DYNAMIC MECHANICAL PROPERTIES OF BLOCK COPOLYMER BLENDS— A STUDY OF THE EFFECTS OF TERMINAL CHAINS IN ELASTOMERIC MATERIALS

Thesis by

Robert E. Cohen

In Partial Fulfillment of the Requirements

for the Degree of

Doctor of Philosophy

California Institute of Technology

Pasadena, California

1972

(Submitted May 19, 1972)

to April May

ACKNOWLEDGMENT

The chance to work closely with Professor N. W. Tschoegl for the past four years has been a rare opportunity indeed. His constant encouragement, guidance, and willingness to give freely of his time and knowledge are deeply appreciated. His interest in the personal lives of all of his students and his willingness to open his home and family life to us was another major factor in making these years so satisfying for me. I thank Dr. Tschoegl now for all that he has done for me, knowing full well that his contribution to the development of my personal life and professional career is just beginning.

Thanks are extended to my colleagues in the Caltech polymer group for the many pleasant experiences and discussions we shared. In particular Don Fesko and Wenji Chang made a number of helpful suggestions concerning my research. Special thanks are extended to my office-mate Satish C. Sharda for four years of close companionship; the long hours at work and the friendship we shared outside will always be remembered. Deep thanks are also due to another member of the polymer family, Mrs. Eileen Finke, not only for the skillful typing of this thesis and countless other manuscripts, but also for the daily smile and the warm friendship she has extended to me since I first arrived at Caltech.

The efforts of Dr. F. Bohnenblust, Ms. Harriet Buhai and Mr. John D. Rynd, Jr. to insure that my studies could continue without

interruption are gratefully acknowledged. Without their help I would just now be starting the research reported here.

I wish to thank my wife, April, for carrying out the yeoman task of typing drafts of this thesis. April has seen me through the vicissitudes of graduate school, and I thank her for her tenderness and patience with me. This thesis is dedicated to her.

Finally, while I can acknowledge the years of patient understanding, encouragement, and financial support provided me by my parents, I will never be able to thank them adequately. As they shared, with enthusiasm, each significant moment of my university education, they took pleasure in the fact that they could provide me with opportunities which were not available to them. This is small compensation for the many personal sacrifices they endured. This thesis is a tribute to my parents and I am certain that only they will see the true significance of its contents.

ABSTRACT

Blends of well characterized polystyrene-polybutadiene SB diblock and polybutadiene continuous SBS triblock copolymers provide rubbery network systems with controlled amounts of terminal chains of known molecular weight. Such systems also provide quantitative information on the concentrations of trapped and untrapped chain entanglements which is not available in conventional elastomers. Three different SB diblocks were synthesized using homogeneous anionic polymerization techniques. These diblocks were blended in various amounts with a single research grade SBS triblock to form three series of samples for mechanical testing.

The mechanical properties of these materials were studied (1) in free oscillation at about 0.2 Hz over a temperature range from -150°C to 100°C, and (2) in dynamic uniaxial compression from 0.1 to 1000 Hz at various temperatures between -87 and 85°C.

The effect of terminal chains on the mechanical properties depends upon their length and concentration in the network. The terminal chains act as a diluent, lowering the storage modulus in the rubbery region. Above a critical molecular weight, the untrapped entanglements provided by the terminal chains can be coupled into a temporary stress-bearing portion of the network; the amount of entanglement coupling is dependent upon temperature. Several low frequency viscoelastic mechanisms appeared as a result of entanglement slippage, and their effect was enhanced as terminal chain content

increased. At very high frequencies in the glassy and transition regions the presence of terminal chains had no effect on the mechanical behavior.

The various mechanisms associated with the terminal chains have been incorporated into a mathematical model whose parameters are given in terms of the structural and compositional features of an entanglement network. The model successfully predicts the level and the location of the low frequency mechanical response for the various materials studied here.

TABLE OF CONTENTS

LIST OF TABLES

LIST OF FIGURES

CHAPTER 1

INTRODUCTION

The major thrust of this research was aimed at gaining an understanding of the effect of terminal chains on the mechanical behavior of elastomeric networks. Particular emphasis was placed on the role of various types of chain entanglements in these networks. In conventional elastomers quantitative information on the effects of terminal chains and chain entanglements is difficult to obtain due to uncertainties in and lack of systematic control over the network structures. This problem was overcome here by using blends of block copolymers to form well-characterized model entanglement networks in which the terminal chain content, their length, and length distribution can all be controlled in a systematic way.

This introductory chapter provides some background information which should help the reader to gain a more complete appreciation of the goals of this research and of the particular approach taken here to attain these goals. The first section briefly discusses the model material approach in the study of polymers. Following this, there are two sections which provide explanations of the occurrence of terminal chains and chain entanglements in conventional elastomers. The final section of this chapter describes the unique features of block copolymer blends which made them particularly useful model materials for this investigation.

1.1 Model Materials

A model polymeric material is one in which important structural features can be varied in a controlled way. The use of such systems has not received widespread attention in the study of the mechanical behavior of polymers. The tendency has been instead to study individually each new polymeric material as it comes along, cataloging the mechanical properties and using these data to estimate the material's structure.

Model materials offer an alternative approach. Because the structure of the model system is well-characterized and can be varied in a known manner, it is possible to identify the effect of each structural feature on the overall mechanical properties. Thus, through the use of model systems, one can study in a systematic way some of the basic molecular mechanisms which contribute to the mechanical behavior of a wide variety of polymers.

Perhaps the absence of an obvious and well-defined model material has prevented this approach from gaining popularity. There is room for much creativity in conceiving model systems for the study of particular molecular mechanisms. Hopefully, the relative degree of success obtained in this investigation will encourage future investigators to use improved model systems in their studies. If a selected model should fail to reveal the desired information, the investigator will have done no worse than to establish the properties of an interesting polymeric system. If the model is a

good one, however, there is the added advantage that the data obtained should contribute measurably to the general understanding of the mechanical behavior of polymers.

In this study, blends of well-characterized block copolymers were used as model materials to study the effect of terminal chains and various types of chain entanglements on the dynamic mechanical properties of elastomers. The major emphasis was directed toward understanding the behavior of the unique rubbery networks formed by the continuous phase of the block copolymer blends and not toward the much studied two-phase nature of these materials. As mentioned above, the important contribution of this work lies in the fact that the model rubbery networks available here contained terminal chains and various types of chain entanglements in reasonably well known amounts, a situation which does not exist in conventionally crosslinked rubbers. Since the two-phase copolymer systems used here offered a convenient method for constructing these well-characterized networks, they became a useful model for studying the behavior of rubber materials in general.

1.2 Terminal Chains in Elastomeric Materials

It has been known for many years that elastomeric networks can be formed by vulcanization of long rubber molecules. The vulcanization process introduces covalent chemical cross-links which

connect the primary[1] molecules at various positions along their lengths. In this way a continuous network of interconnected chains[1] is formed. It is also well known that the finite molecular weight of the primary molecules requires that a certain proportion of the chains will extend from a cross-link point to the end of a primary molecule. A schematic representation of this situation is shown in Fig. 1. Chains of the type BC are known as terminal or dangling chains and they are flaws in the continuous network structure. The terminal chains will not be permanently deformed upon stretching and cannot bear stress at equilibrium. Thus, the terminal chains constitute an elastically ineffective or diluent portion of the network.

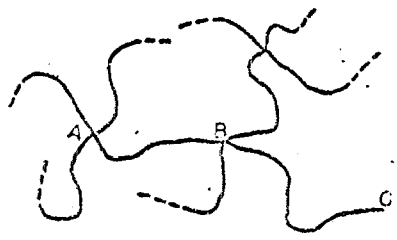

Figure 1. Schematic representation of a network. AB represents a network chain; BC represents a terminal chain; dotted lines imply continuation of network. After Flory (2).

Very early treatments (3-5) of network structure were based on the assumption that the networks were formed from primary

[1] The terminology is that of Flory (1,2). A "primary molecule" refers to the rubber molecules present before cross-linking. A "chain" is the portion of the network extending between cross-links.

molecules of infinite molecular weight. Flory (1) was the first to discuss the effects of finite molecular weight of the primary molecules on the mechanical properties of the vulcanized rubber. Flory reasoned that there should be two terminal chains per primary molecule and that they should have the same length distribution as the network chains. In this way he was able to establish the diluent effect of terminal chains on the equilibrium modulus or compliance of rubbers (2).

For example, the equilibrium shear modulus, G_e, can be written as

$$G_e = G_o (1 - 2M_c/M) \tag{1.1}$$

where G_o represents the modulus expected for a network with no terminal chains, M_c is the number average molecular weight between cross-links, and M is the molecular weight of the primary molecules present before cross-linking. Equation 1.1 explains the observed dependence of the equilibrium mechanical properties on the molecular weight of the primary molecules (2).

More interesting are the possible effects of terminal chains on the viscoelastic mechanical properties. Numerous investigations of the frequency dependent mechanical properties of conventionally cross-linked rubbers have pointed to the importance of terminal chains (6 - 14); however, in every case a clear identification of their role was not possible due to the lack of control

over the network structure formed by conventional cross-linking reactions. In particular the amount of terminal chains, their length, and length distribution could not be controlled in a flexible way, and therefore a clear definition of their contribution to the dynamic properties did not emerge. The results of these studies did indicate, however, that the terminal chains probably contribute most strongly to the dynamic mechanical properties at low frequencies, and that their effect is particularly noticeable in the material's loss properties. Another study has shown that terminal chains can measurably effect the stress relaxation at long times (15).

The contribution of terminal chains, in general, must be viewed in terms of their ability to disengage themselves, through motions of their free ends, from the continuous network. Thus the terminal chains can contribute to a temporary portion of the network structure through engagements known as untrapped entanglements. This temporary structure must have a changing effect on the mechanical properties as time or frequency varies since its effect must disappear at very long times. At equilibrium only the permanent network structure, comprised of trapped entanglements and chemical cross-links, can contribute to the material behavior. In the next section the concept of permanent and temporary network structure will be described including an explanation of the presence of entanglements, both trapped and untrapped, in elastomeric materials.

1.3 Chain Entanglements

In the early 1940's (16) it was recognized that a system of completely uncross-linked polymer molecules could exhibit temporary network structures. The temporary junctions were assumed to be a manifestation of rather strong and widely separated points of coupling among the long-chain molecules. Rearrangements involving molecular segments longer than the characteristic distance between these entanglement points appeared to be greatly restricted, but not permanently excluded as in the case of molecules joined by chemical cross-links. In spite of the large amount of work (See Ref. 17 for a review of these studies) which followed these observations, a rigorous definition of the term "entanglement" as it applies to polymers can not yet be given. It can only be said that an entanglement refers to the temporary constraints on long-range molecular motions mentioned above. The term is not used to describe the short-range intertwining which must occur all along the molecules of any polymeric system.

When a system of entangled primary molecules is vulcanized, the resulting elastomer will have many stress-bearing sites due to permanently trapped entanglement points in addition to the sites provided by the covalent cross-links. This situation, as pictured by Flory (1), is shown in Fig. 2. These entanglement points cannot be disengaged without disrupting the networks, but they are capable of slipping along the chains to accommodate imposed deformations. The slippage motion of the entanglements introduces additional time

dependent mechanisms into the mechanical behavior of cross-linked rubbers. While these mechanisms often have been observed (Ref. 17, Ch. 14), a clear identification of their effect on the mechanical behavior has not been possible because the network structures of the materials studies were not well-characterized. In particular, the number of trapped entanglements could not be determined, only the total number of trapped entanglements and chemical cross-links. The role of these permanent entanglements must be considered to be quite important, however, since in many elastomers they account for a much higher proportion of the stress-bearing sites than do the covalent cross-links.

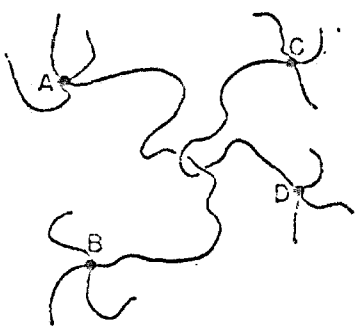

Figure 2. Trapped network entanglement. After Flory (1).

The situation is complicated further by the presence of terminal chains. Clearly, if chain CD had been a terminal chain, the entanglement pictured in Fig. 2 could no longer be permanently trapped. The resulting untrapped entanglement can, because of its free end, become completely disentangled given a sufficiently long time. Its stress-bearing capability will be much less than that of

either a trapped entanglement or a covalent cross-link, and at very long times (equilibrium) it will not support stress at all. Several criteria for distinguishing between trapped and untrapped entanglements have been proposed (10, 17, 18) resulting in slightly different predictions for the equilibrium mechanical properties of cross-linked elastomers. Slow relaxation processes which have been observed at rather long times in cross-linked rubbers are usually attributed to slippage of untrapped entanglements (10, 11, 13, 14). As mentioned above, the particular viscoelastic mechanisms associated with untrapped entanglements have not been clearly identified because of the lack of precise knowledge about the structure of the networks studied.

1.4 Block Copolymer Blends as Model Materials for Conventional Elastomers

This section describes the manner in which blends of diblock and triblock copolymers can be used to provide rubbery networks with controlled amounts of terminal chains and known quantities of trapped and untrapped entanglements. The limitations on using these blends as model materials for studying the behavior of conventional elastomers are also discussed here. In Chapter 6 some suggestions will be given for improving the system and for extending the model to include other structural features in addition to entanglements and terminal chains.

A block copolymer is composed of different homopolymer segments linked sequentially into a single straight-chain molecule. The phase separation of the dissimilar segments of block copolymers has been well established by electron microscopy. It is also well known that a triblock copolymer with relatively short glassy endblocks and a long rubbery center segment possesses elastomeric properties at temperatures below the glass transition temperature (T_g) of the endblocks. This results because the glassy regions or domains act as multifunctional cross-links for the long rubbery chains which comprise the continuous phase. Above T_g of the hard segments the material will flow, and thus the name thermoplastic elastomer (20) has been proposed for block copolymers with such properties. Another useful feature of block copolymers arising from the particular methods used in their synthesis is that a very narrow (nearly monodisperse) molecular weight distribution can be obtained for each of the segments.

A schematic representation of a thermoplastic elastomer is shown at the upper left in Fig. 3. It is immediately apparent that each of the rubbery center segments must have both of its ends pinned in a glassy domain. Thus, at least to the extent that a pure triblock can be made and that phase separation is complete, such materials will contain no terminal chains. The continuous rubbery phase is not cross-linked, but it will bear stress at each of several entanglement points in addition to the glassy cross-links. All of the entanglements are permanent since both ends of each rubbery

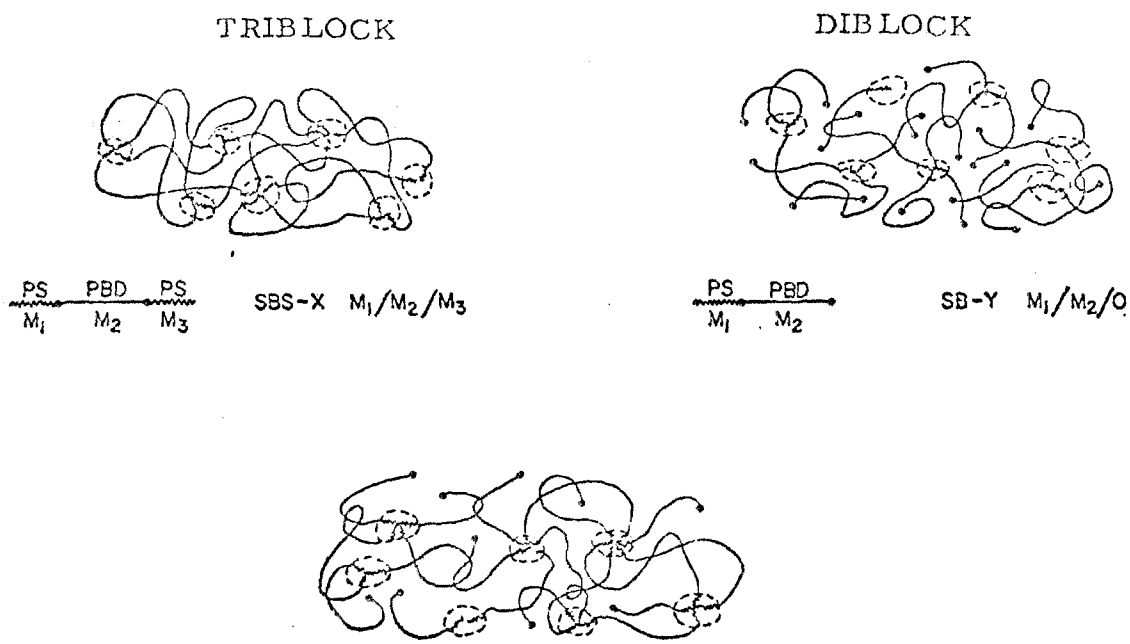

Figure 3.

The Block Copolymer Model System

segment are pinned; however, as discussed earlier, the positions of the entanglement points are not fixed because of the possibility of slippage along the rubbery chains.

The diblock copolymers, shown schematically at the upper right in Fig. 3, will exhibit a similar two-phase morphology. In this case, however, the rubbery segments are pinned in a glassy domain at only one end. Such a diblock copolymer consists of multifunctional star-branched clusters in which the branches are all essentially terminal chains. The material will bear stress only if a temporary entanglement network is formed. The entanglements of this network are not permanent, however, because the free ends allow each rubbery segment to disentangle itself completely over a sufficiently long period of time.

It is a reasonable assumption that the end blocks of diblock and triblock copolymer chains will mix without prejudice (21). Thus by a judicious blending of such copolymers, one can, as shown schematically at the bottom of Fig. 3, introduce a controllable fraction of terminal chains into the continuous rubbery phase of the blend. At the same time it is possible to vary the length and even the length distribution of the terminal chains. Simultaneously there will be a controlled combination of permanent (or trapped) and non-permanent (or untrapped) entanglements. The former arise from the entanglements between two of the triblock rubbery segments, while the latter involve a rubbery segment from at least one diblock molecule. The model system described here

offers no information on possible motions of cross-link points in conventional elastomers since there are no covalent cross-links in these systems. The attachments of the rubbery segments at the domain boundaries do not constitute a model for conventional cross-links since the domains are large and essentially immobile when compared to the chemical linkages found in a typical rubber. A method will be discussed in Chapter 6 for introducing known quantities of tetra- or tri-functional covalent cross-links into the rubbery phase of the block copolymer blends.

Evidently, the diblock-triblock copolymer blends cannot be completely valid model systems for conventionally cross-linked elastomers. Below their glass transition temperature the rigid domains act essentially as a reinforcing filler[2]. However, the time and temperature dependence of the filler affects the mechanical properties of the copolymer even below T_g of the end blocks (22). Furthermore, one cannot, in general, expect a sharp boundary between the two phases. The possibility of a mixed interfacial region in block copolymers has already been postulated in the literature (23, 24). Such an interlayer can seriously affect the mechanical properties in certain regions of time and temperature (25, 26).

---

[2] The diameter of a domain is of the order of hundreds of angstroms which makes them roughly the same size as carbon-black fillers.

The preceeding discussion of the use of diblock-triblock blends as model materials for conventionally cross-linked elastomers is quite general and should apply to a wide variety of block copolymer systems. For a number of reasons, block copolymers of polystyrene (PS) and polybutadiene (PBD) were chosen for use in this work. Firsthand experience with these materials had already been obtained by collaboration in (27) and observation of (25) research projects conducted in this laboratory. Perhaps the most important reason for the particular choice of materials was necessity for a high purity triblock copolymer to serve as the base material for the model system. Any uncertainty concerning a possible diblock portion in the base material would cast serious doubt upon the validity of the model and consequently upon the results of this research. As discussed in the following chapter on materials, high purity polystyrene-polybutadiene-polystyrene triblock copolymers were readily available, and therefore it was decided to build the model system around these materials.

CHAPTER 2

MATERIALS

2.1 Syntheses and Characterization of Polystyrene-Polybutadiene Diblock Copolymers

Homogeneous anionic polymerization techniques, developed in the late 1950's by Szwarc et al (28), make it possible to synthesize an unlimited variety of novel polymeric materials. Of particular interest are block copolymers, which contain sequential segments of different materials linked into a single straight chain molecule. Triblock copolymers of the type polystyrene-polybutadiene-polystyrene (SBS) have received special attention due to their ability to serve as thermoplastic elastomers (20). The Shell Chemical Company has, for several years, produced commercial SBS materials under the trade name "Kraton Rubber".

As discussed in the previous chapter, blends of SB diblocks and SBS triblocks can be used as model materials in the study of terminal chains and various types of chain entanglements in rubbers. It is clear that a supply of several SB diblocks in addition to at least one SBS triblock material will be necessary for this study. Research grade SBS triblocks containing essentially no diblock fraction were generously supplied by the Shell Chemical Company. The characterization information supplied by Shell with

these materials appears in Appendix A. SB diblocks were not readily available and therefore it was necessary to synthesize several samples.

The synthesized diblocks must be compatible with the available triblocks. This means that the size of the polystyrene segments must be nearly identical in the diblocks and triblocks. The microstructure of the polybutadiene moiety of each diblock must be similar to that of the triblocks to avoid a significant shift in the glass transition temperature of the polybutadiene phase. Furthermore, the styrene content of the diblock cannot be too dissimilar from that of the triblock into which it is to be blended. Matsuo (29) and Kawai (30, 31) have shown that drastically different morphologies can result from significant variations in styrene content.

All of the factors mentioned above place certain limitations on the procedures which can be used for synthesizing suitable diblock samples. The information reported in this section is a summary of the results of the various attempts to synthesize SB diblock copolymers and the techniques employed in their characterization. Seven syntheses were carried out, three of which resulted in suitable SB diblocks.

2.11 Purification and Handling of Materials

The procedures required to synthesize diblock copolymers using the method of homogeneous anionic polymerization have been

discussed extensively in the literature (32 - 34). The necessity for extremely high purity materials and an inert atmosphere cannot be over-emphasized. Water and oxygen are especially dangerous impurities which will terminate the growth of one "living" (34) polymer chain for each molecule of impurity present. It has been estimated by Szwarc that a unimolecular layer of water absorbed on the wall of a reactor can destroy all of the active sites in a typical anionic polymerization (34). Trace amounts of impurities not sufficient to terminate the entire reaction will have remarkably strong effects (34) on the molecular weight distribution obtained. Thus, the synthesis of diblock copolymers with essentially monodisperse segments of polystyrene and polybutadiene, while simple in principle, was quite difficult in practice.

The rigorous methods (32, 35-37) employed in the purification and handling of the materials used in the polymerizations are described in the following paragraphs. A high vacuum (10^{-6} torr) apparatus was used to eliminate atmospheric impurities. It is shown schematically in Fig. 4. The vacuum technique was chosen in lieu of the inert gas (nitrogen or argon) method because it allows for thorough flaming and degassing of glassware.

2.111 Initiator

The initiator chosen for use in all reactions was sec-butyllithium. This compound, as do other organolithiums, initiates by anion attack (34). Sec-butyllithium is especially useful for SB

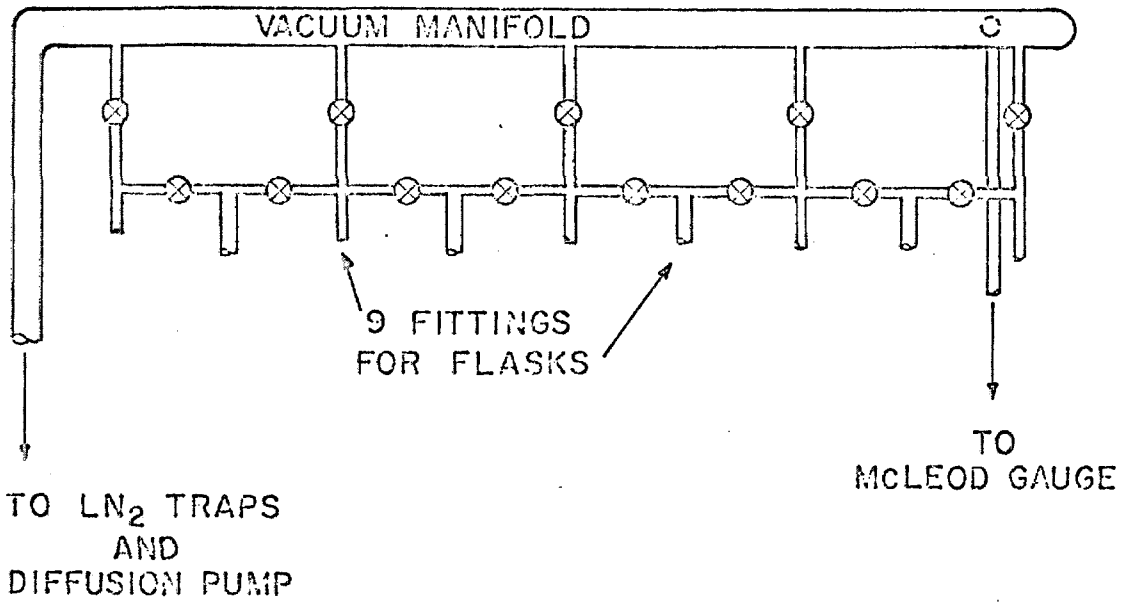

Figure 4.

Vacuum System for Anionic Polymerizations

diblock syntheses because of its relatively high rate of initiation with styrene and butadiene (33). The stock solution (Alpha Inorganics, Inc.) was 2.2N in n-hexane. This solution was transferred to a nitrogen atmosphere and diluted with n-hexane to 0.72N. The diluted initiator solution was then drawn into an evacuated ampul. This was transferred to the vacuum apparatus, degassed, and its contents distributed (32) into ten ampuls containing from 2.5 to 5.0 ml of the 0.72N solution. A typical polymerization carried out in 500 ml of solvent had an initial concentration of sec-butyllithium in the range of 3.6×10^{-3} to 7.2×10^{-3} N.

2.112 Solvents

Several different solvents - tetrahydrofuran, isopentane, n-hexane, and benzene - were purified by identical methods. The solvent was degassed and stirred under vacuum over finely ground (-40 mesh) calcium hydride for several hours. It was then distilled into an evacuated flask containing a liquid alloy of sodium and potassium (32). After several days of stirring over the Na-K alloy to destroy trace amounts of water, the solvent was distilled into a flask which had been mirrored with a thin layer of sodium metal. If no visible degradation of the mirror occurred within 24 hours, the solvent was considered to be dry, and was distilled into a receiving ampul or directly into the reactor.

2.113 Monomers

Styrene cannot be distilled directly onto sodium mirrors because it tends to polymerize. For this reason, the purification procedures had to be modified for this monomer. Stabilized styrene (Matheson, Coleman and Bell) was degassed and stirred for several hours over calcium hydride. The monomer was then distilled to remove the stabilizer and passed twice through chain flasks (32) in which only styrene vapors came into contact with the sodium mirror. The monomer can thus be purified without unwanted polymerization. From the last chain flask the styrene was collected into a monomer receiving ampul, frozen, thoroughly degassed, and sealed. The ampul was then attached to the reactor. Each ampul was preweighed so the weight of the monomer could be determined.

The gaseous monomer butadiene required special handling and purification techniques. A continuous gas flow system was used for initial purification steps (35). The monomer was later handled as a liquid at reduced temperatures with the aid of dry ice-acetone baths. Directly from the gas cylinder, 1,3-butadiene (Baker Chemical Co., Specialty Gas Division) was dispersed by a fritted glass sparger into a 1 M NaOH solution to remove inhibitor. It was then passed through a 0°C chamber which trapped much of the entrained water but did not condense the butadiene (b.p. -4.5°C). The gas was then passed through tubes packed with $CaCl_2$, CaH (4-40 mesh), and Linde 4-A molecular sieves for further drying.

It was then condensed in an evacuated flask on the vacuum line, distilled onto several sodium mirrors, and finally collected in preweighed monomer ampuls.

2.12 Synthesis Methods

The reactor used for the polymerization is shown schematically in Fig. 5. Stopcock grease can be a damaging impurity in prolonged exposure and therefore all ampuls were glass welded onto the reactor's maniford rather than connected with greased fittings. After the solvent was distilled into the flamed and evacuated reactor, the entire reactor-ampul system was sealed off and removed from the vacuum line. The initiator ampul was then cracked open and the walls of the reactor were thoroughly rinsed with the solution to remove any remaining impurities.

Up to this point, all reactions were carried out in the same manner. However, three different approaches were taken for completion of the diblock synthesis. In the first method, the butadiene was polymerized in a hydrocarbon solvent. After several days a small amount (25 - 35 ml) of THF was added to change the polarity of the solvent, and then the styrene ampul was quickly cracked open. This approach was devised in an effort to obtain a polymer with a diene moiety of nearly all 1,4-addition and a monodisperse polystyrene segment. Two major factors are involved (33). Butadiene will polymerize with low amounts of the unwanted 1,2-addition in hydrocarbon solvents. However trace amounts of

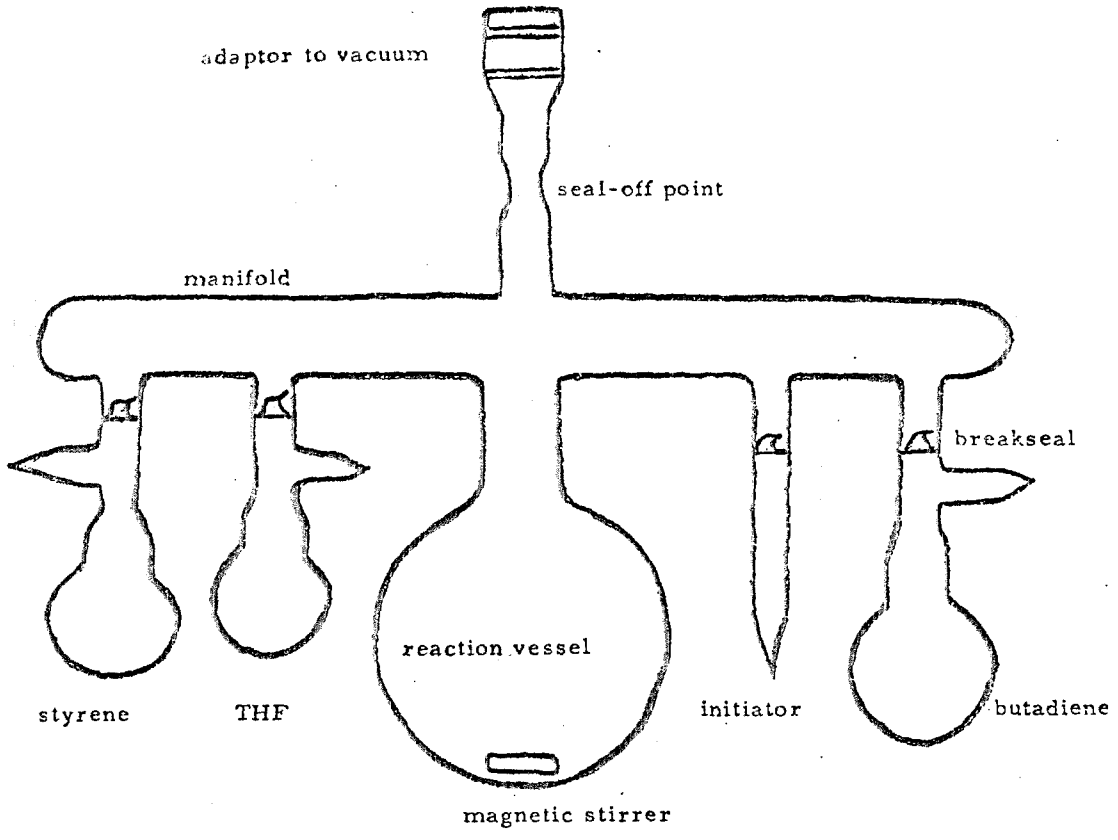

Figure 5.
Reactor Used in the Synthesis of SB Diblock Copolymers

ethers or other polar solvents will greatly increase the amount of the 1,2-adduct. On the other hand, the initiation rate of styrene is slow compared to the propagation rate in non-polar hydrocarbon solvents. Trace amounts of polar compounds such as THF have been found to speed up the initiation and thus help to maintain a narrow molecular weight distribution in the polystyrene moiety of the product.

The first method has several shortcomings. If the THF is added before all of the butadiene has been depleted, unwanted 1,2-polybutadiene may be obtained near the polystyrene segment. Furthermore, because of the slow diene polymerization, the styrene ampul must be cooled continuously for several days to prevent thermal polymerization of the unstabilized monomer in the ampul. Finally, the active end of the polybutadiene chain can attack and react with THF molecules unless quite low temperatures (<-35°C) are maintained (37). However, the molecular weight of the polybutadiene chains already formed may be high enough to precipitate at these temperatures and thus destroy the homogeneity of the system.

With these factors in mind a second method was devised in which the styrene segment was polymerized in a hydrocarbon solvent without addition of a polar solvent by employing a seeding technique (37). This method requires very small amounts of styrene to be added until all of the initiator molecules have been converted into short polystyryl anions. This can be verified visually due to the bright orange color of the styryl anion. When a small addition

of monomer no longer causes a deepening of the orange color, the maximum number of active polystyryl anions has been formed. At this point the remaining monomer is added dropwise with vigorous stirring. This results in nearly monodisperse polystyrene chains. The butadiene is added after several hours and the diene polymerization is allowed to continue for several days. No THF is required for this method. The disadvantage of the seeding technique for our purposes is that the low molecular weight polystyrene segments being sought are near the lower limit of molecular weights for which the technique is successful in producing monodisperse polymers.

A third method was employed in an effort to take advantage of the different reactivity of the two monomers in non-polar hydrocarbon solvents. It has been shown (38, 39) that butadiene will polymerize preferentially to styrene when butyllithium initiator is used in a hydrocarbon solvent. Almost no styrene will react until all of the butadiene has been consumed. The resulting "tapered" block (34) copolymer will have a nearly pure polybutadiene moiety linked to a pure polystyrene moiety by a mixed region of butadiene and styrene. The exact length and nature of the mixed middle segment is difficult to determine. It is interesting to note, however, that mixed segments of this sort would be extremely useful in an investigation of the effects of interlayer regions on the mechanical properties of block copolymers.

When a polymerization was completed, the reaction was terminated by cracking open the neck of the reactor and pouring the viscous solution into a large excess of methanol. A small amount of N-phenyl 2-naphthylamine was added to the methanol as an antioxidant. The collected polymers were stored in the dark at -15°C. A total of seven polymerizations were completed using all three of the synthetic methods described above. The results of these polymerizations will be presented after a discussion of the techniques employed in the characterization of the SB diblocks.

2.13 Characterization Methods

The quantities of interest are the diblock number average molecular weight ($\bar{M}_n$), the styrene weight percentage (ϕ), the diene microstructure, and the glass transition temperature of each segment. $\bar{M}_n$ was determined in toluene solution in a Melabs Membrane Osmometer. Glass transition temperatures of the polybutadiene segments were measured on a DuPont Model 800 Thermal Analyzer. As in previous studies of similar systems (27), the glass transition temperature of the polystyrene segments could not be measured reliably. Percentage compositions were determined in two ways. The first was a quantitative chemical degradation (40) in which the polybutadiene portion of the diblock was cleaved off by oxidation with osmium tetroxide. The oxidation products were exhaustively extracted with ethanol and the remaining insoluble polystyrene was recovered and weighed. Because the low molecular

weight polystyrene segments were difficult to handle quantitatively, a second method based on NMR analysis was used. The NMR technique developed by Senn (41) for analysis of random copolymers of butadiene and styrene was used successfully to determine the compositions of the block copolymers obtained here.

Detailed determinations of polybutadiene microstructure have been accomplished by NMR (42) and IR (43) techniques. For the purposes of this study, it is sufficient to know only the amounts of 1,2- and 1,4-addition in the diene moiety. These quantities can be determined along with the styrene content by the NMR analysis method of Senn (41) in which the amounts of styrene, 1,2-butadiene and 1,4-butadiene in the copolymer are obtained by solving a system of three simultaneous equations. NMR spectra were obtained routinely on an A-60A Varian Spectrometer. Five to ten percent solutions of the polymer in carbon tetrachloride were used for the analysis. The method did not allow for determination of the cis-trans ratio in the 1,4-polybutadiene. The NMR method was tested by determining the compositions of the well-characterized triblock materials supplied by Shell. As indicated in Table 1, the NMR results compare favorably with Shell's characterizations.

Table 1

NMR CHARACTERIZATION OF TRIBLOCKS COMPARED TO SHELL CHEMICAL CO. DATA

A = Shell B = This Investigation

Material		Percent 1,4-addition		Percent 1,2-addition		Weight Percent Styrene	
A	B	A	B	A	B	A	B
TR-41-1647	-	90	92	10	8	48.2	51.2
TR-41-1648	(SBS-8)	90	92	10	8	29.3	28.4
TR-41-1649	-	-	94	-	6	26.8	27.6

2.14 Results and Discussion

Seven polymerizations were completed yielding six copolymers of butadiene and styrene, and one polybutadiene sample. Table 2 summarizes the experimental conditions and the product characterization for each polymerization. To be suitable for blending into the available triblocks, the SB polymers must have a diene microstructure with less than 10% 1,2-addition, contain less than 40% styrene, and have a polystyrene block $\overline{M}_n$ less than 20,000. From Table 2 it is apparent that only reactions 5, 6, and 7 yielded suitable SB diblocks. Reactions 1 to 4 did, however, provide useful information and valuable experience for future work.

Table 2. Results of the Seven Anionic Polymerizations with Sec-Butyllithium Initiator

Reaction Number	Order of Monomer Addition	Time and Temperature of Polymerization		Solvent	$\overline{M}_n$ Diblock	ω_s Wt. % Styrene	$\overline{M}_n$ S / $\overline{M}_n$ B	% 1,2-addition in diene block	T_g B
		S	B						
1	B-S	1 hour - 65°C	3 days 0°C	Isopentane (THF)	42,000	38	16,000 / 26,000	65	-20°C
2	B-S	1 hour -65°C	3 days 0°C	Isopentane (THF)	40,000	49	19,600 / 20,400	55	-
3	B	-	4 days 20°C	n-hexane	103,000	0	0 / 103,000	9	-92°C
4	Simultaneous	7 days 20°C	7 days 20°C	n-hexane	300,000	< 5	<15,000 / >285,000	10	-90°C
5	S-B	2 hours 20°C	4 days 20°C	n-hexane	77,000	13	10,000 / 67,000	5	-89°C
6	S-B	8 hours 20°C	4 days 20°C	n-hexane	60,000	15	9,000 / 51,000	6	-89°C
7	S-B	13 hours 20°C	4 days 20°C	benzene	29,000	24	7,000 / 22,000	8	-90°C

S = Styrene

B = Butadiene

The first two polymerizations were carried out in isopentane by the method in which the butadiene is polymerized first. In both cases the diene polymerization was carried out at 0°C for 3 days before the THF and styrene were added. The addition of styrene produced a bright yellow-orange color somewhat different from the characteristic deep orange color shown by reactive styrene polymers in n-hexane. The color was first attributed to the use of a different solvent, isopentane, instead of n-hexane. Further consideration of the experimental procedures and NMR analysis (which showed a high 1,2-diene content for both polymers), led to the conclusion that the styrene and THF were added before the butadiene was exhausted. This is likely in view of the low temperature (0°C) of the initial polymerization. At this temperature the reaction rate is substantially reduced from that at room temperature. Therefore it is probable that the products of the first two polymerizations were diblocks of largely 1,4-polybutadiene/1,2-butadiene-co-styrene.

The third reaction was carried out in the same manner but with n-hexane solvent. The butadiene was reacted for 4 days at 20°C. A crack developed in the reactor during the attempt to break open the styrene ampul and the reaction was terminated. Thus, the resulting polymer was a pure polybutadiene, but significantly it had a very low percentage of 1,2-adduct as desired.

Reaction number four was an attempt at making a tapered diblock by employing the method of feeding both monomers simultaneously

to the reactor. The reaction medium began as a colorless solution and became increasingly yellow-orange as time proceeded. The yellow color persisted after 7 days indicating that pure polystyrene segments still did not form. At this point the reaction medium was too thick to stir, and the reaction was terminated. The large quantities of monomer and relatively little initiator used in this particular reaction apparently led to a product with a relatively high molecular weight. The product of this reaction probably contains largely 1,4-polybutadiene/1,4-butadiene-co-styrene materials.

The fifth and sixth reactions were carried out according to the seeding procedure. A larger quantity of styrene was employed in the sixth reaction, and the polystyrene chains tended to phase out of solution as they reached their maximum molecular weight. In both cases, however, the deep orange color persisted until the butadiene was added, at which time the solution became colorless and the growing polymers again became soluble. The SB diblocks resulting from these two reactions met the desired molecular specifications, and therefore this polymerization method was also used in the next synthesis.

The seventh reaction was carried out in a manner similar to the previous two, except that benzene was employed as the solvent. There was no tendency for the growing polystyrene chains to phase out of solution in this reaction. Upon addition of the butadiene the orange color again disappeared rapidly. The final

product from this synthesis contained polybutadiene segments with an amount of 1,2-addition similar to the products synthesized in n-hexane solvent. The fact that suitable products can be obtained, with the added advantage of increased solubility during the styrene polymerization, makes benzene the logical choice of solvent for any future SB diblock syntheses using the seeding technique.

All three successful syntheses employed the seeding technique, and so a few remarks will be made concerning the type of product to be expected from this reaction scheme and the usefulness of these products for blending with the available triblocks. As mentioned earlier, the polystyrene moieties are not likely to have very narrow molecular weight distributions. There are several reasons for this. First, styrene is the most difficult of the materials to purify, and impurities have a profound effect on the molecular weight distribution. Second, initiation is not rapid in comparison with propagation for styrene in hydrocarbon solvents, and this condition is necessary for obtaining narrow molecular weight distributions (33). This second problem can, in principle, be overcome by seeding, but as discussed earlier, this technique is only partially successful at the low molecular weights obtained in these syntheses.

Considering the difficulties in obtaining a narrow molecular weight distribution in the polystyrene segments, one must decide whether the diblocks are still useful for building model network systems by blending them with triblocks. In the

interpretation of the mechanical properties of the blends, the polystyrene phase will, in most cases, be considered to be inert filler. Therefore, only the volume or weight fraction of polystyrene in the blend will be significant, not the molecular weight distribution of the polystyrene segments. Furthermore, any impurities in the styrene monomer, or even those added with the butadiene at the beginning of the polymerization of the second segment, will produce terminated or "free" polystyrene segments of various lengths. These short polystyrene chains will enter the polystyrene domains of the blends (21), and thus they offer much less complication to the interpretation of the model network structure than the corresponding amount of free polybutadiene. Another advantage of the seeding technique is the fact that the osmotic pressure determinations of overall molecular weights are rather insensitive to the presence of very short segments. This is due to the permeation limit of the membranes employed in the osmometer.

Thus, the seeding technique has the inherent advantage that most of the problems in the synthesis are overcome by the time the important part of the reaction, namely, the formation of the polybutadiene segments, begins. To be able to assess the structures of the networks formed by the blends, it is necessary to have a narrow polybutadiene molecular weight distribution and no free polybutadiene chains in the sample. The synthetic scheme

in which the polystyrene was synthesized first has helped to assure that these two criteria are fulfilled in the products of reactions 5-7.

The three useful diblocks obtained from the syntheses are given the following designations: SB-5, 10/67/0; SB-6, 9/51/0; and SB-7, 7/22/0. The molecular weights of the individual blocks, in thousands, are separated by the slashes. The third block position has been retained for symmetry with the triblock designations and is indicated by a molecular weight of zero for all the diblocks.

2.2 Sample Preparation

2.21 Preparation of Diblock-Triblock Blends

The three diblocks were blended with one of the Shell triblocks (TR-41-1648, designated here as SBS-8, 16/78/16) to form three series of samples. The blending was accomplished by dissolving known weights of diblock and triblock in benzene to form a solution containing aroung 6 weight percent polymer. A trace amount (ca 0.2% by weight) of N-phenyl 2-naphthylamine was added as anti-oxidant. The solution was stirred vigorously for several hours. It was then poured carefully down a glass plate onto a mercury surface contained in a circular glass dish 10 cm in diameter. The glass plate was submerged below the mercury surface during

pouring; this minimized the number of air bubbles trapped at the mercury-polymer solution interface.

The benzene was allowed to evaporate for several days, during which time the dish was covered, mounted on a vibration absorbing cork-rubber cushion, and stored in a dark, draft-free room. Using this technique, uniform films around 2 mm thick were obtained. The films were, for the most part, free of visible surface flaws or trapped air bubbles.

2.22 Experimental Specimens

Two types of experimental specimens were made from the thin films. Rectangular strips, typically 6.00 cm by 1.00 cm, were cut from the films in a milling machine using a disk-shaped cutter specially modified from a slitting saw. Soapy water was used as a lubricant. These specimens were used in the torsion pendulum apparatus.

Very small (ca 0.20 cm^2 cross section) specimens with irregular hexagonal shapes were required for the dynamic uniaxial compression experiments. The thickness of a typical film was not sufficient for direct use in the dynamic tester (25), and therefore laminated specimens were made. Two or three laminations were necessary, depending upon the thickness of the original film. The particular method of preparing laminated specimens with good adhesion between the layers has been discussed in detail elsewhere (25). Mechanical properties data (25) taken parallel and

perpendicular to the laminations of one triblock specimen were essentially identical and thus the necessity for using multi-layer specimens here is not considered to be a problem. In all of the dynamic compression tests conducted in this investigation, the uniaxial compression was imposed perpendicular to the laminations.

2.23 Annealing of Specimens

During the casting process, some of the soft polymeric material deposits on the sides of the glass container. Because of this adhesion to the walls, each of the circular films had an upward curvature near its outer edge. This portion was always discarded before cutting any test specimens. However, a more serious effect of this adhesion was observed. Figure 6 shows the normalized change in specimen thickness as a function of time at various fixed temperatures. The specimens were cut from the central portion of one of the SBS-8 films. The increase in thickness (the length and width decreased commensurately) indicates that there is significant orientation in the films in the radial direction as a result of the adhesion of the film to the side walls of the container in which it was cast.

Electron photomicrographs of SBS-8 (44) indicate discrete, almost spherical polystyrene domains for annealed specimens; unannealed specimens show slightly elongated domains which appear to touch in some places. These observations are consistent with the annealing data shown in Fig. 6. Especially important is the

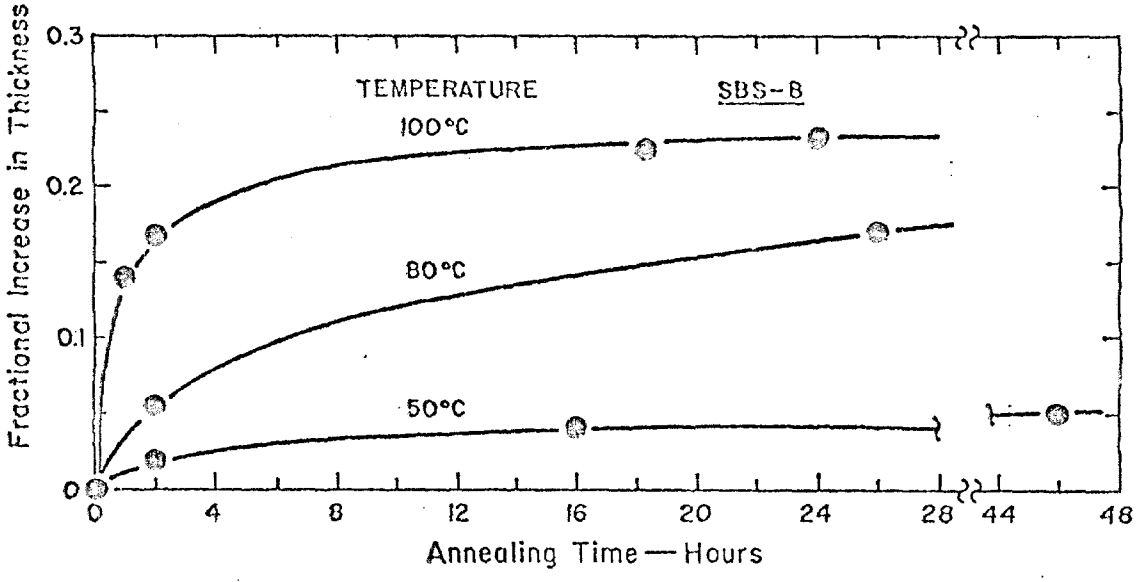

Figure 6.

Effect of Annealing on Specimen Dimensions

fact that at 50°C only minimal dimensional changes can be seen even after very long times. Thus it appears that the radial orientation induced in the specimen during casting can only be removed by annealing at temperatures high enough to allow the polystyrene domains to soften. All of the specimens used in this work were annealed in vacuum at 100°C. The strip specimens for the torsion pendulum were annealed for 24 hours. The small specimens used for the dynamic compression tests were annealed for only 6 hours, but were subjected to additional heat treating (discussed in the next chapter) within the apparatus before any experiments were performed.

CHAPTER 3

EXPERIMENTAL DETAILS

3.1 Overall Experimental Program

The overall program of experiments was designed to yield information on the effects of terminal chains and chain entanglements through comparisons of the mechanical response curves. Figure 7 gives a schematic representation of this approach. Comparing results obtained within each of the three series of blends yields information on the effect of changing network composition at constant terminal chain length. The effect of changing terminal chain length is studied through comparisons of the data from all three series. The compositions of the various blends in the three series are given in Table 3.

The dynamic mechanical properties of these blends were studied in two ways: (1) in free oscillation at about 0.2 Hz over a temperature range from -150°C to 100°C, and (2) in dynamic uniaxial compression from 0.1 to 1000 Hz at various temperatures between -87°C and 85°C. The study of dynamic (rather than transient) properties was especially useful in this work since the energy dissipation or loss properties of the blends turned out to be particularly sensitive to the secondary viscoelastic mechanisms of interest here. The free oscillation experiments were simple but reliable, and they offered a means of obtaining qualitative information on the kinds of changes

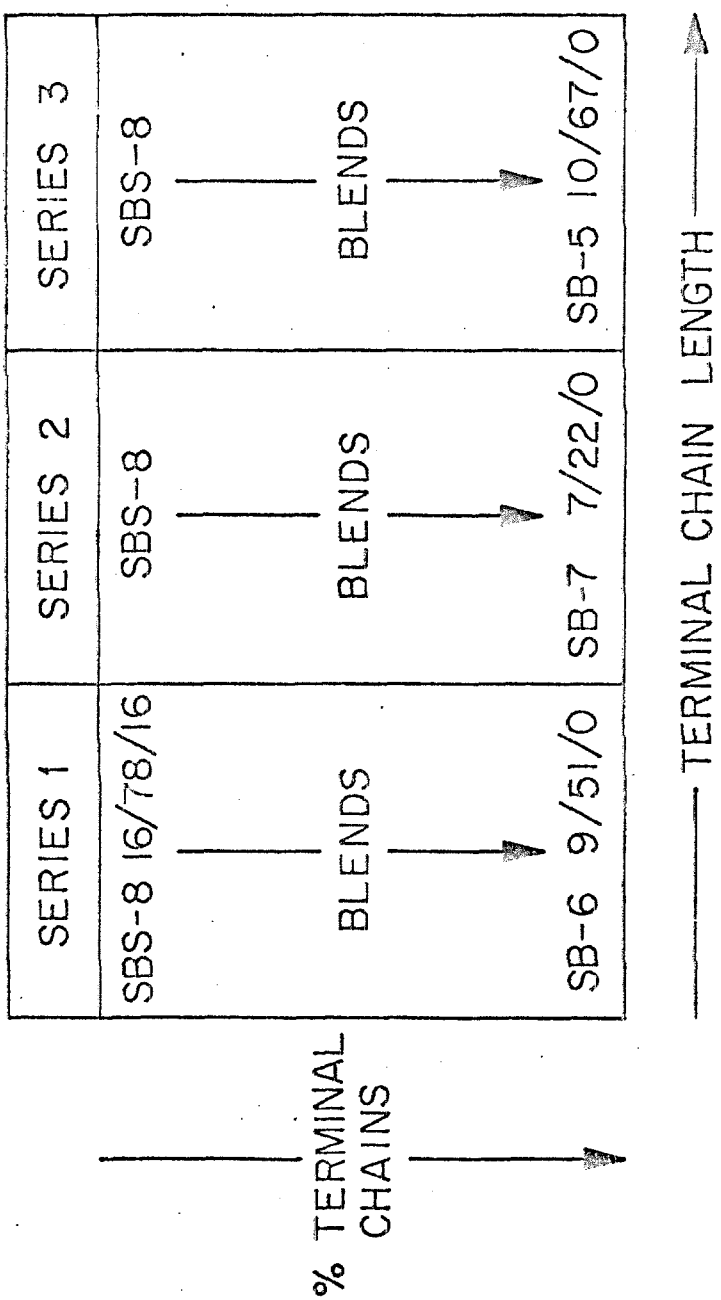

Figure 7.

Overall Experimental Program

Table 3

COMPOSITIONS OF THE DIBLOCK-TRIBLOCK BLENDS

Sample Code	Weight Percent Styrene	Weight Fraction Terminal Chains*
Series 1 Terminal Chain $\overline{M}_n$ = 51,000		
SBS-8	29	0
BL-1.1	26	0.231
BL-1.2	23	0.444
BL-1.3	22	0.577
SB-6	15	1
Series 2 Terminal Chain $\overline{M}_n$ = 22,000		
SBS-8	29	0
BL-2.1	28	0.159
BL-2.2	28	0.315
BL-2.3	27	0.416
SB-7	24	1
Series 3 Terminal Chain $\overline{M}_n$ = 67,000		
SBS-8	29	0
BL-3.1	24	0.334
BL-3.2	22	0.490
SB-5	13	1

*Polystyrene-free basis

to be expected in the various regions of material response as network structure was varied systematically. The regions of greatest interest were then studied in more detail in the forced oscillation experiments. This second experimental method was much more difficult and tedious, but fortunately these data were more adaptable to quantitative interpretation and were, therefore, considerably more valuable than the results of the first method.

3.2 Apparatus and Procedures

3.21 Torsion Pendulum

The mechanical properties of the block copolymer blends were measured as a function of temperature at nearly constant frequency (about 0.2 Hz) on a freely oscillating torsion pendulum. The period and logarithmic decrement (natural logarithm of the ratio between successive displacements) were measured over a temperature range from -150°C to 100°C. The storage and loss moduli were calculated in the usual way (17) using tabulated corrections for a rectangular strip specimen (45).

The torsion pendulum was built essentially along the lines of the apparatus described by Lawson (46). This apparatus is similar to other freely oscillating torsion pendulums except for the displacement sensing device. The oscillating shaft has two magnets mounted on it in a sector-shaped configuration. Centered between the two magnets is a Hall effect device which, under the

influence of a constant current, will convert changes in magnetic field strength to a changing voltage signal. This signal is then displayed without amplification on a strip chart recorder as a damped sinusoidal trace. The Hall device displacement sensor is simpler to balance and align than reflected light beam sensors. Because of its great sensitivity to very small changes in the magnetic field strength, rather small angular displacements (± 1-2 degrees) can be employed. At these small angular displacements the relation between the displacement and the Hall device output may be regarded as linear with sufficiently good approximation (46).

Below room temperature the specimen was encased in a Dewar flask containing a coil of stainless steel tubing. By passing cold nitrogen gas through the coil, temperatures as low as -160°C can be reached. The natural temperature rise is slow enough (around 10°C/hr.) that no further control is necessary. A measurement is taken in less than one minute, and the effect of temperature change over this time interval is insignificant. At very low temperatures, especially near the glass transition temperature of the rubbery phase, the thermal gradient along the specimen caused a serious problem in obtaining reproducible measurements in early runs. This problem was solved by surrounding the specimen with a close-fitting (but not touching) brass cylinder to conduct heat evenly along the length of the specimen. Two thermocouples were placed through small holes in the brass cylinder, one near the top and one near the bottom of the specimen. Even at

the lowest temperatures, the difference between the two thermocouples was less than 1°C.

Above room temperature the specimen, still surrounded by the brass cylinder, was placed in a glass container wrapped with electrical heating tapes. Again the temperature rise was negligible during a measurement, and the thermal gradient along the specimen was under 1°C. At the highest temperatures, around 90 to 100°C, the specimen began to soften and narrow somewhat near the top clamp. The changing shape factor removes any hope of making precise measurements in this region.

A typical set of data obtained from the torsion pendulum experiments is shown in Figure 8. Here, the logarithms of the storage modulus, G', and the loss modulus, G'', are plotted against temperature for SBS-8. The units of the moduli are bars. (1 bar = 10^6 dynes/cm^2 or 14.5 psi.) Each datum point represents an average value taken over at least eight cycles, except in the region of very high damping between -100°C and -90°C. Here the number of cycles which could be obtained varied between eight and two. Figure 8 demonstrates the rather good reproducibility which can be obtained in the intertransition plateau between several repeat runs on the same specimen. The reproducibility was much poorer for unannealed specimens.

Free oscillation data must be interpreted with caution. The complex modulus, $G^*(\omega,\alpha)$, as calculated from such measurements, is a function of both the radian frequency, ω, and the damping, α.

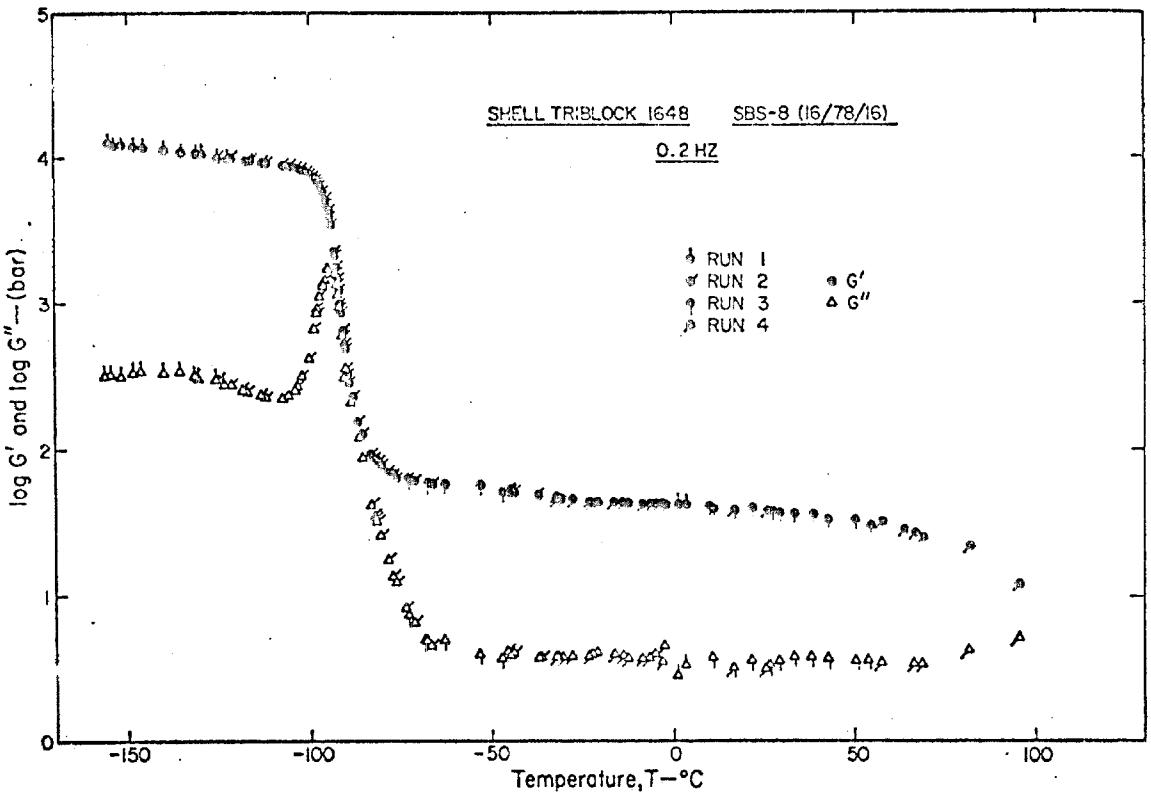

Figure 8.

Typical Data Obtained on the Torsion Pendulum

It becomes comparable to the modulus obtained in forced oscillation, $G^*(\omega)$, only if the damping is negligible. The ensuing difference in notation and terminology has been suppressed here for simplicity but must be borne in mind when comparing the data with similar ones by other authors. A further complication arises from the fact that the measurements are not strictly isochronal. In these measurements the maximum range of frequencies over the temperature range tested was half a logarithmic decade. Isochronal measurements can be obtained by making several measurements at the same temperature in which the moment of inertia, the elastance of the suspension wire, the specimen geometry, or a combination of these factors is varied. In this way one can achieve a spread of frequency allowing interpolation to a constant frequency at each temperature. This method, however, is time consuming and is hardly warranted because damping and frequency cannot be controlled in this way simultaneously. The measurements were made here with the same moment of inertia, suspension elastance and specimen geometry throughout. In this way the data reported here are internally consistent and qualitative comparisons can be made between the various materials tested.

3.22 Dynamic Rheometer

An instrument which enables forced oscillation measurements to be conducted over a wide and continuously variable frequency range as well as a large temperature range is the most

valuable tool available to an investigator studying the viscoelastic properties of polymers. In this respect much of the success obtained in this study can be attributed to several years of patient and persevering labor on the part of D. G. Fesko. In his Ph.D. thesis (25), Fesko described in great detail the manner in which he rebuilt a commercial apparatus which orginally had been designed (47) for use in oscillating shear experiments. The basic operation of this instrument is illustrated in Fig. 9.

As a result of a variable frequency voltage signal being supplied to a confined stack of Cannellite 5400* piezoelectric disks, the driver experiences a sinusoidal displacement. The maximum amplitude of this displacement has been estimated (25) to be around 3000 Å. The polymer specimen acts as the connecting bridge between the driver and the monitor plate. The deformation of the specimen results in a force being transmitted to the monitor plate and this force is converted to an electrical charge signal by a very small deformation of the piezoelectric force transducer. This deformation of the force transducer is small enough to be neglected in comparison with the driver displacement (25). Furthermore, the driver displacement is small enough so that a typical specimen experiences exceedingly small compressional strains (ca 0.01%). It is because of these small strains that the compressional geometry can be used without introducing significant error from bulging of the specimens.

* Channel Industries, Inc., Santa Barbara, California.

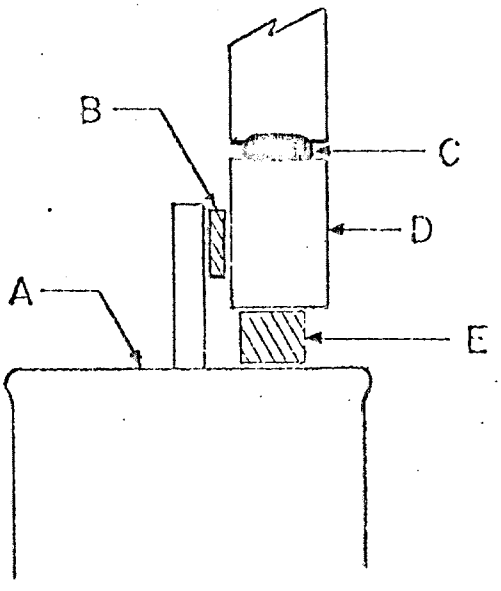

Figure 9.
Diagram Illustrating Compressive Mode in the Modified Melabs Apparatus. A: Driver; B: Specimen in Shear; C: Force Transducer; D: Force Monitor Plate; E: Specimen in Uniaxial Compression.

Figure 10 is a block diagram showing the instrument in its relation to the necessary ancillary equipment. A detailed discussion of all these peripheral devices has been presented elsewhere (25). The input (driver) and output (force transducer) signals were compared using the differential Lissajous method of Tschoegl and Smith (48) which allows very small phase angles to be determined in the subaudio frequency range. In addition, the method enables the amplitude ratio of the two signals to be measured. These two quantities, phase angle and amplitude ratio, along with the specimen geometry are sufficient to determine the dynamic properties of the material. A rather extensive calibration of the instrument (25) was required to relate the observed phase angle and amplitude ratio to the values characteristic of the material under consideration.

Each material was tested over a frequency range of 4 decades (0.1 to 1000 Hz) at a minimum of 17 different temperatures. The temperature range covered was roughly -87°C to 85°C. In each case the first temperature studied was 50°C, and the apparatus with specimen in place was allowed to equilibrate at that temperature for 24 hours. This procedure assured good adhesion between the specimen and the confining plates which in turn improved the reproducibility of the data (25). The 24 hour period also provided for some annealing of the specimens above the 6 hour, 100°C exposure discussed earlier. The test temperature was progressively lowered in intervals of 5 - 10°C until

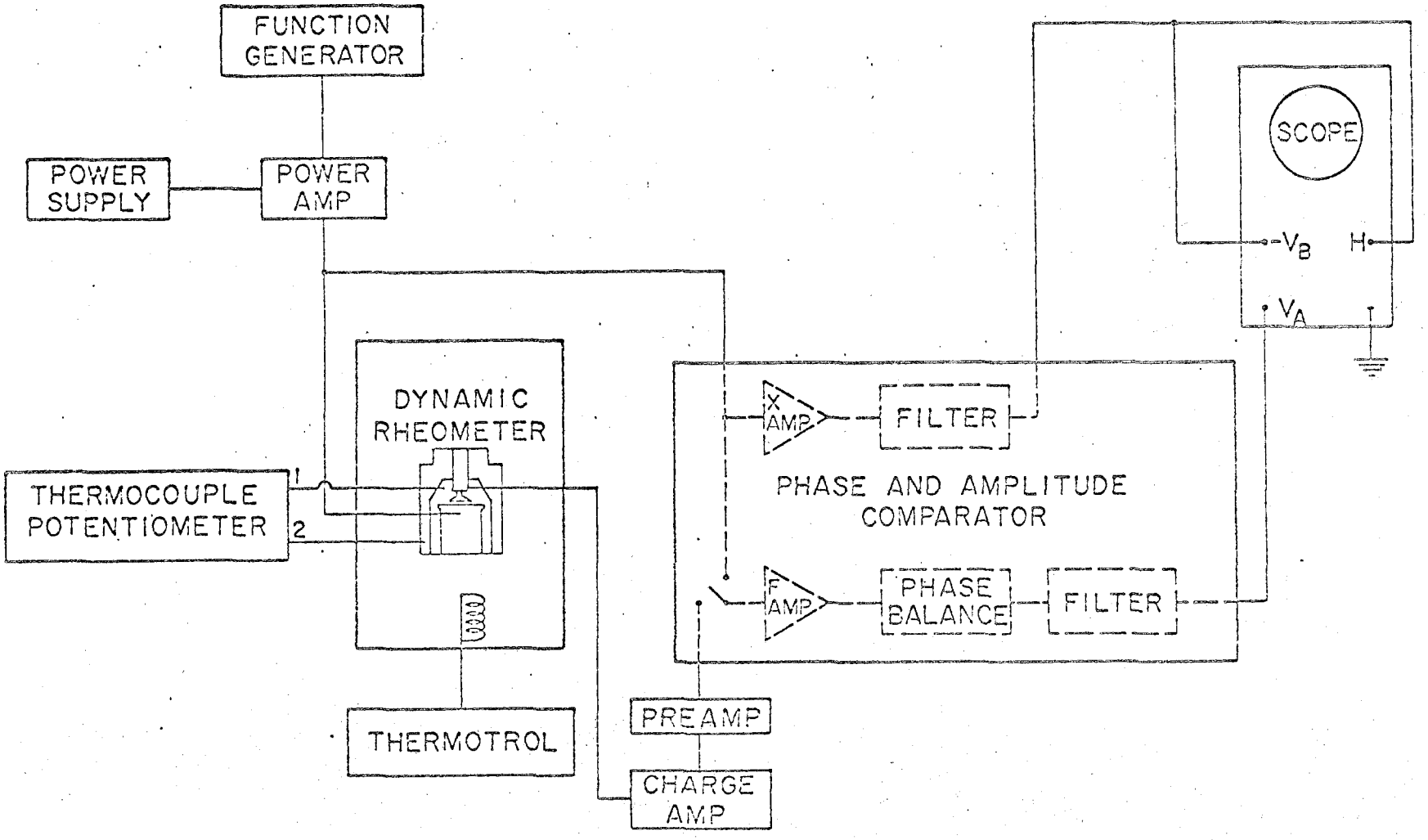

Figure 10. Block Diagram - Dynamic Rheometer and Ancillary Equipment

data had been obtained at the lowest temperature of interest; then data were obtained at temperatures above 50°C. A continuously renewing blanket of dry nitrogen gas was maintained whenever temperatures above -30°C were encountered by the specimen. A period of about 2 - 3 weeks was usually necessary to complete all of the experimental runs for one specimen. All of the forced oscillation data were obtained using these procedures. As well as being internally consistent, these data can be subjected to comparisons with data obtained on other instruments. Fesko (25) has already shown that data obtained on a standardized rubber specimen (49) in compression and in shear on the instrument described here compared favorably with the data obtained on the same material in shear (50) on the apparatus of Ferry and Fitzgerald (51).

A revised version of the dynamic testing instrument described here has recently been constructed. As indicated in Figure 11, the new apparatus has been designed specifically for compressional experiments, although modifications for shear, flexure, and pumping geometries are being considered. The calibration of this new apparatus is discussed in detail elsewhere (52). Work is also in progress (53) to improve the electronic circuitry associated with the instrument. All of these modifications will result in a more efficient research instrument which will be much easier to use. However, the kind of information

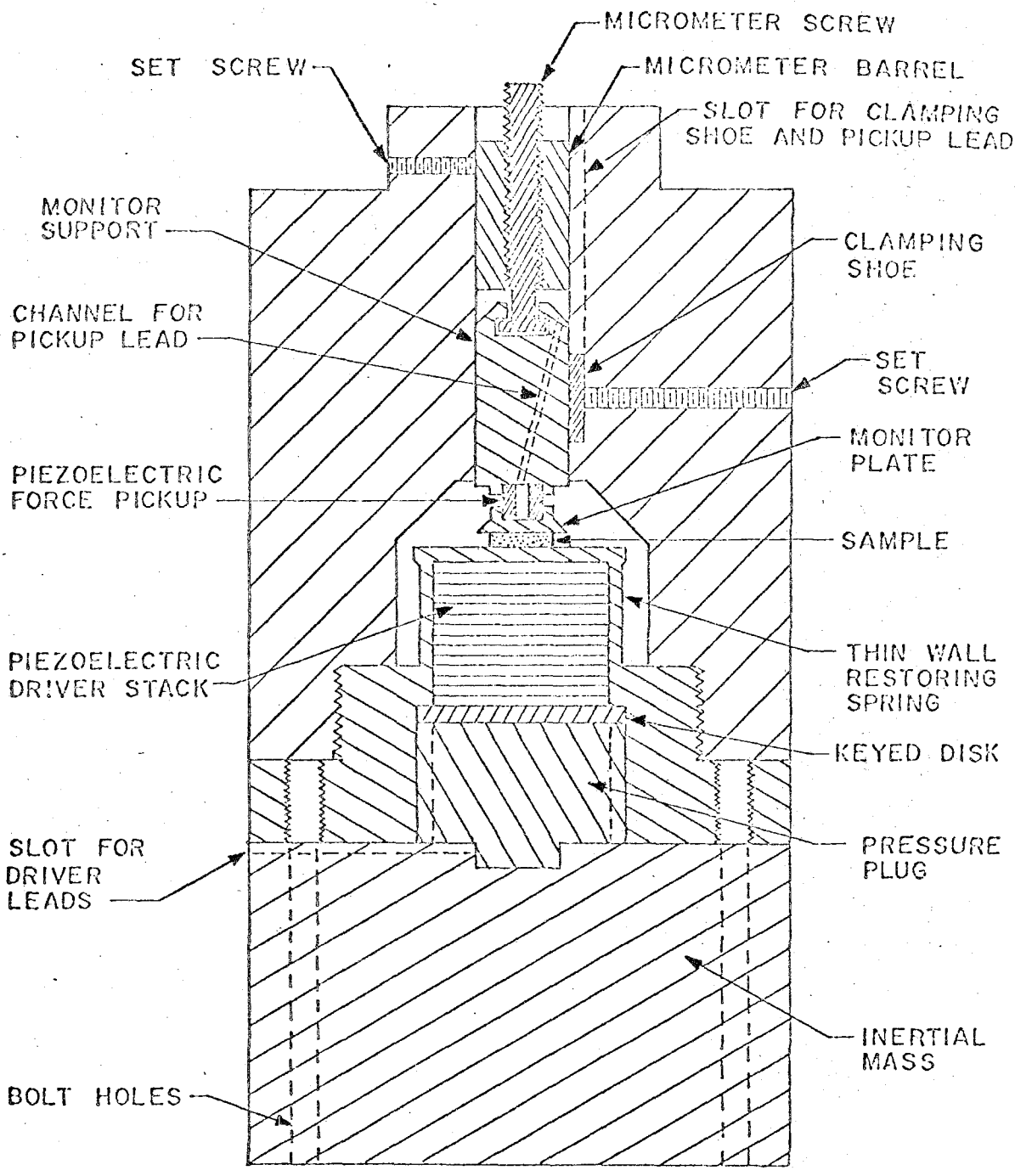

Figure 11.

Rheometer Designed for Dynamic Compression Experiments

which the new instrument can provide is identical to that obtained on the original apparatus. Therefore, aside from the extra time and effort required to obtain the data on the older device, little was lost in not having the improved model available for use in the experiments reported here.

CHAPTER 4

RESULTS AND DISCUSSION

4.1 Results

The experimental program is described here as it developed historically -- the results of the free oscillation experiments are presented first, followed by the information obtained in the forced oscillation tests. It is felt that this method of presentation may allow the reader to feel some of the sense of excitement and discovery felt by the author when the interesting and often surprising results of the free oscillation tests were later corroborated and clarified by the forced oscillation data. In the discussion section, the combined information from the two types of experiments is used to identify and explain the effects of changing network structure on the dynamic mechanical properties of the materials. The discussion is predominantly qualitative with the major effects being identified by comparative inspection of the data. Some preliminary quantitative interpretation is given to several of the observed phenomena, but a detailed treatment is deferred until Chapter 5.

4.11 Free Oscillation Data

Figure 12 shows the behavior of the storage moduli of the materials of Series 1 in which the terminal chains have a number average molecular weight of 51,000. In the glassy and in the polybutadiene transition regions all materials exhibit identical behavior. At the base of the polybutadiene transition the curves diverge, with specimens containing more terminal chains having lower moduli. A quantitative representation of the terminal chain content is given by X, the weight fraction of the polybutadiene phase which is in the form of terminal chains. As X increases, the moduli in the intertransition regions drop away with temperature increasingly more steeply in addition to having lower values overall. The lowest curve, representing diblock behavior, was drawn from a minimum number of points because of experimental difficulties due to the tendency of this material to flow even at relatively low temperatures. For all of the curves, the data at the highest temperatures are in doubt due to a changing shape factor, as discussed in Chapter 3. There is present, however, a clear indication of the approaching polystyrene transition.

In Figures 13 and 14 similar behavior is shown for the storage moduli of the materials in Series 2 and 3, in which the molecular weights of the terminal chains are 22,000 and 67,000, respectively. A suitable specimen could not be prepared from the SB-7 diblock material, and the amount of the SB-5 diblock

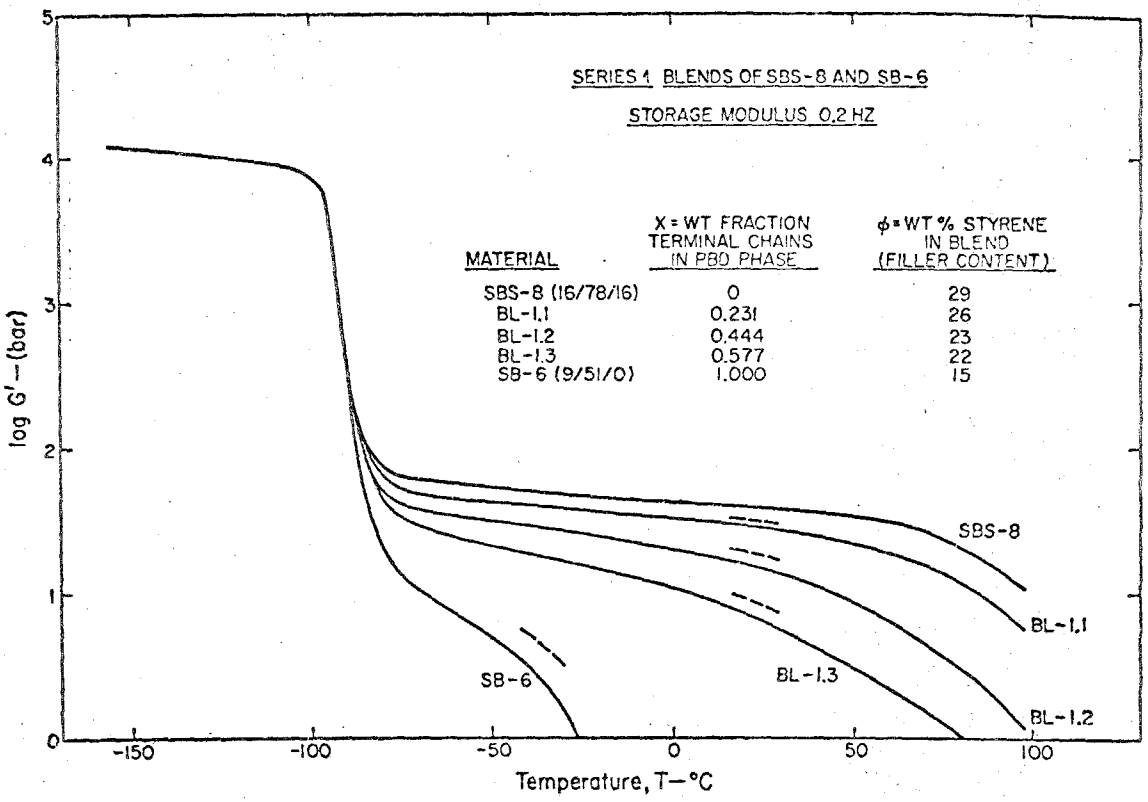

Figure 12.

Storage Modulus - Series 1

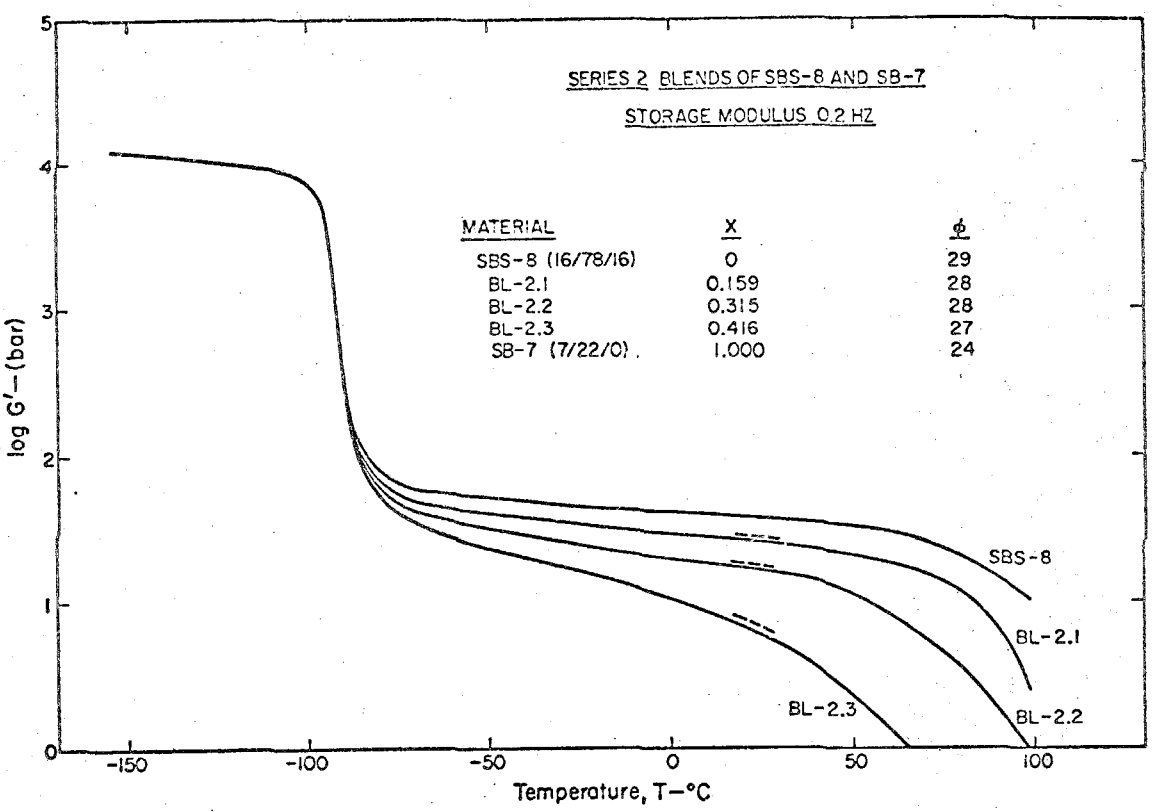

Figure 13.

Storage Modulus - Series 2

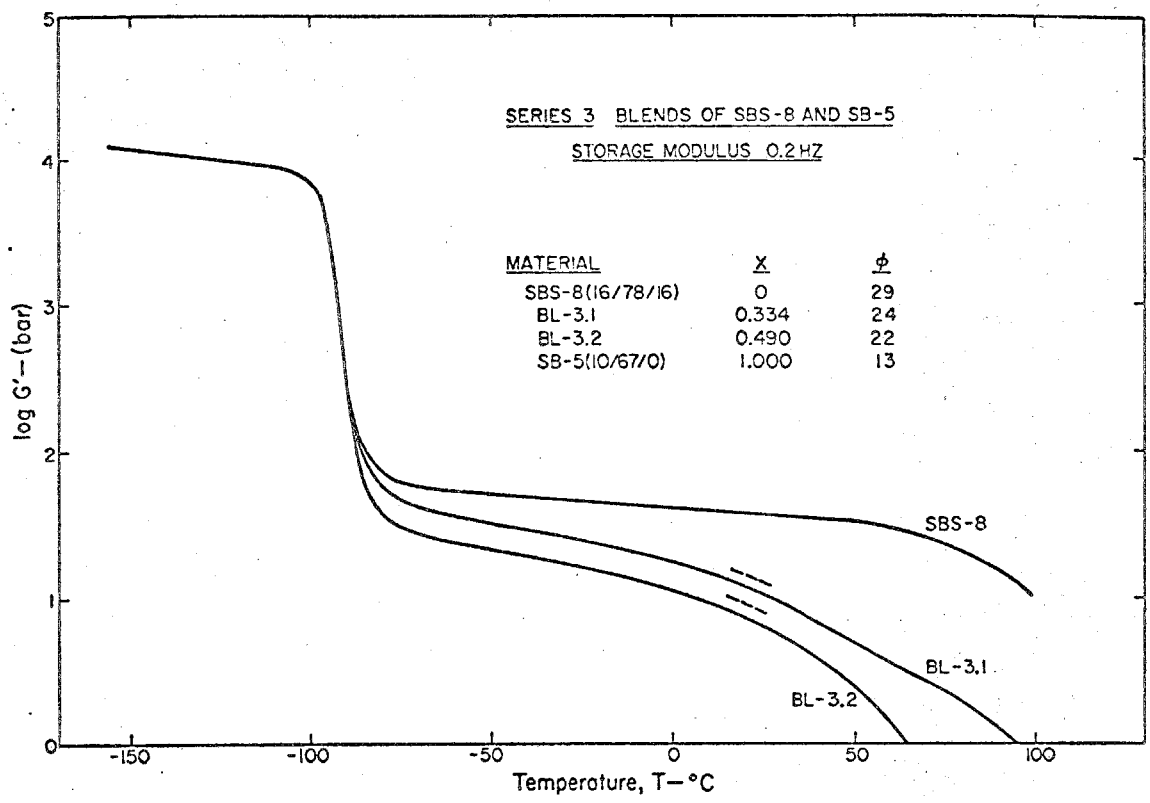

Figure 14.

Storage Modulus - Series 3

was not sufficient for testing. Thus the curves representing diblock behavior do not appear in Figures 13 and 14.

The level of the modulus in the intertransition region is affected by the filler content. In general, a decrease in filler content results in a decrease in modulus. In the diblock-triblock blends the polystyrene domains will be considered, at temperatures below 40°C, to be inert filler particles. Because the triblock and the diblocks contain different amounts of polystyrene, the filler content will vary slightly in a given series of blends. For example, in Series 1 the weight percent of polystyrene in the materials, ϕ, varies from 29% in SBS-8 to 22% in blend BL-1.3. A correction of the data for variations in the filler content is therefore indicated.

There are various correction factors which can be used to normalize the data to constant filler fraction. The correction of the type proposed by Guth (80) has been applied successfully to account for the filler effect of polystyrene domains in triblock copolymers of styrene and isoprene (74). This correction was applied in the intertransition region to normalize all data to a filler content of 29%. The short dashed curves in Figures 12 - 14 indicate the positions of the various curves after this correction. A more sophisticated modulus correction for two-phase polymer systems has been proposed by Uemura and Takayanagi (81). The corrections obtained using their methods are smaller than those shown in Figures 12 - 14. Thus,

only a relatively small proportion of the decrease in the storage modulus is ascribable to decreasing filler content, and the remainder must be attributed to the introduction of terminal chains into the material.

The loss moduli for the blends of Series 1 and 3 are shown in Figures 15 and 16. Each curve has been shifted successively downward by 0.5 decade for display purposes. Again, the glassy and transition regions show no effect of the terminal chains. At the base of the transition, a minimum appears and becomes more pronounced as X increases. From the minimum, the loss rises to a secondary peak and then falls off again at high temperatures. This general behavior appears for all blends of Series 1 and 3, that is, for terminal chains of molecular weight 51,000 and 67,000.

This secondary loss mechanism is quite obviously absent for the blends of Series 2 where the terminal chains have a molecular weight of 22,000. Figure 17 shows that even at rather high concentrations of terminal chains, there is no hint of a minimum at the base of the polybutadiene transition. There is some tendency for the loss to fall off at temperatures above 0°C but not nearly as rapidly as observed for the materials of Series 1 and 3.

The loss tangents ($\tan \delta = G''/G'$) are not shown but can be calculated easily from Figures 12 - 17. The general features of the loss tangent curves are expected from the results

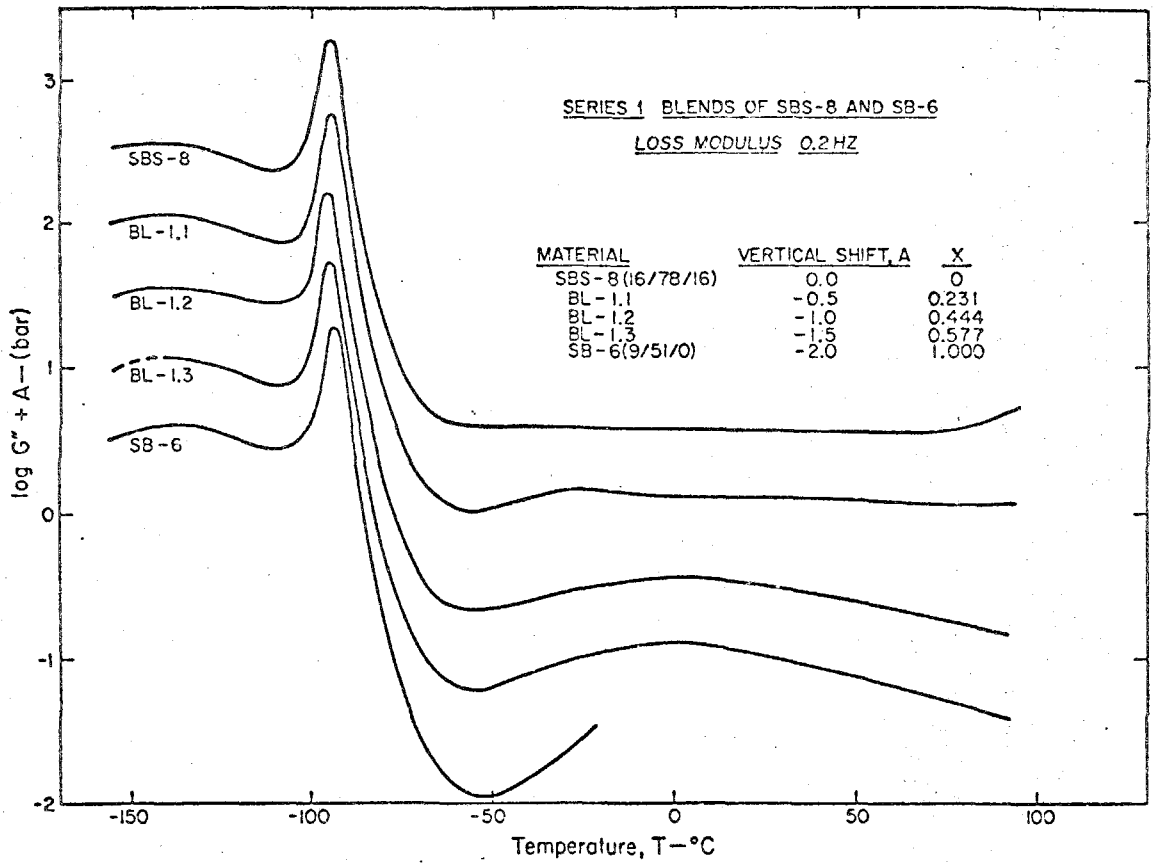

Figure 15.

Loss Modulus - Series 1

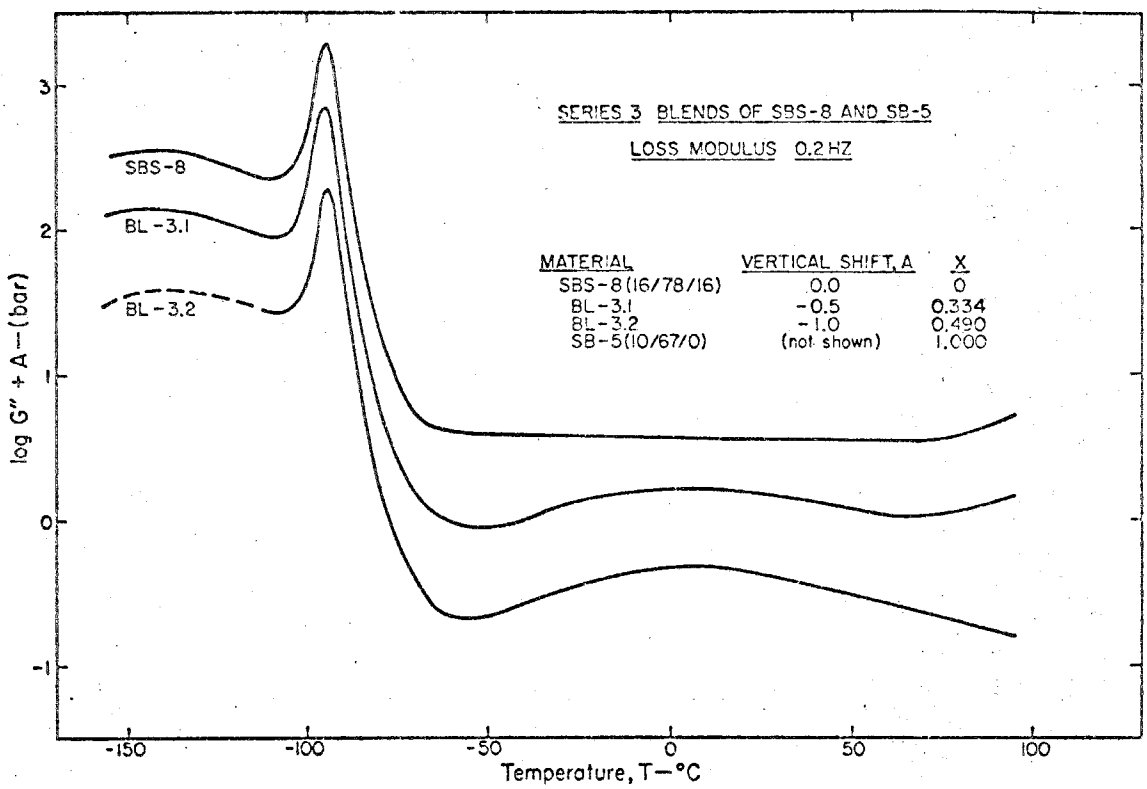

Figure 16.

Loss Modulus - Series 3

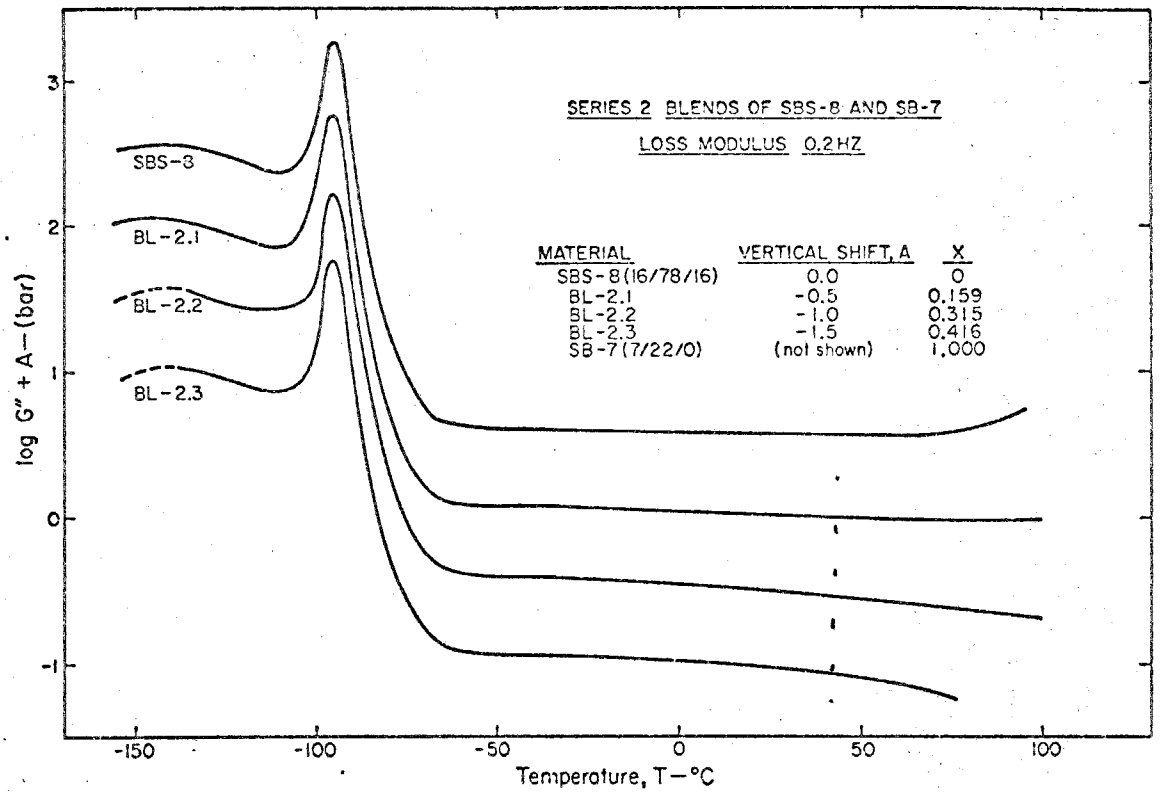

Figure 17.

Loss Modulus - Series 2

already presented: (a) The behavior is essentially identical in the glassy and transition regions, and (b) above the transition region, tan δ increases with increasing terminal chain content. This general behavior was observed for all three series of blends.

4.12 Forced Oscillation Data

4.121 Temperature Reduction

Figure 18 shows the logarithm of the compressional storage compliance[3], $D'(\omega)$, plotted against the logarithm of the circular[4] frequence, ω, for an annealed specimen of the SBS-8 triblock. $D'(\omega)$ is given in reciprocal bars. The results from only a few of the 25 different temperatures employed are shown here; none of the corresponding loss compliance curves is shown. To facilitate comparisons among the various sets of forced oscillation data, it is necessary to remove the dependence of the compliances on the parameter temperature. This temperature reduction is usually accomplished quite successfully by the well known time-temperature superposition principle (Ref. 17, Ch. 11) which relates changes in temperature to shifts in the time (or frequency) scale. For

---

[3] The components of the complex modulus and the complex compliance are simply related for forced oscillation data (17). The compliances are presented here because they fit more naturally into the quantitative treatment presented in Ch. 5 and because previous works (25, 27) have indicated that observed phenomena are more directly related to the compliances in these systems.

[4] The circular frequency, ω, (rad/sec) and the cyclic frequency ν (Hz) are related by $\omega = 2\pi\nu$.

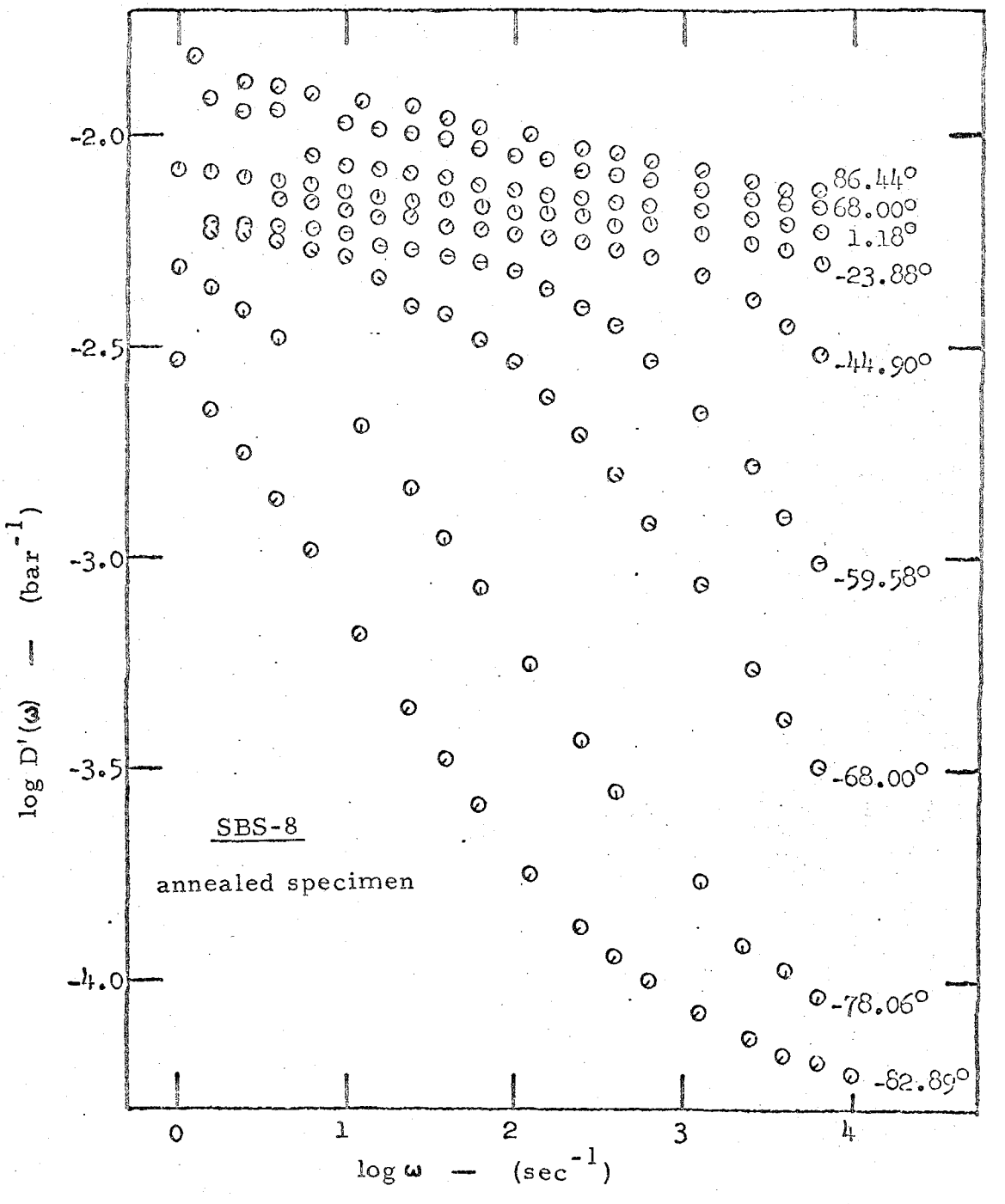

Figure 18.

Storage Compliance - SBS-8

many materials the shifts in the time scale can be established empirically by matching the shapes of the individual isotherms to the segment at an arbitrarily chosen reference temperature. Leaving the details to the discussion section of this chapter, it is merely pointed out here that this type of empirical shifting scheme was used here in the temperature reduction of the forced oscillation data. For reasons also to be discussed later, only the data corresponding to temperatures below about 40°C were used.

The amounts of horizontal shift, log a_T, required to effect superposition are plotted against temperature, T, in Figure 19 for two[5] separate specimens of SBS-8, using -78°C as the reference temperature. The shift factors for the two specimens are in good agreement below 40°C. Very near 40°C and for all higher temperatures (not shown) the data diverged with the shift factors for the unannealed specimen falling off more rapidly. Below about -60°C, the temperature dependence of the mechanical properties of SBS-8 could be described by a WLF equation (17). At higher temperatures the shift factors followed an Arrhenius equation. The solid line in Figure 19 is represented rather well by the following composite equation:

---

[5] SBS-8u, unannealed specimen, compliance data obtained by Fesko (25). SBS-8uA, annealed specimen, compliance data obtained by this author and also discussed by Fesko (25) and by Fesko and Tschoegl (22). All of the triblock behavior reported later in the text has been derived from the data obtained on the annealed specimen, even though very little difference can be seen below 40°C.

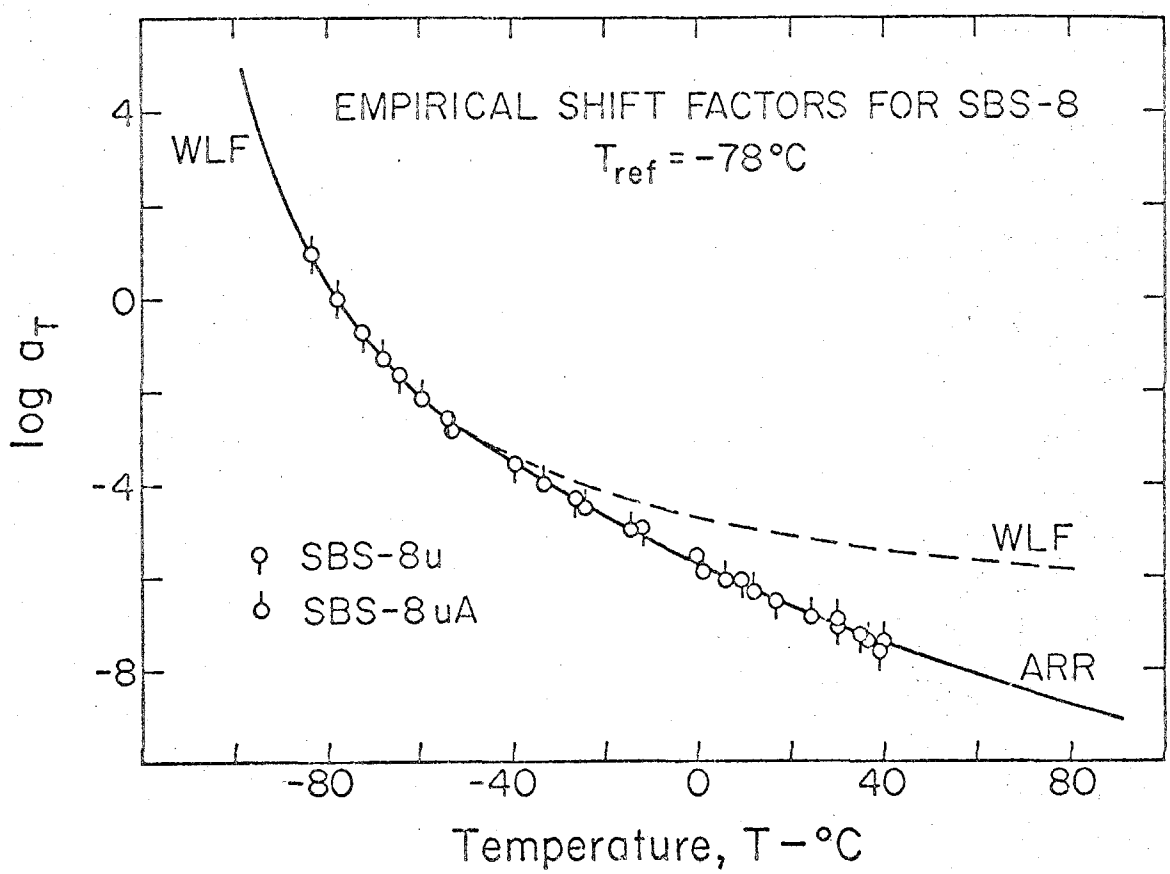

Figure 19.

Temperature Dependence of the Mechanical Properties of the SBS-8 Triblock

$$\log a_T = \begin{cases} -7.76\ (T + 78.0)/(129.1 + T) & T \leq -60°C \\ 3600\ \left(\frac{1}{T + 273.2} - 5.25\right) & T > -60°C \end{cases} \qquad (4.1)$$

where T is the temperature in °C and the various constants are found by suitable curve fitting procedures (17). The implications of this type of temperature dependence will be discussed in detail later.

When the shift factors shown in Figure 19 are applied to the compliance data for the annealed SBS-8 specimen, the master curves shown in Figure 20 are obtained. Here the logarithms of the reduced[6] compressional storage compliance, $D'_p(\omega a_T)$, and the reduced compressional loss compliance, $D''_p(\omega a_T)$, are plotted against the logarithm of the reduced frequency. Data obtained at each temperature are represented by a different symbol as indicated in the figure. The superposition of the data is quite good over the entire reduced frequency range. The superposition is generally somewhat better for the storage compliance, reflecting the smaller amount of uncertainty involved in the determination of that quantity.

---

[6] The compliances have been reduced by a multiplication factor T/T_o, where T is the temperature of the data and T_o is the reference temperature. This slight vertical adjustment accounts for changes in the entropy-spring elasticity(17). The small correction for density changes has been ignored (25). Thus $D''_p = (T/T_o)D'$ and $D''_p = (T/T_o)D''$.

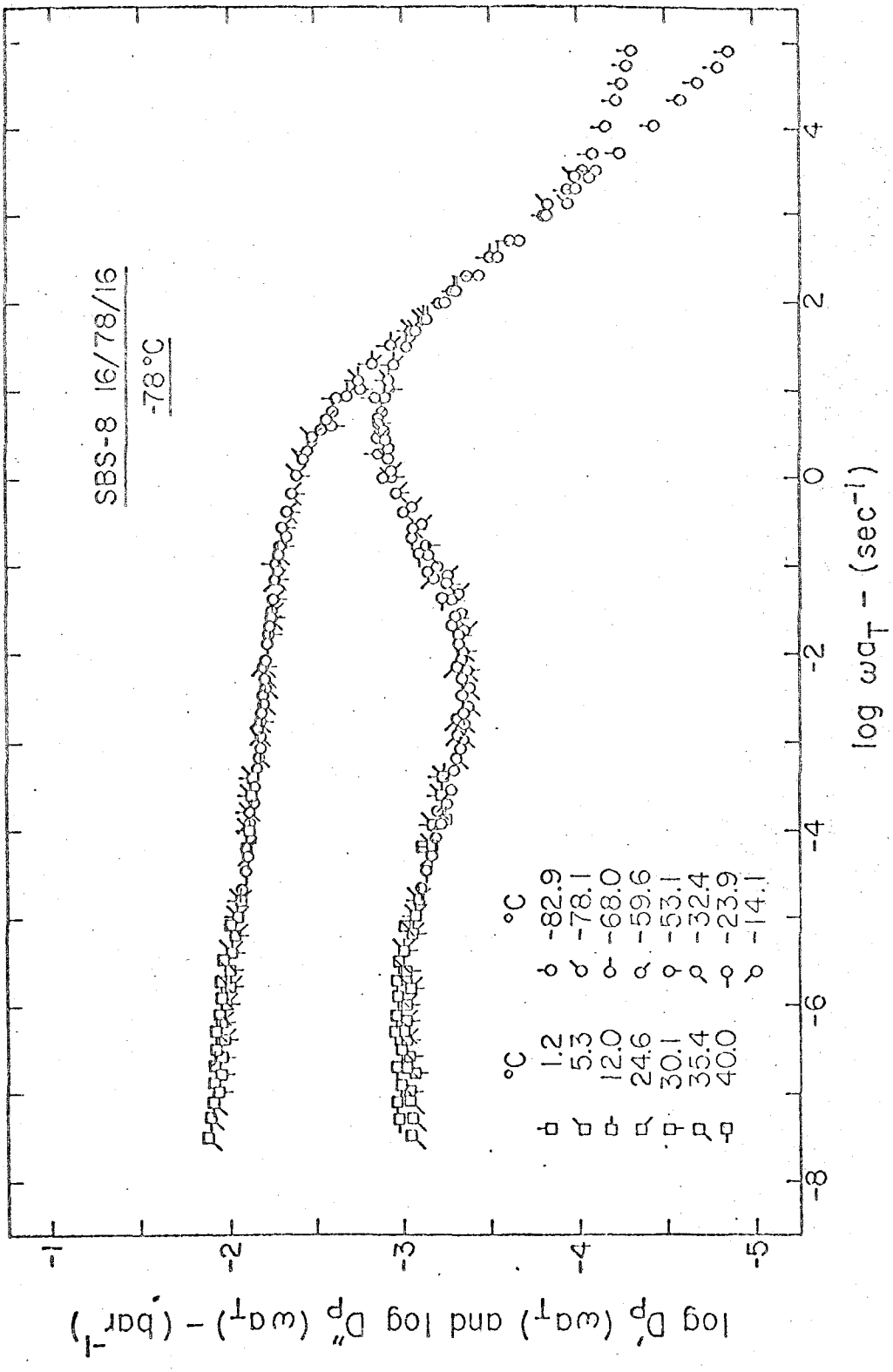

Figure 20. Storage and Loss Compliance Master Surves-SBS-8

The storage compliance rises from very low values in the glassy region (low temperature and high frequency) through the polybutadiene transition and continues to rise, although much more slowly, across the intertransition region. The loss compliance exhibits a peak at high reduced frequencies near the polybutadiene transition and a broad secondary maximum at much lower frequencies. The polystyrene transition would appear at still lower frequencies but is not seen here since all data above 40°C have been excluded.

Five blends were studied in the forced oscillation experiments -- all three blends of Series 1, and one each from Series 2 and 3. The shift factors for these five blends are shown in Figure 21 with the solid line again representing Equation 4.1. Since the triblock represents the base material for the three series, it is reasonable to use its temperature dependence for reduction of the data for all of the blends. In this way it is certain that any differences appearing in the various master curves must be due to changes in material behavior, and not from differences in the method used to reduce the data.

Figure 22 shows the storage and loss compliance master curves for one of these blends, BL-1.2. The data superpose very well, at high reduced frequencies in the glassy and transition regions. At the beginning of the intertransition region there is a significant lack of superposition which is especially noticeable on the low frequency side of the main loss peak. At still lower reduced frequencies the data again superpose very well.

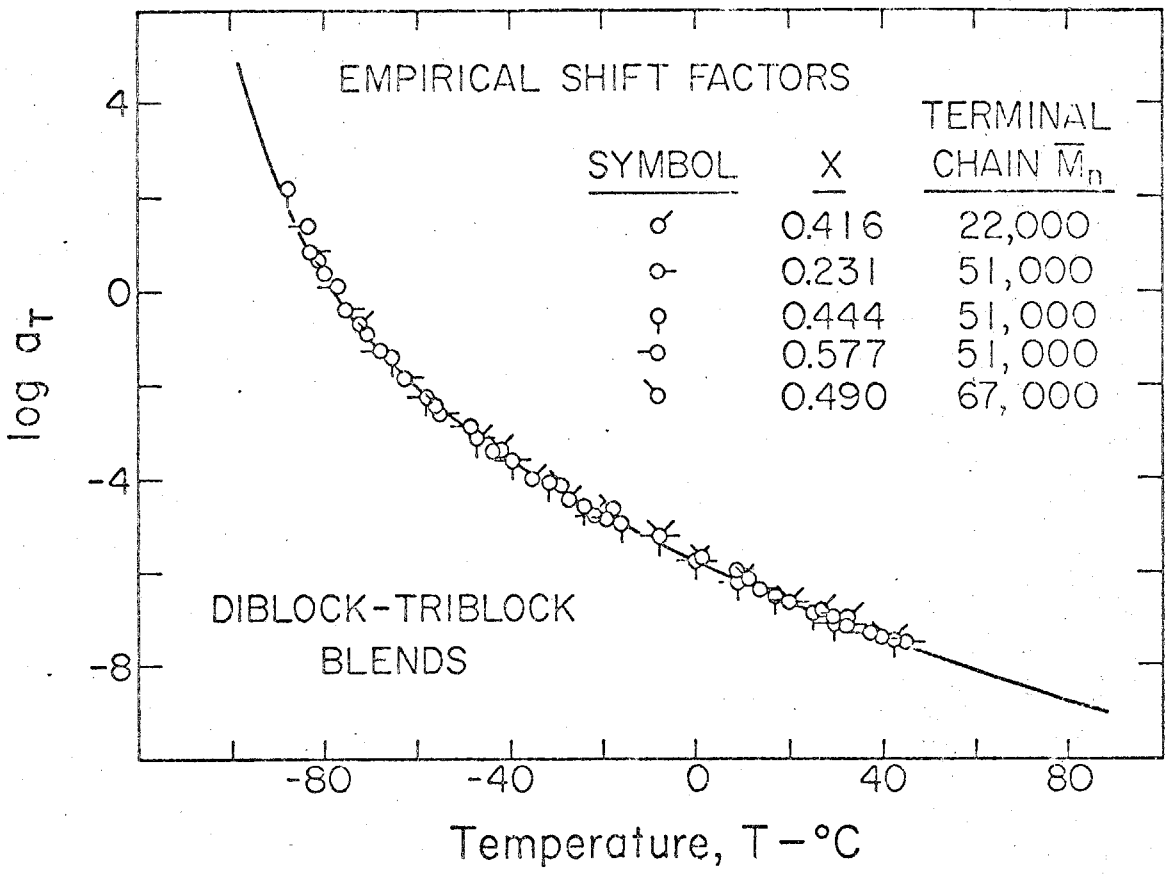

Figure 21.

Temperature Dependence of the Mechanical Properties of the Diblock-Triblock Blends

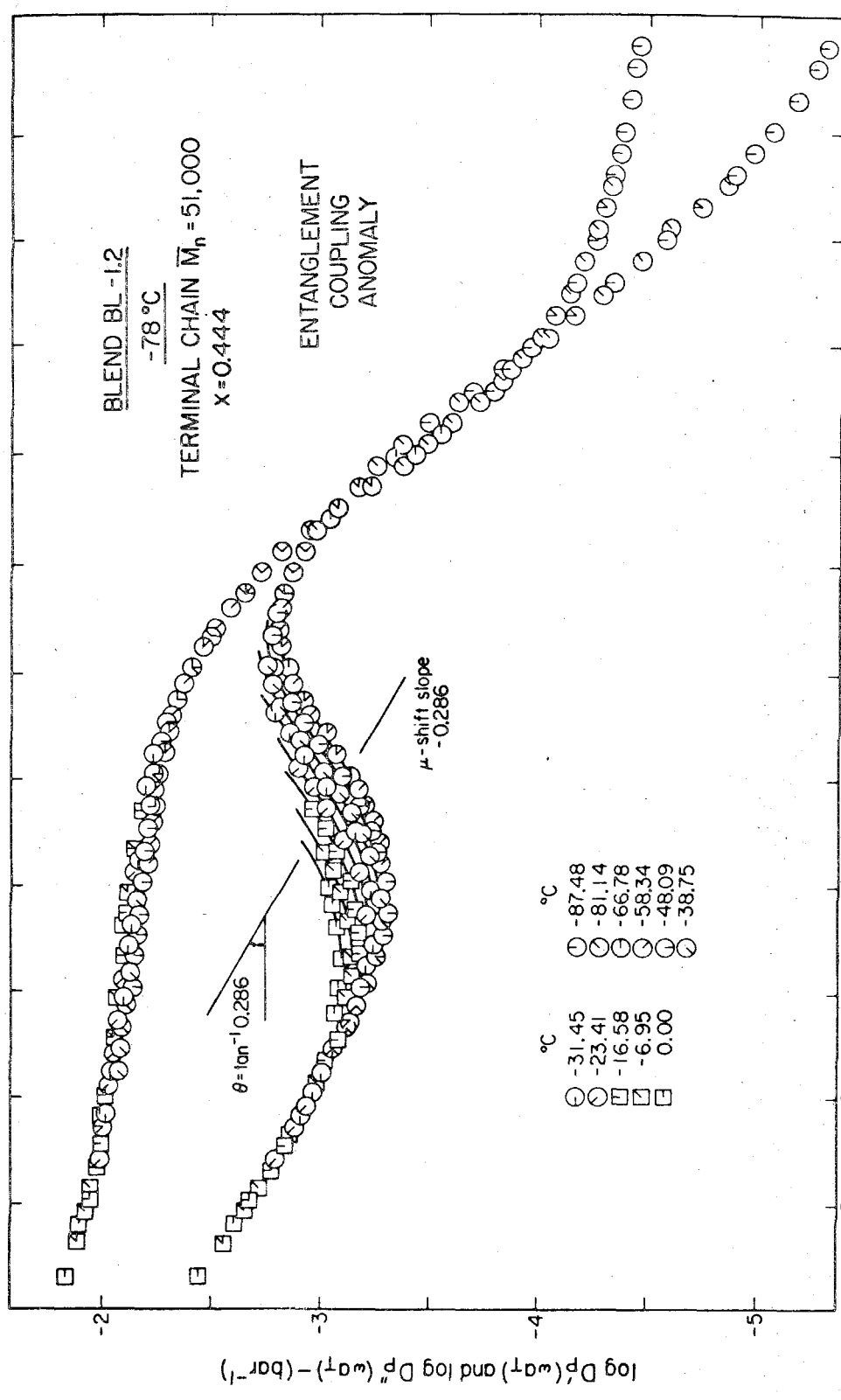

Figure 22. Storage and Loss Compliances for BL-1,2 – Reduced by Shift Factors of Fig. 21

Only data for temperatures 0°C and below are shown here for clarity; the data above 0°C all superposed very well with the low frequency ends of the storage and loss compliance curves. Similar superposition anomalies were observed for the other two blends of Series 1 and for the single blend studied from Series 3.

4.122 The μ-Shift

It was possible to resolve the superposition anomaly seen for the blends of Series 1 and 3 by subjecting the data to a second set of shift factors, this time taken along a diagonal straight line whose slope was chosen parallel to the low frequency rise in the loss compliance (See Figure 22). This choice of slope insures that the good superposition already obtained at low frequencies will not be destroyed by the second shift procedure. By moving the individual isotherms down and to the right along the appropriate slope, the data collapsed into a single master curve exhibiting good superposition over the entire frequency range. Figure 23 illustrates this behavior for blend BL-1.2 where the horizontal and vertical coordinates now include the appropriate component of the diagonal shift or "μ-shift" as it will be called here. The μ-shift factor corresponding to a given temperature is taken as the distance along the diagonal, in logarithmic units, required to effect superposition of the particular isotherm under consideration with the rest of the data. The numerical value of μ must, of course, reflect the appropriate

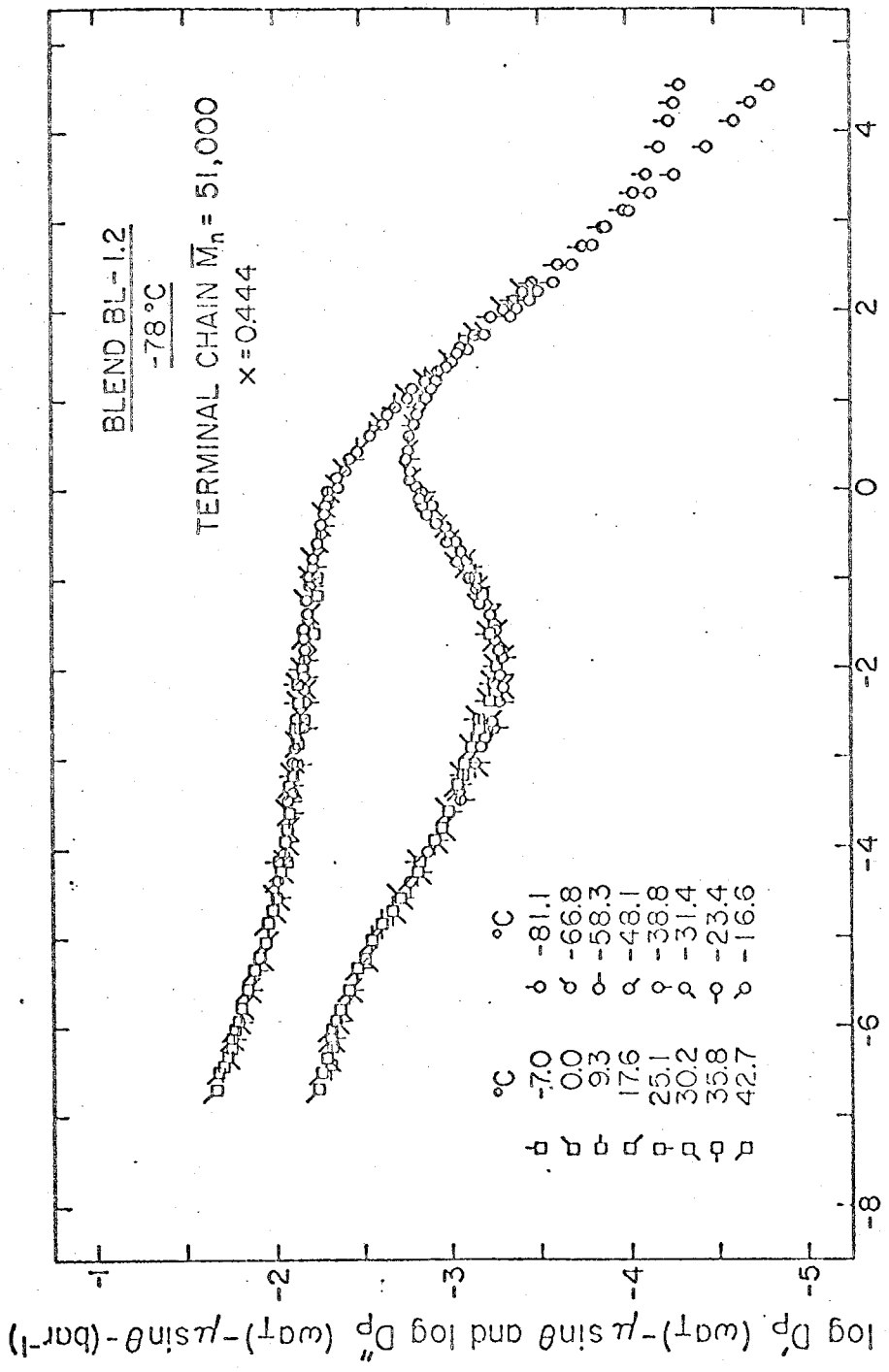

Figure 23. Storage and Loss Compliances for BL-1.2 Reduction Includes Both the Horizontal and the μ-Shift

geometrical considerations for differences in the horizontal and vertical scales.

The μ-shift factors for the four blends under consideration are plotted against inverse temperature in Figure 24. Notice again that a different μ-shift slope was employed for each material with steeper slopes corresponding to higher terminal chain contents. For Series 1 the μ-shift factors for all three blends (circles in Figure 24) scatter reasonably well around a single straight line over the region of temperature in which the superposition anomaly was apparent. At low temperatures the compliance data superposed very well and no μ-shift was necessary; the choice of $\mu = 0$ at low temperatures assures that both shifting procedures ($\log a_T$ and μ) have been referred to a temperature, -78°C, within the transition region. This will prove to be useful later in the comparisons of the various master curves. The maximum value of μ is somewhat arbitrary as a result of the limited length of the compliance isotherms. This upper limit corresponds to the highest temperature for which the compliance data reached into the region where the reduction anomaly was apparent. Data at still higher temperatures superposed quite well and therefore no further μ-shift was required.

For the single blend of Series 3, BL-3.2, the lack of superposition in the compliance data could also be resolved quite successfully by the same μ-shift procedure. As shown by the triangles in Figure 24, the μ-shift factors for this material

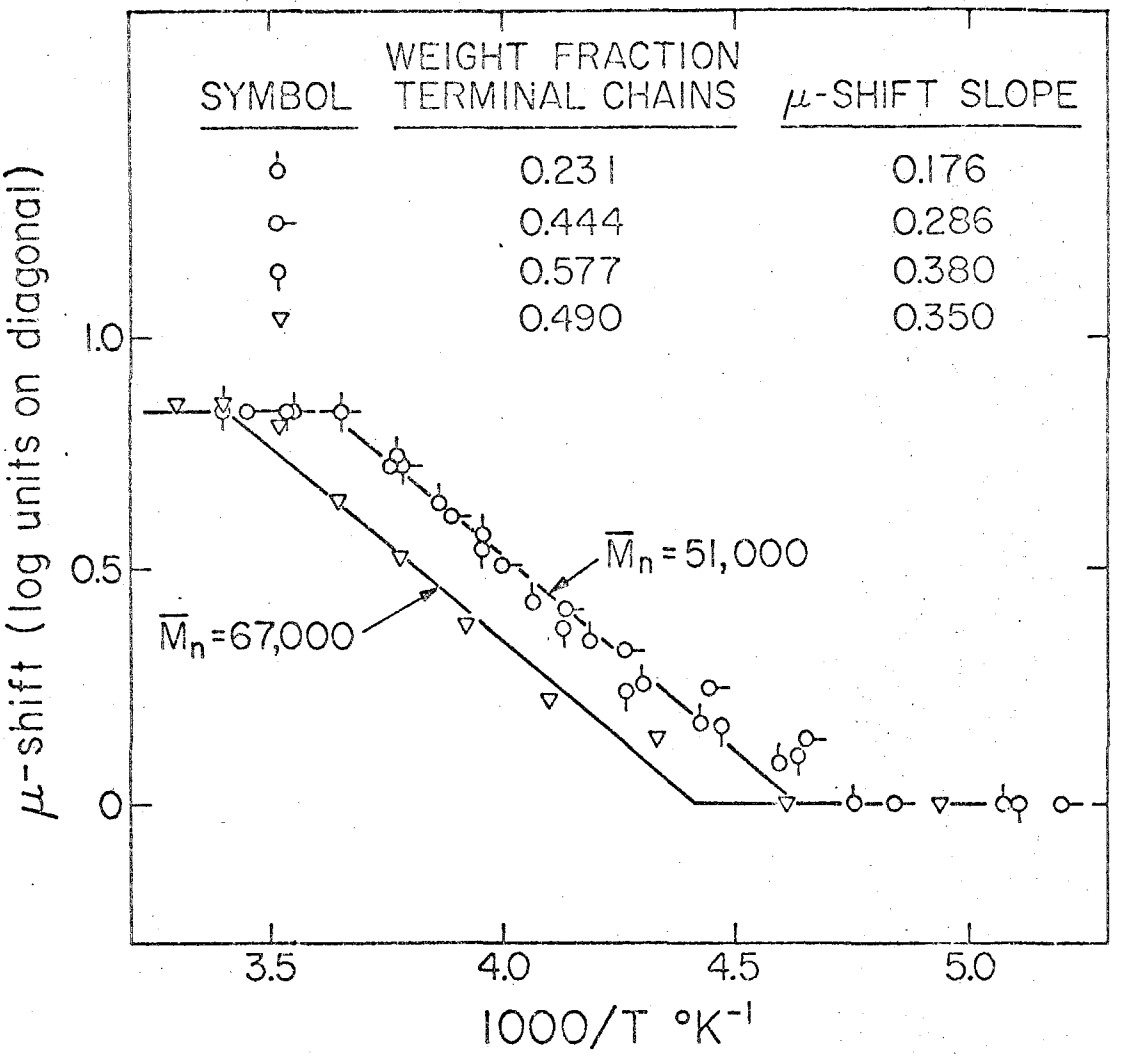

Figure 24.

μ-shift Factors for Series 1 and 3

could be fitted by a straight line parallel to the one used for Series 1. The μ-shift data are sparse and somewhat scattered for this material, but they do indicate that the increase in terminal chain length from 51,000 to 67,000 had no effect on the controlling mechanism except that it was shifted to higher temperatures. Since the abcissa has a nonlinear scale, the change varied from about ten to twenty degrees centigrade. From the slope of the μ vs. 1000/T plot it was possible to calculate a value for the apparent activation energy associated with the μ-shift mechanism. The resulting value for ΔH_a and its interpretation on a molecular level will be treated in detail in the discussion section. Also in the discussion section, the motivation for choosing this particular method for resolving the superposition anomaly will be made clear. At present, it is merely pointed out that, through the use of the μ-shift factors shown in Figure 24, single master curves exhibiting good superposition over the entire frequency range were obtained for all the blends of Series 1 and for the one blend studied in Series 3. Just as knowledge of the horizontal shift factors allows the conventionally superposed data to be decomposed into the original temperature segments, knowledge of the μ-shift factors provides for the regeneration of the superposition anomaly (Figure 22) from the fully reduced data (Figure 23). The data for BL-1.2 have been presented as a typical example of the μ-shift scheme. Working plots for the other blends of

Series 1 and for BL-3.2, both before and after the μ-shift, appear in Appendix B.

The materials of Series 2, terminal chain length 22,000, have been conspicuously absent during the presentation of the μ-shift mechanism. Figure 25 shows the storage and loss compliance data for blend BL-2.3 shifted according to the horizontal (log a_T) shift factors shown earlier in Figure 21. It is immediately apparent that no μ-shift is necessary here since the data superpose very well over the entire frequency range. This was the only material studied from Series 2, but since it contained the largest concentration of terminal chains it offered the most rigid test of the data. Thus, the temperature dependence of the mechanical properties of the materials of Series 2 did not include the additional μ-shift mechanism which was necessary for the reduction of the data from Series 1 and 3. However, even though the overall temperature dependence of BL-2.3 and the base material, SBS-8, were the same, the mechanical properties of the two materials were quite different. Comparing Figures 20 and 25 indicates that BL-2.3 shows a much shallower minimum in its loss compliance behavior at intermediate frequencies than seen for SBS-8. This blend also exhibits significantly higher values of loss at low reduced frequencies. The slope of the storage compliance in the intertransition region for BL-2.3 is significantly steeper than that observed for SBS-8. Thus, the short terminal chains do affect the overall mechanical properties of the materials of

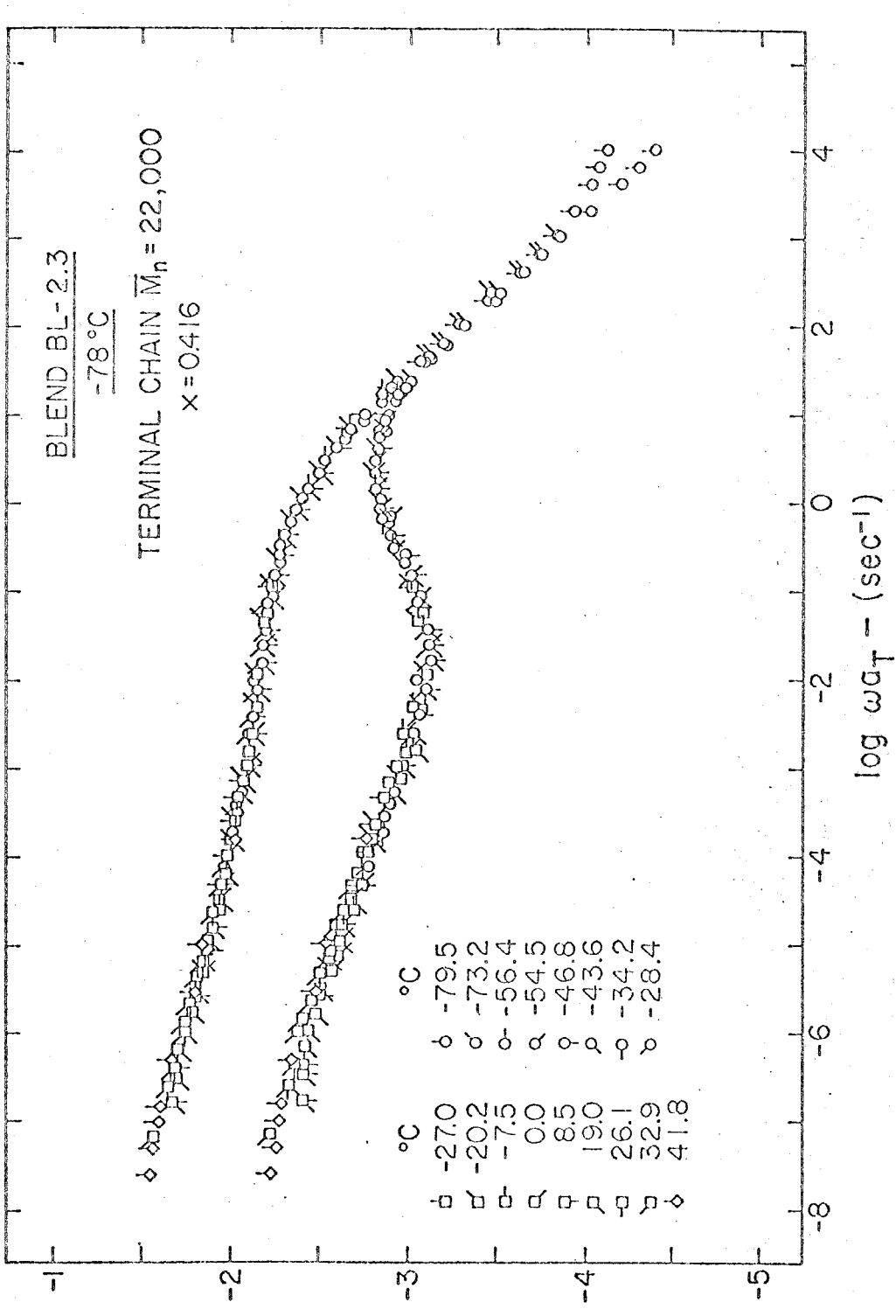

Figure 25. Storage and Loss Compliances for BL-2.3 Reduced by Shift Factors Appearing in Fig. 21

Series 2, but they apparently do not influence the temperature dependence of the mechanical properties.

4.123 Composite Curves for Series 1

All of the materials of Series 1 were studied in the forced oscillation experiment, and therefore it is possible to display the results for the entire series in composite plots to facilitate comparison of the mechanical response curves. Figure 26 shows line plots of the storage and loss compliance master curves for the four materials of Series 1. The double subscript on the compliances, $D'_{p\mu}$ and $D''_{p\mu}$, indicates that the conventional temperature reduction has been performed on all materials and that the second shifting scheme, the μ-shift, has been taken into account where appropriate, i.e. for the blends only. The master curves for the blends have been subjected to small random vertical shifts, usually on the order of 0.05 decade, to match the data with the SBS-8 master curves in the transition and early intertransition regions. This effectively removes from the data any differences in the level of the compliance due to changing polystyrene content and errors incurred in the calculation of the specimen geometry. The small discrepancies seen in the storage compliance in the glassy region can be attributed to the appearance of a noticeable apparatus compliance when the specimen becomes very rigid (25).

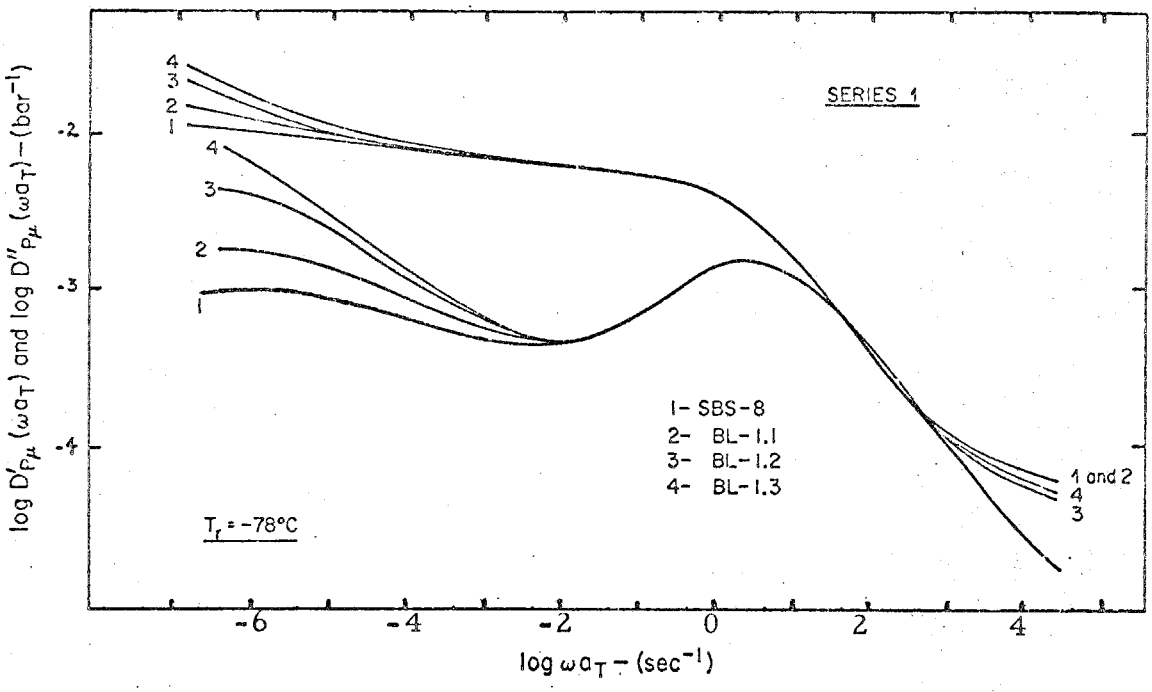

Figure 26.

Storage and Loss Compliances - Series 1

Inspection of Figure 26 indicates that the storage and loss compliance behavior for all the materials in Series 1 is essentially identical in the glassy and transition regions. Both the level and the steepness of the storage compliance at low reduced frequencies are increased by the introduction of terminal chains. No significant difference in the loss compliance curves can be seen for reduced frequencies above 0.01 sec^{-1}. Below this frequency, however, the curves diverge sharply with higher levels of loss being attained for higher terminal chain contents. For the two blends of highest terminal chain content, the level of loss at the lowest reduced frequencies becomes greater than that attained at the peak value of loss located near the polybutadiene transition. A clearly defined maximum in the loss compliance at low frequencies is visible only for the triblock material. However, there is evidence that the secondary loss maximum is shifting to lower frequencies as terminal chain content increases. The reasons why the data could not be extended above 40°C to reveal these peaks will be discussed in detail later. A final observation to be made from Figure 26 is the change in slope of the linear region of the loss compliance at low frequencies. These are the slopes which were mentioned earlier during the application of the μ-shift to the data for Series 1.

The loss tangents for all the materials of Series 1 are plotted against reduced frequency in double logarithmic coordinates in Figure 27. Because it is a ratio of compliances,

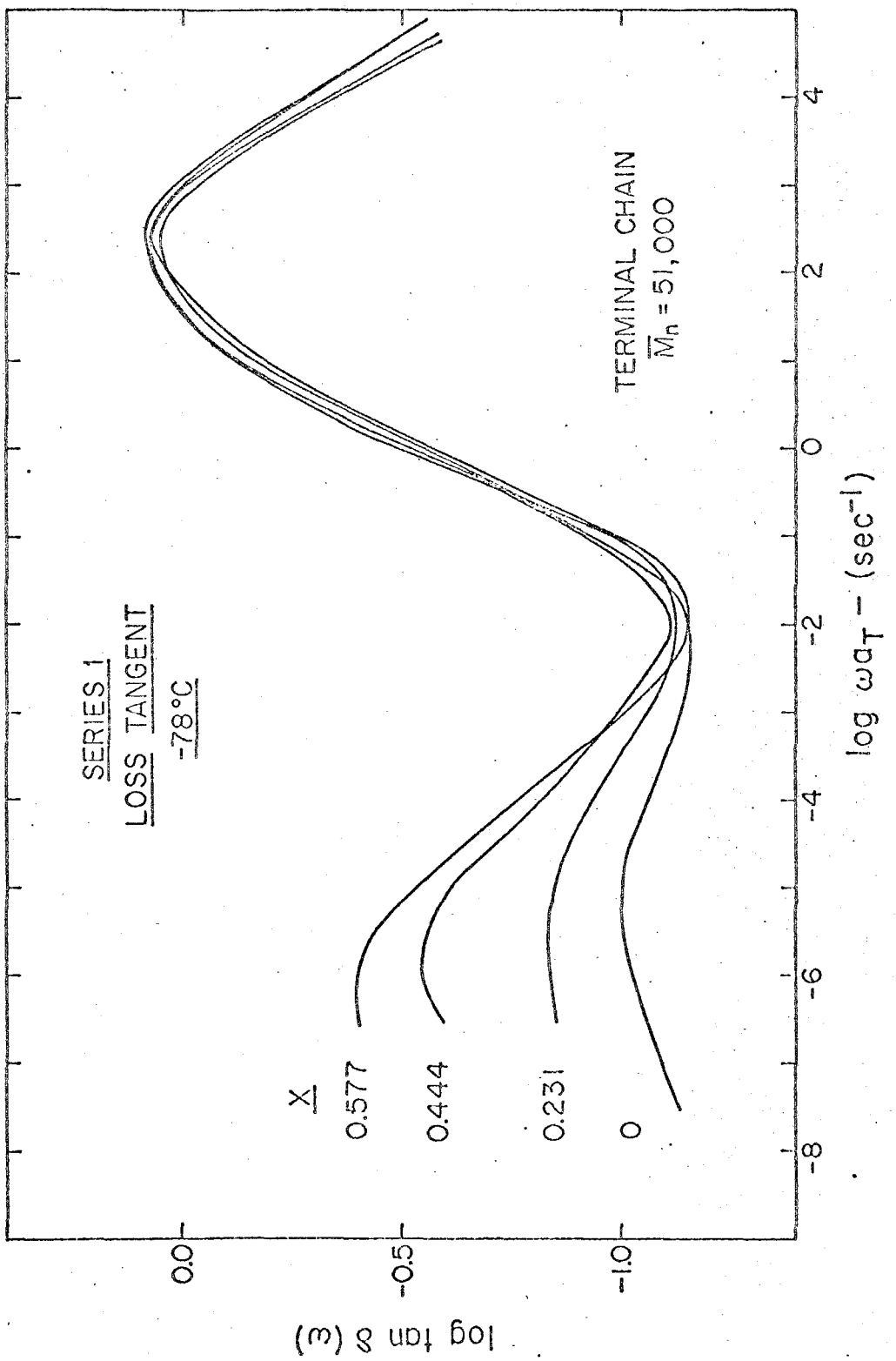

Figure 27. Loss Tangent - Series 1

tan $\delta = D''/D'$, the loss tangent is not affected by differences in styrene content or by errors in calculation of the specimen geometry. Therefore values of tan δ calculated from the individual sets of reduced data (not the matched curves of Fig. 26) reveal the true amount of discrepancy at high frequencies where the mechanical behavior has been considered to be identical. Near $\log \omega a_T = -2$ the spread of the four curves becomes greater, but no systematic behavior of the minimum in the loss tangent is apparent. These low values of tan δ are subject to the greatest amount of uncertainty anyway since very small phase angles must be measured here. At still lower reduced frequencies the loss tangent curves diverge rapidly and rise to much higher values for larger terminal chain contents. A secondary peak in tan δ which shifts to lower frequencies with increasing terminal chain content is evident in Figure 27. However, for all the materials the level of tan δ at low frequencies was always less than that of the main peak associated with the polybutadiene transition near $\log \omega a_T = 2$.

For two of the materials of Series 1, SBS-8 and BL-1.3, the retardation spectra (17) were calculated using the approximation methods of Tschoegl (54). The calculated values of the retardation spectra appear in Figure 28 plotted logarthmically against the corresponding retardation time, τ. The symbol L''_2 indicates that the spectra shown here have been calculated from loss compliance data and that the second central approximation formula (54) has been used. As presented here the spectra are

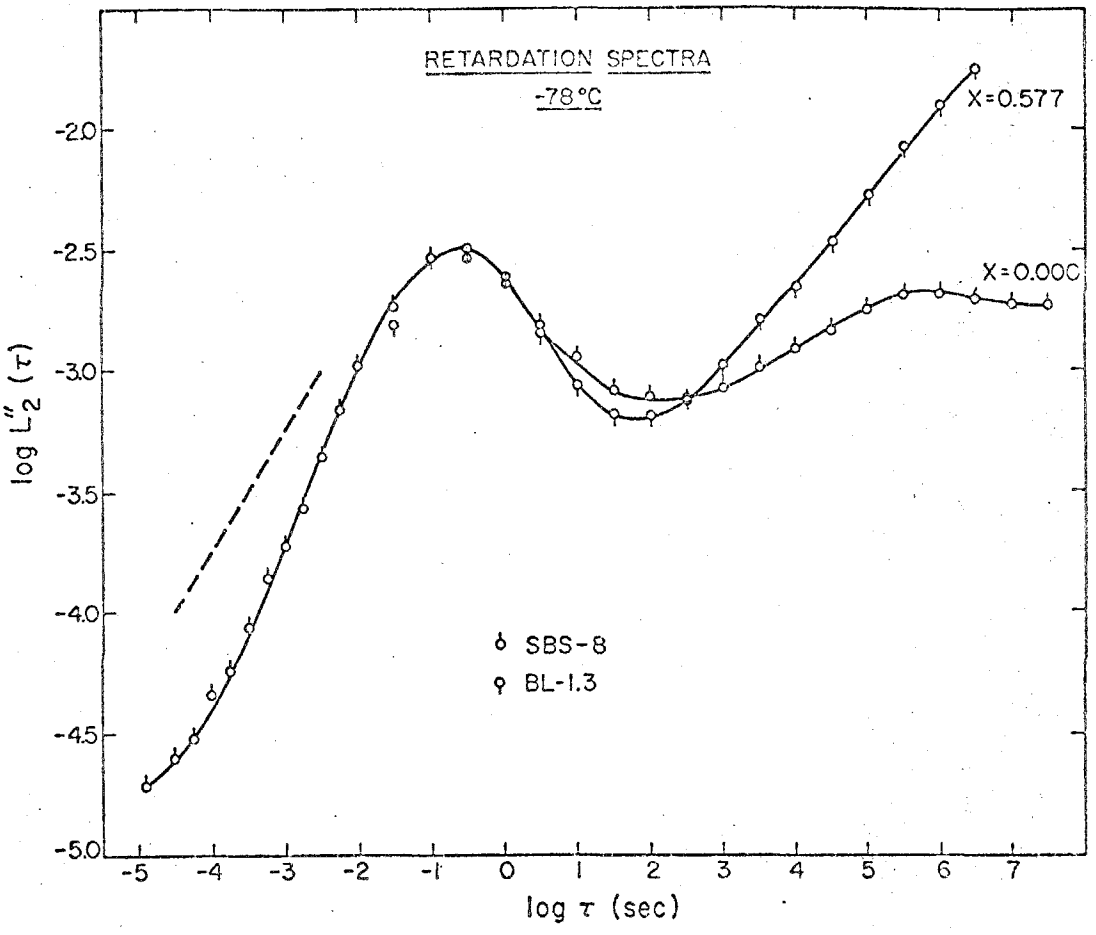

Figure 28.

Retardation Spectra — SBS-8 and BL-1.3

not normalized and have units of inverse bars. The shapes of the spectra shown in Figure 28 are not markedly different from mirror images of the loss compliance curves for these two materials. These plots are quite useful, however, since the level of the retardation spectrum represents a measure of the concentration of the retardation processes as they affect the compliance of a viscoelastic material (17). From Figure 28 it is clear that the addition of terminal chains has enormously increased the number of retardation processes at long times. At intermediate times (near log τ = 1 or 2) it appears that there may be fewer retardation processes when terminal chains are present. The spectra for the two materials converge below log τ = 0.5, and they are assumed to be identical in the transition region where the loss compliance curves were essentially identical. The dashed line appearing in Figure 28 near the transition region has been drawn with a slope of 1/2. This is the prediction of several molecular theories (17) for the slope of the retardation spectrum in this region.

4.2 Discussion of Results

A rather substantial body of data has been presented in the previous section as representative of the dynamic mechanical behavior of the block copolymer blends. In this section the important features of these response curves will be discussed, with special emphasis placed upon the relationship between

changes in the polybutadiene network structure and the observed changes in the mechanical behavior.

One approach to the discussion of the results could be to deal first with the body of data obtained in free oscillations and then show how the forced oscillation data uphold the proposed explanations of the mechanical behavior. However, it is felt that the reader has probably been engaged in this mental process while reading the previous section and inspecting the data. Therefore the major interesting features of the mechanical response of the various blends will be dealt with directly, using the combined information from both types of experiment as evidence to support the proposed explanations of the material response. This is a particularly useful approach since various effects of changing network structure are not equally evident in the two sets of data. Therefore, by discussing the combined results, all the evidence for a particular explanation of an observed phenomenon can be presented at one time.

The overall plan of the discussion will be to work upward in temperature, beginning with the short range viscoelastic processes occurring in the glassy region and proceeding toward the long time response observed in the rubbery region. The discussion deviates from this plan at first, however, because the effects of the polystyrene phase and the interlayer must be examined. Also, discussion of the empirical shifting procedure which has been used to reduce the temperature dependence of the forced

oscillation data requires that the entire temperature range of the data be considered. Discussion of contributions to the mechanical behavior from sources other than the polybutadiene networks is aimed primarily at establishing the regions of time and temperature in which these contributions are negligible. This leaves the behavior of the polybutadiene networks clearly exposed and allows for meaningful discussion of the relationship between network structure and mechanical properties.

4.21 Contribution to the Mechanical Response from the Polystyrene Phase and the Interlayer

Whenever the viscoelastic response is affected significantly by the polystyrene domains or by a mixed polystyrene-polybutadiene interlayer region, the behavior of the rubbery phase of the material is not easily interpreted. For example, Figure 8 shows that for SBS-8 the slope of the log G´ vs. temperature plot becomes noticeably steeper aroung 50°C, clearly indicating the onset of softening effects. It is well known that triblock copolymers will flow when the glass transition temperature of the polystyrene domains is exceeded. As indicated earlier, 83°C is a reasonable estimate of the polystyrene T_g in the SBS-8 triblock. From consideration of the mechanical behavior of a low molecular weight ($\bar{M}_n$ = 16,400) polystyrene fraction (55), Fesko (25) was able to show that the compliance of the pure polystyrene domains in SBS-8 should be entirely negligible

compared to the matrix compliance below about 80°C. Therefore, only the highest temperature region of the storage modulus curve for SBS-8 reflects the onset of flow behavior due to softening polystyrene domains.

The observed increase in the slope of the storage modulus of SBS-8 at temperatures as low as 50°C must result from the softening of a mixed interfacial region with a characteristic modulus which is intermediate between that of pure polystyrene and pure polybutadiene. The existence of such an interlayer has been postulated many times (23-26), but a clear visualization of this mixed phase through electron microscopy has never been produced. The common model proposed for the interlayer morphology involves a series of spherical shells enclosing each of the pure polystyrene domains (24-26). The compositions of the individual shells, and therefore their mechanical properties, have been estimated as smoothly varying functions which reduce to the values characteristic of the homogeneous phases at the interlayer boundaries (25). For the purposes of this work it is important that there be a limited region in which the interlayer has a significant effect on the mechanical behavior of these materials. If, for example, the interlayer contributed to the slow decrease in the storage modulus seen in Figures 12 - 14 over the entire intertransition region, then a difficult and imprecise decomposition would be necessary to elucidate the contribution of interest, namely that of the pure polybutadiene phase.

Fortunately, an earlier study of the dynamic properties of the SBS-8 triblock material indicated that the contribution of the interlayer region becomes noticeable only at temperatures above about 45°C when frequencies above 0.1 Hz are employed (25). This fact is shown quite clearly in Figure 29 where the entire body of SBS-8 data is displayed. The data here have been shifted according to the temperature reduction scheme developed by Fesko and Tschoegl (22) which predicts point-wise shifts of the data from a model based on the assumed additivity of the compliances of the polystyrene and polybutadiene phases. The effect of the softening interlayer is seen clearly in the loss compliance and to a smaller extent in the storage behavior. The softening of the interlayer causes an increase in the overall compliance, and therefore at each succeeding temperature the level of the data is correspondingly higher. There is no observable effect of the interlayer below about 45°C. Thus, data obtained below that temperature can safely be assumed to reflect the behavior of the polybutadiene phase alone. Another interesting and gratifying piece of information to be gained from Figure 29 lies in the few data available above 80°C. At 82 and 86°C, we see in the storage and loss compliances the onset of the polystyrene transition at the low-frequency end of the data. (The lowest experimental frequency was 0.1 Hz.) This is in excellent agreement with the observations already made from the free oscillation (0.2 Hz) data which showed a very rapid decrease of the SBS-8 storage modulus around 80°C.

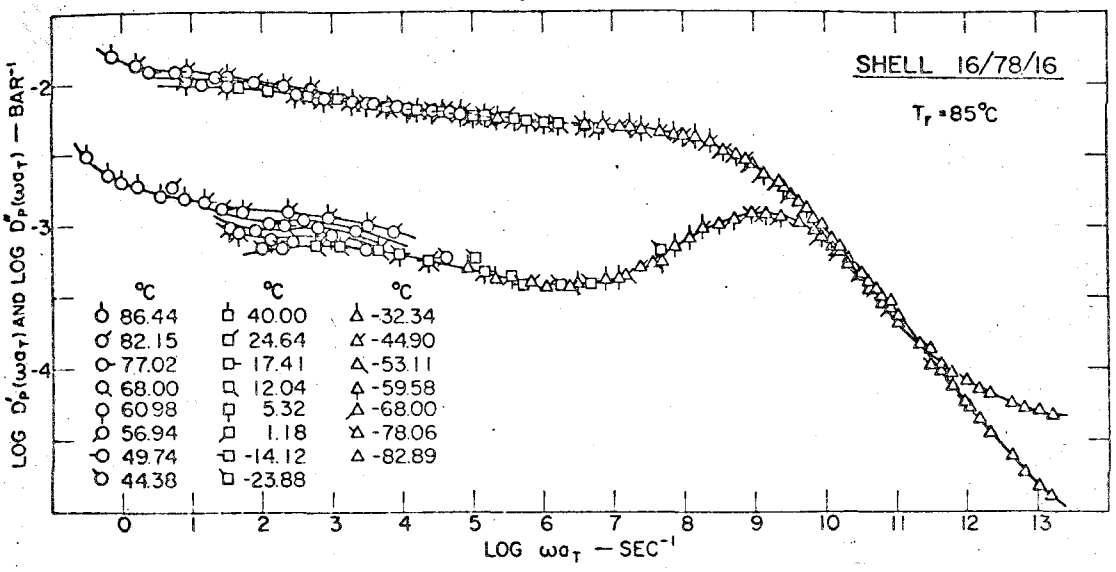

Figure 29. Effect of the interlayer on the mechanical properties of SBS-8.

In earlier studies of the transient mechanical properties of block copolymers it was proposed (26) that the mechanical behavior of these materials is dominated by the interlayer over the entire intertransition region. Figure 29 shows that this is clearly not the case and furthermore gives an indication of why this conclusion was reached. The transient viscoelastic properties all exhibit monotonic behavior similar to the storage compliance shown here. Because of this, the vertical shifts introduced by the softening interlayer are not easily recognized and instead could be incorporated into the horizontal shifts. It was from observations of the shift behavior (26) not of modulus or compliance curves, that the over-assessment of the interlayer's contribution was made. As will be seen in more detail later, knowledge of a material's loss behavior is not only useful, but often necessary, for correct interpretation of small secondary effects such as the interlayer behavior seen here.

Plots similar to the ones seen in Figure 29 could have been constructed for all of the materials studied here. For example Figure 30 shows the effect of the interlayer again appearing around 45°C in one of the blends of Series 1. Again, the loss compliance is affected more strongly. Only data above 0°C are shown here for clarity. In all of the master curves to be shown henceforth, only data below 40°C are used since these can be assumed to reflect the dynamic mechanical behavior of the polybutadiene network alone. By restricting the analysis of the forced oscillation data to temperatures below 40°C, then, one is assured that softening of the polystyrene domains or of the interlayer has not yet begun to affect the observed mechanical properties.

4.22 Thermorheological Complexity

Turning our attention again to the free oscillation data for the triblock shown in Figure 8, we can see quite clearly that there are two major viscoelastic transitions associated with these two-phase materials. The polybutadiene transition is located near -95°C, and the polystyrene transition is becoming evident above 80°C. In general one would expect each of these transitions to have a different frequency dependence since each reflects the behavior of a completely different material. This means that the locations of the two transition in Figure 8 should shift to lower temperatures with decreasing frequency at different rates, and therefore the separation observed between the two

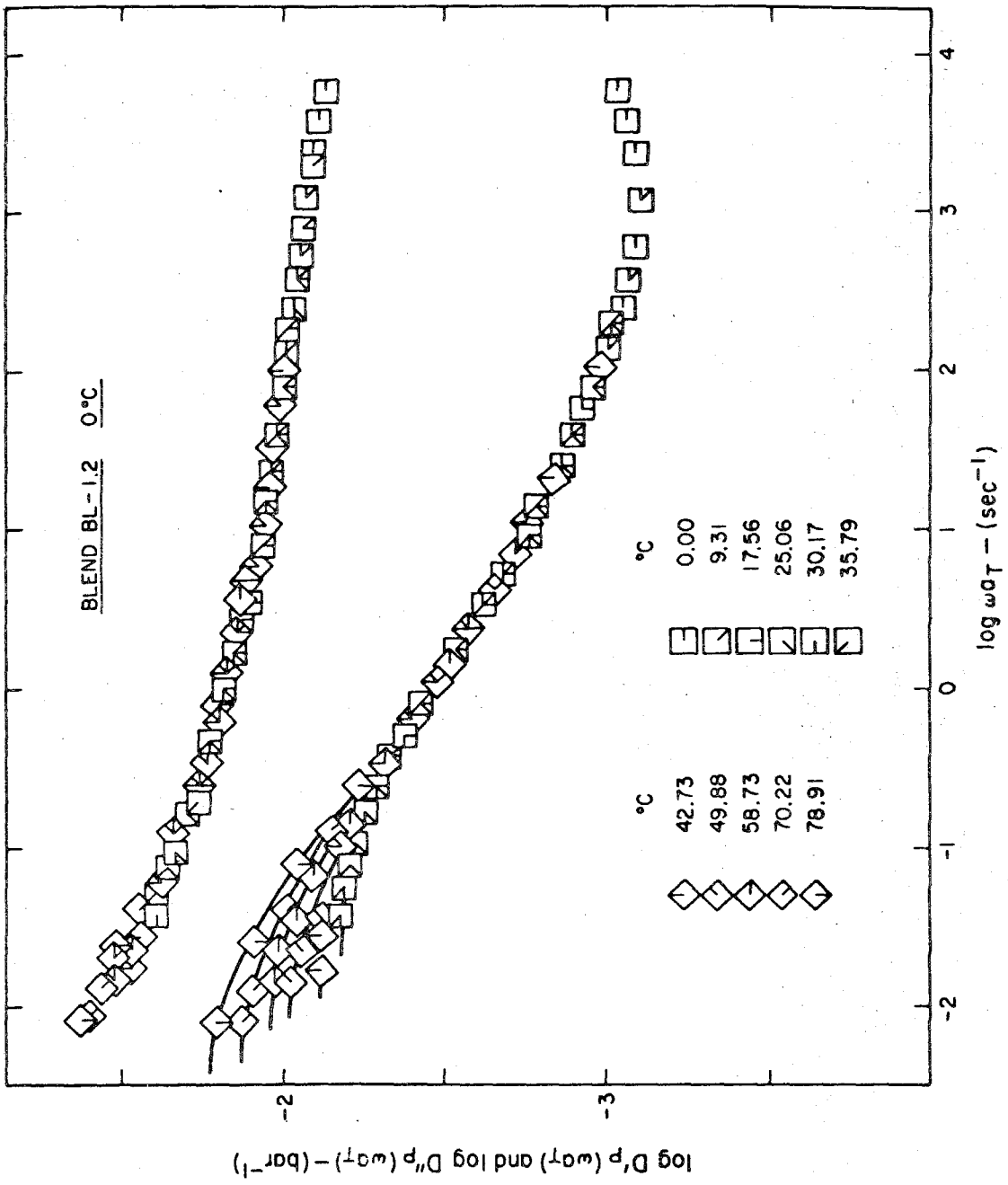

Figure 30. Effect of the Interlayer on the Mechanical Properties of BL-1.2

transitions becomes dependent upon the frequency of the experiment. One example of this was observed in isochronal forced oscillation measurements (56) on Shell Thermoelastic 125, a triblock copolymer similar to SBS-8. Those data showed that the frequency dependences of the polybutadiene and polystyrene loss modulus peaks were associated with activation energies of 82 and 158 kcal/mole respectively.

When considering isothermal forced oscillation data, the presence of two large transitions in the material becomes critical. In particular, the validity of the empirical shifting scheme for reducing the temperature dependence of the data is predicated upon the assumption that the material under consideration is thermorheologically simple, i.e., all of its relaxation times are affected equally by changes in temperature. Early studies (23, 26, 27) indicated that block copolymers are in general probably not thermorheologically simple materials, although there have been some claims to the contrary (57). Fesko and Tschoegl (22) have shown in a theoretical study that empirical shifting cannot lead to valid[7] master curves for a thermorheologically complex material. They did not, however, provide clear experimental proof of thermorheological complexity in block copolymers.

As mentioned earlier, the compliance of the polystyrene domains is essentially negligible over most of the temperature range

---

[7] When a master curve is valid, the behavior indicated by superposing the isothermal data is identical to that which would have been obtained if the entire reduced frequency range had been covered at the selected reference temperature.

of the forced oscillation data obtained here. However, a detailed analysis of time-temperature superposition in thermorheologically complex materials (22, 25) shows that the proper shift for a datum point at a given time and temperature depends not only on the level of the compliance in each phase and its rate of change with frequency, but also upon the steepness of its characteristic tempera-dependence curve. Thus, it is quite possible for the polystyrene phase to affect the shift factors even at temperatures well below its glass transition temperature. When this is the case, the shifts will be complicated functions of both frequency and temperature, and therefore empirical shifting will definitely lead to invalid master curves. By considering the compliances of the two phases to be additive, Fesko and Tschoegl (22) were able to generate, at various frequencies, the expected shift behavior for an SBS triblock material. Their results indicate quite clearly that for temperatures below about 50°C the shift factors were essentially insensitive to any realistic frequency range encountered experimentally. Thus below about 50°C the shift factors predicted by their model were essentially identical to those obtained by empirical shifting of the segments. This is a particularly useful result for the purposes of this work, since only data below 40°C were used to assemble the master curves. Thus, there was no great error introduced because of the thermorheologically complex behavior of the two phase material when the data were shifted empirically. Below 40°C the polystyrene domains can safely be considered as inert

filler particles. In this region of temperature their compliance is negligible compared to the polybutadiene phase, and, in addition, their temperature dependence has a negligible effect on the mechanical properties.

From the discussion presented above one can conclude that the major problem of thermorheological complexity arising from the presence of polystyrene domains can be safely ignored by considering only the data below about 40°C. Here the polybutadiene phase completely dominates the mechanical behavior and the material's temperature dependence. The suggestion has been made (25) that whenever this is the case empirical shifting should lead to valid master curves. However, there is a subtle but very important point to be made here concerning the validity of empirical shifting even when a single phase dominates the mechanical behavior. It is well known that certain polymethacrylates (58-60) exhibit thermorheologically complex behavior since the mechanical properties are comprised of two contributions, each with different sets of relaxation mechanisms. In the methacrylates these two contributions arise from motions of the chain backbone and the side chains, respectively. Plazek (61, 62) has found that the steady-state viscosity and the steady state compliance of polystyrene cannot be described by the same WLF equation. All of these materials consisted of a single phase, yet all exhibited thermorheologically complex behavior.

Thus, the master curves predicted by empirical shifting of the data obtained on SBS-8 below 40°C may still not be entirely valid if the polybutadiene phase is in itself a thermorheologically complex material. That is, if the mechanical behavior of the polybutadiene phase is controlled by more than one mechanism, each having a different temperature dependence, empirical shifting will necessarily introduce some errors into the master curve. The errors involved will no doubt be much smaller than those introduced by the effect of the two-phase thermorheological complexity, but the possibility of thermorheologically complex behavior within the polybutadiene phase should be recognized nonetheless.

Evidence of thermorheological complexity in the polybutadiene phase of SBS-8 has already been seen, but to a large extent ignored, in the study of time-temperature superposition conducted by Fesko (25). In that work a composite WLF-Arrhenius temperature dependence was observed below 40°C and was taken to be representative of the polybutadiene matrix. The added Arrhenius mechanism appearing at 0°C was assumed to be an indication of the onset of an entanglement slippage mechanism involving the trapped entanglements in the polybutadiene phase of the triblock. This observation is probably correct, but the implied validity of the shift factors employed must be questioned. First, the sudden appearance of entanglement slippage at one given temperature is unlikely. Furthermore, the particular choice of 0°C for the change in the shift behavior cannot be explained any better than the

arbitrary break points seen in very early and relatively unsophisticated studies of time-temperature superposition in block copolymers (23, 26, 27). Even more important is the fact that the incorporation of two different mechanisms into the shift behavior is essentially an admission of thermorheological complexity within the polybutadiene phase of the triblock. It will be seen later that the introduction of terminal chains into the polybutadiene phase results in several additional entanglement slippage mechanisms each of which is likely to have a temperature dependence different from standard WLF behavior. Therefore thermorheological complexity in the polybutadiene phases of the blends is also to be expected.

In view of the above discussion, it is admitted and indeed emphasized that the master curves which are shown to represent the behavior of the filled polybutadiene networks cannot be strictly valid. To obtain truly valid master curves it would be necessary to know, in advance, the temperature dependence of each contributing mechanism and a method for combining them to yield the overall behavior. The situation is not as alarming as one might think, however. As evidenced by Figure 20 excellent superposition can still be obtained for all the SBS-8 data below 40°C by using simple empirical shifts. The segments do not show serious non-superposition because of their limited length (25) and because the region of material response between the WLF and Arrhenius behavior is relatively flat and therefore insensitive to the shifts employed. In addition,

the difference between the two temperature dependences of Equation 4.1 is relatively small, certainly not anywhere near the great difference seen in the temperature dependence of polystyrene and polybutadiene. Therefore the master curves obtained by simple empirical shifting of the data below 40°C, while not strictly valid, are probably not very different from the master curves which would be predicted by a more sophisticated shifting scheme which accounts for the thermorheological complexity within the polybutadiene phase.

The basic shift behavior, shown in Figures 19 and 21 and described by Equation 4.1, does not differ markedly from the empirical shifts used by Fesko (25) for the SBS-8 data below 40°C. The shifts employed here did result in somewhat better overall superposition of the data and were not overly weighted to yield perfect superposition in any one region of material response. The result of this approach is a more satisfying log a_T vs. T curve which is smooth over the entire temperature range rather than exhibiting a sudden break at some arbitrary temperature. Essentially, this means that a visual averaging process has been employed in determining the empirical shifts in the region of temperature where the two mechanisms (WLF and Arrhenius) overlap. There was no consciousness of this averaging process, however, probably because the small effect on the superposition of the data arising from the overlap of the two different mechanisms was lost in the scatter of the data due to experimental error.

The constants of the WLF portion of Equation 4.1 are identical to those determined by Fesko (25). However, as seen in earlier studies of block copolymers of the SBS type (26, 27), the WLF coefficients are quite different from those established by Ferry and coworkers (7) on homopolymers of polybutadiene of similar microstructure. Above -60°C the shift factors fit smoothly into the Arrhenius equation given in the second part of Equation 4.1, and thus there was no need for a step function (25, 27) to enter the expression in this case. The apparent activation energy associated with this Arrhenius equation is around 17 kcal/mole. It would be unwise, however, to associate this apparent activation energy directly with the entanglement slippage mechanisms since, as discussed above, the shifts must represent some average over the various processes occurring in this region of temperature.

Equation 4.1, in fact, was never used to reduce the data, the point values of log a_T shown in Figures 19 and 21 being used in every case. This equation should be regarded merely as a convenient description of the empirical shifting scheme used to assemble the master curves, recognizing that it does not follow any of the simple forms found for most polymeric materials. However, as mentioned earlier, the fact that all of the shift factor data fall very closely along the single curve described by Equation 4.1 indicates that the temperature reduction has been carried out in a consistent and orderly manner. Therefore, it is possible to make valid comparisons among the various sets of data regardless of the

fundamental uncertainties involved due to the thermorheologically complex behavior of the polybutadiene.

It is reasonable to question the concept of thermorheological complexity in the polybutadiene phase of these block copolymers since all experience with moderately cross-linked (7), lightly cross-linked (11), and linear (11) polybutadiene of similar microstructure has indicated that a simple WLF equation is satisfactory for reducing the data. Furthermore, studies of 1,2-polybutadiene (12), and other cross-linked elastomers (6, 8-10) also revealed simple WLF behavior even when entanglement slippage was important. However, studies of poly(dimethylsiloxane) networks (13, 64) showed that far above T_g, where entanglement slippage became the dominant molecular mechanism the shift factors followed an Arrhenius equation, whereas a WLF equation would be more appropriate near T_g. Thus it is clearly possible that entanglement slippage can contribute to a second temperature dependence of the material properties.

If one considers morphological differences, it is not surprising that the temperature dependence of the polybutadiene phase of the triblock is different from that found for homopolybutadienes of the same microstructure. In SBS triblocks, both ends of the polybutadiene molecules are attached to large and essentially immobile polystyrene domains. These attachments restrict any motion of the ends of the polybutadiene molecule and require that all molecular motions occur over a specified maximum length (78,000 for SBS-8). This is quite different from the situation which exists

in an uncross-linked polybutadiene where there are no permanent restrictions on the molecules at all. Even in a cross-linked polybutadiene network in which there are permanent restrictions on molecular motions, the linkage points are small and somewhat mobile. Thus, it is not surprising, and indeed it perhaps should be expected, that the polybutadiene phase of the block copolymers does not exhibit the same temperature dependence as homo-polybutadiene. It will be seen later that the two-phase structure also causes the polybutadiene of the block copolymers to have a much more loosely entangled structure than homo-polybutadienes. Therefore entanglement slippage should occur more easily in the block copolymer polybutadiene phase, and perhaps this accounts to some extent for the more predominant effect of entanglement slippage on the temperature dependence in these materials. In any case, it is quite clear that the polybutadiene present in the continuous phase of the block copolymers behaves quite differently from homopolymers of the same microstructure and this must be kept in mind throughout the discussion. However, the continuous phase of the block copolymer blends is meant to be a more general model system than just for polybutadiene. The major effects of terminal chains and chain entanglements appear clearly in the data even though the overall behavior is not identical with that of any single known elastomer.

4.23 Mechanical Behavior of the Model Polybutadiene Networks

All of the previous discussion has been aimed primarily at establishing which regions of material response are likely to reflect the true mechanical behavior of the model polybutadiene networks. Analysis of the polystyrene and interlayer contributions has shown that for the frequencies encountered in the experiments conducted here, data below about 40°C contain negligible effects from these sources. Empirical shifting was seen to be a useful, although not entirely valid, method for carrying out the temperature reduction of the forced oscillation data. The nature of the temperature dependence indicated that the polybutadiene phase of the block copolymer materials behaves quite differently from conventional polybutadiene networks. The data were handled in a consistent manner so that comparisons of the response curves would be justified.

Thus we are finally at the point in the discussion which we have been seeking all along. It is now possible to inspect the response curves and relate observed changes in mechanical response to the controlled changes made in the structure of the model networks. The mechanical behavior of the model networks will be discussed by starting with the lowest temperature (short-time) effects and working upward toward the highest temperatures for which the model remains valid. It is convenient to divide the mechanical response of the model networks into three distinct

regions: (1) the glassy and transition region in which all the materials behaved nearly identically, (2) the region just above the main polybutadiene transition where temperature effects on the amount of entanglement coupling are important, and (3) the inter-transition region (up to 40°C) where the rubbery behavior is dominated by entanglement slippage mechanisms.

4.231 Glassy and Transition Regions

All of the model network systems tested in this investigation exhibited essentially identical behavior in the glassy and transition region; both the location and the shape of the main transition from glassy to rubbery behavior was unaffected by the introduction of terminal chains into the networks. This is perhaps an expected result since all of the polybutadiene segments in the various materials had roughly the same glass transition temperature (about -90°C). The similar T_g's reflect the closely matched microstructures (approximately 90% 1,4 addition) in all of the polybutadiene segments.

It is well known that the mechanical behavior in the glassy state is largely independent of network structure since only very limited short-range molecular motions occur in this region of material response. The forced compressional measurements do not really enter into the glassy region and any data in or near this region would probably be erroneous due to a significant apparatus compliance (25). However, the free oscillation measure-

ments extend below -150°C, well into the glassy region, and thus some qualtitative assessment can be made of the mechanical behavior in the glassy state.

Figures 12 - 14 indicate that the level of the storage modulus in the glassy region is around 10^4 bars, a value which is roughly the same for a wide variety of polymers below their glass transition temperatures. These figures show further that between -150°C and -110°C the storage modulus undergoes a slow, nearly linear, decrease with temperature, with the slope, d log G´/dT , having a value of about 3×10^{-3} logarithmic decades/°C. This slope indicates that there is some small amount of viscoelasticity at these temperatures. Since the polybutadiene segments have no side groups, the viscoelastic properties probably result from oscillations and rotations around bonds in the backbone structure. There is also some evidence that the slight temperature dependence in this region may be partially attributed to a dispersion in small crystalline regions which perhaps can form at these low temperatures. Takayanagi (65) has observed small peaks near -140°C in the loss moduli of semicrystalline specimens of trans 1,4-polybutadiene. In Figures 15 - 17 similar peaks, centered around -140°C, are seen in the loss moduli for all of the materials studied here. If there is some small degree of crystallinity in these polybutadiene networks at very low temperatures, the preponderance of evidence, both from mechanical properties data and thermal analysis, indicates that these regions must disappear above the polybutadiene glass transition temperature.

We now turn our attention to the location and the shape of the transition region. The free oscillation storage modulus data given in Figures 12-14 show that the rapid decrease in G´ covers nearly 2.25 logarithmic decades and takes place over a rather narrow (around 20°C) temperature range. The inflection or midpoint temperature (17), T_m, is roughly -90°C for all samples. It is interesting to note that this value of T_m agrees well with the values of T_g determined in DTA measurements even though these two parameters are not necessarily expected to agree in all cases. Figures 20, 23 and 25 show that a corresponding rise is observed in the reduced forced oscillation storage compliance. The slope of the log D´ vs. log ωa_T plot is roughly -0.6 in the transition region for all the materials studied, slightly steeper than the slope of -0.5 predicted for the transition region by the modified Rouse theory (17). Figure 28 shows that the retardation spectra derived from the loss compliance data also exhibit slopes which are steeper (the dashed curve is drawn with a slope of 0.5) than expected from theoretical considerations. The increased steepness cannot be explained by the presence of the polystyrene domains since reinforcing fillers generally tend to decrease the slope in the transition region. Dynamic measurements on homopolymers of polybutadiene (7, 11) with microstructures similar to the materials studied here, revealed slopes which were much steeper than the -0.6 slope observed here in the transition region. Therefore the polystyrene filler particles apparently do tend to

reduce the steepness of the transition region as expected. The lack of agreement with theory must be considered to be a characteristic of the material and not an experimental artifact.

The location of the transition region on the frequency or temperature scale is determined by the monomeric friction coefficient which in turn depends upon the amount of free volume in the material. The frictional resistance per monomer unit decreases with increasing free volume and results in a shift of the transition to higher frequencies. The presence of chain ends in polymeric systems can cause a significant increase in free volume; however, when the molecular weight of the polymer molecules is greater than about 20,000, the effects of changing free volume due to differences in the amount of free chain ends becomes imperceptible (17). This explains the observed insensitivity of the location of the transition region to the terminal chain content in this study. Since terminal chains introduce only one free end each, they affect the free volume in a manner similar to homopolymer polybutadiene chains of twice the molecular weight. Thus the shortest terminal chains employed here ($\bar{M}_n$ = 22,000) are much too long to cause significant changes in the free volume, and therefore the location of the transition region was unaffected by their presence. A significant fraction of terminal chains of molecular weight below 10,000 would be necessary to change the location of the transition region along the frequency scale.

The appearance of maxima in the loss modulus curves in Figures 15 to 17 is a result of greatly increased energy dissipation associated with configurational rearrangements of the polybutadiene molecules near the glass transition temperature. These particular dissipation processes must be unaffected by terminal chains since the peaks in G'' are essentially identical for all the materials. Figure 8 shows clearly that the magnitudes of the storage and loss moduli are closely similar throughout the high-temperature half of the transition region. This is the region of highest damping in these materials, and the loss tangent, G''/G', is close to unity here. Although the loss tangent curves derived from the free oscillation measurements have not been presented, their maxima appear slightly to the right (near -90°C) of the peaks in G'' as expected. The only loss tangent curves presented here were derived from the forced oscillation data obtained on the materials of Series 1. As shown in Figure 27, the maximum values of tan δ occur in the transition region. The narrow band of curves indicates the typical amount of disagreement among the various sets of data in the transition region. Other plots essentially provide a best-fit curve to represent all the materials whenever the curves are this close to being identical. The half band-width is roughly 0.04 logarithmic decades, and this probably is a good representation of the reproducibility of the data in these experiments.

The maximum in the reduced loss compliance is also related to the configurational rearrangements of the network chains in a

rubbery material. Maxima in the loss compliances of conventionally cross-linked rubbers reflect the supression of very long range configurational rearrangements by the covalent cross-links and the entanglements in the network. Since very long range motions are permanently excluded in these materials, the loss compliance falls off at low frequencies instead of continuing to increase, thus generating a maximum in the response curve. Maxima also appear in uncross-linked polymers of sufficiently high molecular weight indicating that entanglements are capable of supressing long range motions in a manner closely resembling the behavior of covalent cross-links. As will be discussed in more detail in later sections, in an uncross-linked polymer the restrictions imposed by entanglements are temporary, and therefore the loss compliance rises again at lower frequencies.

The maxima appearing in the loss compliances of the triblock and the blends are a result of the physical restrictions on the polybutadiene segments which arise at the polystyrene domain boundaries and at the multitude of entanglement points in the continuous polybutadiene networks. The shapes and peak locations of the maxima in D'' (after the appropriate temperature reductions, both log a_T and μ, have been taken into account) were essentially identical for all the materials throughout the transition region. This indicates that whenever the mechanical response is dominated by molecular motions of segments shorter than the

distance between junction points in the network, the material is oblivious of any differences between network chains and terminal chains.

The location of the reduced loss compliance and its peak height in the transition region are both strongly affected by the average distance between entanglements or equivalently the total number of entanglements in the network. We have seen quite clearly that, when the data are properly reduced to a common reference temperature, these features of the loss compliance curves are not affected by variations in terminal chain content or length. This indicates that, at a reference temperature of -78°C, the average spacing between all types of entanglements in the blends is not perceptibly different from the spacing between trapped entanglements in the triblock material. In the terminology of Ferry (17) this means that D_{eN} (the compliance level associated with all the entanglements and cross-links, if any, in a network) is essentially the same for all the materials studied here. Thus, the main viscoelastic transition from D_g (the glassy compliance) to D_{eN}, was unaffected by changes in the terminal chain content of these networks. It will be seen later that the terminal chains begin to play a dominant role once this transition to D_{eN} has been completed.

4.232 Effect of Temperature on Entanglement Coupling

In the previous section dealing with the mechanical behavior in the glassy and transition regions it was pointed out that an entanglement network was responsible for the maximum in the loss compliance appearing near log $\omega a_T = 1$. Furthermore, at a given reference temperature the shape and location of this maximum were both essentially unaffected by changes in the relative proportions of trapped and untrapped entanglements in the networks or by changes in the length of the terminal chains which enter into these untrapped entanglements. In this section it will be shown that, under certain circumstances, a change in temperature can have a pronounced effect on the mechanical properties in the region near the peak in the loss compliance by causing changes in the amount of entanglement coupling in the networks. The structural features of the networks which are important in this temperature dependent mechanism are the proportion of untrapped entanglements and the length of the terminal chains engaged in these untrapped entanglements. It will become clear that trapped entanglements provided by the triblock polybutadiene segments do not enter into this mechanism.

Pronounced effects of temperature on entanglement coupling in uncross-linked polymethacrylates have been observed by Ferry and coworkers (65-69). Such effects have not been observed in homopolymers of polybutadiene, but as mentioned earlier,

the model network systems studied here should not be expected to behave identically to conventional polybutadiene networks. In fact, it will be shown later that certain features of the overall morphology of the block copolymer systems make it reasonable to expect that a temperature dependent entanglement coupling mechanism should occur in these model networks but not in conventional polybutadienes.

With this introduction, the following proposition, based on the earlier work of Ferry (67), is made concerning the effect of temperature on entanglement coupling in these networks: In certain regions of temperature (roughly -60°C to 0°C) the number of entanglements is susceptible to readjustment as temperature is changed. It is further proposed that the readjustment will take place in such a way so that fewer entanglements are associated with higher temperatures. Keeping in mind the unique structure of these model networks, it is clear that only the untrapped entanglements can change in number; the number of trapped entanglements is fixed as long as the polystyrene domains, which pin both ends of the triblock polybutadiene segments, remain intact. Therefore, it is postulated that a certain fraction of the entanglement network, the exact amount depending upon the terminal chain content, becomes more loosely entangled as temperature is increased. The data obtained on the model network systems will be used to defend and elaborate upon this proposed mechanism.

Before discussing the proposed mechanism in relation to the behavior, a few words are in order concerning the nature of entanglement coupling in polymers. In a study of the dependence of the steady-flow viscosity on molecular weight for a number of polymers, Berry and Fox (70) showed that at a characteristic molecular weight M_c, the slope of the log η vs. $\bar{M}_w$ plot changed rather abruptly from 1.0 to 3.4. The observed change in the viscosity behavior was attributed to the presence of a temporary network of coupled entanglements whenever the molecular weight was greater than M_c. The observation that $M_c \simeq 2\ M_e$ (M_e is the average molecular weight between entanglement points) is consistent with this explanation of the viscosity behavior since it would take an average of two (17) coupling points for every polymer molecule before the entanglement network would extend throughout the entire system. Otherwise the effect of an entanglement would be felt only locally. These observations become relevant to the networks under consideration here because different terminal chain molecular weights were employed. Since the terminal chains are responsible for the untrapped entanglements in these systems, it will be their molecular weight which will determine whether or not the untrapped entanglements are coupled with each other and with the rest of the network structure. In analogy with the viscosity experiments discussed above one would expect to find coupled untrapped entanglements when the terminal chain molecular weight is roughly twice the characteristic entanglement length of these systems.

However, the factor of two must be regarded as being approximate since the exact relationship between M_c and M_e has not been clearly established for all materials. Vinogradov and coworkers (71) have shown that the onset of a coupled entanglement network in 1,4-polybutadiene is not expected unless the molecular weight is around four times the entanglement molecular weight.

We not turn to the data to find manifestations of the proposed temperature effects on the amount of entanglement coupling in the model networks. In addition we will be looking for differences in the behavior of the various series of blends since the terminal chain lengths differ significantly in the three series. The only storage modulus data obtained on any of the pure diblock materials appears in Figure 12. The storage modulus of the SB-6 diblock reveals a slight tendency between -80°C and -50°C to level into a plateau, indicating that the entangled chains are coupled into a temporary stress bearing network in this region. The polybutadiene segments of SB-6 have a molecular weight of 51,000 and it is clear that this value must be larger than M_c for this system. Thus, the SB-5 diblock (terminal chain length 67,000) would also be expected to exhibit a temporarily coupled network. At this point one can only speculate on the behavior to be expected for the much shorter, 22,000 molecular weight terminal chains. The general behavior observed for SB-6 in Figure 12 indicates that the coupled network of untrapped becomes weaker (decreasing G´) as temperature increases.

The weakening of the coupled network with temperature means that fewer stress bearing sites, i.e. fewer coupled untrapped entanglements, are present at each higher temperature.

A somewhat more definitive picture of the role of changes in entanglement coupling with temperature can be gained by viewing the entire body of loss modulus data shown in Figures 15 to 17. Considering first the SB-6 curve in Figure 15 one sees that the loss modulus continues to decrease from the base of the main transition until about -50°C where the loss begins to rise again. The decrease in the modulus with temperature between -80°C and -50°C reflects the general weakening of the network through a decrease in the number of entanglement points. At -50°C the terminal chains are sufficiently decoupled from each other to slip and introduce internal frictional mechanisms which cause the loss to rise again. This slippage phenomenon will be discussed in detail in the next section. The resulting minimum in the loss curves is seen for all the blends of Series 1 and 3. The minimum is deeper for increased terminal chain content. This is quite reasonable since a larger fraction of the network is susceptible to changes in entanglement coupling for higher terminal chain contents. It is also gratifying that the SBS-8 triblock shows no hint of a minimum, supporting the earlier proposal that the trapped entanglements are fixed in number and cannot enter into this mechanism.

There has been some previous evidence to support the contention that the minima seen in the loss data for Series 1 and 3 arise from changes in entanglement coupling involving the terminal chains. In a study of very lightly cross-linked rubbers, Nielsen (72) observed minima in the loss moduli similar to those seen in this work. His materials were so lightly cross-linked that they contained a significant sol fraction; furthermore, molecular weight between cross-links was large and chain entanglements must have been contributing to the observed moduli in addition to cross-links. In a conventionally cross-linked rubber, a high molecular weight between cross-links indicates the presence of long terminal chains. Therefore, the minima seen by Nielsen probably arise from the same effect of temperature on the number of untrapped entanglements as seen here. Highly cross-linked rubbers were studied for comparison, and no minima were observed for those materials (72). In general, a minimum on the low frequency side of the main loss peak derived from isothermal measurements of the viscoelastic functions is usually attributed to the presence of network strands which are coupled by entanglements (17). In loss modulus vs. temperature curves, this corresponds to the high temperature side of the loss peak, exactly where the minima in the data occur in Series 1 and 3.

The entanglement coupling mechanism is quite obviously absent for all the materials of Series 2 since there is no evidence of a minimum in the loss modulus curves near -50°C for these materials

(see Figure 17). The implication is that the 22,000 molecular weight terminal chains were too short to engage in coupled entanglements with the rest of the network; i.e. 22,000 appears to be less than M_c for these systems. Evidently the shorter terminal chains of Series 2 are already free enough at the base of the main transition to slip and contribute to the frictional loss mechanisms which began to occur around -50°C for the longer terminal chains of Series 1 and 3. Thus no minimum forms in the loss modulus vs. temperature curves for the blends of Series 2.

In the presentation of the forced oscillation data it has already been pointed out that the materials studied from Series 1 and 3 exhibited noticeable reduction anomalies in their mechanical response curves. If one considers the frequency range of the forced oscillation data (0.1 - 1000 Hz), the temperatures for which the data do not superpose (roughly -60 to 0°C) correspond rather well to the region in which the loss modulus curves were exhibiting the minima attributed changes in entanglement coupling. Thus, it is reasonable to assume that the systematic lack of superposition, seen for example in Figure 22 for one of the blends of Series 1, is a manifestation of this same mechanism, namely a decrease in the number of coupled untrapped entanglements with increasing temperature. The difference here, however, lies in the fact that the forced oscillation measurements were carried out isothermally. Therefore, a different (more weakly coupled) network system was being studied over the entire frequency range at each higher temperature.

Reduction anomalies of the type seen in Figure 22 have already been observed by Ferry and coworkers in the behavior of several high molecular weight methacrylate polymers and their solutions (66-69). In one of these studies (67) a method for reducing the anomaly was developed through considerations of temperature effects on the temporary entanglement networks formed by these materials. Their major premise was based on the predictions of the molecular theories for cross-linked and entanglement networks (Ref. 17, Ch. 10), which indicate that the magnitude of the complex compliance is inversely proportional to the number of junction points in a network while the location of the compliance value along the reduced frequency scale is directly proportional to the square of this number. They reasoned that in an entanglement network the number of junction points, i.e. the number of untrapped entanglements, could be affected by changes in temperature. In particular, a change in temperature which would alter the number of entanglement points by a factor f would consequently result in a change in magnitude of the compliance by a factor 1/f and a shift in its location on the frequency scale by a factor f^2.

Ferry was able to determine the unknown factor f associated with each temperature by shifting the anomalous compliance data along a slope of -1/2 on the log-log plots and recording the distance required to obtain superposition. The "f-shift" (67) factors obeyed Arrhenius equations with apparent activation energies

ranging from 1.6 to 2.3 kcal/mole depending upon the material. The method did result in excellent reduction of the superposition anomalies for the various methacrylates polymers. The basic reasons for the observed nonsuperposition were also made apparent by Ferry's analysis. Experiments carried out at different temperatures, while conducted on the same specimen, actually tested a material with a different structure in each case. At higher temperatures there was a larger average distance between entanglement points and therefore fewer entanglements comprising the network. Consequently the material became more compliant (shifted up) and its overall mechanical response shifted to lower frequencies than predicted by the conventional temperature reduction. These changes in structure of the material were compensated for by carrying out the f-shift as described above, and therefore the superposition of the data was restored.

The changes in material response seen in these methacrylate polymers resulted from a change in the number of entanglement points in the networks at each temperature. This phenomenon should not be confused with entanglement slippage which occurs at much lower reduced frequencies. Once the material has adjusted itself to the change in temperature so that the appropriate number of entanglement points has been established, the entanglements are as resistant to slippage at high reduced frequencies as they were before the change in temperature occurred. However, a completely

satisfactory explanation of this apparent equilibrium between entanglement points and entanglement sites (17, 67) has not been given.

It is also not clear why the f-shift is so apparent in the methacrylate polymers but completely absent in essentially all other systems whose properties have been documented in the literature. One explanation has been proposed (17, 67) which is based on the presence of high molecular weight aggregates in the methacrylate polymers due to regions of tactic ordering (73). Presumably the effects of temperature on entanglement coupling are more prominent when the entanglement structure is enhanced by these regions of high aggregation (17). It is interesting that an entanglement coupling mechanism so strikingly similar to the "f-shift" mechanism seen in the methacrylates should appear in the mechanical behavior of the model networks studied here. Especially interesting is the fact that the glassy domains act as multifunctional linkage points from which the uncross-linked polybutadiene segments emanate. The domains may behave in much the same way as the regions of tactic ordering do in the methacrylates, and perhaps this accounts for the appearance of prominent entanglement coupling effects in the data obtained here.

The superposition anomalies in the mechanical behavior of the methacrylate polymers are remarkably similar to the non-superposition seen for blend BL-1.2 in Figure 22, for the remaining two blends of Series 1 and for the single material, BL-3.2, studied

from Series 3. Therefore, there was strong motivation for using a diagonal shifting scheme similar to the "f-shift" to resolve the anomalies here. A major difference in the overall behavior of the blends, however, lies in the fact that only a portion of these networks, the untrapped entanglement portion, will be affected by the change in entanglement coupling with temperature. The methacrylate networks were comprised entirely of untrapped entanglements and therefore the total system was affected by changes in temperature. Qualitatively, then, one would expect the vertical, or compliance component of the diagonal shift to be smaller for the model networks than for the methacrylates. Following this line of reasoning, one should use slopes of magnitude less than 1/2 to resolve the superposition anomalies in the blends, and furthermore these slopes should increase toward a limiting magnitude of 1/2 as terminal chain content increases.

Another limitation on the slope used for the diagonal shifting procedure arises from the differences seen in the low frequency rise in the loss compliance for the various blends. As mentioned in Chapter 3, if the diagonal shift is carried out along a slope very different from that of the linear portion of the low frequency losses, resolving the anomaly near the main loss peak will result in a serious lack of superposition at lower frequencies. In Ferry's work (67) the slope of the low frequency losses was steep enough (about -0.4) so that shifting the data along a slope of -1/2 did not significantly disturb the superposition at low

frequencies, although some small spread was introduced. Since the magnitudes of the slopes of the low frequency losses in the blends were always less than 1/2 and increased with increasing terminal chain content (see Figure 26, for example) it was decided that shifting along these slopes would be a convenient and meaningful way to resolve the superposition anomalies in these materials. Since the slopes were composition dependent and different from -1/2, the diagonal shift scheme used here has been designated as the "μ-shift" to distinguish it from Ferry's "f-shift". The μ-shift slopes are plotted against terminal chain content, X, in Figure 31. The point at X = 1 was placed on the assumption that -1/2 is the limiting value for the slope of the diagonal shift; zero slope has been assumed to correspond to the absence of any diagonal shift when only trapped entanglements (X = 0) are present in the network. The four blends studied fit very well into the pattern, and this lends confidence to the method of choosing the μ-shift slope parallel to the rise in the low frequency losses.

Still further confidence in the method lies in the excellent resolution of the reduction anomalies obtained by employing the μ-shift. Also, the fact that all of the μ-shift factors for Series 1 clustered around the same straight line in Figure 24 indicates that the particular choice of slopes was sufficient to account for the composition dependence of the mechanism. The μ-shift data for Series 3 are shifted to higher temperatures in Figure 24, but otherwise follow the same mechanism.

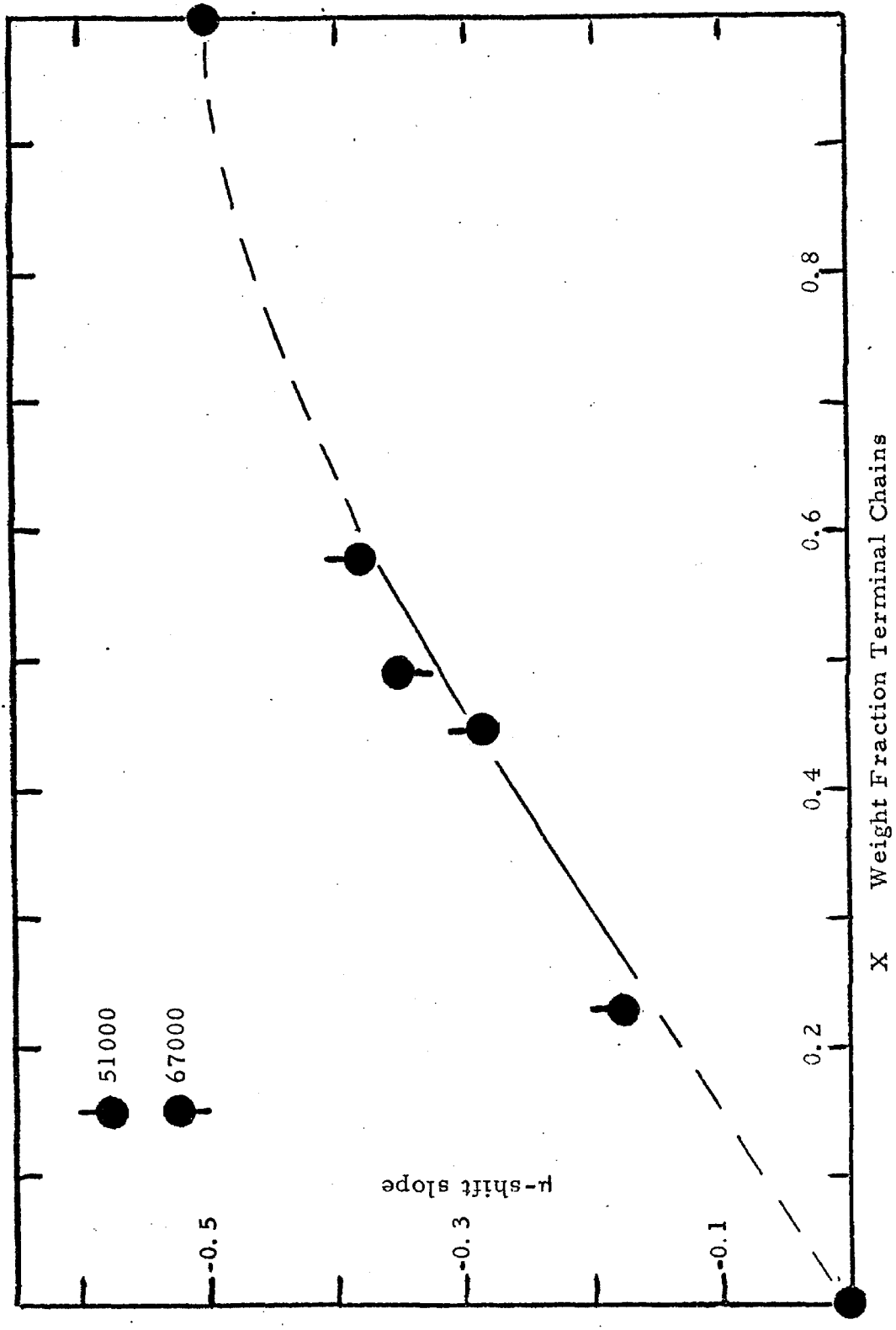

Figure 31. μ-shift Slopes

This is reasonable behavior since the longer terminal chains in Series 3 should provide untrapped entanglements which are more strongly coupled with the rest of the network. Therefore the effects of changing entanglement coupling appear at, and persist to, somewhat higher temperatures.

The practice of shifting the data down and to the right when carrying out the μ-shift insures that the location of the glassy and transition region remains unaffected by the analysis. This is desirable since the reference temperature for the conventional (log a_T) temperature reduction was chosen in this region. Thus, both sets of shift-factors, μ and log a_T, have values of zero at -78°C. Referring the μ-shift to low temperatures also insures that the compliance level in the intertransition region reflects the behavior of a network containing the maximum number of entanglements and not a network "weakened" by changes in entanglement coupling.

It is easily shown that the μ-shift used here reduces to the f-shift when the slope employed has a magnitude of 1/2. In Ferry's work the factor f was a measure of the vertical shift in the compliance on a linear scale. In this analysis μ was taken to be the shift (in log units) along the particular diagonal employed. When this diagonal has a slope of -1/2 the relationship between μ and f becomes $\mu = (1/0.447) \log f$, where $0.447 = \sin \psi$ and $\psi = \tan^{-1} 1/2 = 26.6°$. We then obtain the following relations for the vertical and horizontal components of the μ-shift along a

slope of -1/2: Vertical, $-\mu \sin 26.6° = -0.447\,\mu = -\log f$; Horizontal, $\mu \cos 26.6° = 0.894\,\mu = 2 \log f$. Thus at the limiting slope of -1/2 when one plots $\log D'' - \mu \sin \psi$ against $\log \omega a_T + \mu \cos \psi$, this is equivalent to Ferry's treatment (17, 67) where plots of $\log D''/f$ against $\log \omega a_T f^2$ are produced. Thus the μ-shift reduces properly to the f-shift at a slope of -1/2.

Since the analyses are equivalent (The μ-shift is more flexible since it allows for a composition dependent slope) it is possible to compare the apparent activation energies found by Ferry for the methacrylates and the value determined here for the model polybutadiene networks. Taking into account the appropriate geometry discussed above, one obtains the apparent activation energy associated with the Arrhenius equation describing the μ-shift mechanism as follows: $\Delta H_a = 0.447\ (2.303 \cdot R \cdot S)$, where R is the gas constant in appropriate units and S is the magnitude of the slope of the μ vs. 1000/T plot shown in Figure 24. This results in a value of about 1.7 kcal/mole for ΔH_a in very good agreement with the values of 1.6 to 2.3 kcal/mole reported by Ferry (67) for the methacrylate polymers. The meaning of this close agreement is obscure since the systems are quite different. In fact the general interpretation of these apparent activation energies as heats of dissociation, with an implied equilibrium existing between the untrapped entanglements and a large excess of entanglement sites (17, 67) should not be taken too literally. It is perhaps sufficient to view the μ-shift as a convenient

method for reducing superposition anomalies of the type shown in Figure 22 to yield the single smooth master curves of Figure 23 and not subject the treatment of the data to detailed molecular interpretations. There is, however, ample evidence from this work and the earlier studies on methacrylate polymers to suggest that systematic superposition anomalies near the main peak in the loss compliance result from a decrease in the amount of entanglement coupling with increasing temperature. Furthermore, it appears that these effects are enhanced by the presence of regions of high aggregation within the entanglement network.

Still remaining in this discussion is an explanation of the obvious absence of any entanglement coupling effect in Series 2, terminal chain length 22,000. Figure 25 shows clearly that no μ-shift was required to obtain good superposition of the data for blend BL-2.3. The region in which the superposition anomaly was present for the blends of Series 1 and 3 shows very good superposition for the BL-2.3 data. This is consistent with the earlier observation that no minima developed in the loss modulus curves derived from free oscillation data for Series 2. The conclusion is that the 22,000 molecular weight terminal chains are short enough to be below M_c for these systems. As a result the terminal chains do not become engaged in the coupled network which is necessary for the material to be affected by changes in temperature in the manner discussed above.

At first this may not seem likely since, as discussed earlier, one would expect entanglement coupling to extend throughout the system when the molecular weight of the rubbery segments is greater than twice the entanglement molecular weight (M_e) for the material. For homopolymers of polybutadiene the values of M_e range between 2,000 and 4,000 depending upon the microstructure of the material (17). The linear weighted average M_e for a polybutadiene containing about 45% cis-1,4, 45% trans-1,4, and 10% 1,2 addition is 2530. Thus, one should expect the onset of an entangled network system for molecular weights greater than about 5,000 for homopolymers of polybutadiene. Berry and Fox (70) have observed an M_c value of 5,900 for a 50% cis-1,4 polybutadiene.

The fact that the entanglement coupling mechanism did not appear in the materials containing terminal chains of molecular weight 22,000 is difficult to understand in the light of the above discussion. However, it is important to note that the values of M_e quoted above were determined on <u>homopolymers</u> of polybutadiene. The terminal chains in the polybutadiene networks which we are studying will very likely have different entanglement characteristics because one of the chain ends is constrained to be at or near a polystyrene domain. Intuitively one would expect this constraint to increase the average length between entanglements because of a decrease in the relative freedom of movement. Thus it is quite possible that terminal chains of molecular weight 22,000 are not long enough to engage into a coupled network in the diblock-triblock

copolymer blends. Similar considerations should also apply to the distance between permanent entanglements in the triblock. Perhaps even more important is the fact that in a cast triblock elastomer the entanglements are formed simultaneously with the formation of the two-phase structure. By contrast, in a conventionally cross-linked rubber the entanglements were already present before cross-linking.

To resolve this problem swelling measurements were conducted on the triblock material, SBS-8, to determine the average distance between entanglement points in the network. Triblock copolymers can be swelled with a solvent which will penetrate the continuous rubbery phase and leave the dispersed glassy domains essentially untouched. Bishop and Davison (74) found that isooctane satisfies these requirements for triblocks of polystyrene and polybutadiene. They also determined that it is necessary to correct the observed swelling ratio for the constraint on the swelling around each polystyrene domain, and that a correction of the type proposed by Kraus (75) for carbon black filled rubber could be applied successfully.

The equilibrium swelling ratio of the polybutadiene phase in isooctane was determined for two separate specimens of SBS-8 with excellent reproducibility. No swelling creep (74) was detected even after several days, and less than 1% extractable material was found in the swelling solvent. The Kraus correction

was applied, and the concentration of effective chains, ν_e, was calculated from the Flory-Rehner equation (76, 77) as used by Kraus (78).

$$\nu_e = -\frac{1}{V_s} \frac{\ln (1 - v_r) + v_r + \chi v_r^2}{v_r^{1/3} - 2 v_r/f} \tag{4.2}$$

Here V_s is the molar volume of the isooctane solvent, v_r is the volume fraction of polybutadiene in the swollen network (corrected according to Kraus), f is the functionality of the cross-links (trapped entanglements act as a tetrafunctional link), and χ is the polymer-solvent interaction parameter. The interaction parameter used for the polybutadiene-isooctane system was determined by Bishop and Davison (74) as

$$\chi = 0.406 + 0.522\, v_r \tag{4.3}$$

The resulting value for ν_e was 0.75×10^{-4} moles/cc. The molecular weight between entanglements was then determined from the relation, $M_e = \rho/\nu_e$ where ρ is the density of polybutadiene in grams/cc. This results in a value of about 13,000 for M_e in SBS-8; Bishop and Davison determined M_e to be about 16,000 for their SBS materials.

Since D_{eN} and the properly reduced location of the main loss peak were unaffected by terminal chain content, it is reasonable to assume that the total concentration of entanglements, and therefore the value of M_e, is the same in the triblock and the blends.

Then, since M_e was determined as 13,000 and $M_C \geq 2\ M_e$, it is clear that terminal chain molecular weights greater than 26,000 are necessary to exceed the critical molecular weight for entanglement coupling in these networks. This provides a satisfactory explanation for the absence of the temperature dependent entanglement coupling effect in Series 2 where the terminal chains had a molecular weight of only 22,000.

There have been some objections raised concerning the validity of the entanglement molecular weights determined by swelling for block copolymer systems (79). In particular the level of the modulus in the rubbery region is much too large to be accounted for by an entanglement molecular weight of 13,000, even after applying the correction (80) for filler content. There are several ways (Ref. 17, Ch. 13) to determine M_e from mechanical properties data. In every case entanglement weights under 2,000 are predicted, and in many cases unreasonably low M_e values result. For example, M_e is simply related to D_{eN} (corrected, of course, to remove filler effects on the compliance level) by the relation

$$g_N \rho RT/M_e = 1/(3D_{eN}) \tag{4.4}$$

where g_N is a numerical factor assumed to be very close to unity (17), R is the gas constant in appropriate units, ρ is the density, and T is the temperature in °K. D_{eN} can be obtained in a number

of ways. By considering the retardation spectrum for SBS-8 seen in Figure 28 one obtains D_{eN} as

$$D_{eN} = \int_a^b L''_2 \, d \, \ell n \, \tau \tag{4.5}$$

where the integration limits are chosen to include only the contribution to the spectrum from the main peak (9). Another method (82) relates the peak in D'' to D_{eN} by

$$D'' = k \, D_{eN} \tag{4.6}$$

where k is a constant ranging from 0.240 to 0.417 depending upon the material and the distribution of strand lengths in the network (17).

From equations 4.4 to 4.6 one obtains M_e values ranging from 370 to 750 which are all unreasonably small. Fesko (25) found even smaller M_e values for a similar triblock system when using calculations of this sort. One may be tempted to use D_e (the equilibrium compliance associated with the trapped entanglements in the SBS-8 networks) in equation 4.4 rather than D_{eN}. In a triblock system where all the entanglements are trapped and fixed in number, any difference between D_{eN} and D_e must be associated with some kind of relaxation due to trapped entanglement slippage. Since the storage compliance rises continuously across the intertransition region, this must be the case for the SBS-8 triblock. However, D_e cannot be obtained reliably since polystyrene and interlayer

contributions to the compliance become important before equilibrium is reached. However a reasonable estimate can be made simply by choosing the highest value of D´ attained by SBS-8 in Figure 20. Correcting this value for filler content and then substituting into equation 4.4 results in a value of about 1700 for M_e, still lower than the 2500 value expected for homopolybutadiene.

Although not as reliable for calculations of this type, the free oscillation data can also be used to estimate values of M_e for SBS-8. From the rubbery modulus, G, one obtains M_e from the relation

$$G = \rho RT/M_e \tag{4.7}$$

One can estimate G from the various values of G´ across the intertransition region; again the correction (80) for filler content is required. Choosing the value of G´ at -50°C results in a value for M_e of about 800. At 40°C, the highest temperature for which interlayer and polystyrene effects are negligible, one obtains 2000 as the estimate for M_e.

A final calculation, based on minimum value of the loss tangent, gives a direct estimate of M_c, the critical molecular weight for entanglement coupling in these networks. Since tan δ is a ratio of compliances, the correction for filler effects is unnecessary here. From Figure 27 one can estimate the minimum

value of the loss tangent, tan δ_m, and then obtain M_C from the following expression (17, 82)

$$\tan \delta_m = 1.04 \ (M/M_C)^{-0.8} \qquad (4.8)$$

where M is the molecular weight of the entangled linear polymers, 78,000 for SBS-8. The resulting value for M_C is around 1800, and since $M_e \leq M_C/2$, the entanglement molecular weight predicted by this method is under 900.

The M_e values calculated from the mechanical properties data are rather low, but they are much closer to the M_e values characteristic of homopolymers of polybutadiene than the value of 13,000 determined by swelling. The discrepancy between the calculated values and those obtained by swelling could arise for several reasons. The swelling data could conceivably be in error due to some solubility of the polystyrene domains, but as mentioned earlier only a minute quantity of extractable material could be recovered from the swelling solvent. The Kraus correction may not be applicable to these systems as assumed. In particular, it might over-correct the swelling ratio to yield the rather large M_e value of 13,000. However completely ignoring the Kraus correction still results in M_e values greater than 7000 from the swelling data. It is also possible that the calculation of the entanglement density from the mechanical properties data is not completely valid for these filled systems. Also, the effective

volume fraction of filler may be significantly larger than predicted by the measured polystyrene content if there is a significant volume of interlayer present or if the domain geometry is not spherical as presumed. In addition, the polybutadiene may not have reached equilibrium, although at these frequencies near 40°C it should be quite close.

The important point here is not that the true value of M_e is in question. Instead the major concern is that if one accepts the rather low values of M_e calculated from Equations 4.4 to 4.8, the absence of entanglement coupling effects in Series 2 cannot be explained on the basis of the terminal chain length being less than twice the entanglement length for the system and therefore less than M_c. However, it has been suggested (79) that for these model networks the observed entanglement coupling phenomenon arises for reasons slightly different from those discussed above. If the domains are assumed to be separated by a distance which is determined by 78,000 molecular weight of the polybutadiene segments in the triblock, then diblock polybutadiene segment molecular weights in excess of 39,000 would be required before the terminal chains from neighboring domains could span the required distance to entangle with each other. Thus the terminal chains of molecular weights 51,000 and 67,000 are involved in coupled entanglements in this sense, whereas the shorter terminal chains of Series 2, $\bar{M}_n \approx 22{,}000$, are not. This means that entanglements involving terminal chains from neighboring

domains are required before the temperature effects on entanglement coupling become apparent. In this case the particular value of M_e characterisitc of these systems is unimportant to the explanation of the mechanism's presence or absence. This is so because M_C, the critical terminal chain molecular weight for the appearance of the entanglement coupling effects, is no longer defined in terms of M_e. Instead M_C depends only upon the molecular weight necessary to span the half-distance between neighboring domains and is roughly equal to half the triblock polybutadiene segment molecular weight.

In any case, there is overwhelming evidence in the data that M_C is greater than 22,000 for these systems. Assuming that the swelling data are correct and the value of M_C is roughly 2 M_e, one would expect to see the entanglement coupling effects in the data for terminal chains molecular weights greater than 26,000. If M_C is defined by the distance between domains as discussed above, the effects should not appear until the terminal chains have molecular weights in excess of 39,000. Further studies of these systems using many more terminal chain lengths should help to decide which of these interpretations is the more reasonable.

4.233 Entanglement Slippage

The slippage of trapped and untrapped entanglements will cause secondary relaxation or retardation effects to appear in the mechanical response curves at high temperatures or low reduced frequencies. The untrapped entanglements become completely disengaged through this entanglement slippage process so that their contribution to the mechanical properties disappears at very long times. The model networks studied here contain two distinct types of untrapped entanglements -- diblock-diblock and diblock-triblock polybutadiene segment engagements. The retardation processes associated with each of these two types of entanglements will no doubt be quite different, and therefore their effects should appear at different points along the frequency scale. The position of a particular untrapped entanglement along the contributing terminal chain should have a large influence on the characteristic range of retardation times over which the slippage processes for that particular entanglement take place; clearly, those entanglements near the free end of a terminal chain will disengage more easily than those nearer to the fixed end. The influence of neighboring entanglements is likely since trapped entanglements should be more restrictive to neighboring motions than untrapped entanglements. Thus, both terminal chain length and terminal chain content should affect the untrapped entanglement slippage mechanisms. Trapped entanglements (triblock-triblock) cannot become disengaged since all four chains radiating form these entanglements eventually

find their way to a glassy domain. However at low enough frequencies or high enough temperatures when slippage of these chains is permitted, the positions of the trapped entanglements will be continuously changing as the network seeks the most comfortable configuration to accommodate imposed stresses or strains. Thus one can picture a kind of vibrational sliding motion for the chains which take part in trapped entanglements, even though these entanglements cannot become completely disengaged. The characteristic distances (and therefore the associated retardation times) for the sliding of these network chains will depend upon the composition of the network. For example, in the pure triblock where all of the entanglements are trapped, the average distance that a chain can move before meeting another trapped entanglement corresponds to the length of a polybutadiene segment of molecular weight 13,000. (The swelling results are assumed to be correct here.) As the terminal chain content is increased, the probability also increases for the neighboring entanglement to be untrapped and therefore completely or partially disengaged from the network. Thus, the average distance available for the slippage of trapped entanglements increases with terminal chain content, and therefore the characteristic time scale of the process also increases.

The preceeding discussion has been offered to aid the reader in forming a mental picture of the kinds of molecular motions which contribute to the entanglement slippage mechanisms.

In addition, it introduces the concept of multiple overlapping low frequency mechanisms which are sensitive to changes in network structure. Probably the most important and unique feature of this research project is the ability to characterize these mechanisms in terms of known changes in network structure. In earlier studies of entanglement slippage in conventionally cross-linked rubbers conducted by Ferry and coworkers (6-14) this was not possible. For example, in the earliest of these studies (6, 7) it was noticed that low frequency losses increased as cross-link density decreased. However, simply decreasing the cross-link density results in a multitude of structural changes in the network, namely -- increased length of the terminal chains, a greater proportion of untrapped entanglements, longer distances between trapped entanglements, and fewer and more widely spaced points of chemical cross-linking. Interpretation of the results from studies designed to vary the terminal chain content by varying the molecular weight of the primary molecules before cross-linking (7,8) was also difficult owing to the fact that the individual structural features mentioned above could not be controlled independently, and also due to the unknown amount of chain scission which always accompanies cross-linking reactions. It was correctly pointed out (9) that the major effect of entanglement slippage mechanisms was to cause an increase in the compliance from D_{eN}, where all forms of entanglements contribute, to D_e, the equilibrium compliance which contains contributions only from those entanglements

which are permanently trapped. Redefinition of the criteria for entrapment of an entanglement resulted from later studies (10, 19), and this made it possible to attribute this rise in the compliance primarily to relaxation of untrapped entanglements. The possibility of a contribution to low frequency mechanisms from trapped entanglement slippage was not included. Furthermore, although some qualitative predictions for the magnitude and location of the overall low frequency losses were discussed (13, 19), no attempt was made to explain these effects in terms of the several individual mechanisms which contributed to these losses.

A detailed quantitative treatment of the entanglement slippage processes associated with the various types of molecular structural features appearing in the model networks will be given in the next chapter. For the present, the discussion will be aimed primarily at showing that the low frequency slippage processes observed by other authors are also present in the data obtained here. Furthermore, it will be pointed out that the observed low frequency mechanical response changes dramatically as network composition is changed. The discussion will begin with the free oscillation data where the effects of entanglement slippage appear as high temperature (i.e. above the main polybutadiene transition) effects. As usual, the free oscillation data are really useful only to obtain a simplistic picture of the important changes which are occurring. The forced oscillation data are much richer in information concerning the individual molecular mechanisms contributing to the low frequency mechanical response.

It is perhaps easiest to think of the entanglement slippage processes in terms of a viscoelastic transition between two levels of compliance (D_{eN} to D_e). This is formally equivalent, then, to the larger transition between the glassy and rubbery states in polymers. A serious problem arises when one attempts to investigate the mechanisms contributing to the transition between D_{eN} and D_e through the use of the model networks employed here. The viscoelastic transitions associated with the polystyrene and interlayer portions of these materials appear before the transition of interest is completed. In fact, only about one third of the transition form D_{eN} to D_e can be covered before the data begin to reflect polystyrene and interlayer contributions. Even so, the data are very useful for analyzing the individual contributions of the various entanglement slippage mechanisms. The limited range of the data does point out, however, that a better study of entanglement slippage processes could be carried out by using a block copolymer model system with glassy domains of much higher T_g. The limitations of the model are perhaps best seen in the free oscillation storage modulus data shown in Figures 12 to 14. The G' curves never level off completely indicating that the equilibrium modulus of the filled rubbery system is not reached. This means that the entanglement slippage processes are still taking place within the polybutadiene phases of all the model networks when, around 40°C or 50°C, the interlayer and polystyrene contributions become important.

However, below about 40°C where the polybutadiene phase alone is contributing to the decrease in the storage moduli, one can obtain from the free oscillation data useful qualitative information about the entanglement slippage processes. For example, inspection of Figures 12 to 14 shows clearly that the level of the storage modulus across the intertransition region is lowered by the introduction of terminal chains. At equilibrium the terminal chains would constitute a diluent portion of the network as discussed by Flory (2). During the approach to equilibrium the untrapped entanglements are continuously slipping free from their engagements with the network, and thus they behave as an "active diluent" in this region of material response. It is also clear that increased amounts of terminal chains tend to steepen the log G′ vs. T plot in the intertransition region indicating that increased amounts of relaxation are taking place when there are more untrapped entanglements in the network. The small but persistent slope of the storage modulus curve for the SBS-8 triblock results in a much larger drop in G′ than predicted by a temperature correction to an equilibrium modulus. This indicates that slippage of trapped entanglements is also contributing to relaxation processes in the intertransition region.

In an attempt to gain a somewhat more quantitative understanding of this reduction of the storage modulus in the intertransition region, the data from Series 1 were plotted as shown in Figure 32. The values of G′ were corrected for variations

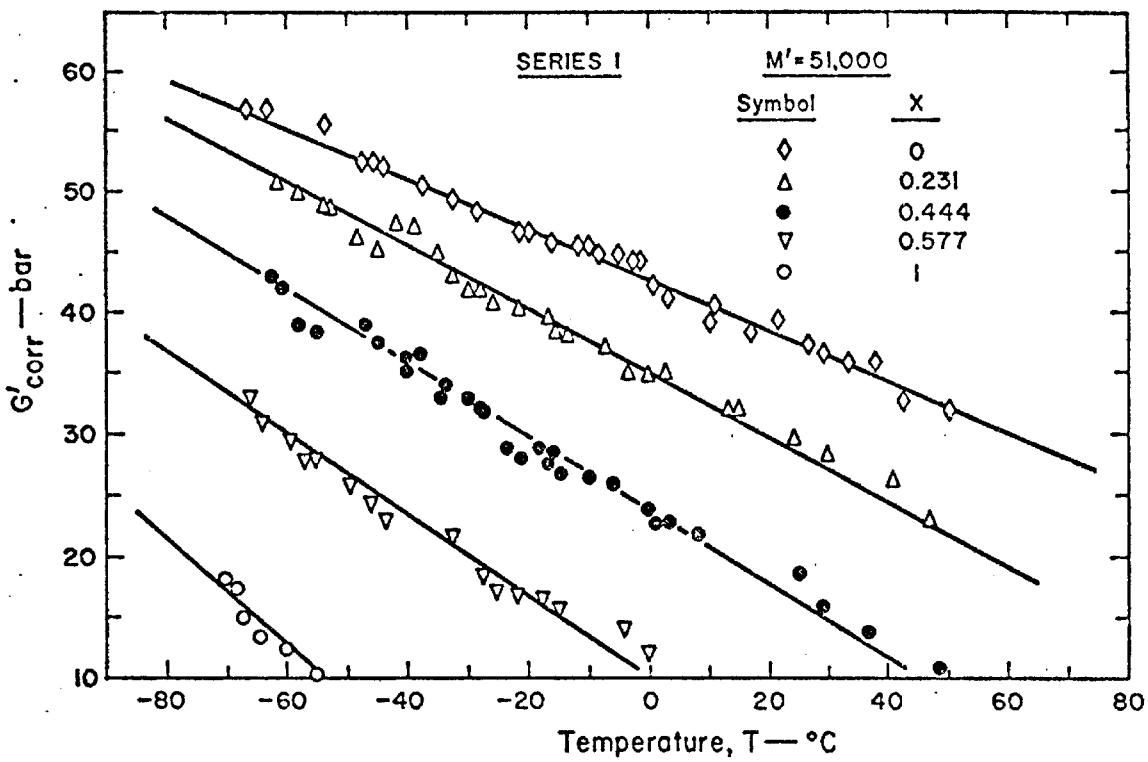

Figure 32.

Corrected Storage Moduli in the Intertransition Region - Series 1

in styrene content as discussed earlier, removing, in this way, any filler effect on the level of the modulus. The fact that there is no equilibrium value of G´ is even more apparent from this figure. It is quite clear that slow relaxation processes are continuously taking place over the entire region. For each of the materials of Series 1, the dependence of G´ on temperature in the intertransition region can be described by a straight line.

Such plots were also made from the data obtained with Series 2 and 3 and showed similar behavior. The slopes of the straight lines were plotted against the amount of terminal chains, X. As shown in Figure 33 this again results in reasonable straight line fits. The point at X = 0.334 is clearly an outlier. These plots are offered merely as an observation because the free oscillation data do not warrant a detailed quantitative interpretation. It will be shown clearly in the next chapter that the behavior seen here must be a consequence of an interplay between several overlapping mechanisms. Figures 32 and 33 do serve, however, to show that the storage modulus in the intertransition region decreases with temperature and that the decrease is more rapid as either the amount of terminal chains increases, or their length decreases. This means that the amount of high temperature relaxation is increased by the introduction of terminal chains. This is to be expected since slippage of untrapped entanglements is the predominant mechanism here and the amount of untrapped entanglements

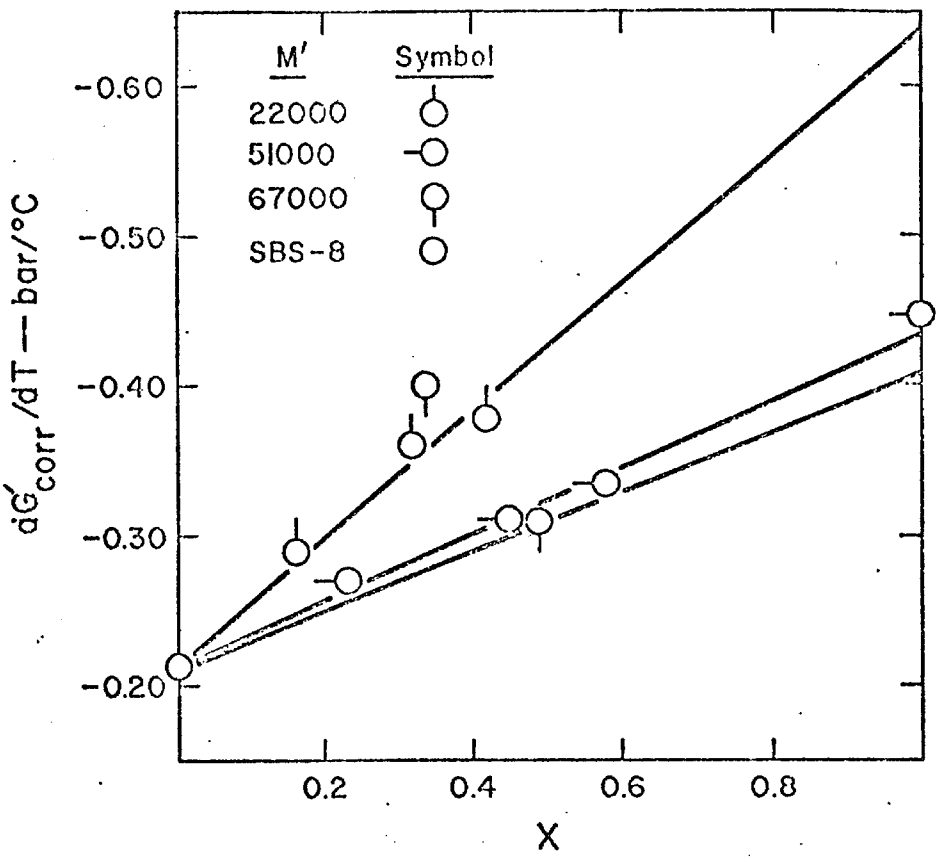

Figure 33.

Effect of Terminal Chain Content and Terminal Chain Length on the Slope of the Storage Modulus in the Intertransition Region

in the network increases with terminal chain content. Figure 33 also indicates that at a fixed terminal chain content, a given amount of relaxation takes place more slowly (i.e. over a wider temperature range) for longer terminal chains.

A relaxation mechanism which is evidenced by a drop in the storage modulus is generally accompanied by the development of a maximum in the loss modulus. In Figures 15 and 16 secondary loss modulus peaks are seen for the blends of Series 1 and 3. These maxima, which become more prominent with increased terminal chain content, are attributed to the relaxation mechanisms and frictional effects associated with the slippage of the untrapped entanglements provided by the terminal chains. There is only one broad secondary peak indicating that the mechanisms associated with the two distinct types of untrapped entanglements must overlap considerably. While it is a very tenuous piece of information, it does appear that the peak value of G'' in the secondary maximum is shifted to slightly higher temperatures for longer terminal chains. The peaks appear near 0°C and 10°C for Series 1 and Series 3 respectively. This is consistent with the observations of the storage modulus behavior which indicated a shift of the entanglement slippage mechanisms to higher temperatures for longer terminal chains.

The absence of any secondary loss peak in Series 2 is also related to this shift in location with terminal chain length. It has already been shown that the short terminal chains of Series 2

are not coupled tightly with the continuous entanglement network. Thus the slippage motions can occur at much lower temperatures for these terminal chains. Their contribution to the loss is already apparent at the base of the main transition and thus no minimum appears from which the loss can rise to form a secondary peak. Relaxation mechanisms due to slippage of the untrapped entanglements are taking place, however, as evidenced by the increased tendency of the Series 2 loss modulus curves to fall off above about -10°C as terminal chain content increases. Perhaps the best way to visualize entanglement slippage for the short terminal chains of Series 2 is to consider the major portion of the intertransition region as the right side of the broad secondary maximum contributed by these mechanisms, with the peak and the left side occurring near the base of the main transition. More convincing evidence will be given later to substantiate this shift of the entanglement slippage process to lower temperatures for the shorter terminal chains of Series 2.

No secondary maximum appeared in the loss modulus data for the SBS-8 triblock to correspond to the observed slow decrease in the storage modulus which has been attributed to trapped entanglement slippage. The peak would be expected to be quite small and very broad since only a small amount of relaxation associated with the trapped entanglements is seen in this type of experiment. Most likely, then, this small peak could not be ovserved and, within experimental error, the loss modulus curve

for SBS-8 appeared to be flat. The forced oscillation measurements were much more sensitive to secondary loss effects and therefore trapped entanglement slippage effects were observed quite clearly.

In Figure 20 a secondary peak in the loss compliance master curve for SBS-8 is clearly evident near log $\omega a_T = -6$. Since, as discussed in detail earlier, polystyrene and interlayer contributions have been effectively removed by restricting the analysis to data obtained below 40°C, and since there are no terminal chains in the triblock, this secondary peak must represent the contribution of trapped entanglement slippage to the low frequency losses. Fesko (25) has already discussed this contribution in some detail. The corresponding storage compliance curve for SBS-8 is slightly sloped across the entire region of frequency above the main transition, also indicating the presence of slow retardation processes. The master curves for SBS-8 are very similar to those obtained by Ferry and coworkers on SBR (9) and polybutadiene (7) vulcanizates of intermediate cross-link densities. As mentioned before, in their studies the molecular sources of the secondary loss peaks were uncertain owing to the lack of precise knowledge of the network structure.

In Figure 26 the entire set of storage and loss compliance master curves for Series 1 were presented. It is clear from this figure that increasing the terminal chain content causes substantial increase in the amount of low frequency retardation processes. The effects appear in both storage and loss behavior, but the loss

compliance is clearly the more sensitive indicator of entanglement slippage effects. The loss tangents for Series 1 shown in Figure 27 reflect this larger effect on the loss compliance. As terminal chain content increases, the secondary (low frequency) peak in the loss tangent ($\tan \delta = D''/D'$) moves to higher values since the loss compliance is increased to a greater extent by the addition of terminal chains. It is also apparent from Figure 27 that the secondary peak in $\tan \delta$ shifts to lower frequencies with increasing terminal chain content, an effect which will be treated in detail in the next chapter.

These compliance master curves and $\tan \delta$ plots for Series 1 behave in a manner qualitatively similar to any series of elastomers of decreasing cross-link density (6-13). As discussed earlier, the observed behavior of the conventionally cross-linked elastomers is a result of several inseparable effects. In these model networks, the observed increase in the amount of low frequency retardation processes can be attributed directly to the increased proportion of untrapped entanglements. With a greater proportion of untrapped entanglements in the network the transition from D_{eN} to D_e is larger and therefore more retardation processes are seen at low frequencies. This is manifested more clearly in the retardation spectra shown in Figure 28 where the number of long retardation times is increased enormously by the introduction of terminal chains, or equivalently untrapped entanglements, into the network. There is some indication that there fewer retardation processes occurring at

intermediate values of time for the material containing a significant proportion of terminal chains. This can be explained qualitatively by recognizing that there are fewer trapped entanglements in this network and therefore longer distances between them. This combination of fewer and more widely spaced trapped entanglements probably resulted in a decrease in their overall contribution to the retardation spectrum and a shift in their contribution to longer times, thus depleting the amount of intermediate-time retardation processes.

The compliance master curves for the single blend studied from Series 3 (terminal chain $\bar{M}_n$ = 67,000) showed qualitatively similar behavior to that just discussed for Series 1. Both the storage and loss compliance of blend BL-3.2 were increased at low reduced frequencies, with the loss again being affected more strongly. There was a slightly deeper minimum in the loss compliance curve for BL-3.2 than observed for the materials of Series 1. This indicates that the overall low frequency process has been shifted somewhat farther downscale for these longer terminal chains so that still fewer retardation processes were seen at intermediate frequencies.

As shown in Figure 25 the blend studied from Series 2 (terminal chain $\bar{M}_n$ = 22,000) also exhibited increased loss and storage compliances at low frequencies. There is a major difference in the behavior of this material, blend BL-2.3, at intermediate frequencies however. The minimum in the loss compliance near log ωa_T = -2 was not as deep as seen in the other

two series. Furthermore, the loss compliance values at frequencies immediately above log $\omega a_T = -2$ were noticeably higher than those seen in Series 1 and 3. Also, the storage compliance rises more steeply just above the main transition indicating that there are retardation processes occurring in this material at relatively high frequencies. These processes reflect the same untrapped entanglement slippage mechanisms seen in Series 1 and 3; their location at higher reduced frequencies is a result of the rather short terminal chains involved here.

In the most general sense, the entanglement slippage processes contribute to the rise in compliance from D_{eN} to D_e; if one considers D_e to be a measure of the total number of retardation processes available to the material, then the effect of increasing the proportion of untrapped entanglements through the addition of terminal chains is to greatly increase this total number of retardation processes. At equilibrium the length of the terminal chains in the network is unimportant since the level of D_e depends only upon the relative proportions of stress bearing and diluent components in the network. Thus, all blends with the same terminal chain content, X, should have the same equilibrium compliance, and therefore they should undergo the same total <u>amount</u> of retardation processes over whatever frequency range is necessary to make the transition from D_{eN} and D_e. However, the nature of the <u>approach</u> to equilibrium, or equivalently the location along the

frequency scale of the various mechanisms which contribute to the rise from D_{eN} to D_e, will greatly depend upon the particular length of the terminal chains in the network.

We have covered only the very beginning of this approach to equilibrium with the data discussed here. Even so, it has been seen clearly that shorter terminal chains contribute their retardation processes at higher frequencies or lower temperatures. It has also been apparent that the contributions from various entanglement slippage processes occur at different positions along the frequency scale depending upon the relative amounts of trapped and untrapped entanglements in the network. The mathematical model developed in the next chapter treats the individual contributions of trapped and untrapped entanglements in a more quantitative manner and accounts for the possibility of a changing location along the frequency scale for each contributing retardation mechanism. However, before launching into the development of this mathematical model, it will be useful to pause briefly to summarize the rather lengthy discussion given here and to draw some conclusions.

4.3 Summary and Conclusions.

One hesitates to make sweeping summarizing statements or to draw narrow conclusions from the large body of information presented in this chapter. However, readers of lengthy works often look for statements of this sort hoping to find a key concept or result of particular interest. Hopefully anyone who begins his reading with

this section will return to the discussion for details and to the data presented in advance of the discussion so that he may consider more deeply the implications of the brief statements made here.

(1) In the most general sense, this research project has shown rather clearly that model systems can be used successfully to study the effects of varying network structure on the mechanical properties. The model networks generally behaved similarly to conventional elastomers, but there was the added advantage here that changes in mechanical behavior could be correlated with controlled changes in network structure. This will be considered in still more detail in Chapter 5. The model systems studied here had some inherent limitations, but a significant amount of useful information still was obtained. Proposed improvements in the model system will be discussed in Chapter 6.

(2) Annealing of the block copolymer samples produced significant irreversible dimensional changes which reflected the orientation induced during the casting process. Annealing temperatures above the glass transition temperature of the polystyrene phase were required for nearly complete removal of these orientation effects.

(3) The polystyrene and interlayer contributions to the mechanical properties of these two-phase materials overlapped with some of the interesting effects occurring in the polybutadiene phase. However, to a very good approximation, the data below 40°C

reflected viscoelastic mechanisms which were characteristic of the polybutadiene phase alone.

(4) The mechanical behavior of the polybutadiene phase of the model networks was thermorheologically complex. The horizontal shift factors used to carry out the temperature reduction of the forced oscillation data did not follow any of the commonly observed equations. Instead the shift behavior appeared to reflect two different temperature dependent mechanisms, with significant overlap between them. Even so, the data were reduced by conventional shifts with the knowledge that the resulting master curves were probably not strictly valid. All data were handled in a consistent manner so that differences in the master curves would truly reflect differences in the mechanical behavior of the materials.

(5) The terminal chains in all three Series had no effect on the mechanical behavior of the materials in the glassy and polybutadiene transition regions.

(6) The mechanical properties of the blends of Series 1 and 3 reflected the presence of a temporary entanglement coupling network which involved the rather long terminal chains of these materials. This portion of the network tended to weaken as temperature increased; as a result, minima appeared in the free oscillation loss modulus curves and a superposition anomaly became evident in the forced oscillation data. The superposition anomaly was resolved by a second temperature reduction known as the μ-shift.

The materials of Series 2 contained much shorter terminal chains and the effects of a temperature dependent entanglement coupling mechanism were not seen in the mechanical response curves. Two different explanations were proposed for the absence of the mechanism in Series 2; both were related to the inability of the short terminal chains to engage in a coupled entanglement network.

(7) The entanglement slippage of the trapped and untrapped entanglements contributed to low frequency retardation mechanisms. There was generally more viscoelastic response occurring at low frequencies for materials containing larger quantities of terminal chains. The overall effect of terminal chains was to increase both the storage and the loss compliance at low frequencies; the loss was affected more strongly, however, so that increased terminal chain content increased the level of tan δ. The locations of the various low frequency retardation mechanisms were not fixed and appeared to be related to both terminal chain content and terminal chain length. It was evident that longer terminal chains contributed to the mechanical response at lower frequencies.

CHAPTER 5

DEVELOPMENT OF A MATHEMATICAL MODEL FOR A QUANTITATIVE TREATMENT OF THE EFFECTS OF TERMINAL CHAINS AT LOW REDUCED FREQUENCIES

A major goal of this research was the identification of the roles of terminal chains and various types of chain entanglements in elastomeric materials. This goal has been accomplished, at least qualitatively, by supplying the data which were presented and discussed in the previous chapter. Because the rubbery networks of the block copolymer blends were reasonably well characterized, it was possible to examine the various regions of material response and identify, in a systematic way, changes in material behavior with changes in network structure. This procedure resulted in the list of conclusions given at the end of the previous chapter.

It is tempting to carry the analysis one step further; namely, to combine in a non-arbitrary manner the various effects already identified and then compare the synthesized response curves with those obtained experimentally. Of course, if each response curve is broken down into separate contributions and then recombined to yield observed behavior, no information is gained. If, however, the data obtained on one or two materials can be used to predict the response of all the others, the model used to accomplish this

may contain some useful information concerning the nature of the individual molecular mechanisms and the manner in which they combine to give the overall material response.

The model developed in this chapter should not be considered to constitute a molecular theory for polymers containing significant amounts of chain entanglements. Such theories have been the object of numerous investigations, and the varying degrees of success and applicability of these studies have been summarized adequately (17). These theories generally provide a spectrum of relaxation times which is expressed in terms of molecular parameters. The spectrum can then be used to calculate the overall material response, and often certain features of the spectrum enable the low frequency response associated with entanglement slippage to be predicted adequately. However little information is available on the fine structure, i.e. on the individual viscoelastic mechanisms which make up this spectrum. In the approach taken here a beginning spectrum is estimated from the data. The spectrum is then changed by shifting the weight of the various separate contributions and by changing the location of each contributing mechanism along the frequency scale. These changes in weighting and location are predicted, through the use of the model to be developed, in terms of the known changes made in the structure of the networks studied here. It will be desirable to have a minimum of arbitrary parameters in the model so that one can obtain a clear picture of the manner in which the

characteristics of the network affect the mechanical properties. Useful parameters, then, are those which are well known for the block copolymer blends, namely:

M_e - molecular weight between entanglements in the pure triblock; determined as 13,000 from swelling measurements.

M' - molecular weights of the polybutadiene segments of the various diblocks, i.e. the terminal chain molecular weights; 51,000, 22,000 and 67,000 for SB-6, SB-7 and SB-5 respectively.

M - molecular weight of the polybutadiene segments of the triblock; 78,000 for SBS-8.

X - weight fraction of terminal chains in the polybutadiene phase of the diblock-triblock blends.

A considerable portion of this chapter will be devoted to the task of determining the parameters of the model in terms of the network parameters listed above. After this has been accomplished, the response curves predicted by the model will be compared with those obtained experimentally.

5.1 The Model

A generalized Voigt model is often used to represent the linear viscoelastic behavior of polymers. The appropriate expressions for the storage and loss compliances are

$$D'(\omega) = D_g + \sum_i D_i/(1 + \omega^2 \tau_i^2) \tag{5.1}$$

$$D''(\omega) = \sum_i D_i \omega\tau_i/(1 + \omega^2\tau_i^2) \tag{5.2}$$

In these expressions the summation over i accounts for a distribution of retardation times, τ_i, with associated spectral strength, D_i. Equations 5.1 and 5.2, depending upon the choice of the D_i and τ_i values, can represent a single viscoelastic mechanism (usually the main transition near the T_g of the material) rather well. The constant D_g appearing in Eq. 5.1 represents the glassy compliance of the material. The value of D_g is roughly the same for a wide variety of polymers, and, except at the very highest frequencies of interest, it is entirely negligible in comparison with the summation.

A simple modification of the generalized Voigt model, allowing for the possibility of additional viscoelastic mechanisms each with its own spectrum of retardation times, results in the following expressions for the storage and loss compliances:

$$D'(\omega) = D_g + \sum_{k=1}^{n} \sum_{i=1}^{n_k} D_{ik}/(1 + \omega^2 \tau_{ik}^2) \qquad (5.3)$$

$$D''(\omega) = \sum_{k=1}^{n} \sum_{i=1}^{n_k} D_{ik}\, \omega\tau_{ik}/(1 + \omega^2\tau_{ik}^2) \qquad (5.4)$$

The value of the index k indicates which of the n contributing viscoelastic mechanisms is being considered. Each of the mechanisms will have a different set of retardation times associated with it, a total of n_k values of τ_{ik} for the kth mechanism. The D_{ik} values represent the weighting or degeneracy for each τ_{ik}.

Equations 5.3 and 5.4 are formally equivalent to the transient network model of Lodge (83), but the interpretation of the parameters on a molecular level is somewhat different. Furthermore there is no method for weighting the various mechanisms in the Lodge model. The expressions actually represent the addition of several groups of Voigt elements whose contributions appear at various positions along the frequency scale. In this sense Equations 5.3 and 5.4 can be considered as a generalization of the more restricted model for the behavior of entangled polymers proposed by Ferry and coworkers (84).

If left completely unrestricted in terms of the choices of values for n and the various τ's and D's, Eqs. 5.3 and 5.4 could be made to fit nearly any observed response. From this point of view they represent an extremely convenient starting point from which to build a model. Curve fitting is not the

purpose of this work however, and thus the choice of values for the parameters of the model will be dictated by the molecular structure of the networks. If the structure is not reasonably well characterized in terms of quantities such as M_e, M', M and X, then the choice of values for the parameters becomes arbitrary and the model is of little practical importance.

5.2 Determination of the Model Parameters from Known Network Structure

It is apparent from Eqs. 5.3 and 5.4 that the parameter which should be determined first is n , the number of viscoelastic mechanisms contributing to the mechanical response. For the triblock, containing no terminal chains, it is easily seen from the data that n = 2 is the appropriate value, k = 1 corresponding to the main transition and k = 2 accounting for the trapped entanglement slippage mechanism. The model is not expected to account for interlayer or polystyrene behavior because it is concerned with the behavior of the polybutadiene phase only.

For the diblock-triblock blends, the value of n is not immediately apparent. However, knowing the structure of the rubbery networks, it is easy to decide upon n = 4 with the following mechanisms being assumed:

k=1 short range motions near T_g of the polybutadiene phase

k=2 trapped entanglement slippage motions involving two triblock polybutadiene segments

k=3 slippage of untrapped entanglements involving diblock polybutadiene segments (terminal chains) and triblock polybutadiene segments

k=4 slippage of untrapped entanglements involving two terminal chains

Each of these mechanisms must now be identified with a certain number of retardation times which distribute themselves in some manner along the time or frequency scale.

If we first consider the region of material response at very low frequencies, each of the viscoelastic mechanisms will have contributed its entire effect in Eq. 5.3. The storage compliance will have reached some limiting equilibrium value, D_e, which is a sum of the individual contributions from each of the four mechanisms listed above. Thus, the following condition holds at very low frequencies:

$$\sum_{k=1}^{4} \sum_{i=1}^{n_k} D_{ik} = D_e - D_g \simeq D_e \qquad (5.5)$$

where, as indicated earlier, the glassy compliance can be neglected.

Equation 5.5 gives D_e as the total number or total degeneracy of all the retardation times characterizing the material. It does not indicate how these are distributed among the individual mechanisms and does not give any means of deciding upon a numerical value for D_e. To solve both of these problems we begin by using the base material, SBS-8, as a reference.

The numerical value of the equilibrium modulus for the triblock material, designated D_e^t here, can be obtained by integrating over the entire retardation spectrum. In Figure 34 the retardation spectrum for SBS-8 is replotted using a linear vertical scale. The right side of the secondary peak has been assumed to be symmetric with its left side. The apparent persistence of the calculated spectrum at long times above the assumed shape may be explained, at least partially, by the onset of polystyrene and interlayer contributions. The validity of the symmetry assumption cannot be proven; this simply represents a reasonable way to estimate the total long-time contribution to the equilibrium compliance. The resulting value for D_e^t is $10^{-1.84}$ bar^{-1}.

In the triblock there are only two contributing mechanisms, corresponding to k=1 and k=2. The total number of retardation times for the triblock can therefore be split into two fractions, Z_t associated with the main transition and $1-Z_t$ with the trapped entanglement slippage mechanism. The linear scale of Figure 34 allows the spectrum for SBS-8 to be separated easily into two peaks. The numerical value of Z_t is then

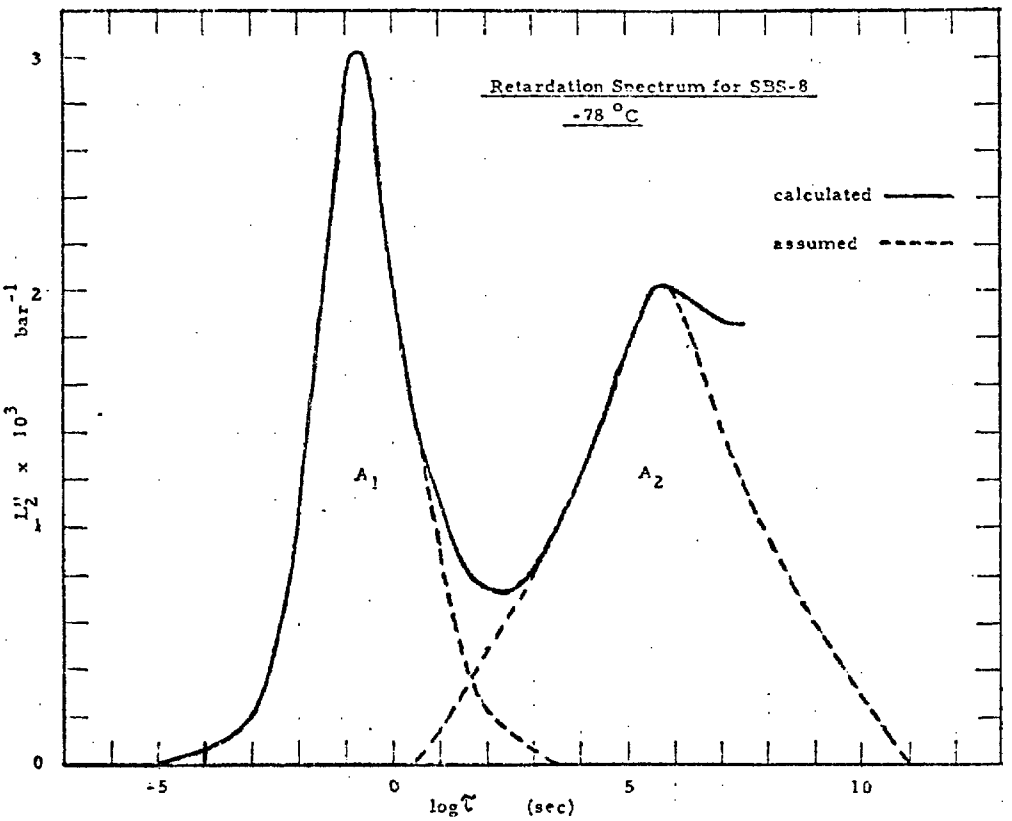

Figure 34.

SBS-8 Retardation Spectrum - Linear Scale

determined as the ratio of the area under the main peak to the total area, or

$$Z_t = A_1/(A_1 + A_2) \tag{5.6}$$

where the A's represent the areas shown in Figure 34. This results in a value of 0.419 for Z_t, and this value represents the fraction of the SBS-8 equilibrium compliance contributed by the main transition.

Having established that there are $D_e^t Z_t$ retardation times associated with the main transition and $D_e^t (1 - Z_t)$ for the entanglement slippage mechanism, and knowing the distribution of these times as given by Figure 34, it is possible to duplicate the experimentally observed response curves for the triblock material. This is accomplished by choosing values of τ_{ik} at equally spaced intervals of 0.25 decade along the time scale, reading the corresponding value of L_{ik} (i.e. the strength of the spectrum at τ_{ik} on the kth peak), and calculating the appropriately weighted spectral strength for use in Eqs. 5.3 and 5.4 from the relations

$$D_{i1} = D_e^t Z_t (L_{i1} / \sum_{i=1}^{n_1} L_{i1}) \tag{5.7}$$

$$D_{i2} = D_e^t (1 - Z_t)(L_{i2} / \sum_{i=1}^{n_2} L_{i2}) \tag{5.8}$$

where the division of each L_{ik} by the summation constitutes a normalization of the area under each peak to unity. In this way the total number of retardation times is assured to be equal to D_e^t regardless of the vertical scale of the L vs. log τ plot. The values of n_1 and n_2 were 34 and 43 respectively. It will be seen later that this procedure results in excellent reproduction of the experimental curves for SBS-8. This indicates that the assumed shape of the right side of the retardation spectrum was reasonable.

As stated earlier, curve fitting is not the purpose of this work. However it was necessary to use the triblock data to establish these base constants, D_e^t and Z_t, which provide a reference point for calculating the parameters associated with the diblock-triblock blends. It will become clear that the value of D_e^t actually represents a scale factor which assures that the calculated response curves will appear at the same numerical level as the observed behavior. The entire scheme could be made dimensionless by dividing the observed material response data and both sides of Eqs. 5.3 and 5.4 by D_e^t.

It is now possible to determine the model parameters corresponding to a general diblock-triblock blend containing a weight fraction X of terminal chains of molecular weight M'. Inspection of the data, has revealed that the presence of two additional retardation mechanisms in the blends results in an increase in the total number of retardation times from D_e^t to some

larger value, say $D_e(X)$, where a dependence on terminal chain content is already anticipated. However, the shape and numerical values for all the material response curves were identical in the main transition region. These two observations result in the following two conditions:

$$D_e(X) = D_e^t/f(X) \tag{5.9}$$

$$D_e(X)\ Z(X) = \text{const.} = D_e^t\ Z_t \tag{5.10}$$

where $D_e(X)$ and $Z(X)$ represent the parameters for a blend of terminal chain content X, and $f(X)$ represents the fraction of all the entanglements in the blend which are effective at equilibrium, i.e. the fraction of trapped entanglements. An explicit expression for $f(X)$ will be developed presently.

Equation 5.9 is simply a restatement of Equation 1.1 which predicted a decrease in the equilibrium modulus as the number of effective linkages decreased. Since the equilibrium compliance and modulus are related reciprocally, Equation 5.9 follows immediately. Equation 5.10 is a mathematical formulation of an effect already observed in the data, namely that D_{eN} is identical in all materials. This is so because D_{eN} is simply the integral over the first peak in the retardation spectrum and this is precisely the contribution accounted for by Equation 5.10. Since D_{eN} is a reflection of the total number of entanglements

comprising a network before any slippage or long range molecular rearrangements begin to occur, both diblock and triblock polybutadiene segments must have the same characteristic entanglement length so that the total concentration of entanglements can be independent of X. Equation 5.10 also carries the implicit assumption that any μ-shift scheme has been referred to some low temperature within the main transition. In addition any differences in the level of the compliances due to variations in filler content must be taken into account. These requirements are consistent with the manner in which the data were handled.

The major significance of Equation 5.10 as far as the model is concerned is that it introduces an adjustable parameter, Z(X), which assures that all of the response curves calculated from the model will be identical in the region of the main transition. Thus, the model defines the main transition by curve fitting to agree with experimental observation, and therefore it cannot generate any useful information concerning the behavior of these materials in the transition region.

Equations 5.9 and 5.10 define for any blend the total number of retardation times, $D_e(X)$, and the fraction of these, Z(X) which are associated with the main transition. This leaves a fraction 1 - Z(X) of the total number of retardation times to be distributed among the three remaining mechanisms. This breakdown can be handled in terms of network parameters if two assumptions are made. First, it is necessary to assume that diblock and

triblock polybutadiene segments have the same characteristic entanglement length, an assumption already discussed in some detail in the previous chapter and in connection with Equation 5.10 above. The second assumption involves the effectiveness of the various types of entanglements in their contribution to the frequency dependent material behavior. It is assumed here that each type of entanglement contributes in such a way so that the number of retardation times attributed to each of the three mechanisms associated with entanglements (k=2-4) will be proportional to the probability of finding each type of entanglement in the network.

The probabilities of finding a diblock segment or a triblock segment at some point in the network are X and 1-X respectively. Under the first assumption above, the probabilities that a diblock or a triblock segment will enter into some kind of entanglement are also equal to X and 1-X respectively. Then the chance of finding two triblock segments at the same point, i.e. the probability of finding a trapped entanglement, can be expressed as 1-X times 1-X, or $(1-X)^2$. Similarly, a diblock-diblock untrapped entanglement would be expected to occur with probability X^2. The diblock-triblock untrapped entanglements involve two possibilities, chain A originating from a diblock segment and chain B from a triblock segment, or vice versa. Thus a factor of two enters the expression 2 X(1-X) which is the probability of finding an untrapped

entanglement of the diblock-triblock type. The probabilities sum to unity as required. In summary:

$$\begin{aligned} p(k=2) &= p \text{ (trapped entantlements)} &&= (1-X)^2 \\ p(k=3) &= p \text{ (diblock-triblock entanglement)} &&= 2\,X(1-X) \\ p(k=4) &= p \text{ (diblock-diblock entanglement)} &&= X^2 \end{aligned} \tag{5.11}$$

$$\sum_{k=2}^{4} p(k) = 1$$

Knowledge of these probabilities allows the number of retardation times in each of the four mechanisms to be expressed in terms of the terminal chain content of the material. Writing W_k for the number of retardation times associated with mechanism k, we obtain

$$\begin{aligned} W_1(X) &= [D_e(X)][Z(X)] \\ W_2(X) &= [D_e(X)](1 - Z(X)][(1 - X)^2] \\ W_3(X) &= [D_e(X)][1 - Z(X)][2\,X(1 - X)] \\ W_4(X) &= [D_e(X)][1 - Z(X)][X^2] \end{aligned} \tag{5.12}$$

where[8]

$$D_e(X) = D_e^t/(1 - X)^2 \tag{5.13}$$

and

$$Z(X) = Z_t(1 - X)^2 \tag{5.14}$$

The first of Eqs. 5.12, along with Eqs. 5.13 and 5.14, clearly satisfies the condition set on Z(X) by Eq. 5.10. To obtain Eq. 5.13 the expression $(1 - X)^2$, the fraction of trapped entanglements in a blend, was substituted for the unknown function f(X) appearing in Eq. 5.9.

The set of equations 5.12 to 5.14 completely determines the change in weighting of the various mechanisms, i.e. the change in the number of retardation times in each, as the terminal chain content, X, is varied. Equations 5.12 are plotted in Figure 35 using the values of D_e^t and Z_t determined earlier. The absolute weighting factors, W_k, are plotted here, and the transfer of weight among the various mechanisms is difficult to see since the total number of retardation times is always increasing with terminal chain content. For this reason, the relative weighting factors, W_k/D_e, are plotted in Figure 36. The change in the relative importance of each of the individual

---

[8] It is clear that a restriction of $X < 1$ is required here. It will be seen later that the entire analysis must be restricted to values of X less than some critical value which is characteristic of the model system. It is also interesting to note that Oberth (15) observed that the measured equilibrium moduli of urethane elastomers containing significant amounts of terminal chains decreased by a factor $(1-V)^2$, where V was the volume fraction of terminal chains. Since $V \simeq X$ this is a good indication that Eqs. 5.12 to 5.14 have been formulated correctly.

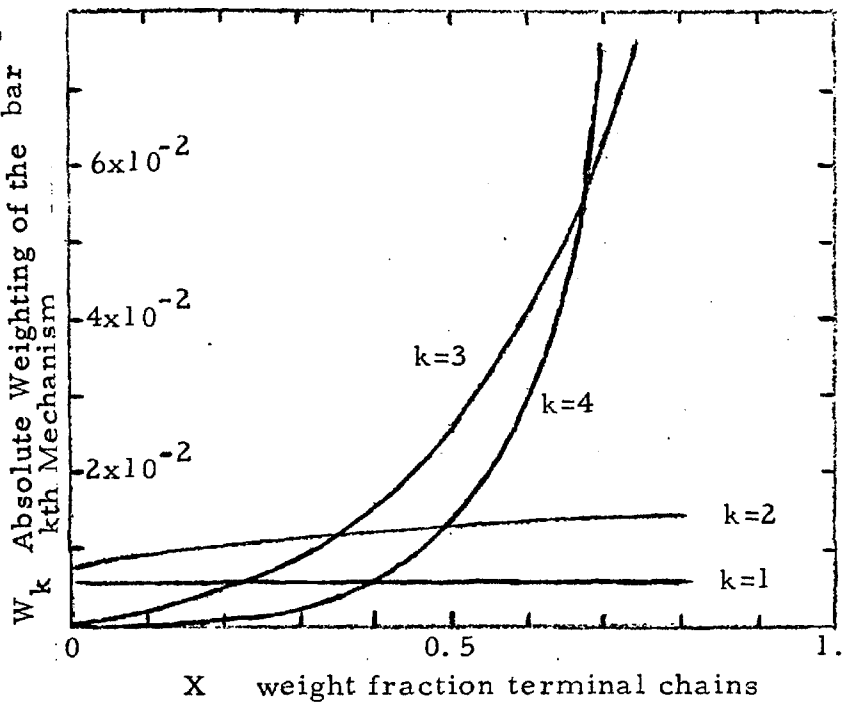

Figure 35.

Absolute Weighting of the
Individual Retardation Mechanisms

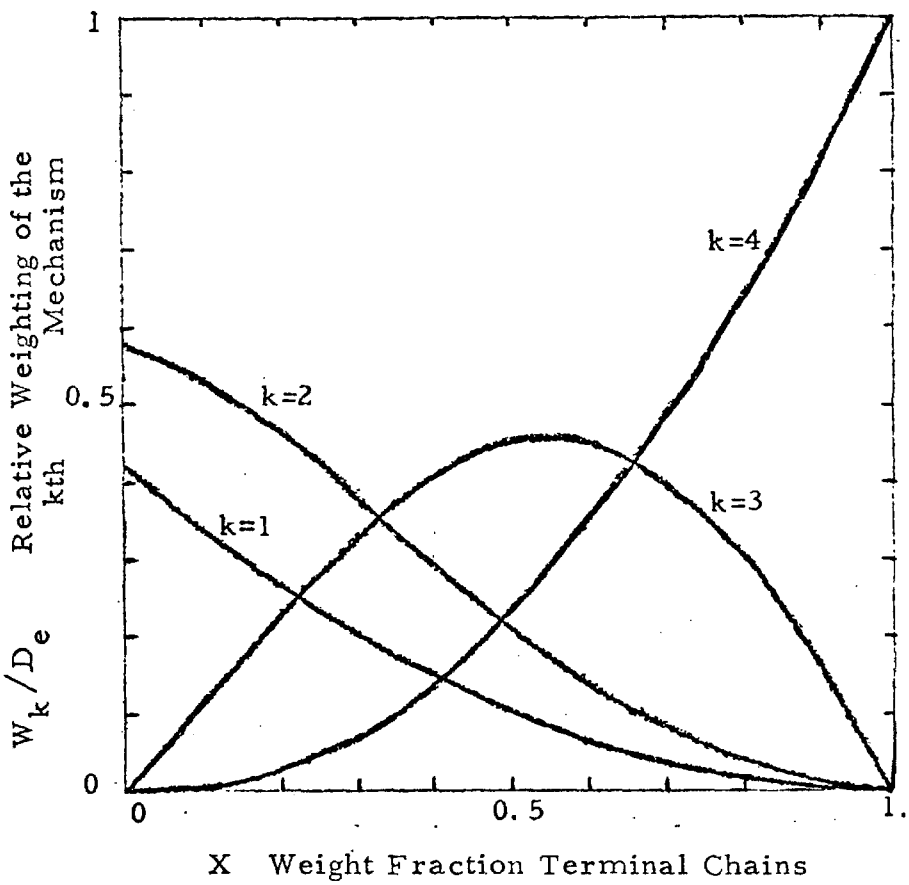

Figure 36.

Relative Weighting of the
Individual Retardation Mechanisms

mechanisms is apparent when the equations are plotted in this way. It is particularly interesting to see the manner in which the dominance in the entanglement slippage process changes progressively from mechanism 2 to 3 to 4 as terminal chain content increases.

Knowing the manner in which the retardation times are distributed among the four mechanisms, each D_{ik} value which enters into Eqs. 5.3 and 5.4 can be written as

$$D_{ik} = W_k \left(L_{ik} / \sum_{i=1}^{n_k} L_{ik}\right) \tag{5.15}$$

for each selected value of τ_{ik}. As before, the factor in parentheses gives the normalized value of the strength of the retardation spectrum for the kth mechanism at position τ_{ik} on the time scale. For the triblock, the values of L_{ik} for the two mechanisms contributing to the mechanical behavior could be determined directly from Figure 34. However, at this point the L_{ik}'s and corresponding τ_{ik}'s are unknown for the diblock-triblock blends. Thus, we are confronted with the problem of determining both the location and the shape of the four individual retardation spectra contributing to the mechanical response of the blends.

5.3 Location of the Retardation Spectra of the Individual Entanglement Slippage Mechanisms

It has already been shown that both the shape and the location of the main peak are fixed for all the materials. Thus only mechanisms 2 to 4 need to be considered in this section. For the triblock, the location of the trapped entanglement slippage mechanism was established by the peak in the calculated retardation spectrum at $\log \tau = 5.75$. It is now necessary to decide whether this location should also characterize the slippage of trapped entanglements in a blend containing a significant proportion of terminal chains.

It was pointed out in the previous chapter that the average distance between trapped entanglements increases as terminal chains are added to the network. In particular, with M_e indicating the known molecular weight (13,000) between trapped entanglements in the triblock, the molecular weight between trapped entanglements in a blend, M_{e*} can be found from the expression

$$M_{e_*} = M_e\left\{\frac{\text{total number of sites available for trapped entanglements}}{\text{number of trapped entanglements in the network}}\right\}.$$

The probabilities presented in Eqs. 5.11 can be used to evaluate the ratio in parentheses above. The denominator will clearly be proportional to $(1 - X)^2$, the probability of finding a trapped entanglement in the network. The numerator should reflect only the probabilities of triblock-triblock and diblock-triblock

entanglements, since diblock-diblock junctions do not constitute possible sites for trapped entanglements. Thus the numerator incorporates the sum of the first two of Eqs. 5.11 and is proportional to $1 - X^2$. The proportionality constant is the total number of entanglements in each case, and therefore it cancels from the expression for M_{e*}. The resulting expression for the molecular weight between trapped entanglements in a blend is

$$M_{e*} = M_e (1 + X)/(1 - X) \tag{5.16}$$

Equation 5.16 is not completely unrestricted in terms of terminal chain content. Since M_e is known to be 13,000, all values of X greater than 5/7 will predict a molecular weight between trapped entanglements which is greater than 78,000, the molecular weight of the triblock polybutadiene segments. This situation is clearly not physically realistic, and therefore a critical value of $X = 5/7$ must not be exceeded for the analysis to be meaningful.

This critical value of terminal chain content, X_c, represents the point at which it is no longer possible to have, on the average, one trapped entanglement on every triblock polybutadiene segment. At this point the system may no longer be regarded as one continuous interconnected entanglement network, and therefore the analysis should not be expected to be valid. The value of 5/7 for X_c resulted from the particular values of M and M_e for the system used in this study. In general

$$X_c = \frac{(M/M_e) - 1}{(M/M_e) + 1} \tag{5.17}$$

Returning to Eq. 5.16, we see that the distance between trapped entanglements increases in a well defined manner with X as long as X is less than X_c. Therefore, it might be expected that the time scale of the trapped entanglement slippage mechanism would also vary with X. A rather general prediction of several of the molecular theories (Ref. 17, Ch. 10) for cross-linked and entanglement networks is that the retardation time characteristic of a given viscoelastic mechanism increases as the square of the length of the molecular strands entering into the mechanism. Thus one should expect the location of the retardation spectrum characterizing the trapped entanglement slippage mechanism to shift to longer times in proportion to the square of the distance between trapped entanglements. Using Eq. 5.16 and the known value of $\log \tau = 5.75$ for the location of the peak associated with trapped entanglement slippage in the triblock, one obtains

$$\log \tau_{p2} = 5.75 + 2 \log (1 + X)/(1 - X) \tag{5.18}$$

Here τ_{p2} represents the location of the peak of the spectrum for the mechanism corresponding to $k = 2$, i.e. the slippage of trapped entanglements. The shape of the spectrum around the shifted peak location will be treated in the next section.

The location of the peak for the retardation spectrum associated with mechanism 4, which accounts for slippage of diblock-diblock entanglements, can be calculated by an analogous procedure. The value of log τ = 5.75 is chosen again as the location characteristic of a mechanism involving polybutadiene strands of molecular weight 13,000. Since the diblock segments cannot enter into any trapped entanglements, the effective strand length characterizing the location of the peak in their retardation spectrum is the entire length of the diblock polybutadiene segment, M'. Thus the peak in the spectrum for mechanism 4 will be located by the relation

$$\log \tau_{p4} = 5.75 + 2 \log (M'/M_e) \tag{5.19}$$

As with Eq. 5.18 this relation locates the peak in the spectrum but does not give any information concerning the manner in which the appropriate number of retardation times for mechanism 4 are distributed around this peak value.

Locating the peak for the spectrum of mechanism 3 is more difficult because it is not possible to identify clearly an effective strand length associated with the diblock-triblock junctions. Along the triblock chain which enters into the entanglement, there will be a distance between trapped entanglements as defined by Equation 5.16. The diblock chain will not see any trapped entanglement along its entire length as discussed above. Taking a simple average of the

two characteristic lengths, one along the diblock segment and the other along the triblock segment, results in the following expression for the location of the peak in the retardation spectrum for mechanism 3:

$$\log \tau_{p3} = 5.75 + 2 \log \left[\frac{M_e (1+X) + M'(1-X)}{2 M_e (1-X)} \right] \qquad (5.20)$$

There are several interesting and important features of the particular manner in which the peaks of the various spectra were located. The peak positions were determined in a non-arbitrary way by determining shifts from the position of the one mechanism which could be located in the data. The shifts were calculated under the assumption that the locations of the peaks of the various spectra were related to the average distance to the nearest trapped entanglement as seen from the particular type of entanglement in question. Because the networks of the diblock-triblock blends were well characterized, these shifts could be described in terms of known quantities.

The locations of the peak values of the spectra for mechanisms 1 to 4 are plotted in Figure 37 as a function of terminal chain content for a terminal chain molecular weight of 51,000. It is interesting that different mechanisms contribute to the lowest-frequency response of the material depending upon the terminal chain content. The behavior shown in Figure 37 explains to some extent the observation that very lightly cross-linked polymers exhibit retardation

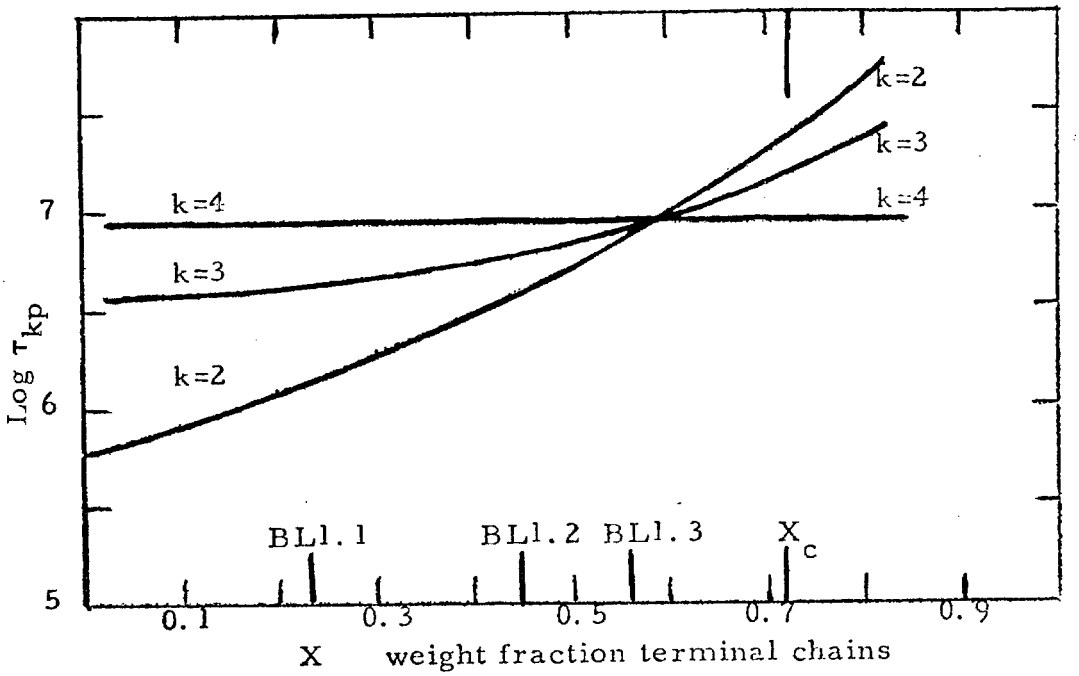

Figure 37.

Locations of the Spectra for the Individual Retardation Mechanisms - Series 1

mechanisms at significantly longer times than the corresponding uncross-linked polymer (11). The crossover of the curves in Figure 37 clearly indicates that one must be cautious in placing the mechanisms associated with various types of network junctions in a particular order along the time scale because the order is likely to change as the network composition changes. Figures 36 and 37 give a very clear indication of the complicated and changing manner in which the different mechanisms contribute to the low frequency response.

Having determined the number of retardation times associated with each mechanism and the location of the peak in the retardation spectrum for each mechanism, it is now necessary to define a shape for each of the retardation spectra. That is, it is necessary to establish the manner in which the appropriate number of retardation times associated with each mechanism distribute themselves around the peak value located in this section.

5.4 Shapes of the Individual Retardation Spectra

For the main transition in all the materials and for the trapped entanglement slippage mechanism in the triblock, the spectral shapes are given by the two separate peaks of Figure 34. It is reasonable to assume that the shift to longer times of the trapped entanglement slippage mechanism occurs without any significant change in shape of its retardation spectrum. If this is the case, the second peak of Figure 34 defines the retardation spectrum for mechanism 2 in the blends also. Thus, Figure 34 defines the shapes of the spectral distributions for mechanisms 1 and 2 for all the materials.

Defining spectral shapes for mechanisms 3 and 4 is particularly troublesome because their effects have not been separated clearly anywhere in the data. However, if one is willing to assume that the spectra for mechanisms 3 and 4 will exhibit the same shape, it is possible to use the available data to obtain an estimate of this shape. Figure 28 shows the calculated retardation spectra for SBS-8 (X=0) and for BL-1.3 (X=0.577). Use of Eqs. 5.18 to 5.20 reveals that the peaks in the spectra for mechanisms 2 to 4 in BL-1.3 lie nearly in coincidence around a position of log τ = 7.0 on the time scale. (See Figure 37.) This fortuitous result allows the shape of the left side of the spectrum for mechanisms 3 and 4 to be calculated by subtracting the spectrum for mechanism 1, after shifting its peak to log τ = 7, from the corresponding portion of the spectrum for BL-1.3. From a peak value of log τ = 7.0, the shape of the descending right side of the spectrum for both mechanisms 3 and 4 is assumed to be identical with that of mechanism 2.

This rather rough estimate results in a somewhat steeper ascent from the left to the peak value for the spectrum of mechanisms 3 and 4 when compared to the spectrum characterizing mechanism 2. That is, the spectrum for mechanisms 3 and 4 is skewed toward longer times, a result which may have been anticipated intuitively. Figure 38 shows the shapes of the individual spectra for mechanisms 1 to 4 plotted on a linear vertical scale. Because the earlier analysis included a normalization before assigning a particular number of

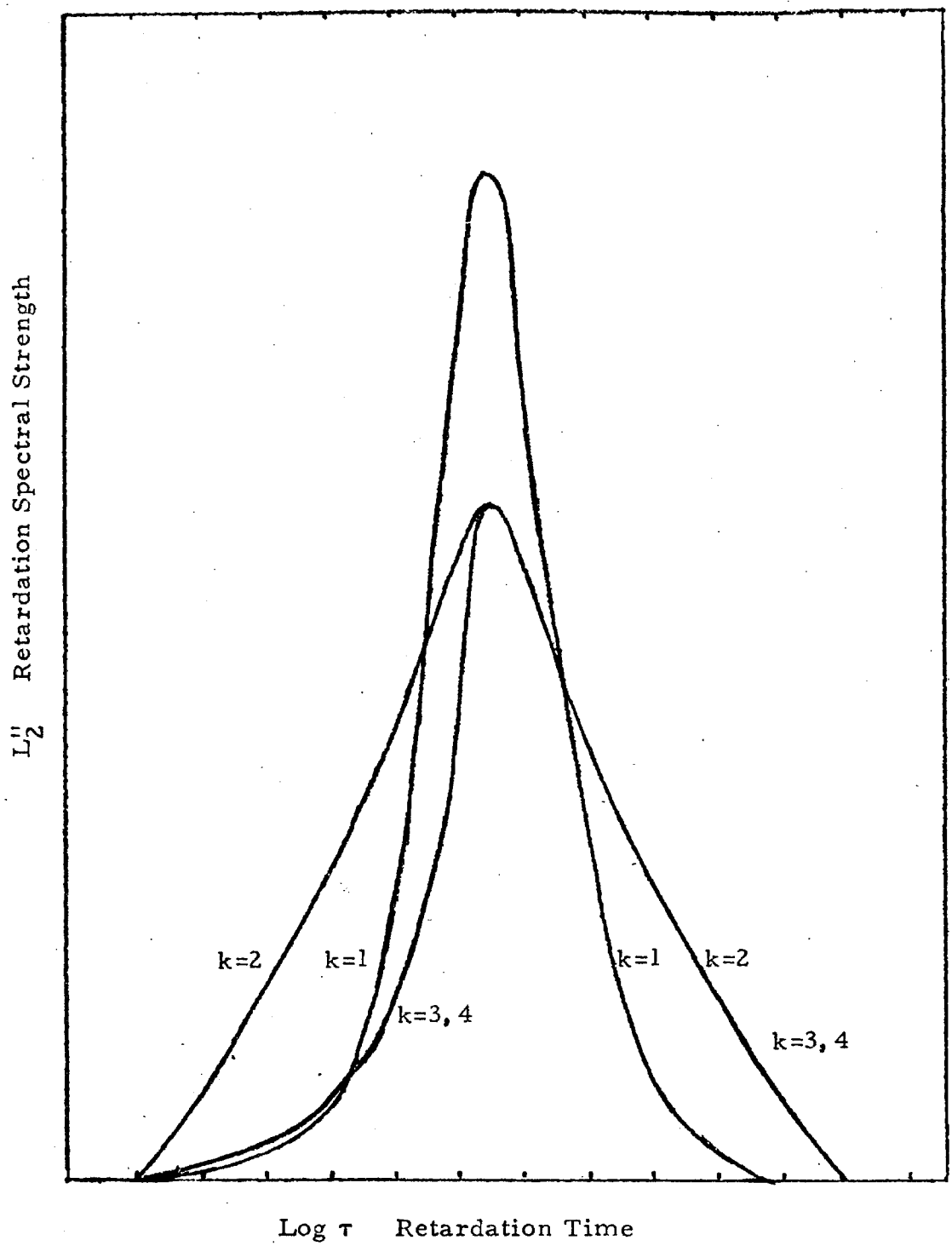

Figure 38.
Qualitative Comparison of the Shapes of the Retardation Spectra for the Individual Mechanisms

retardation times to each mechanism, the areas under the various curves in Figure 38 have no significance. Also, the peak positions have been made to coincide in this figure so that the characteristic shapes for the various mechanisms can be compared easily.

5.5 Using the Model

Before using the model to predict response curves of the various materials, a brief review will be given of the manner in which the parameters of the model were related to the structure of the networks. First, the appropriate number of mechanisms was determined from inspection of the data and knowledge of the various types of network entanglements likely to be present in block copolymer blends. Next, the number of retardation times in each mechanism was related to the network composition. An adjustable fraction of the total number of retardation times was attributed to the main peak for every material so that the shape and position of this portion of the response curves remained fixed. The remaining retardation times were divided among the other mechanisms by considering the probability of occurrence of each type of entanglement in the network. The location of each mechanism on the frequency scale was determined by calculating an effective strand length for each type of entanglement which in turn defined the proper amount of frequency shift from the position of the one slippage mechanism which could be located experimentally. The shapes of the spectra for the various mechanisms were estimated from considerations of the shapes of the retardation spectra of SBS-8 and BL-1.3.

It is now possible to use Eqs. 5.3 and 5.4 to generate response curves for materials of varying terminal chain content and varying terminal chain length. First, equations 5.12 are used to calculate the value of W_k for each mechanism. Then the normalized spectral strength at each value of τ_{ik} is determined from Eq. 5.15

$$D_{ik} = W_k(L_{ik}/\sum_{i=1}^{n_k} L_{ik}).$$

The choice of the spacing of the τ_{ik} values is unimportant as long as they are close enough so that smooth curves are obtained. In practice, a spacing of 0.25 decade was used, resulting in values for n_k of 34 for mechanism 1 and 43 for mechanisms 2 to 4.

Figures 39 to 41 show the comparison between calculated response curves (dashed lines) and those obtained experimentally (solid lines). The table included with each of the figures indicates the values of the network parameters used to calculate the various dashed curves. The particular experimental curve which corresponds to each of the calculated curves is indicated by the geometrical symbol at the low frequency end of the curve and also in the table. Several of the calculated curves have no experimental counterpart. They have been included to indicate the wide spread of response predicted by the model.

Figure 39 shows the calculated and observed response curves for Series 1. The agreement in the glassy and transition regions is, of course, expected since the model has been fitted to the experimental

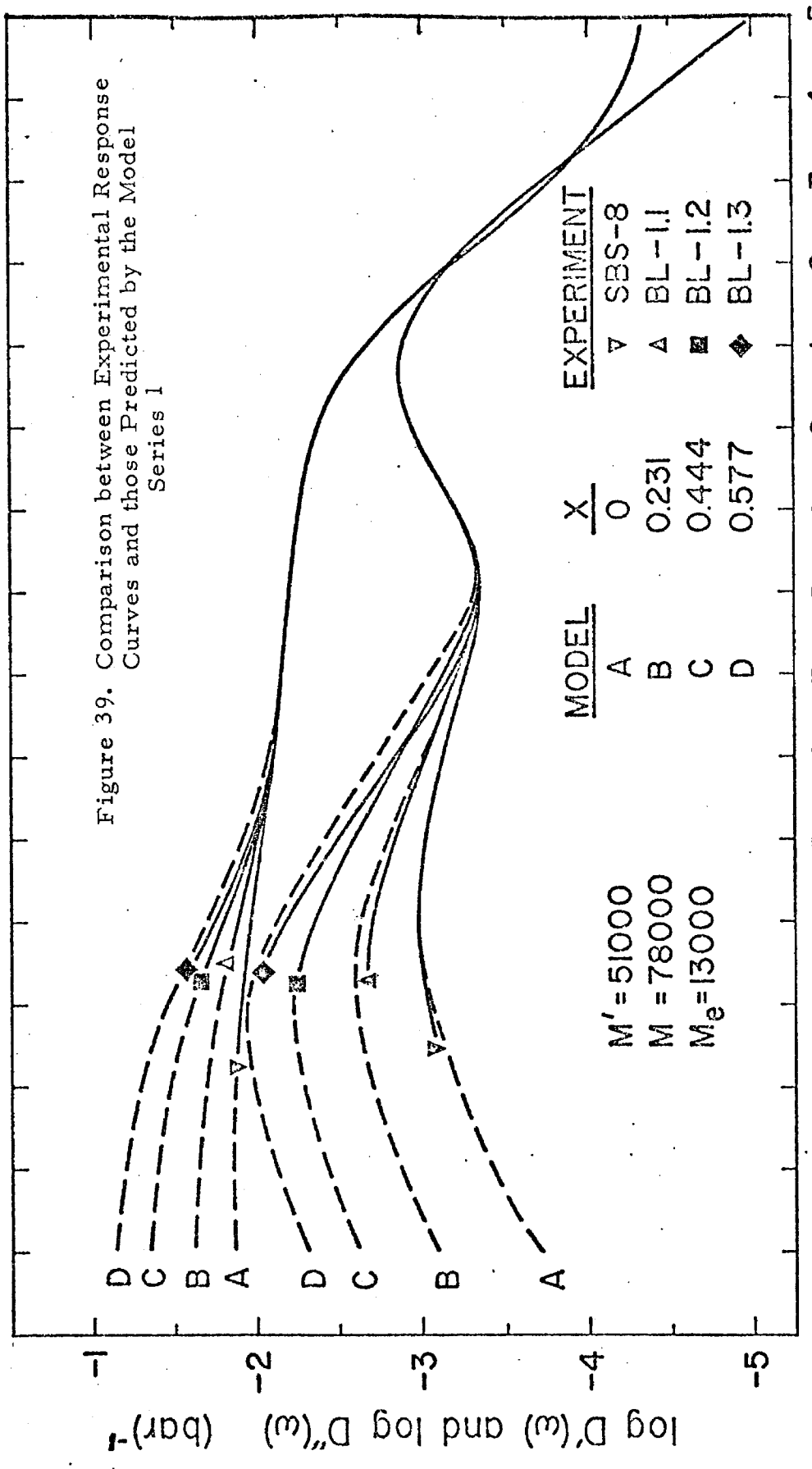

Figure 39. Comparison between Experimental Response Curves and those Predicted by the Model Series 1

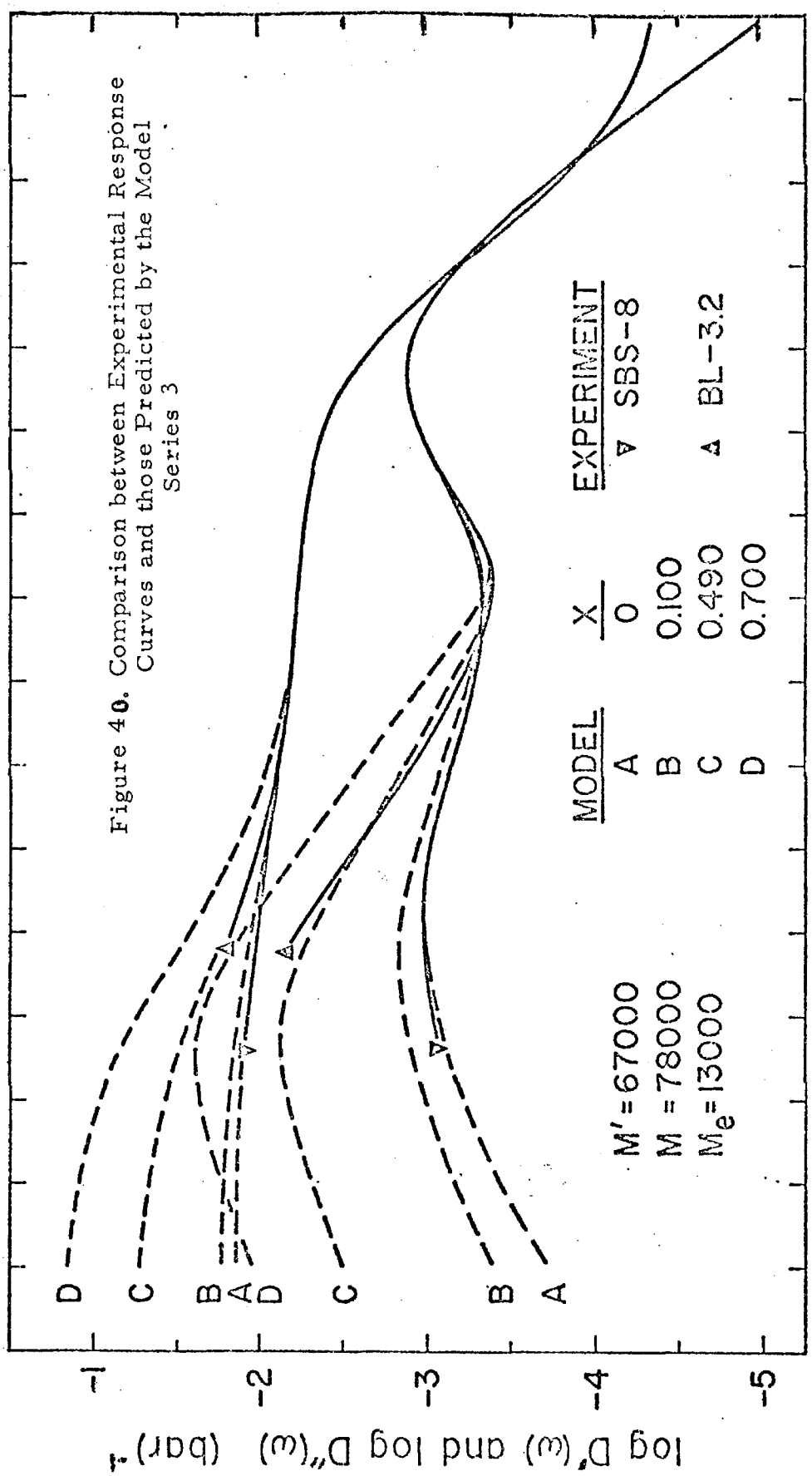

Figure 40. Comparison between Experimental Response Curves and those Predicted by the Model Series 3

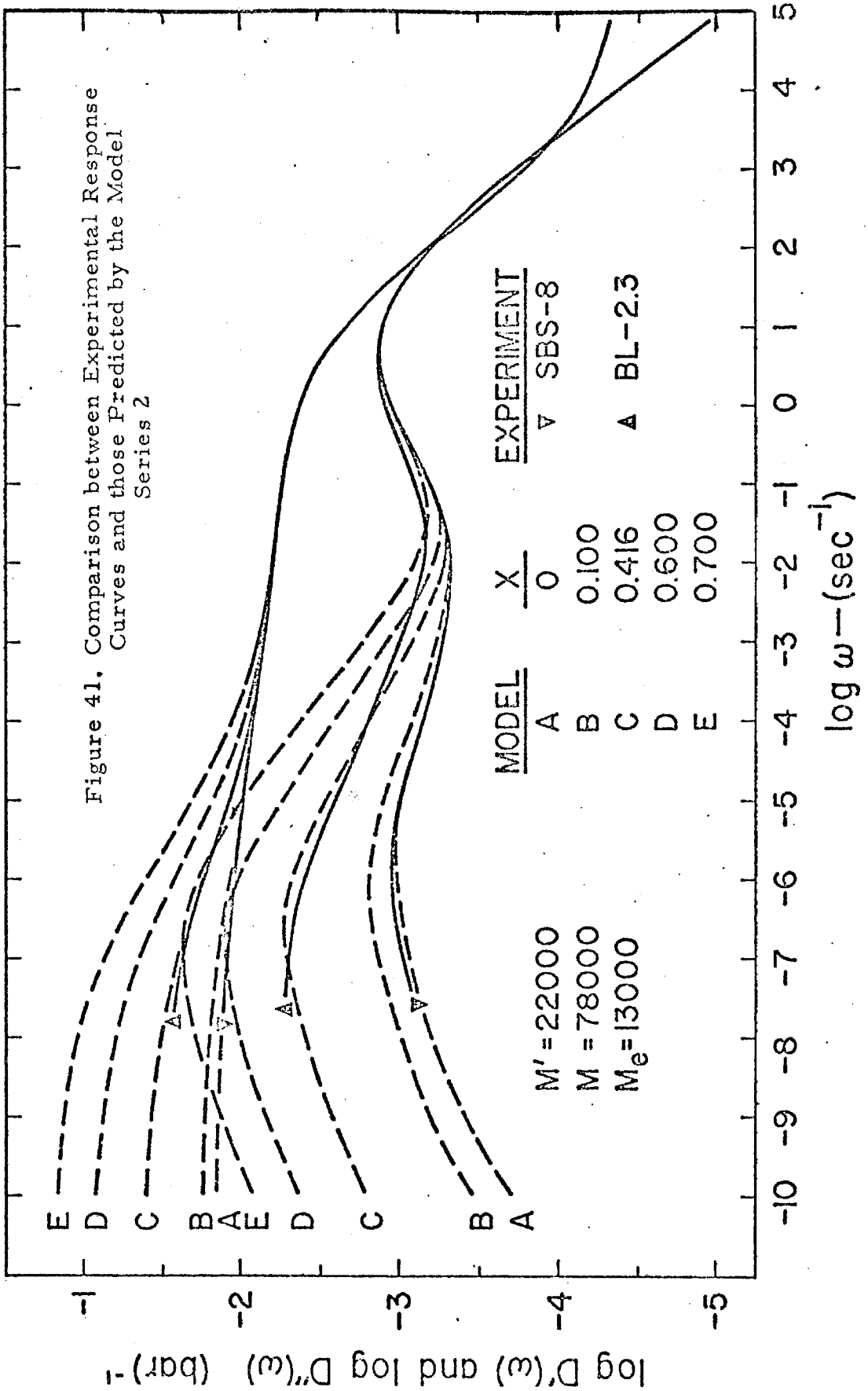

Figure 41. Comparison between Experimental Response Curves and those Predicted by the Model Series 2

curves in that frequency range. At lower frequencies the curves predicted by the model diverge. The loss compliances calculated from the model pass through distinct maxima which shift to lower frequencies and higher values as terminal chain content increases. The model predicts storage modulus curves which rise through steeper secondary transitions to attain higher values of D_e with increasing terminal chain content. The amount of spread in the predicted curves is not insignificant and is especially large in the loss compliance. Thus, comparison with the experimental curves is not an insensitive test.

In Figure 39 the agreement between the model response curves and the experimentally determined mechanical properties is quite good for all three blends of Series 1. Especially significant is the close agreement in the level of the loss since this is the more sensitive response function to these low frequency mechanisms. Furthermore, the shapes of the experimental curves are in reasonably close agreement with the calculated curves, although the data end before most of the interesting changes in shape begin to develop. It was necessary to cut off the data at the indicated points because, as discussed in Chapter 4, polystyrene and interlayer contributions become important at still lower reduced frequencies. Thus, Figure 39 points out very clearly that the particular model materials used in this study were of somewhat limited value. Clearly a much better study could have been made by employing a block copolymer system containing the glassy domains with a much higher T_g.

Figure 40 shows the comparison for Series 3. We see very good agreement between the experimental curves for BL-3.2 and the corresponding curves calculated from the model. Again the loss behavior is more sensitive to network structure and so the agreement of the loss compliance is not as good as the near identical matching found for the storage compliance. As mentioned above, the extra curves corresponding to X - 0.7 and X = 0.1 are included to show that the agreement is not simply a result of insensitivity of the model to changes in the parameter X. The secondary maximum again shifts to lower frequencies with increasing amounts of terminal chains. Furthermore, although it is difficult to see in this figure, the various curves predicted by the model exhibit a deepening minimum near log ω = 2 as X increases. As discussed in the previous chapter and made even more clear in the development of the mathematical model in this chapter, the deepening of the minimum is caused by a downscale shift of some of the low frequency retardation mechanisms leaving a reduced contribution to the loss at intermediate frequencies.

The response curves predicted from the model using the parameters corresponding to the materials of Series 2 are shown in Figure 41. The experimental curves for blend BL-2.3 do not agree very well with the corresponding set of curves predicted by the model. Especially apparent is the discrepancy in the overall shape of the loss compliance curves. However, in spite of the relatively poor agreement with experiment, there are some interesting features

of these predicted response curves which should be mentioned here. The general level of the low frequency response for BL-2.3 is correctly predicted by the model even if the overall shapes of the compliance curves are in doubt. Also, the model correctly predicts that the minimum in the loss compliance becomes shallower as terminal chain content is increased in Series 2. The shallower minimum is a direct result of the relatively high frequency location of the k = 4 mechanism (diblock-diblock entanglement slippage) for Series 2. Since these terminal chains are so short ($M' = 22,000$) their contribution appears at high enough frequencies to affect the level of the minimum in the loss compliance. Furthermore, the location of this particular mechanism is fixed (independent of X) for a given terminal chain length. Therefore increasing the terminal chain content continues to raise the level of the minimum by increasing the number of retardation times in this region. At the same time the secondary peak in the loss at lower reduced frequencies still shifts downscale with increased terminal chain content. This is a result of the shift of the k = 2 and k = 3 mechanisms to longer times as the terminal chain content of the network increases.

5.6 Concluding Remarks

Through the proper use of the mathematical model developed in this chapter, it should be possible to estimate the location and the relative importance of some of the secondary retardation mechanisms affecting the mechanical response of a rubbery material if the amount

and length of the terminal chains in that material can be determined. In the development and use of this model it has become quite clear that the "secondary" effects often observed in the storage and loss compliances of rubbery materials must arise from the complicated interplay of numerous overlapping viscoelastic mechanisms. The weighting and location of the contributions from these various mechanisms are complicated, yet interrelated, functions of the network composition. It is clear, then, that a lumping of these low frequency effects into a single mechanism must involve a significant amount of oversimplification. Thus it appears from the results presented here that any model or theory which includes only a single mechanism to account for the effects of entanglements in elastomers is likely to lack correlation with the true physical situation.

The model has included only the effects of terminal chains and the various types of chain entanglements present in elastomeric materials. It could certainly be extended to include the contributions of other structural features, such as motions of covalent cross-link points, if their low frequency mechanisms could be separated and identified. In fact the analysis could be extended to include additional polymer phases. For example, one can visualize introducing mechanisms corresponding to $k = 5$ and $k = 6$ to account for the interlayer and polystyrene contributions. This has not been attempted here since only the behavior of the polybutadiene phase was under investigation. The model completely ignores the temperature dependence of each contributing mechanism, and therefore the overall

response predicted by the model is strictly applicable only at the reference temperature chosen here. However, if one could somehow establish the characteristic temperature dependence of each separate mechanism, the model could be used successfully to predict the mechanical response at any temperature. In that case the model would constitute an additive compliance analysis of thermorheologically complex behavior in single phase materials.

The rather good agreement between the calculated curves and those obtained experimentally lends support to the conclusions drawn and assumptions made during the development of the model. Furthermore the successful development and use of this mathematical model has made it clear that fruitful studies can be carried out through the use of model network systems. It was possible to compare the calculated response curves to the appropriate experimental curves in a nonarbitrary way only because the networks studies were reasonably well characterized. Otherwise the model developed here could not have been tested meaningfully.

CHAPTER 6

SUGGESTIONS FOR FUTURE WORK

6.1 Introduction

When viewed in total, it appears that this investigation has raised as many new and interesting problems as it has solved. Some of these problems have already been mentioned in the preceding text. More attention is given to these unanswered questions in this final brief chapter along with some suggested directions for continued study. Some of the suggestions involve direct extensions of this project; others deal with more tangential, but equally interesting, studies. Hopefully, some of the suggestions given here will lead to fruitful research projects which can perhaps begin to provide answers to the interesting problems which appeared during the course of this work.

6.2 Extensions of this Investigation

From the experience gained and the information reported here, one can easily suggest several meaningful ways to extend this work. Of primary importance is the necessity for a better model system. Eliminating or at least minimizing the interlayer region would be desirable since its presence requires that much of the high-temperature data be rejected even before the glassy domains begin to soften. This

can probably be accomplished to a large degree by choosing the proper solvent or solvent mixture for use in the sample casting process. Choosing a system which is a very good solvent for polybutadiene and a poor solvent for polystyrene will result in samples with a continuous rubbery phase and a minimum amount of intermixing around the glassy domains. Benzene, the system used in this study, is a farily good solvent for both phases.

The glassy domains of the model system should have a much higher T_g so that more of the low frequency response of the polybutadiene phase can be studied before the domains begin to soften. One useful system, for example, would be provided by block copolymers of polybutadiene and poly(α methyl styrene) since the T_g of the glassy domains is around 172°C for these materials.

Having obtained a better model system, one would be in a position to conduct the following studies: First, it would be useful to test, at constant composition, a much wider range of terminal chain molecular weights with smaller molecular weight intervals between the various samples. In this way one could establish quite clearly at what terminal chain molecular weight the entanglement coupling effects become noticeable. Using these same diblocks it would be possible to study the effects of a changing molecular weight <u>distribution</u> in the terminal chain portion of the networks. This would be accomplished by blending several of the monodisperse diblocks with the base material. This would be particularly useful since the terminal chains in a conventional elastomer are not

monodisperse but most likely have the same molecular weight distribution as the network chains. Finally, one would like to incorporate into the model system another important structural feature, covalent cross-links. If one could introduce a controlled amount of covalent cross-links into the system it would be possible to study the effects of cross-link mobility on the mechanical properties and possible differences between the contribution of a covalent cross-link and a trapped entanglement.

Clearly one cannot hope to introduce controlled amounts of covalent cross-links by conventional vulcanization techniques. However, it would be possible to introduce small amounts of covalent cross-links by employing the star-branched block copolymers shown in Figure 42. These materials have been prepared at the Phillips Petroleum Company and essentially consist of three and four diblock chains held together at the polybutadiene ends by covalent linkages. These linkages should be equivalent to tri- and tetra- functional cross-links in a conventional elastomer.

With respect to the further development of the mathematical model, it would be useful to obtain some idea of the individual temperature dependences of the various entanglement slippage mechanisms. A better model polymeric system would make this task easier since one could hope to cover more of the low frequency peak in the loss compliance. Furthermore, an improved apparatus such as the one described in Chapter 3 should allow forced oscillation

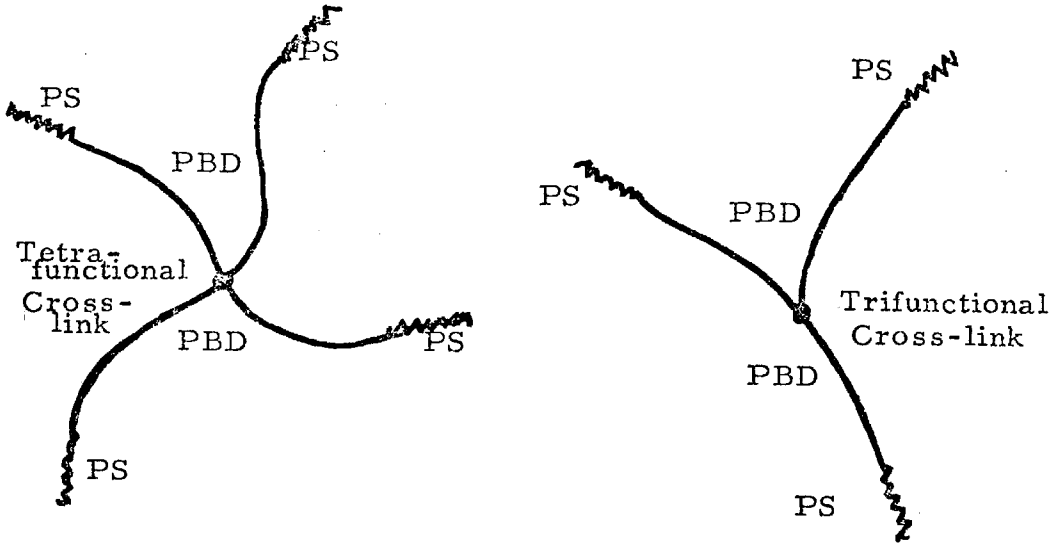

Figure 42.

Star-branched Block Copolymers Containing a Central Covalent Cross-link

measurements to be conducted on pure diblock materials. In this way the untrapped entanglement slippage mechanisms could be studied independent of trapped entanglement effects.

6.2 Related Studies

Several interesting observations were made during the course of this work which were related to the behavior of the block copolymer model systems but did not directly enter into the study of terminal chains and chain entanglements. Some thoughts on these observed phenomena are presented in this section.

One major problem in the characterization of the two-phase block copolymers systems has been the inability to determine the glass transition temperature of the dispersed phase in a reliable way. The observed effects of annealing on the dimensions of a solvent cast specimen may provide a method for accomplishing this. It was pointed out that minimal changes in thickness were observed until annealing temperatures approached what was presumed to be the polystyrene T_g. A reasonable definition of the temperature at which the dimensional changes first became significant could be obtained by cross-plotting isochronal data from plots similar to Figure 6. Several more annealing runs at different temperatures would be necessary, of course, to obtain a meaningful cross-plot. The resulting reduced thickness vs. temperature plot should resemble an ogive-shaped breakthrough curve. Extrapolating back to the onset temperature should give a reasonable estimate of the T_g of the domains.

The T_g value obtained by this method would probably depend upon the particular isochrone chosen for the cross-plot. However, this is a general short-coming of all methods for determining glass transition temperatures.

The interlayer region in block copolymers has been the subject of much speculation. By introducing known amounts of the "tapered" block copolymers described in Chapter 2 into conventional di- and tri-block systems, one could enhance the proportion of the interlayer region at will. Characterization of the tapered region of these polymers is difficult, but reasonable qualitative studies could still be made. In particular, it would be useful to see if the regions of mechanical response currently attributed to the interlayer are enhanced by the addition of tapered block copolymers. Furthermore, it would be very interesting to see whether or not the mixed portion of these tapered block systems could be visualized as a region of gray, intermediate exposure in electron photomicrographs of suitably stained samples.

The controversy concerning the presence or absence of thermorheological complexity as a result of the two-phase structure of block copolymers can be resolved in several ways. One of these would be to establish clearly, over and above experimental error, that isothermal forced oscillation data cannot be superposed by conventional empirical shifts. This difficult task should be made somewhat easier by investigating the behavior of a block copolymer system whose separate phases have relatively closely spaced transitions.

Another approach involves the observed separation of the two transitions on the temperature scale when the material is studied isochronally. If the separation of the transitions changes as the isochronal frequency is changed, then the material must be thermorheologically complex and simple empirical shifts cannot lead to valid master curves. Consideration of the individual WLF equations for the two phases of the system studied here indicates that if the material is thermorheologically complex, the separation between the transitions should change by about 13°C for a four decade change in the isochronal frequency. Since this is a realizable frequency range and an easily observed temperature shift, this should be a rather easy proposition to test.

Finally, there is the interesting observation that the domain structure of the block copolymer system apparently enhanced entanglement coupling effects in much the same way that regions of tactic ordering appear to affect this behavior in certain methacrylate polymers. Studies of other systems containing regions of high agglomeration within a continuous entangled matrix should prove very interesting in this respect.

REFERENCES

1. P. J. Flory, Chem. Revs., 35:51 (1944).
2. P. J. Flory, Ind. Eng. Chem., 38:417 (1946).
3. P. J. Flory, J. Rehner, Jr., J. Chem. Phys., 11:512 (1943).
4. E. Guth, H. M. James, Ind. Eng. Chem., 33:624 (1941).
5. L. R. G. Treloar, Trans. Farad. Soc., 39:36 (1943).
6. J. D. Ferry, R. Mancke, E. Maekawa, Y. Ōyanagi, R. Dickie, J. Phys. Chem., 68:3414 (1964).
7. E. Maekawa, R. Mancke, J. D. Ferry, J. Phys. Chem., 69:2811 (1965).
8. R. Dickie, J. D. Ferry, J. Phys. Chem., 70:2594 (1966).
9. R. Mancke, J. D. Ferry, Trans. Soc. Rheol., 12:335 (1968).
10. R. G. Mancke, R. A. Dickie, J. D. Ferry, J. Polymer Sci. A-2, 6: 1783 (1968).
11. R. H. Valentine, J. D. Ferry, T. Homma, K. Ninomiya, J. Polymer Sci. A-2, 6:479 (1968).
12. J. F. Sanders, J. D. Ferry, R. H. Valentine, J. Polymer Sci. A-2, 6:967 (1968).
13. N. R. Langley, J. D. Ferry, Macromolecules, 1:353 (1968).
14. S. D. Morton and J. D. Ferry, J. Phys. Chem., 66:1639 (1962).
15. A. E. Oberth, Rubber Chem. Tech., 44:152 (1971).
16. L. R. G. Treloar, Trans. Farad. Soc., 36:538 (1940).
17. J. D. Ferry, "Viscoelastic Properties of Polymers", 2nd ed., Wiley, N. Y. (1970).
18. A. M. Bueche, J. Polymer Sci., 19:297 (1956).

19. N. R. Langley, Macromolecules, 1:348 (1968).

20. G. Holden, E. T. Bishop, N. R. Legge, J. Polymer Sci. C, 26: 37 (1969).

21. M. Morton, Adv. Chem. Ser., 99:490 (1971).

22. D. G. Fesko, N. W. Tschoegl, J. Polymer Sci. C, 35:51 (1971).

23. J. F. Beecher, L. Marker, R. O. Bradford, S. L. Aggarwal, J. Polymer Sci. C, 26:117 (1969).

24. D. H. Kaelble, Trans. Soc. Rheol., 15:235 (1971).

25. D. G. Fesko, Ph.D. Thesis, California Institute of Technology, (1971).

26. M. Shen, E. H. Cirlin, D. H. Kaelble, "Colloidal and Morphological Behavior of Block and Graft Copolymers", G. E. Molau, ed. Plenum Press, N. Y. 1971.

27. C. K. Lim, R. E. Cohen, N. W. Tschoegl, Adv. Chem. Ser. 99: 397 (1971).

28. M. Scwarc, M. Levy, R. M. Milkovich, J. Am. Chem. Soc., 78: 2656 (1956).

29. M. Matsuo, Japan Plastics, p. 6, 1968.

30. T. Inoue, T. Soen, T. Hashimoto, H. Kawai, Macromolecules, 3:87 (1970).

31. T. Inoue, T. Soen, T. Hashimoto, H. Kawai, J. Polymer Sci. A-2, 7:1283 (1969).

32. L. J. Fetters, J. Res. N.B.S., 70A:421 (1966).

33. L. J. Fetters, J. Polymer Sci. C, 26:1 (1969).

34. M. Szwarc, "Carbonions, Living Polymers, and Electron Transfer Processes", Interscience, N.Y. 1968.

35. A. Rembaum, F. R. Ellis, R. C. Morrow, A. V. Tobolsky, J. Polymer Sci., 61:155 (1962).

36. R. J. Angelo, R. M. Ikeda, M. L. Wallack, Polymer, 6:141 (1965).

37. M. Morton, A. Rembaum, J. L. Hall, J. Polymer Sci. A, 1 (1963).

38. I. Kuntz, J. Polymer Sci., 54:569 (1961).

39. A. F. Johnson, D. F. Worsfold, Die Makromol. Chem., 85:273(1965).

40. I. M. Kolthoff, T. S. Lee, C. W. Carr, J. Polymer Sci., 1: 429 (1946).

41. W. R. Senn, Jr., Anal. Chim. Acta., 29:505 (1963).

42. H. Y. Chen, Anal. Chem., 34:1134 (1962).

43. R. Silas, J. Yates, V. Thornton, Anal. Chem., 31:929 (1959).

44. D. G. Fesko and N. W. Tschoegl, to be published.

45. C. J. Nederveen, C. W. van der Wal, Rheol. Acta, 6:316 (1967).

46. D. D. Lawson, JPL-NASA SPS Report No. 37-55, Vol. III, Feb. 28, 1969.

47. D. O. Miles, J. Appl. Physics, 33:1422 (1962).

48. N. W. Tschoegl, J. R. Smith in T. L. Smith, J. R. Smith, N. W. Tschoegl, Final Report on "Viscoelastic Properties of Solid Propellants and Propellant Binders", SRI Projects PRU-3939, 4660, 5174, Stanford Research Institute, Menlo Park, California (1966).

49. W. G. Knauss, J. F. Clauser, R. F. Landel, "Second Report on the Selection of a Crosslinked Polymer Standard", MATSCIT PS 66-1, California Institute of Technology, AFRPL-TR-66-21, Edwards, California, January, 1966.

50. D. G. Fesko, M. Masterson, R. F. Landel, N. W. Tschoegl, in N. W. Tschoegl, et al., "A Research Program on Solid Propellant Physical Behavior", CHECIT PL 70-1, California Institute of Technology, AFRPL-TR-70-143, Edwards, California, August, 1969.

51. E. R. Fitzgerald, J. D. Ferry, J. Colloid Sci., 8:1 (1953).

52. R. E. Cohen, Polymer Laboratory Internal Report No. 71-2, Division of Chemistry and Chemical Engineering, California Institute of Technology, July 1971.

53. W. V. Chang, N. W. Tschoegl, Polymer Laboratory, Division of Chemistry and Chemical Engineering, California Institute of Technology, 1972.

54. N. W. Tschoegl, Rheol. Acta, 10:582 (1971).

55. D. J. Plazek, V. M. O'Rourke, J. Polymer Sci. A-2, 9:209 (1971).

56. T. Miyamoto, K. Kodama, K. Shibayama, J. Polymer Sci. A-2, 8:2095 (1970).

57. V. A. Kaniskin, A. Kaya, A. Ling, M. Shen, to be published.

58. J. D. Ferry, N. C. Child, Jr., R. Zand, D. M. Stern, M. L. Williams, R. F. Landel, J. Colloid Sci., 12:53 (1957).

59. W. C. Child, Jr., J. D. Ferry, J. Colloid Sci., 12:327 (1957).

60. W. C. Child, Jr., J. D. Ferry, J. Colloid Sci., 12:389 (1957).

61. D. J. Plazek, J. Phys. Chem., 69:3480 (1965).

62. D. J. Plazek, J. Polymer Sci. A-2, 6:621 (1968).

64. D. J. Plazek, W. Danhauser, and J. D. Ferry, J. Colloid Sci., 16:101 (1961).

65. M. Takayanagi, Pure and Applied Chemistry, 15:555 (1967).

66. T. E. Newlin, S. E. Lovell, P. R. Saunders, J. D. Ferry, J. Colloid Sci., 17:10 (1962).

67. J. W. Berge, P. R. Saunders, J. D. Ferry, J. Colloid Sci., 14: 135 (1959).

68. P. R. Saunders, D. M. Stern, S. F. Kurath, C. Sakoonkim, J. D. Ferry, J. Colloid Sci., 14:222 (1959).

69. D. M. Stern, J. W. Berge, S. F. Kurath, C. Sakoonkim, J. D. Ferry, J. Colloid Sci., 17:409 (1962).

70. G. C. Berry, T. G. Fox, Adv. Polymer Sci., 5:261 (1968).

71. G. V. Vinogradov, V. G. Yanovsky, A. I. Isayev, V. P. Shatalov, V. G. Shalganova, Intern. J. Polymeric Mater., 1971, 1:17 (1971).

72. L. E. Nielsen, J. Appl. Polymer Sci., 8:511 (1964).

73. R. Chiang, J. J. Burke, J. O. Threlkeld, T. A. Orofino, J. Phys. Chem., 70:3591 (1966).

74. E. T. Bishop, S. Davison, J. Polymer Sci. C, 26:37 (1968).

75. G. Kraus, J. Appl. Polymer Sci., 7:861 (1963).

76. P. J. Flory, J. Chem. Phys., 18:108 (1950).

77. P. J. Flory, J. Rehner, Jr., J. Chem. Phys., 11:521 (1943)

78. G. Kraus, Rubber World, 135:67 (1956).

79. T. Smith, Personal communication (1972).

80. E. Guth, J. Appl. Phys., 16:30 (1945).

81. S. Uemura, M. Takayanagi, J. Appl. Polymer Sci., 10:113 (1966).

82. H. Oser, R. S. Marvin, J. Res. Nat. Bur. Standards, 67B:87 (1963).

83. A. S. Lodge, Rheol. Acta, 1:379 (1968).

84. J. D. Ferry, R. F. Landel, M. L. Williams, J. Appl. Phys., 26:359 (1955).

Appendix A

Information Supplied by Shell Chemical Company with the Research Grade Block Copolymers

EXPERIMENTAL BLOCK COPOLYMERS

In recent years, there has been a great deal of interest in block copolymers which have the unique property of being both rubbers and thermoplastics. As a commercial manufacturer of these products, the Shell Chemical Company has received many requests for samples to be used for research. Three polymers have now been specially made and carefully characterized for this purpose.

All three polymers have the general configuration poly (styrene-b-butadiene-b-styrene)* and were synthesized by sequential anionic polymerization in a hydrocarbon solvent. Details of quite similar systems have been discussed in recent articles[2,3]. In these particular polymerizations, to keep the molecular weight distribution of the final polystyrene segments as narrow as possible, a small amount (about 0.5% volume of the total solution) of diethyl ether was added to the reaction mixture at the end of the butadiene polymerization[4]. This increases the ratio between the initiation rate and the propagation rate of the polymerization of the subsequent polystyrene segment. Polymerization of each segment was continued for greater than 10 half lives of the reaction before the next monomer increment was added, thus avoiding tapering of one segment into another.

The polymers were characterized by measuring the intrinsic viscosities of the first segments in toluene at 30°C and the styrene content of the subsequent materials by infrared spectroscopy. These values, together with the segmental molecular weights calculated from them, are given in Table I.

The molecular weight of the first (S1) segment was obtained from the intrinsic viscosity measurement using the relationship given in Table I. The molecular weight of the second (B) segment was obtained from the S1 molecular weight and the measured styrene content of the S1-B polymer by the relationship,

$$\bar{M}_B = \frac{\bar{M}_{S1}}{\phi_{S1-B}} - \bar{M}_{S1}$$

where ϕ_{S1-B} is the styrene content of the S1-B polymer and $\bar{M}_B$ and $\bar{M}_{S1}$ are the molecular weights of the B and S1 segments, respectively.

The molecular weight of the final (S2) segment was obtained from the molecular weight of the previous S1 segment and the measured styrene content of the S1-B and S1-B-S2 polymer by the relationship,

---

* The nomenclature is that of Ceresa[1].

1) R. J. Ceresa. "Block and Graft Copolymers", Butterworth, Inc., Washington, D. C. 1962.
2) R. Zelinski and C. W. Childers. Rubber Chem. and Tech. 41 161 (1968).
3) L. J. Zeltmers. J. Poly. Sci. C26 1 (1969).
4) "Carbanions, Living Polymers and Electron Transfer Processes", M. Szwarc. Interscience Publishers, New York 1968, Chapter 7.

Experimental Block Copolymers

$$\bar{M}_{S2} = \bar{M}_{S1} \cdot \frac{\phi_{S1\text{-}B\text{-}S2} - \phi_{S1\text{-}B}}{(1-\phi_{S1\text{-}B\text{-}S2}) \cdot \phi_{S1\text{-}B}}$$

where $\phi_{S1\text{-}B\text{-}S2}$ is the styrene content of the final S-B-S polymer and $\bar{M}_{S2}$ is the molecular weight of the final polystyrene segment.

The intrinsic viscosities of the S1-B-S2 polymer was also measured and are given in Table I for reference purposes.

The relative amounts of cis 1,4, trans 1,4 and 1,2 addition in the butadiene portion of two polymers were measured by infrared spectroscopy and are also given in Table I. The other one is expected to be similar.

Stabilization and Purification

The polymers are essentially pure materials, containing only ~ 0.2% of Antioxidant 330**. If further purification is required for light scattering measurements, etc., they may be dissolved, filtered as required, and reprecipitated***.

If the polymers are to be exposed to relatively high temperature (> 100°C), it is suggested that up to 0.5% each of Plastanox LTDP**** and Antioxidant 330** be added. This can be done by dissolving and reprecipitating as previously described. Like other polymers containing unsaturation in the backbone chain, these materials can be degraded by excessive exposure to light. If prolonged exposure is necessary, they can be established by the addition of Tinuvin P*****.

Credit

The polymerization and characterization of these materials should be credited to Mr. A. R. Bean and Mrs. M. J. Papavasiliou, Elastomers Technical Center, Shell Chemical Company, Torrance, California.

These polymers were produced for research purposes and are not intended to be representative of commercial products.

** 1,3,5-Trimethyl-2,4-tris (3,5-di-tert-butyl-4-hydroxybenzyl) benzene, ex Ethyl Corporation.

*** Our usual procedure is to make a 10% solution of the polymer in cyclohexane and to add 1 volume of this solution to 5 volumes of well stirred methanol. The mixture is stirred for about one hour, the excess liquid decanted off and the precipitate filtered and vacuum dried. If it is desired to have n% of some additive (i.e., an antioxidant) in the dried polymer, then about 5 n gm/liter of this material should be dissolved in the methanol.

**** Dilaurylthiodipropionate, ex American Cyanamid Co.

***** 2(2' Hydroxy-5' methylphenol) benzotriazole, ex Geigy Chemical Company.

TABLE I

Characterization of Experimental Block Polymers

	Polymer Number		
	TR-41-1649	TR-41-1648	TR-41-1647
Intrinsic Viscosity, $[\eta]$, $dl/gm^{a)}$			
$[\eta]_{S1}$	0.130	0.141	0.089
$[\eta]_{S1-B-S2}$	0.648	1.004	0.662
Styrene Content, ϕ, (Weight Fraction)			
ϕ_{S1-B}	0.319	0.170	0.164
$\phi_{S1-B-S2}$	0.482	0.293	0.268
Calculated Molecular Weights, $\bar{M}$ (in thousands)			
$\bar{M}_{S1}$ [b)]	14	16	7
$\bar{M}_{B}$	30	78	36
$\bar{M}_{S2}$	14	16	6
Polybutadiene Microstructure, (%)			
cis 1,4	-	41	44
trans 1,4	-	49	46
1,2	-	10	10

a) In toluene at 30°C.
b) Using the relationship $\log [\eta] = 0.648 \log \bar{M}_{S1} - 3.564$.

Appendix B

Working Plots of the Forced Oscillation Data for Series 1 and 3

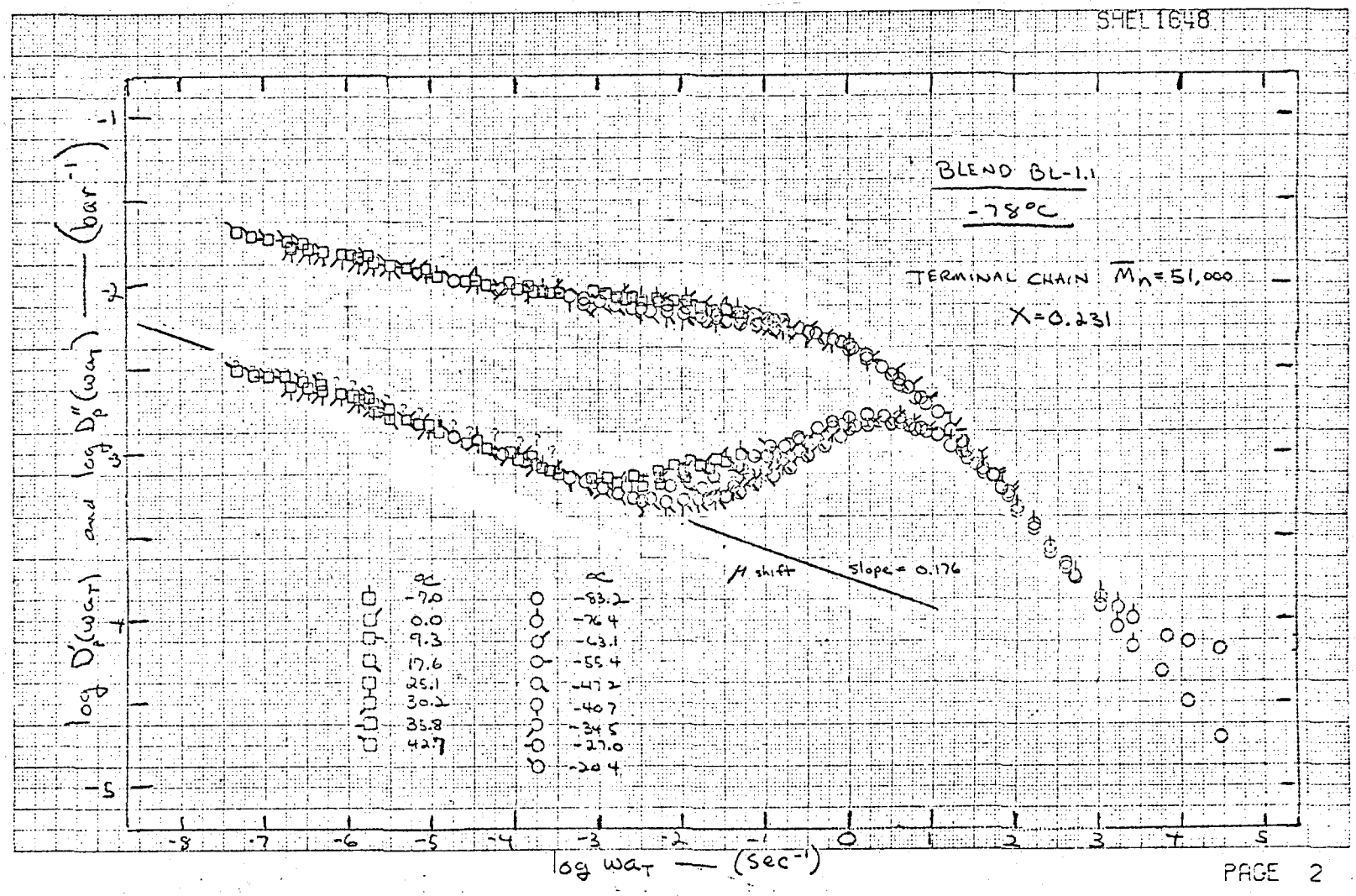
SHELL 648
BLEND BL-1.1
-78°C
TERMINAL CHAIN $\overline{M}_n$ = 51,000
X = 0.231
μ shift
slope = 0.176
log D'_p(w,T) and log D''_p(w,T) — (bar^{-1})
log w$_{aT}$ — (sec^{-1})
α
-70
0.0
9.3
17.6
25.1
30.2
35.8
42.7
α
-83.2
-76.4
-63.1
-55.4
-47.2
-40.7
-34.5
-27.0
-20.4

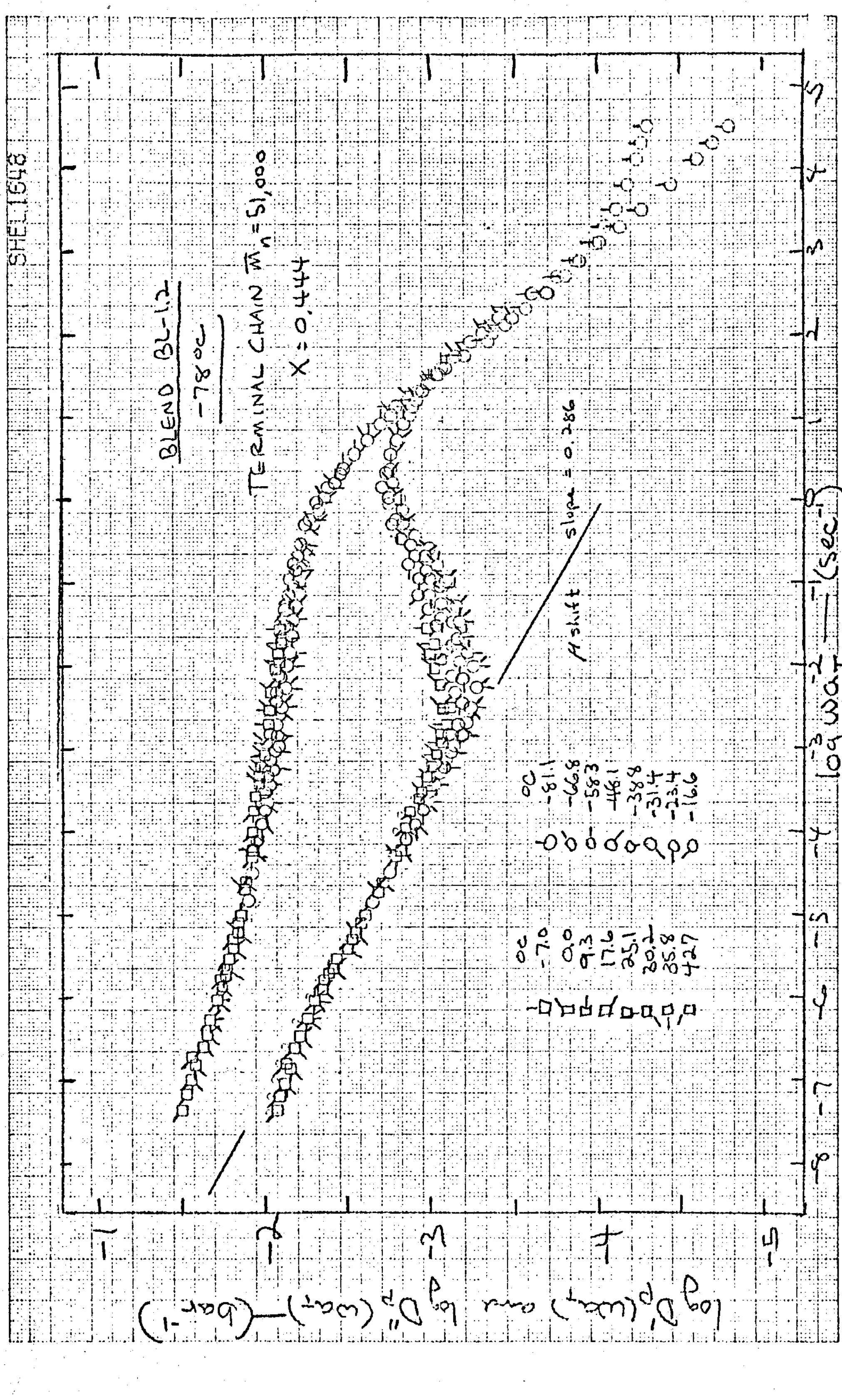
BLEND BL-1.2
-78°C
TERMINAL CHAIN $\overline{M}_n$ = 51,000
X = 0.444
slope = 0.286
A shift
°C -7.0 0.0 9.3 17.6 25.1 30.2 35.8 42.7
°C -81.1 -66.8 -58.3 -46.1 -38.8 -31.4 -23.4 -16.6
log ωa_T —— (sec^{-1})
log $D'(\omega a_T)$ and log $D''(\omega a_T)$ —— (bar^{-1})
-8 -7 -6 -5 -4 -3 -2 -1 0 1 2 3 4 5
-1 -2 -3 -4 -5
SHEL 1648
PAGE 4

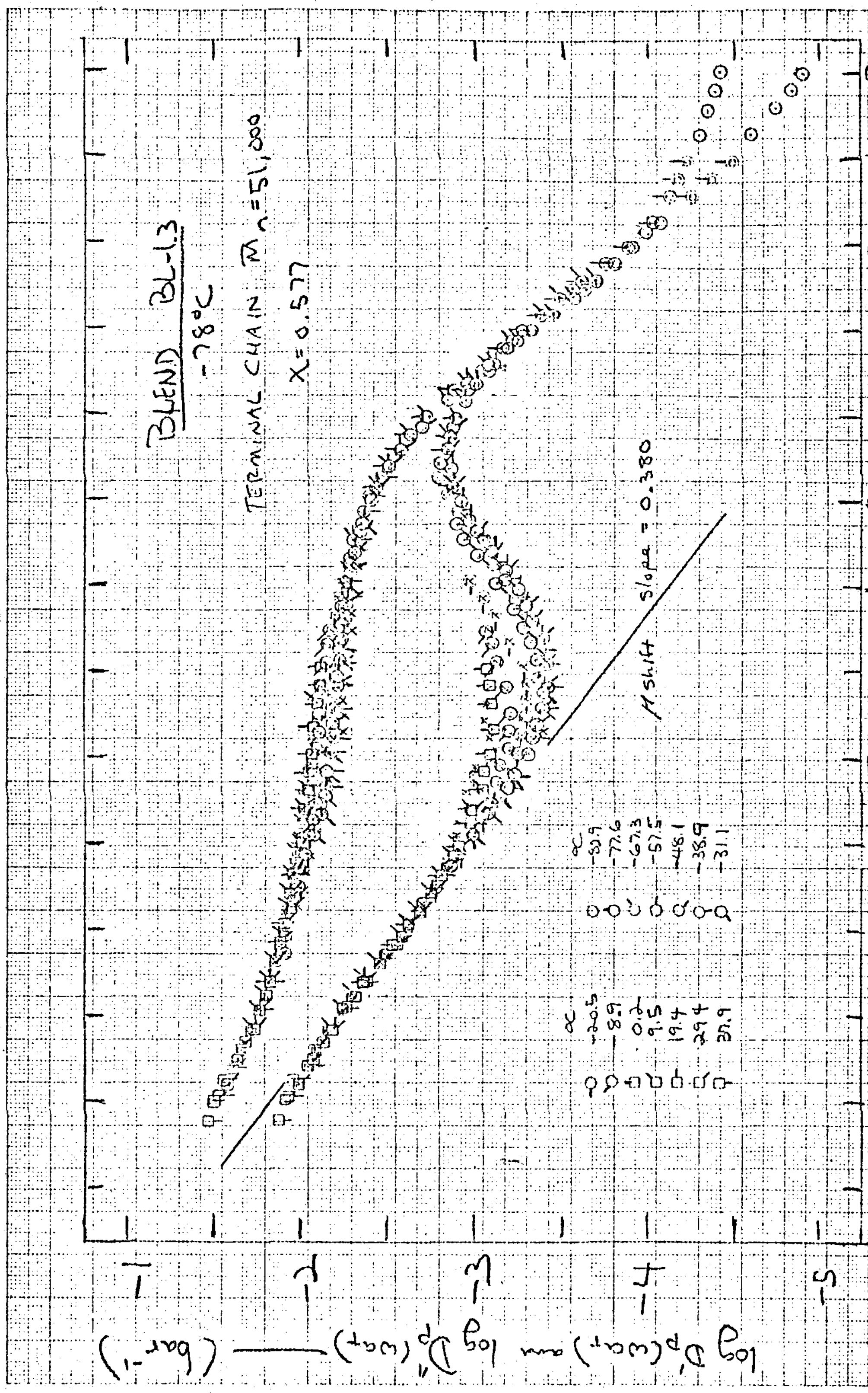
BLEND BL-13
-78°C
TERMINAL CHAIN M̄n = 51,000
X = 0.577
slope = 0.380
log ωaT — (sec⁻¹)
log D'p(ωaT) and log D''p(ωaT) — (bar⁻¹)
α
-20.5
-8.9
0.2
9.5
19.4
29.4
35.9
α
-50.9
-77.6
-67.3
-57.5
-48.1
-38.9
-31.1

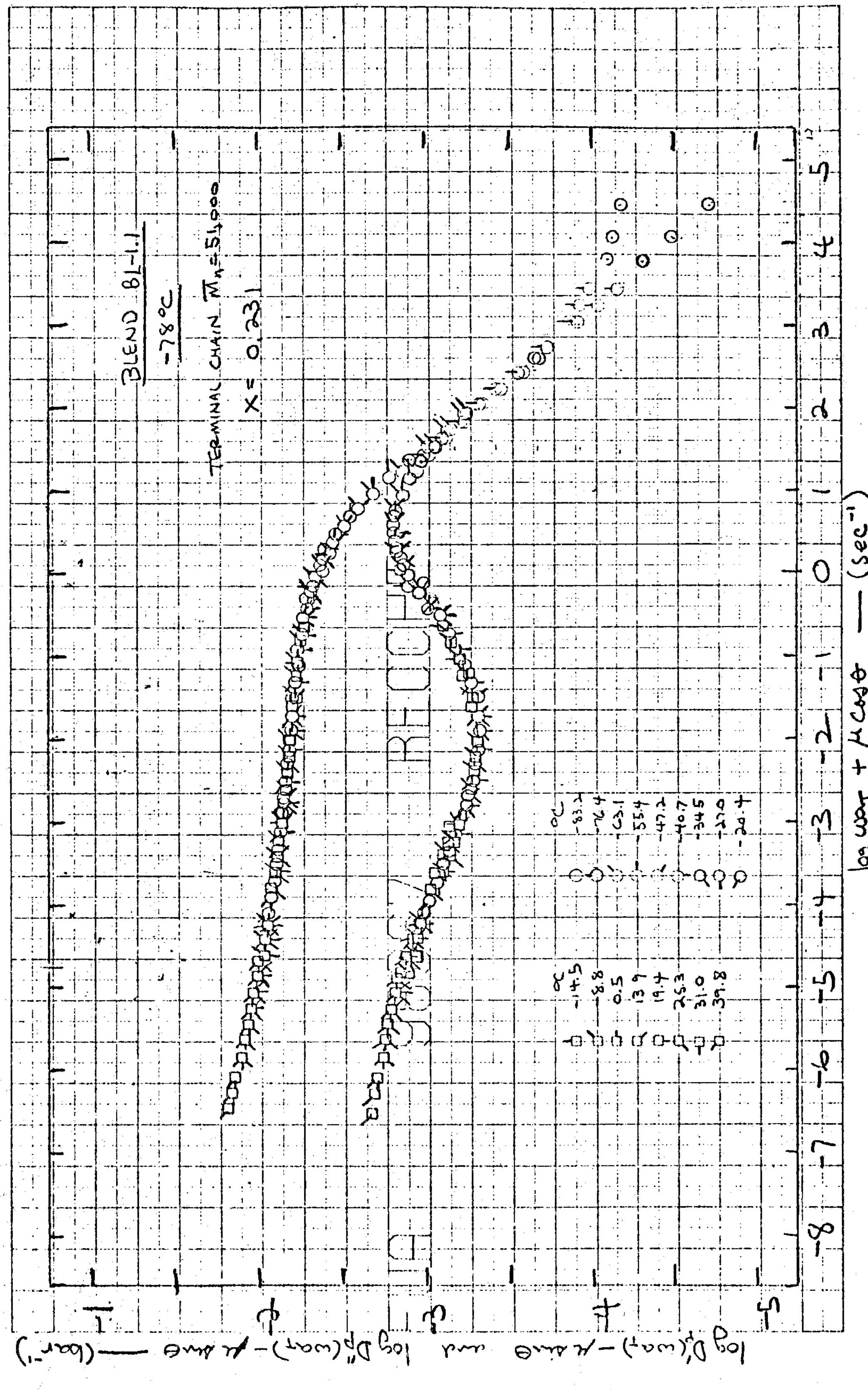
BLEND BL-1.1
-78°C
TERMINAL CHAIN $\bar{M}_n$=51,000
X = 0.231
°C
-14.5
-8.8
0.5
13.9
19.4
25.3
31.0
39.8
°C
-83.2
-76.4
-63.1
-53.4
-47.2
-40.7
-34.5
-27.0
-20.4
log ωa_T + μ cos φ — (sec⁻¹)
log D'_p(ωa_T) − μ sin φ and log D''_p(ωa_T) − μ sin φ — (bar⁻¹)

BLEND BL-1.2
-78°C
TERMINAL CHAIN Mn 51,000
X = 0.444
PAGE 4

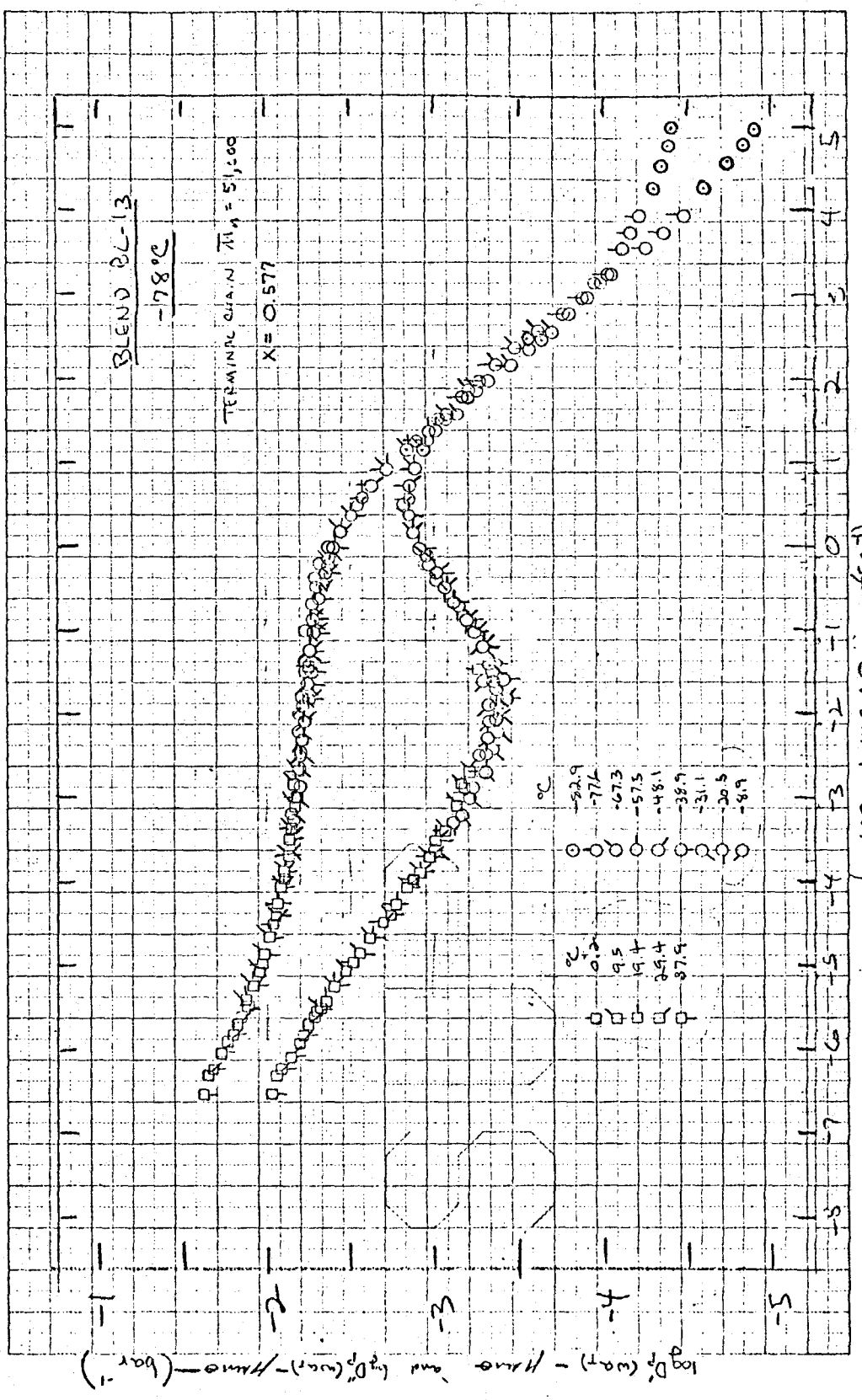
BLEND BL-13
-178°C
TERMINAL CHAIN $\overline{M}_n$ = 51,000
X = 0.577
°C
0.5
9.5
19.4
29.4
37.9
°C
-52.9
-47.4
-42.3
-38.1
-31.1
-25.5
-18.9
$\log D_r^0$ (sec^{-1}) — $\log \omega\tau + \mu\cos\theta$
$\log D_r^0(\omega\tau) - \log D_r^0(\omega\tau)_{\text{max}}$ — $\log \omega\tau + \mu\cos\theta$ — (sec^{-1})

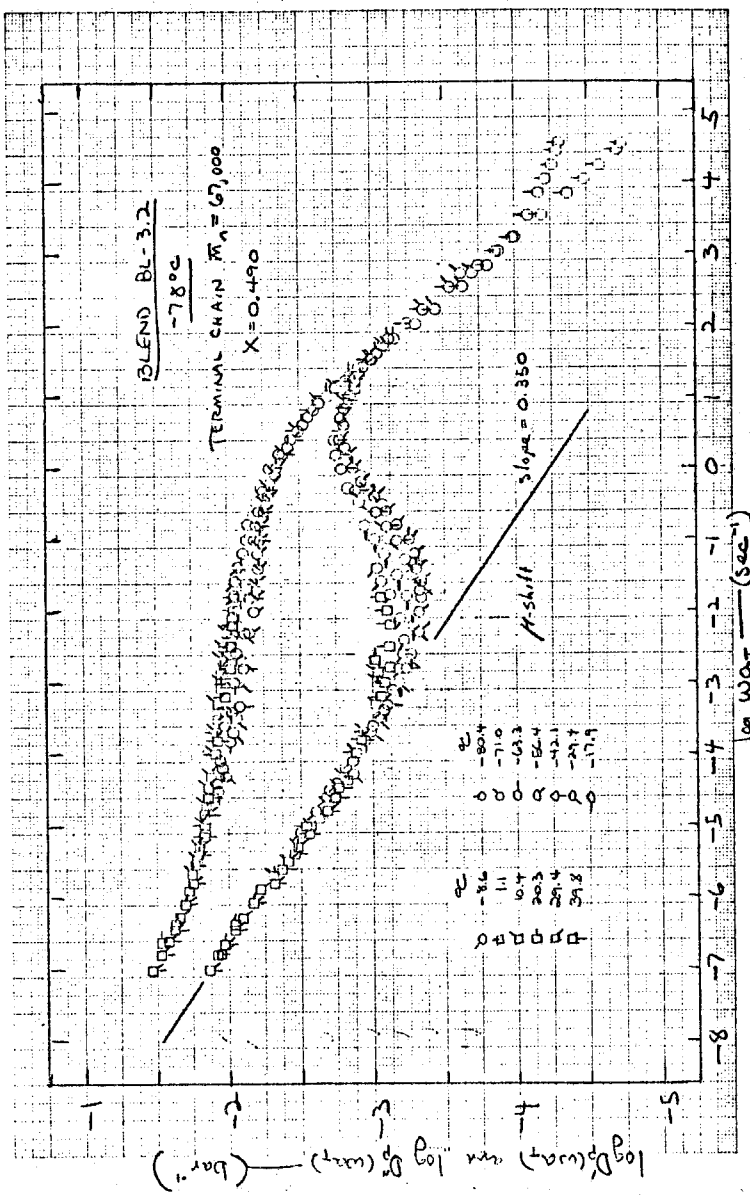
BLEND BL-3.2
-78°C
TERMINAL CHAIN $\bar{M}_n$ = 67,000
X = 0.490
slope = 0.350
log $G_p'(\omega_T)$ vs log ω_T
log $G_p'(\omega_T)$ (dyn cm^{-2})
log ω_{aT} (sec^{-1})
E
-80.4
-71.0
-63.3
-54.4
-42.1
-29.4
-17.9
E
-8.6
1.1
10.4
20.3
29.4
39.8

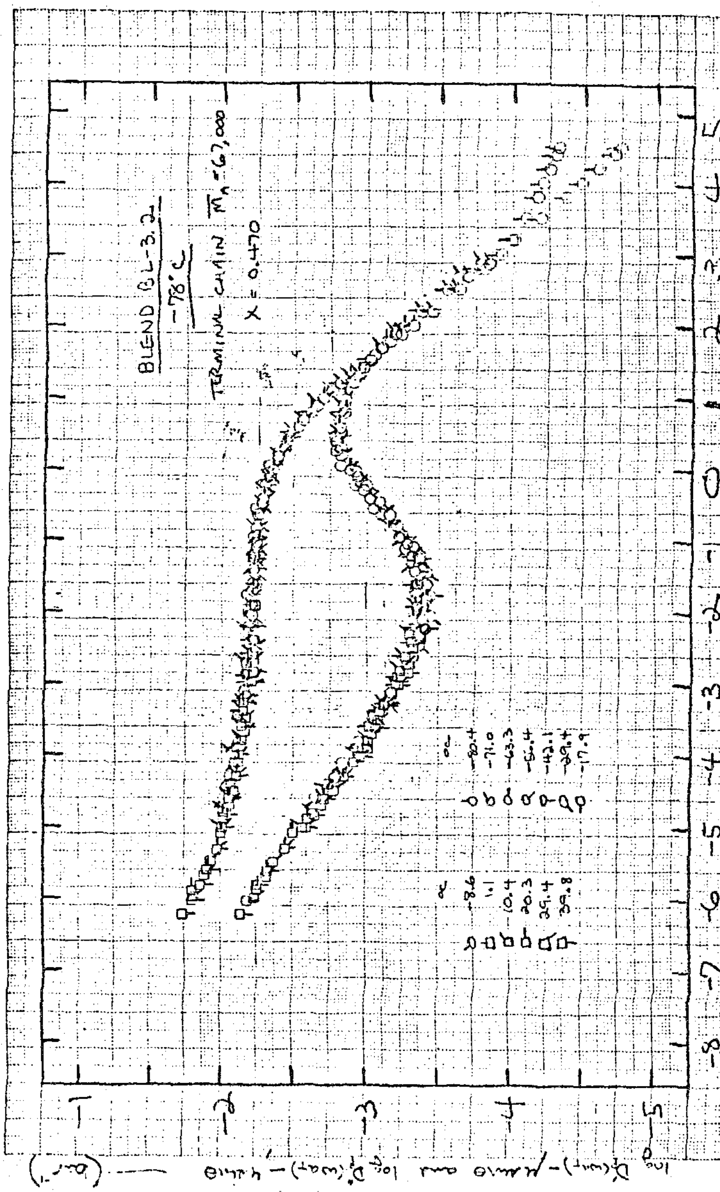
BLEND BL-3.2
-78°C
TERMINAL CHAIN $\overline{M}_n$ = 67,000
X = 0.470
log ωa_T

PROPOSITION 1

PART I

A COMPARISON OF THE RESPONSE OF VISCOELASTIC MATERIALS TO TRIANGULAR PULSE AND DELTA FUNCTION EXCITATIONS

Abstract

General expressions for the viscoelastic response to two excitation functions, the triangular pulse and the delta function, are presented. Proper comparisons of the response curves result in the formulation of criteria useful in the consideration of high speed loading rates.

A three parameter viscoelastic model is used to show representative behavior. A power law model, approximating the behavior of polyisobutylene, is also considered.

The relation of high speed testing to impact characteristics of polymeric materials is discussed. Also the possibility of directly measuring the fundamental viscoelastic parameters, relaxance and retardance, is discussed. Conclusions are drawn concerning the sufficiency of presently available loading rates for measuring these parameters.

Introduction

In polymeric materials, the segmental motions of the long chain molecules occur on a time scale that can affect the normal laboratory observation. Thus, these materials are viscoelastic or rate dependent in their mechanical behavior. That is, the mechanical response will differ depending upon the rate of excitation imposed upon the material. However, in the testing of mechanical properties of materials, it is often assumed that loading rates of rather moderate magnitudes can be considered to be equivalent to an infinitely fast excitation. One aspect of this paper deals with the range of validity of this assumption.

A second consideration deals with the concept of impact testing. It is generally accepted that impact characteristics of a material are related to the ability to withstand a high speed blow, but no particular value of loading rate is generally accepted as the beginning of the impact range. It has been suggested[1,2] that the velocity resulting from a two-foot free fall, 4.8×10^5 in/sec, be considered as the mimimum velocity for impact testing. A survey of modern impact testing methods[3] shows that devices producing loading rates as high as 2×10^7 in/sec are now being used. In this paper a minimum velocity for impact loading will be developed to determine whether such rates are sufficient for testing in the impact range.

Proposition

It is proposed that a delta function of imposed excitation be considered as the limiting condition for loading rates. The delta function causes the load to be applied and removed with infinite speed. It is further proposed that a triangular pulse be used as an approximation to the delta function. In this case the load is applied and removed at the same finite rate.

Responses to both the delta function and triangular pulse can be calculated. Comparison of the responses will give an indication of how close the triangular pulse is coming to duplicating the effect of the delta function. From these comparisons it will be possible to develop two criteria useful for guides in testing materials.

The first criterion deals with the concept of a delay time for taking data. For any given loading rate, it is possible to determine the time at which differences between the finite rate response and the response to the delta function are within the range of normal experimental error. This time, defined as the delay time, t_o, must be allowed to elapse after completion of the finite loading if meaningful data is to be obtained. The second criterion, a minimum rate for impact loading, is developed by seeking the finite rate response which closely approximates the infinite rate response over the entire time scale.

Motivation

The answers to two basic questions are being sought. First, if a material is subjected to a finite loading rate, how much time should be allowed before the data nearly duplicate that which would have been obtained if an infinite loading rate could have been imposed. Secondly, can the load be applied fast enough so that meaningful data can be taken as soon as the loading has been completed.

Aside from the above questions, there is further motivation for seeking the conditions necessary for approximating a delta function. If a true delta function of excitation could be imposed upon a viscoelastic material, the response would embody one of the fundamental material parameters, relaxance or retardance. For example, a delta function of imposed strain would yield a stress response identical to the relaxance of the material under consideration. Because of the necessity for an infinitely fast excitation, relaxance and retardance have been considered to be unattainable from real experiments. However, no criterion has been established which clearly indicates how closely one can approximate these parameters by employing properly applied finite rate excitations. For this reason, the criteria developed in this paper are of fundamental importance, and as a result, the triangular pulse could become a very useful tool to be employed in the testing of polymeric materials.

Limiting Rate of Loading - The Delta Function

It has been proposed that a delta function be considered as the limiting condition for imposed loading rates. In this section a mathematical formulation of this excitation function is presented.

A unit impulse, I(t), shown graphically in Figure 1, is defined as follows:[4]

$$I(t) = \begin{cases} 1/t' & 0 \leq t \leq t' \\ 0 & t > t' \end{cases} \qquad (1a)$$

$$\int_0^\infty I(t)dt = 1 \qquad (1b)$$

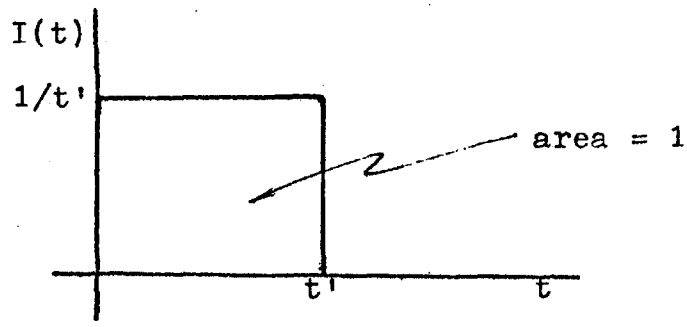

Figure 1. The Unit Impulse Function

It should be noted that Equation 1b imposes the constraint of unit area on the impulse function.

As t' approaches zero, the unit delta function, $\delta(t)$, is defined by:[5,6]

$$\delta(t) = \begin{cases} \infty & t = t' = 0 \\ 0 & t > 0 \end{cases} \qquad (2a)$$

$$\int_0^\infty \delta(t)dt = 1 \qquad (2b)$$

Figure 2 is a graphical representation of the unit delta function. Again it is useful to note that Equation 2b defines the area or "strength" of the delta function to be unity.

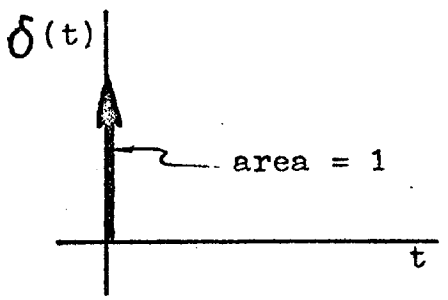

Figure 2. The Unit Delta Function

Finite Loading Rates - The Triangular Pulse

One method of approximating a delta function is by the use of a triangular excitation function, or triangular pulse. In this case, the excitation increases at a constant finite rate until a certain time, t', is reached. At this point the excitation is decreased at the same constant rate until it reaches zero at 2t'. The excitation remains zero after 2t'. Such an excitation function is shown in Figure 3. The height of the pulse must be $1/t'$ to normalize the area to unity. This is an absolute requirement if comparisons are to be made with the previously defined delta function. The unit area constraint further fixes the loading rate, or slope of the triangular excitation function, at $1/(t')^2$.

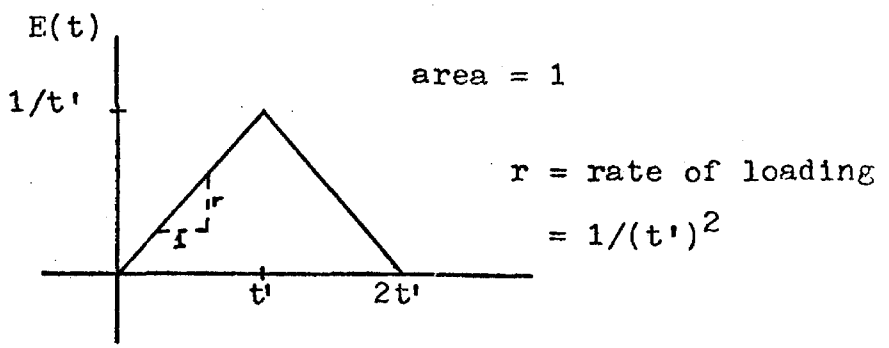

Figure 3. The Unit Triangular Pulse

In order to obtain an analytical expression for a triangular pulse, the concept of the unit step function must be introduced. The unit step function is defined as follows:

$$h(t-a) = \begin{cases} 1 & t \geq a \\ 0 & t < a \end{cases} \qquad (3)$$

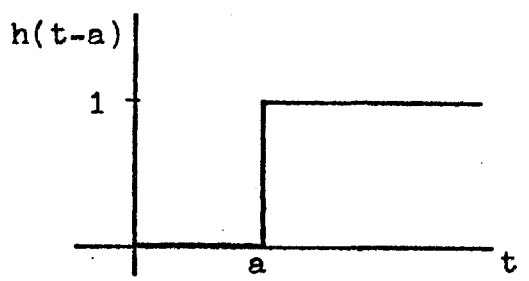

Figure 4. The Unit Step Function

The unit step function can be used to bring single terms into an expression at a given time, and it will retain the term for all succeeding time. By employing the unit step function, it is possible to express the triangular pulse as follows:(7)

$$E(t,t') = r\left[th(t-0) - 2(t-t')h(t-t') + (t-2t')h(t-2t')\right] \quad (4)$$

Equation 4 defines a family of triangular pulses; the value of t' determines the height and base dimensions of the particular pulse under consideration. Figure 5a shows how each term is brought into Equation 4 by the appropriate step function. Figure 5b shows that the individual terms sum to give the triangular pulse.

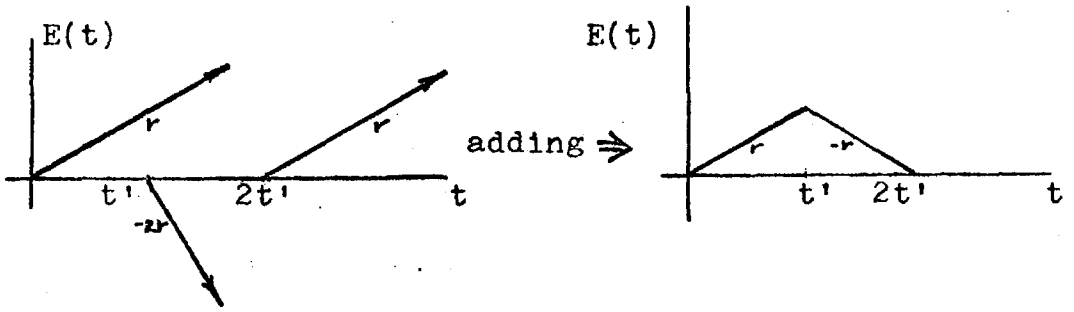

Figure 5. Graphical Formulation of the Triangular Pulse

As shown earlier, the value of the slope, r, must be $1/(t')^2$ in order to conform to the unit area constraint. Therefore, the final expression for the triangular pulse is

$$E(t,t') = (1/t'^2)\left[th(t-0) - 2(t-t')h(t-t') + (t-2t')h(t-2t')\right] \quad (5)$$

Equivalence of the Excitation Functions

If valid comparisons are to be made between the two previously defined excitation functions, the two must be equivalent in the limit of zero loading time. That is, as the rate of loading is steadily increased, the triangular

pulse must become equivalent to the delta function. It is sufficient to show that the following limiting operation is valid.

$$\lim_{t'\to 0} E(t,t') \stackrel{?}{=} \delta(t) \tag{6}$$

Substituting the expression given by Equation 5 for $E(t,t')$ gives:

$$\lim_{t'\to 0} \left| (1/t'^2)\left[th(t-0) - 2(t-t')h(t-t') + (t-2t')h(t-2t') \right] \right| \stackrel{?}{=} \delta(t) \tag{7}$$

At this point it is advantageous to remove the time dependence through the use of the Laplace transform. The Laplace transformed function, $\bar{f}(s)$, of a time dependent function, $f(t)$, is defined by:

$$\bar{f}(s) = \int_0^\infty \exp(-st) f(t)\,dt \tag{8}$$

Applying this transformation termwise to Equation 7 yields:

$$\lim_{t'\to 0}\left[(1/t'^2)\left[\int_0^\infty \exp(-st)th(t)dt - 2\int_0^\infty \exp(-st)th(t-t')dt + \int_0^\infty \exp(-st)th(t-2t')dt \right] + (1/t')\left[2\int_0^\infty \exp(-st)h(t-t')dt - 2\int_0^\infty \exp(-st)h(t-2t')dt \right] \right] \stackrel{?}{=} \int_0^\infty \exp(-st)\delta(t)dt \tag{9}$$

Recognizing that the step functions are zero unless the argument is greater than or equal to zero, and further that the Laplace transform of a delta function, that is, the right hand side of Equation 9, is defined as unity[4], allows

Equation 9 to be simplified as follows:

$$\lim_{t'\to 0}\left[(1/t'^2)\left[\int_0^{\infty} t\exp(-st)dt - 2\int_{t'}^{\infty} t\exp(-st)dt + \int_{2t'}^{\infty} t\exp(-st)dt\right] + (1/t')\left[2\int_{t'}^{\infty}\exp(-st)dt - 2\int_{2t'}^{\infty}\exp(-st)dt\right]\right] \stackrel{?}{=} 1 \quad (10)$$

Integrating each term of the left side of Equation 10 gives:

$$\lim_{t'\to 0}\left[1/(t's)^2 - (2/t's)\exp(-st') - (2/(t's)^2)\exp(-st') + (2/t's)\exp(-2st') + (1/(st')^2)\exp(-2st') + (2/t's)\exp(-st') - (2/t's)\exp(-2st')\right] \stackrel{?}{=} 1 \quad (11)$$

Collecting terms:

$$\lim_{t'\to 0}\left[\left[1/s^2t'^2\right]\left[1 - 2\exp(-st') + \exp(-2st')\right]\right] \stackrel{?}{=} 1 \quad (12)$$

The numerator and denominator of the left side of Equation 12 both approach zero as t' approaches zero. The limit is evaluated using L'Hospital's rule.

$$\lim_{t'\to 0}\left[\left[1/2st'\right]\left[0 + 2\exp(-st') - 2\exp(-2st')\right]\right] \stackrel{?}{=} 1 \quad (13)$$

Applying L'Hospital's rule a second time:

$$\lim_{t'\to 0}\left[\left[1/2\right]\left[0 - 2\exp(-st') + 4\exp(-2st')\right]\right] = 1 \quad (14)$$

qed

The equality in Equation 14 is sufficient to show that the delta function is the limit of the triangular

pulse function as the loading time, t', approaches zero.

The proof has been included for two reasons. First it gives motivation for the earlier proposal that the delta function be considered as the limit of finite loading rates. Secondly the proof assures that valid comparisons between triangular pulse and delta function loadings can be made, and further, that differences resulting from the two types of loading should disappear as the loading rate, $1/t'^2$, becomes large.

Response to Excitations

For a viscoelastic material, the relationship between excitation and response are most clearly analyzed when the time dependence is converted through the use of Laplace transforms. In general for a viscoelastic material[8]:

$$\bar{R}(s) = s\bar{M}(s)\bar{E}(s) \qquad (15)$$

where $\bar{R}(s)$, $\bar{E}(s)$, $\bar{M}(s)$ represent the response, excitation, and material parameter, respectively, and s is the Laplace transform variable. The corresponding time dependent functions are R(t), E(t), and M(t).

Equation 15 can be interpreted as follows: If the expression for the excitation is transformed into the Laplace plane, and further, if the material function can be similarly transformed, then the Laplace transformed response of the material is immediately given by Equation 15. Laplace inver-

sion of this response, $\bar{R}(s)$, gives the time dependent response, $R(t)$.

Using this method, the general time dependent response to a triangular pulse of arbitrary loading rate can be found. Similarly, the response to a delta function excitation can be found. A comparison of the responses offers a criterion for determining how close the triangular pulse is coming to duplicating the effect of the delta function. As the rate of excitation is increased in the triangular pulse, the response should approach that produced by a delta function.

For the present it will be assumed that a material parameter, $M(t)$, is known which can be transformed to $\bar{M}(s)$ for use in Equation 15. As indicated earlier, the Laplace transform of a delta function is unity. Therefore, for the case of delta function excitation, Equation 15 reduces to:

$$\bar{R}_{\delta}(s) = s\bar{M}(s) \tag{16}$$

where $\bar{R}_{\delta}(s)$ indicates that the response to a delta function is being considered. Laplace inversion of this general expression yields:

$$R_{\delta}(t) = M'(t) + M(0)\delta(t) \tag{17}$$

Equation 17 is the general expression for the time dependent response, $R_{\delta}(t)$, of a material characterized by the parameter $M(t)$, when this material is subjected to a

delta function of excitation. M(0) is the value of the material parameter at zero time, and M'(t) is the first time derivitive. It is clear that the material parameter must be at least once continuously differentiable to be useful in this analysis.

The general response to a triangular pulse is similarly determined by inserting the transformed expression for the excitation into Equation 15 and then inverting the resulting expression back to obtain the time dependent response. In this case Equation 15 becomes:

$$\bar{R}_{\Delta}(s) = \left[\left[s\bar{M}(s)\right] \quad \left[1/(st')^2 \left[1-2\exp(-st')+\exp(-2st')\right]\right]\right] \quad (18)$$

The expression in the brackets is the Laplace transformed triangular pulse excitation. The expression is rewritten to show the form of each term that must be inverted.

$$\bar{R}_{\Delta}(s) = \left[1/(t')^2\right]\left[\bar{M}(s)/s - 2\exp(-st')\bar{M}(s)/s + \exp(-2st')\bar{M}(s)/s\right] \quad (19)$$

The first term of Equation 19 can immediately be inverted to integral form. Yagii and Tschoegl[7] have noted that the second and third terms can be inverted by employing the transform pair technique. Using this method, Laplace inversion of Equation 19 gives the following expression, where u is a dummy variable of integration.

$$R_{\Delta}(t,t') = (1/t'^2)\left[\left(\int_0^{t} M(u)du\right)h(t) - \left(2\int_0^{t-t'} M(u)du\right)h(t-t') + \left(\int_0^{t-2t'} M(u)du\right)h(t-2t')\right] \qquad (20)$$

Here $R_{\Delta}(t,t')$ defines a family of time dependent responses of a material characterized by the material parameter $M(t)$ when this material is subjected to a triangular pulse of arbitrary loading rate $1/t'^2$. The material parameter must be integrable for use in Equation 20.

Equations 17 and 20 are the general expressions for the response of a material to the two types of loading. In subsequent sections, strain excitations, $\epsilon(t)$, will be considered. The response, therefore, will be stress, $\sigma(t)$, and the material parameter will be the modulus, $G(t)$.

Response of the Three Parameter Material

One of the simplest expressions for the modulus is the three parameter model:

$$G(t) = G_1 + G_2\exp(-t/\tau) \qquad (21)$$

The dimensions of G_1 and G_2 are chosen as Bars(1 Bar = 10^6 dynes/cm^2). The relaxation time, τ, has units of seconds. The nature of the material being considered will depend upon the numerical values of G_1, G_2, and τ. For simplicity in the first set of calculations, G_1, G_2, and τ will be chosen as unity. The following results are easily

obtained.

$$G(t) = 1 + \exp(-t) \tag{22}$$

$$\sigma_{\updownarrow}(t) = -\exp(-t) + 2\delta(t) \tag{23}$$

$$\sigma_{\Delta}(t) = \left[(1/t'^2)\right]\left[(t-\exp(-t)+1)h(t) - 2(t-t'-\exp(-t+t')+1)h(t-t') + (t-2t' - \exp(-t+2t') + 1)h(t-2t')\right]$$

Here $\sigma_{\updownarrow}(t)$ is the stress resulting from a delta function of imposed strain, and $\sigma_{\Delta}(t)$ is the stress resulting from a triangular pulse of imposed strain. These can be rewritten in a more convenient form which more clearly shows the separate time intervals involved.

$$\sigma_{\updownarrow}(t) = \begin{cases} \infty & t=0 \\ -\exp(-t) & t>0 \end{cases} \tag{24}$$

$$\sigma_{\Delta}(t) = (1/t'^2) \begin{cases} 1 + t - \exp(-t) & 0<t\leq t' \\ -1-t+2t' +2\exp(-t+t')-\exp(-t) & t'\leq t\leq 2t' \\ 2\exp(-t+t')-\exp(-t+2t')-\exp(-t) & t\geq 2t' \end{cases}$$

Equations 24 are plotted in Figure 6. Various values of t', and thus various values of loading rate $1/t'^2$, are considered.

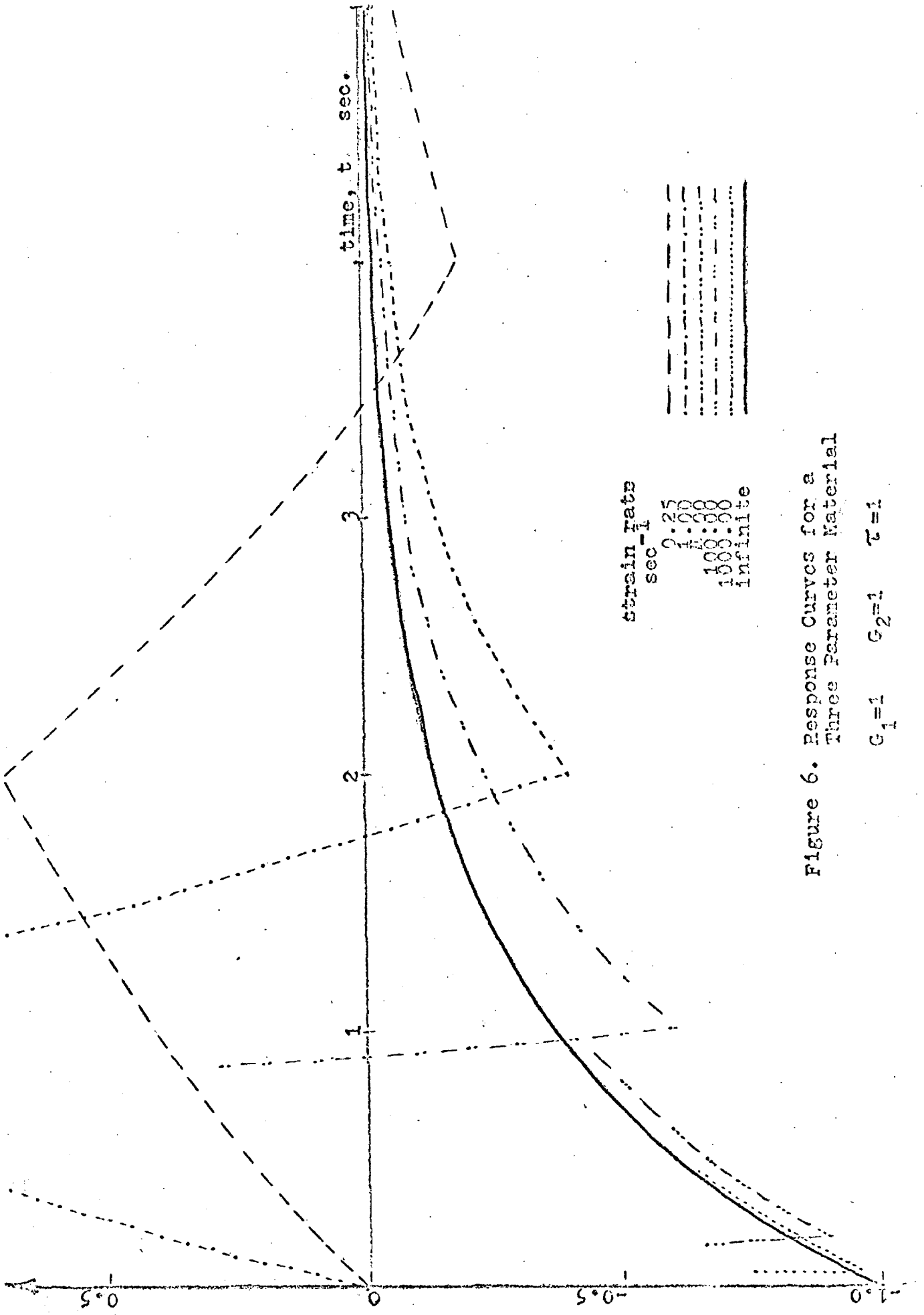

Figure 6. Response Curves for a Three Parameter Material

$G_1=1 \quad G_2=1 \quad \tau=1$

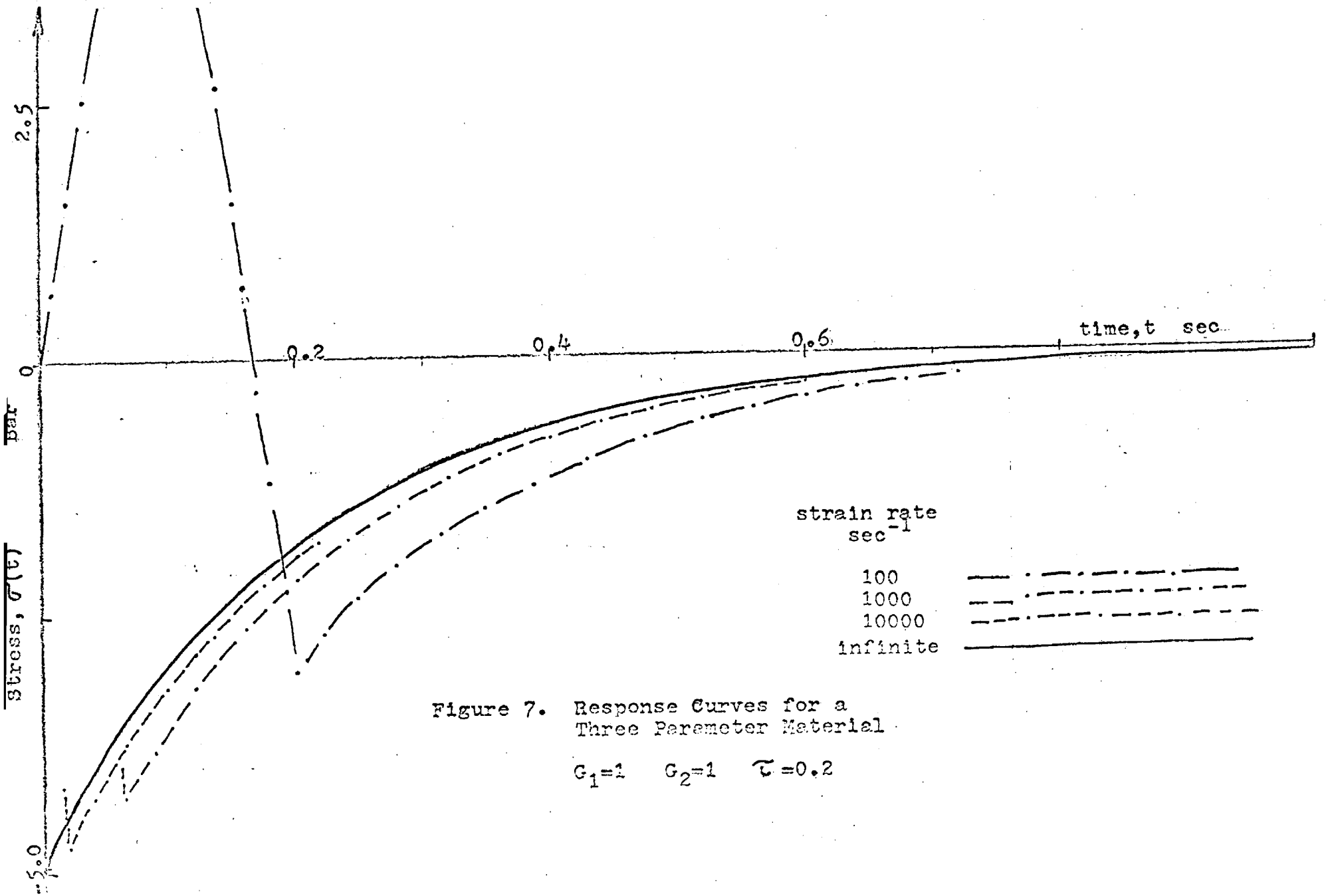

Figure 7. Response Curves for a Three Parameter Material

$G_1=1 \quad G_2=1 \quad \tau=0.2$

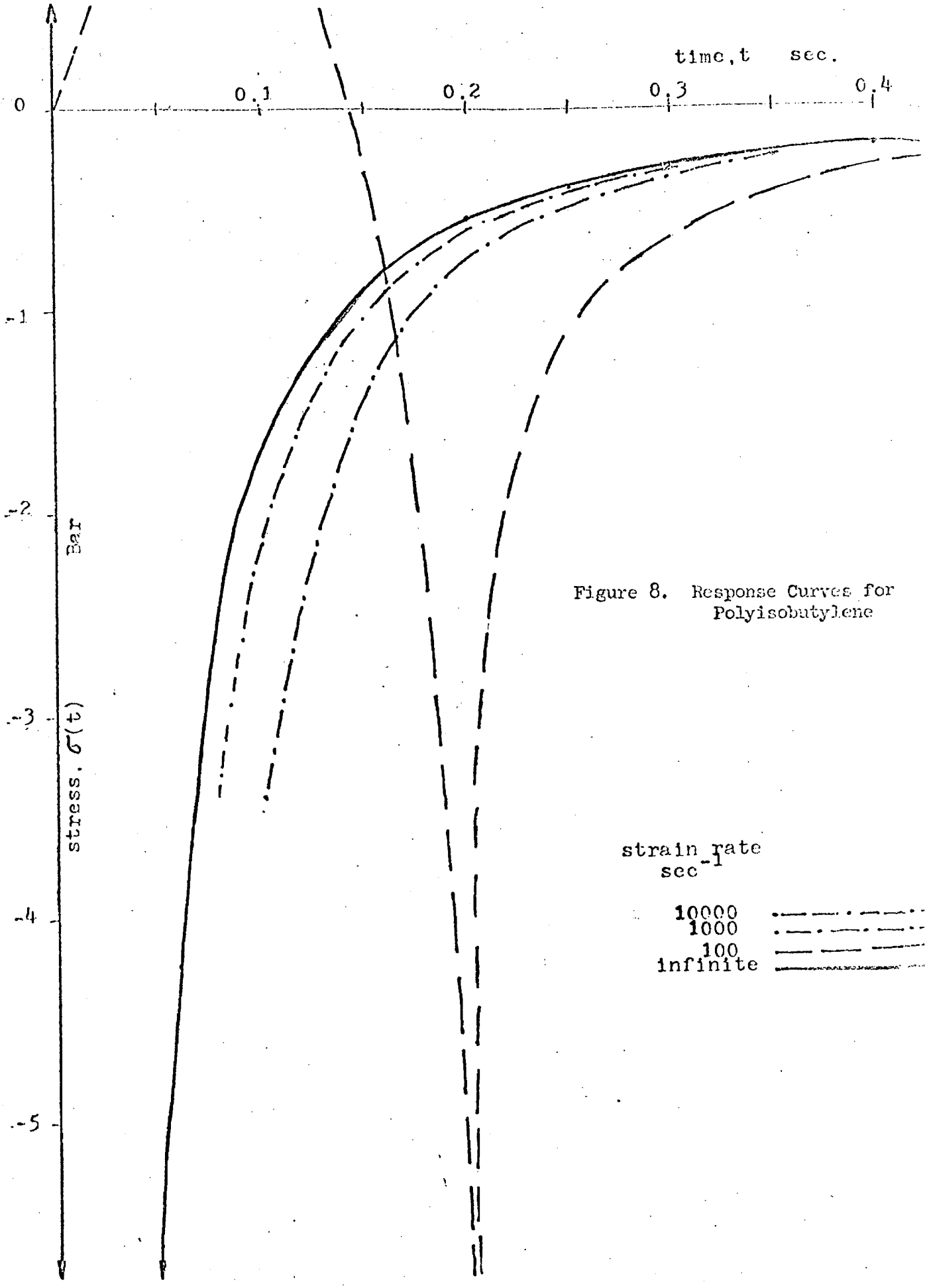

Figure 8. Response Curves for Polyisobutylene

Delay Time - Criterion for Useful Data

The curves of Figure 6 contain valuable information for anyone dealing in testing of rate sensitive materials. It is clear from this figure that at sufficiently long times, all loading rates will yield response data which is identical to within normal experimental error. The experimenter will wish to know how long he must wait before this condition is reached. This delay time, t_o, will depend upon the material under consideration and upon the loading rate.

For the three parameter material of Figure 6, it is assumed that responses can be measured to within 0.01 Bar. The delay time now becomes the time at which the difference between the finite rate response and the limiting response becomes less than 0.01 Bar. The values of t_o for the various loading rates are tabulated below.

Table I Delay Times for Three Parameter Material
$G_1 = 1 \quad G_2 = 1 \quad \tau = 1$

Rate, r, sec^{-1}	Delay time, t_o, sec
0.25	6.82
1.00	5.23
4.00	4.17
100.00	2.34
1000.00	1.13

As shown in Figure 9 the values of logarithm of delay time plotted against logarithm of rate yield a straight line.

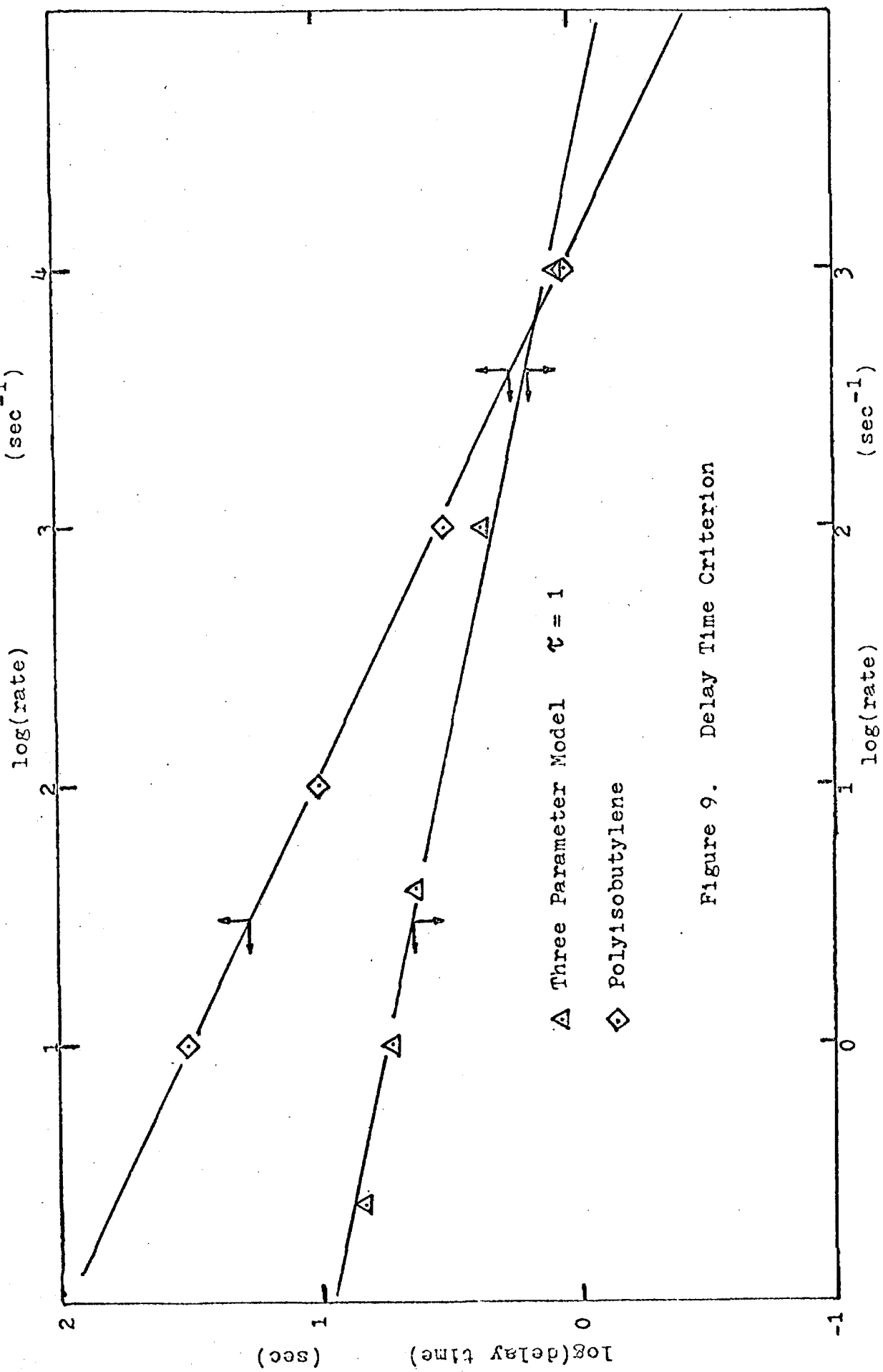

Figure 9. Delay Time Criterion

Thus the following criterion for delay time is established.

$$t_o = 5.4r^{-0.214} \qquad (25)$$

Thus, knowing the rate which was imposed, the experimenter can now estimate how long he must wait before data becomes significant. The criterion of Equation 25 is not general. It holds only for the three parameter material under consideration. However, a similar criterion can be derived for any material by analogous procedure.

Effect of Relaxation Time in the Three Parameter Model

The three parameter model considered in previous sections is useful for showing representative behavior but does not approximate the behavior of any real polymeric material. Relaxation times for typical polymeric materials are of the order of 10^{-9} sec. For the three parameter model, a value of τ in this range would compress the interesting portion of the response curves into a very short time interval. Figure 7 shows the effect of changing τ to 0.2 sec. This behavior is a result of having only a single relaxation time, and this is not physically realistic.

It should be noted that while the three parameter model does not represent a real material, the kinds of changes observed as τ is changed should be in the same direction as in real materials. Comparing Figures 6 and 7 clearly shows

that as τ is decreased, higher loading rates are necessary to similarly approximate the limiting curve.

Impact Loading Criterion and Material Impact Parameter

It is clear from Figure 6 or 7 that as loading rate is increased, the resulting response curves more closely approximate the limiting curve which results from an infinite loading rate. Furthermore there will be some rate at which a response comes close enough to the limiting curve that there would be very little to gain by increasing the loading rate further. This leads to the development of the following impact loading criterion: When the response which results from a finite loading rate comes within tolerable limits, say 5%, of duplicating the response to an infinite loading, the material can be considered as being tested in the impact range. Mathematically, this criterion can be formulated as follows:

$$\sigma_{\Delta}(2t')/\sigma_{\uparrow}(2t') = 1.05 \qquad (26)$$

The argument must be 2t' because that is the point at which the triangular pulse response begins its approach to the limiting curve. As shown in Figures 6 and 7 the nature of the responses is such that they cannot be meaningfully compared before 2t'.

There will be a unique value of t' which will satisfy

the above impact criterion. This value designated by t'_{crit}, will depend upon the material under consideration and thus could be considered to be a parameter which characterizes the impact properties of materials. This is directly related to a critical loading rate, r_{crit}, for testing in the impact range. The larger the rate necessary to satisfy the impact loading criterion the better the impact properties of the materials should be. Results for the three parameter models considered earlier are given in Table II.

Table II Impact Parameters for Three Parameter Models

	Material 1 $G_1=1$ $G_2=1$ $\tau=1$	Material 2 $G_1=1$ $G_2=1$ $\tau=0.2$
t'_{crit}	0.49 sec	0.0098 sec
r_{crit}	416.00 sec^{-1}	10400 sec^{-1}

It takes a much higher rate of loading to get Material 2 into the impact test range. Again it should be noted that neither of these are good approximations to the behavior of a real material; however the established criterion, Equation 26, is completely general and can be used with any suitable material model.

Behavior of A Power Law Material -- Polyisobutylene

As mentioned in earlier sections the three parameter models do not give a good approximation to any real material. Several expressions have been developed which give a fairly good representation of material behavior. One such expression for the modulus is given by the power law expression:

$$G(t) = G_e + (G_g - G_e)/(1+at)^b \qquad (27)$$

By fitting the above equation to the data on the modulus of polyisobutylene taken by Catsiff and Tobolsky[9], Smith[10] was able to determine all of the adjustable parameters in Equation 27. Thus for polyisobutylene the power law expression for the modulus in units of Bars and seconds becomes:

$$G(t) = 7.59 + 30190/(1 + 2.964 \times 10^8 t)^{0.6767} \qquad (28)$$

Equation 27 is now the material function which is introduced into the general response expressions, Equations 17 and 20. The theoretical response curves for polyisobutylene under various rates of loading are shown in Figure 8. The behavior is qualitatively similar to that observed in the three parameter materials. As rate of loading is increased, the response curves successively approach the limiting curve.

The delay times for polyisobutylene are calculated and tabulated below:

Table III Delay Times for Polyisobutylene

Rate, r, sec^{-1}	Delay Time, t_o, sec
10	32.8
100	9.9
1000	3.3
10000	1.2

Again, plotting the logarithm of rate against the logarithm of delay time gives a straight line. From the slope of this plot, shown in Figure 9, the following relationship is obtained:

$$t_o = 100(r)^{-0.5} = 100(t') = 50(2t') \qquad (29)$$

This says that for polyisobutylene, the delay time is roughly fifty times the time required to complete the application of the triangular loading function. This is somewhat more restrictive than the general rule of thumb, t_o=10×loading time , often employed in the testing of viscoelastic materials.

Finally turning to the impact criterion for the polyisobutylene model, we find that no value of t' clearly satisfies Equation 26. For even the most rapidly applied load, the response to the delta function is much smaller in absolute value than the response to the triangular pulse at $t = 2t'$. However the response curves slope upward very steeply and converge very rapidly immediately after 2t'. If 0.001 seconds

is allowed for this to occur, the response curve corresponding to a loading rate of $10^{8}sec^{-1}$ comes close to satisfying the criterion. While this is not a completely rigorous solution, it does show that for a real material such as polyisobutylene, extremely high loading rates are necessary to even approach impact conditions.

Summary and Conclusions

The triangular pulse excitation has been shown to be a valid method of approximating a delta function. Comparisons of responses to the two types of excitation led to the development of general delay time and impact loading criteria. Consideration of a three parameter viscoelastic model resulted in representative behavior qualitatively similar to real materials. A power law model, approximating polyisobutylene behavior, showed the necessity for extremely large loading rates in order to satisfy the impact loading criterion.

The first significant conclusion that can be drawn involves the range of rate sensitivity of polymeric materials. It was originally felt that perhaps very large loading rates were unnecessary because they essentially exceeded the rate sensitivity of the materials being tested. The single real material considered here clearly shows that this is not the case. The response of polyisobutylene is dependent on the rate of loading for rates at least as high as 1×10^{8} sec^{-1}.

Conclusions concerning the impact properties of materials can perhaps be drawn from knowledge of the rate necessary to satisfy the impact loading criterion. As suggested earlier, the more difficult it is to impose a loading rate which satisfies this criterion, the better the impact properties of the material may be. The validity of this correlation could be checked if

suitable expressions were available for the moduli of materials whose relative impact properties are known. However, the excellent impact properties of two-phase polymeric materials suggest that other considerations such as shock wave dissipation and crack propagation may be more fundamental to the understanding of impact properties. This would involve failure criteria not considered here.

Finally, perhaps the most important conclusions which result from this work are concerned with the feasibility of obtaining the fundamental material parameters relaxance and retardance from real experiments. Analysis of the power law model shows that approximate measurements of the relaxance of polyisobutylene would require a triangular strain pulse with a loading rate equal to 1×10^{8} sec^{-1}. This is clearly a difficult experiment to perform. However, the analysis further shows that if the strain excitation could be applied and removed at a more moderate rate of 100 sec^{-1}, after a delay of ten seconds the response data would essentially duplicate the relaxance. Thus a method for segmentally duplicating the relaxance curve becomes apparant. Employing triangular pulses of various rates, along with the delay time criterion developed in this paper, allows a portion of the relaxance curve to be closely approximated. The amount of the relaxance curve which can be determined in this manner depends upon the rates of triangular loading functions which can be produced.

The range of currently available loading rates discussed earlier is for simple extensional loading patterns. The possibilities of producing rapid triangular pulse loadings have not been fully explored. However, if an apparatus could be designed which developed a triangular pulse of variable rate, a great deal of information concerning the nature of the relaxance and retardance functions could be obtained. Thus it is concluded that at least portions of these fundamental parameters can be obtained experimentally. However,this conclusion should be regarded with caution. Obtaining the interesting portions of the relaxance curve will demand rather forbidding strain rates. At very high loading rates, inertial effects, shock waves, and and end effect complications require careful consideration. All of these things will affect experiments designed to measure relaxance and retardance. However, it is clear from this paper that the triangular pulse deserves careful consideration as a fundamental method of testing polymeric materials. The development of a device producing triangular pulse excitations could result in the determination of information about polymeric materials which was formerly considered to be unattainable.

LIST OF TABLES

LIST OF FIGURES

REFERENCES

1. P.D. Ritchie, Physics of Plastics, Van Nostrand (1965)

2. E. Baer,ed., Engineering Design for Plastics, SPE Polymer Science and Engineering Series, Reinhold(1964)

3. R.E.Cohen,"Brief Discussion of Impact Testing" Polymer Laboratory Seminar,Spalding Laboratory,Caltech,May,1968

4. M. Spiegel, Theory and Problems of Laplace Transforms , Schaum(1965)

5. C.R. Wylie, Advanced Engineering Mathematics, McGraw-Hill(1960)

6. E. Kreyszig, Advanced Engineering Mathematics,Wiley(1967)

7. K. Yagii and N.W.Tschoegl,First Annual Report,CHECIT PL 68-1, June,1968

8. J.D.Ferry, Viscoelastic Properties of Polymers, Wiley(1967)

9. E. Catsiff and A.V.Tobolsky, J.Colloid Sci.,10,375(1955)

10. T.L. Smith, Unpublished Results

PROPOSITION 1
PART 2

ANALYSIS OF THE CRITICAL POINTS AND OF THE EFFECTS OF A CHANGING DISCRETE SPECTRUM ON THE PHENOMENOLOGICAL EQUATIONS FOR RELAXATION IN LINEAR SYSTEMS

Abstract

The equations which describe the phenomenology of relaxation in linear systems are analyzed for various sets of relaxation times and associated parameters. In the first section of this paper, particular emphasis is placed on the locations of the critical points (maxima and inflections) when these equations are plotted on double logarithmic coordinates. The critical points are determined analytically for the simplest case involving a single relaxation time. Comments are made concerning the validity of using the various critical points of the response curves as a means for classifying and comparing the response of different systems.

In the second section of this work the effects of a changing discrete spectrum of relaxation times are elucidated by graphical means. The results are mostly interesting from a didactic point of view, but some quantitative information is obtained concerning the range of influence of a single relaxation time.

Introduction

Phenomenological theories are formulated to predict the behavior of a system under a given set of conditions after having already observed the behavior under other conditions. Such theories do not uncover unkown properties of a system, but instead describe the known behavior. Therefore, it is not surprising that quite often one phenomenological theory based on a given set of mathematical equations can be used to describe the behavior of a number of very different physical systems. The equations under consideration here are used to describe relaxation phenomena in a variety of cases. For example, one can use the same set of equations to describe relaxation in electric circuits, mechanical systems of springs and dashpots, dielectrics, and viscoelastic materials. Some of the interesting interrelations which exist among the four examples listed above have appeared in literature (1,2,3,).

In this paper the equations and discussion are couched in the formalism of time and frequency dependent moduli since the author was most familiar with the nomenclature and terminology in that particular area. However, as discussed above, the equations themselves are independent of any physical interpretation, and therefore the analysis is quite general. Equations 1-3 listed below are the particular expressions of interest here;

in each case the type of time or frequency dependent modulus associated with the equation is also listed since this will greatly facilitate the discussion. In addition to Equations 1-3, the commonly used loss tangent, $\tan\delta$ is also discussed in several places.

Relaxation modulus $$G(t) = G_e + \Sigma\, G_i\, e^{-t/\tau_i} \qquad (1)$$

Storage modulus $$G'(\omega) = G_e + \Sigma\, G_i \omega^2 \tau_i^2/(1+\omega^2\tau_i^2) \qquad (2)$$

Loss modulus $$G''(\omega) = \Sigma G_i\, \omega\tau_i/(1+\omega^2\tau_i^2) \qquad (3)$$

The sums are easily evaluated on a digital computer, and therefore the number of terms taken in the series expressions was not limited by the amount of time or effort involved. However at most three terms were used, and this was found to be sufficient to gain some understanding of the effect of adding relaxation times to the equations. The advantage of the computer lies in the ability to calculate and plot values for the various expressions at closely spaced intervals over a very large range of the parameter t or ω. In this way it was possible to study the effect of spacing and the range of influence of the particular set of relaxation times incorporated into the equations.

McCrum et al (2) have discussed the critical points of these equations when plotted semilogarithmically, i.e. G(t), G'(w) or G"(w) against the logarithm of t or ω. However, the wide range of system response often observed

in relaxation phenomena tends to make this an unrealistic analysis. For example, McCrum's model systems containing a single relaxation time allowed for a decay in the value of G(t) from 1 X 10^{10} to 1 X 10^{9}. If G(t) is taken to represent the relaxation modulus of a typical amorphous polymer, this range of relaxation is too small by about a factor of 1000. Therefore it is much more meaningful to consider the locations of the critical points of the double logarithmic plots since the observed phenomena are usually represented more clearly in this way. In some cases the locations of the critical points of the double logarithmic plots are taken to be meaningful characteristics of a particular system and are often used for first-order comparisons with the response of other systems. The analysis presented here will show which of the critical points are reliable for comparisons of this sort and why others may give rise to meaningless comparisons.

Representative Behavior - Single Relaxation Time

Figure 1 shows the response curves for a spectrum containing a single relaxation time. Several things are apparent from inspection of these plots. The maximum in the loss modulus appears exactly at $\omega = 1/\tau_1$. The maximum in the loss tangent, G"/G', is shifted to the right (i.e. toward lower frequencies) of this value The inflection points of the relaxation modulus and storage modulus curves are also shifted to the right of τ_1.

For a single relaxation time, the position of the critical points in the response curves can be found analytically. For the inflection point in the plot G(t) against log t we must have a first derivative which exists and goes through a maximum. Thus we seek the value of t for which

$$\frac{d^2 \log G(t)}{d \log^2 t} = 0 \tag{4}$$

The operator can be transformed as follows

$$\frac{d^2 \log}{d \log^2 t} = \frac{d}{d \log t}\left(\frac{d \log}{d \log t}\right) = \frac{d}{d \log t}\left(\frac{d \ln}{d \ln t}\right) =$$

$$2.303 \frac{d}{d \ln t}\left(\frac{d \ln}{d \ln t}\right) = 2.303\, t \frac{d}{dt}\left(\frac{d \ln}{d \ln t}\right) \tag{5}$$

The derivative in parenthesis can be evaluated readily for the case of a single relaxation time.

$$\frac{d \ln G(t)}{d \ln t} = \frac{d \ln (G_e + G_1 \exp -t/\tau_1)}{d \ln t} = \frac{t\, d \ln (G_e + G_1 \exp -t/\tau)}{dt}$$

$$= -\frac{G_1}{\tau_1}\left(\frac{t \exp -t/\tau_1}{G_e + G_1 \exp -t/\tau_1}\right) \tag{6}$$

Substituting this result into Equation (5) gives

$$\frac{d^2 \log G(t)}{d \log^2 t} = \frac{2.303\, G_1\, t \exp -t/\tau_1}{(G_e + G_1 \exp -t/\tau_1)^2}\left(\frac{-G_e t}{\tau_1} + G_e + G_1 \exp -t/\tau_1\right) \tag{7}$$

Setting the second derivative equal to zero for the point of inflection gives the following relation

$$(R - 1) = \frac{G_1}{G_e} \exp - R \qquad (8)$$

where $R = t_{infl}/\tau_1$. Thus the point of inflection, t_{infl}, is seen to be greater than τ_1, i.e. the inflection point occurs to the right of τ_1. Furthermore the point of inflection depends upon the ratio, G_1/G_e. This means that the amount of drop between glassy and equilibrium moduli on logarithmic coordinates will determine how far the inflection point is shifted from $t = \tau_1$.

Identical procedures carried out on the expression for the storage modulus of a single relaxation time model gives

$$G_e/(G_e + G_1) - \omega^4 \tau_1^4 = 0 \qquad (9)$$

The point of inflection, w_{infl}, must be less than $1/\tau_1$, i.e. lying to the right of τ_1 in Figure 1. As before, the value of w_{infl} depends upon the values of the glassy and equilibrium limits.

The location of the maximum in the log G"(w) vs log w curve is found by seeking value of w for which the first derivative is zero and the second derivative is negative. For the single relaxation time case we have:

$$\frac{d \log G''(\omega)}{d \log \omega} = G_1 \left(\frac{1 - \omega^2 \tau_1^2}{1 + \omega^2 \tau_1^2}\right) \qquad (10)$$

$$\frac{d^2 \log G''(\omega)}{d \log^2 \omega} = \frac{-4.606\, \omega^2 \tau_1^2 G_1}{(1 + \omega^2 \tau_1^2)^2} \qquad (11)$$

Clearly the two conditions are satisfied at $\omega = 1/\tau_1$. It is interesting to note that the lack of an equilibrium constraint in the expression for G"(w) is responsible for the resulting occurrence of the maximum exactly at $\omega = 1/\tau_1$.

The maximum in the loss tangent, $\tan\delta = G''/G'$, can be located in a similar fashion. However the equilibrium constraint appears in the denominator of $\tan\delta$, and therefore the maximum does not appear at $\omega = 1/\tau_1$. Instead the location of the maximum in the loss tangent is defined by the relation

$$G_e/(G_e + G_1) - \omega^2\tau^2 = 0 \qquad (12)$$

which predicts that $\tan\delta_{max}$ appears at a different (and lower) frequency from that of the inflection in the log G' vs log w curve.

McCrum's analysis of the semilogarithmic plots showed that the inflection in G(t) occurred at $t = \tau_1$ Furthermore the peak in G" and the inflection in G' both appear at $w = 1/\tau_1$. This is a direct result of the disappearance of the constant G_e during the semilogarithmic differentiation. However as in the double logarithmic case, the equilibrium constraint must appear in the denominator of the loss tangent and does not drop out during the semilogarithmic differentiation. Thus the peak in tan δ appears at the same position on both double and semilogarthmic plots.

It is immediately apparent that the inflection

points of Equations 1 and 2 appear at different locations along the time or frequency axis depending upon how the equations are plotted. Thus the nature of the particular plot employed should accompany any reference to an "inflection frequency" characteristic of a given system. An even more important result is the observation that all of the critical points, except for the peak in G", are affected by the amount of relaxation which the system undergoes. This is seen quite clearly, for example, in Equations 8,9,and 12, all of which relate the particular critical point of interest to the upper and lower (i.e. the unrelaxed and relaxed) limits of the system response in addition to the relaxation time governing the process. Therefore comparisons of the inflection points in G(t) and G'(w) and of the peak locations of $\tan\delta$ for various systems do not give a clear indication of the differences in the controlling relaxation times for these systems. Only the location of the peak in G" is independent of the magnitude of the relaxation process. For this reason the maximum in G" is the most useful of the critical points for comparing the location of the relaxation processes of different systems.

The Discrete Spectrum

The summation in Equation (1) implies that each relaxation time, τ_i , is being associated with a definite

spectral strength, G_i. Alternatively, this spectral strength can be envisioned as resulting from a total of G_i distinct relaxation times, all of unit spectral strength degenerating to superpose at $t=\tau_i$ on the time scale. In terms of a Maxwell model these two interpretations correspond to the following two equivalent representations: (a) one Maxwell element for each relaxation time τ_i, with spring modulus G_i; or (b) G_i Maxwell elements all with relaxation time τ_i and with unit spring modulus. As will be discussed later, it is often necessary to weight the smaller relaxation times with larger values of spectral strength to elucidate the behavior of the individual relaxation times. The ramifications of this weighting procedure as it affects the discrete spectrum and associated model, should be kept in mind when considering the results presented here. Thus for a large number of relaxation times we can construct the following equivalent spectra.

1 τ's weighted with appropriate unequal G's and spaced equally along the time scale

2 τ's with equal spectral strength and spaced equally on the time scale, with G_i of these relaxation times degenerating to superpose at various points on the time scale

Effect of the Weighting Parameter, G_i

Figures 2 and 3 show plots of G'(w) and G"(w) in double logarithmic coordinates for a discrete spectrum of three relaxation times separated from each other by 4 decades on the frequency scale. In Figure 2, the G_i were all chosen equal to 0.333×10^{10} while in Figure 3 the values of G_i were 0.9×10^{10}, 0.9×10^{9}, 0.9×10^{8} respectively for the corresponding τ_i in order of increasing time. Comparison of these two figures reveals that the numerical value of G_i can have a significant effect on the shape of the response curves. The choice of equal weighting parameters results in a symmetric effect on the loss modulus but a marked anti-symmetric effect on the storage modulus. Properly chosen values of G_i as in Figure 3 can equalize the effect on G'(w) but gives rise to anti-symmetric behavior in G"(w). As indicated earlier, the spectrum of Figure 3 must be considered differently from a spectrum containing only three equal relaxation times. Using the concept of degenerate relaxation times superposing at some point along the time scale this particular spectrum can be considered as containing 100 relaxation times of unit spectral strength at $t=\tau_3$ and 10 unit relaxation times at $t=\tau_2$ for every 1 unit relaxation time at $t=\tau_1$.

The Effect of Spacing of the Relaxation Times

The curves in Figures 4 and 5 were generated using a spectrum weighted as Figure 3 above, while the spacing between relaxation times was decreased. The separation was 4 decades in Figure 3, 2 decades in Figure 4 and 1 decade in Figure 5. It is apparent from Figure 3 that a spacing of four decades is sufficient for the effect of the relaxation times to be completely independent of each other. The relaxation and storage moduli drop from glassy to equilibrium values in equal steps with a distinct plateau between each step. The loss modulus has three distinct peaks with the highest peak occurring at $t=\tau_3$ and the two smaller peaks occurring at $t=\tau_2$ and $t=\tau_1$, respectively. Moving the relaxation times to a smaller spacing of 2 decades results in the beginning of interaction between neighboring relaxation times. The plateaus between drops in the relaxation and storage moduli are no longer well defined. The loss modulus now shows shoulders at each of the two highest relaxation times with a distinct peak remaining at the lowest relaxation time, τ_3. Moving the relaxation times to a spacing of 1 decade results in behavior qualitatively similar to that observed in Figure 1 for a single relaxation time. The loss modulus has a single peak at the lowest relaxation time, and the relaxation and storage moduli pass through their transitions in a single step. The shapes of the curves

are different from those obtained from a single relaxation time, the multiple transition-time curves being extended to the right. Quantitative aspects of this shape change will be discussed in a later section.

Effect of Adding Relaxation Times to the Spectrum

Figure 6 shows plots of the storage modulus for three cases. Curve A was calculated for a single relaxation time, τ_3, with $G_3 = 1 \times 10^{10}$. Curve B had a second relaxation time, τ_2 added to the spectrum at a distance of 1 decade upscale, with $G_3 = 0.969 \times 10^{10}$ and $G_2 = 0.309 \times 10^9$. Curve C was generated using 3 values of τ_i spaced 1 decade from each other with $G_3 = 0.9 \times 10^{10}$, $G_2 = 0.9 \times 10^9$, $G_1 = 0.9 \times 10^8$. All of the curves are nearly identical below $t=\tau_3$. However above τ_3 the curves are shifted to the right by adding to the spectrum upscale. Figure 6 also shows the effect on G" for the same three spectra Here the peak always appears at $t=\tau_3$, but the curve is broadened to the right by added relaxation times upscale. Again, it should be emphasized that we are not really dealing with three single relaxation times. Due to the manner in which the weighting parameters were chosen, the time corresponding to τ_3 had many more relaxation times associated with it than did the others.

Equally weighted relaxation times were used to generate the curves in Figures 7 and 8. From Figure 7 it is apparent that adding relaxation times of equal

strength upscale in the spectrum, changes position of the G" peak as well as the shape of the curve. However, adding relaxation times of equal strength symmetrically about a position on the frequency axis results in a stationary peak with symmetric broadening of the curve. Figure 8 shows the effect of the same spectral changes on the storage modulus. The curves are displaced upscale by any addition of relaxation times, symmetric or not.

Range of Influence of a Relaxation Time

From Figures 6,7, and 8, it is possible to obtain the differences between the curves calculated for the various spectra. Plotting this difference will show the region in which an additional relaxation time makes significant changes in the shape of the curves. In Figure 9, the differences between the curves of Figure 6 are shown. The spectra for these curves had been weighted so that most of the relaxation times were positioned at the lowest relaxation time, τ_3. For the storage modulus, there is little effect below τ_3. However, as shown by curve 1 of Figure 9, the influence of the relaxation time added upscale begins to increase rapidly at $t=\tau_3$. This influence passes through a maximum and is small for times greater than one decade above τ_2. Similarly, the effect of two relaxation times added upscale is shown by Curve 2. The loss modulii of Figure 6 show for $t<\tau_3$ a slight decrease in value upon addition of relaxation times upscale.

Above τ_3 the difference between curves for one and two relaxation times rises steeply and then levels off to a constant value around one decade above τ_2. Similar behavior is observed for two additional relaxation times.

Figure 10 shows the results of a similar analysis performed on the curves of Figures 7 and 8 for the case in which the equally weighted relaxation times were placed symmetrically about the point log w = 0. The effect on G'(w) is negative below zero and then passes through a maximum. The G" behavior is different from that observed in Figure 9. Here the difference between curves passes through a minimum at log w = 0 and then rises steeply to reach a constant value for times above and below this point.

From both Figures 9 and 10, it can be seen that the addition of one relaxation time shows a strong shape-changing effect on G' or G" over a rather narrow (approx. 2 decade) time scale.

Outside of this range, the effect is not necessarily zero, but it has leveled off to some constant value which is maintained over the rest of the time scale. Thus, it may be concluded that the effective range of influence of a single relaxation time is around ±1 decade from its own position.

Comments about Continuous Spectra

The addition of a single relaxation time to a discrete spectrum has been shown to cause a rapidly changing effect only in a range of about two decades. Outside this range the effect of the added τ may have nearly zero value, slightly negative values, or rather substantial positive constant values, depending upon the particular function under consideration and the weighting of the added relaxation time. Regardless of the value, the effect of an added τ remains at some finite level over the entire $(-\infty < t < \infty)$ time scale. This becomes important when one considers a continuous spectrum of relaxation times, $H(\tau)$. When a continuous spectrum is used to calculate a viscoelastic function at a <u>particular value of time</u> (or frequency), the integration is carried out over the <u>entire spectrum</u> of relaxation times. For example in the calculation of $G''(w)$ we have

$$G''(\omega) = \int_{-\infty}^{\infty} H \frac{\omega\tau}{1 + \omega^2\tau^2} \, d\ln\tau \qquad (13)$$

In view of the analysis above, showing that any τ exerts an influence over the entire time scale, the limits of integration in Equation13 may become more meaningful.

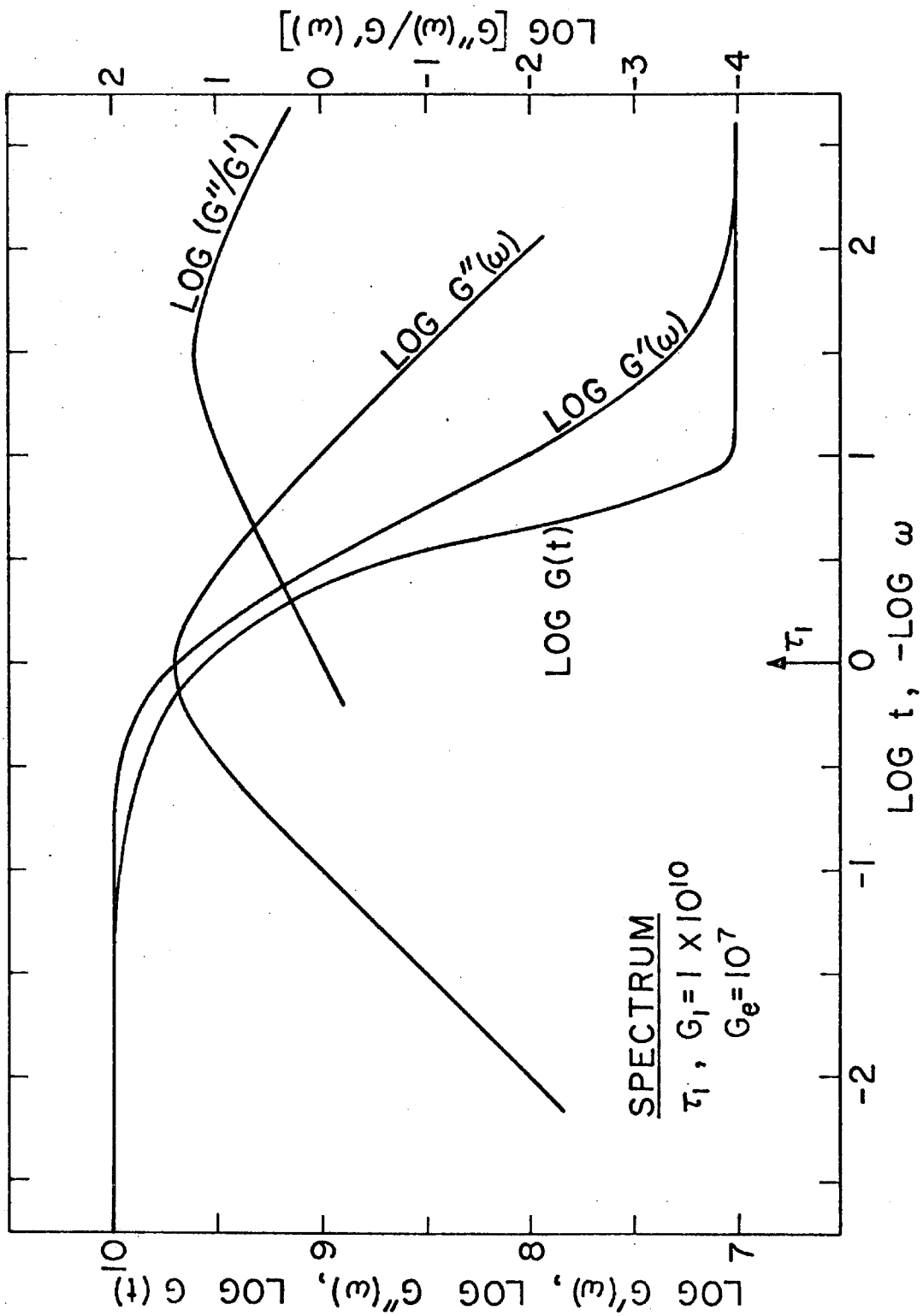
LOG [G''(ω)/G'(ω)]
2
1
0
-1
-2
-3
-4
LOG (G''/G')
LOG G''(ω)
LOG G'(ω)
LOG G(t)
τ1
SPECTRUM
τ1 , G1= 1 X 10^10
Ge=10^7
LOG t, -LOG ω
2
1
0
-1
-2
LOG G'(ω), LOG G''(ω), LOG G (t)
10
9
8
7

Figure 1.

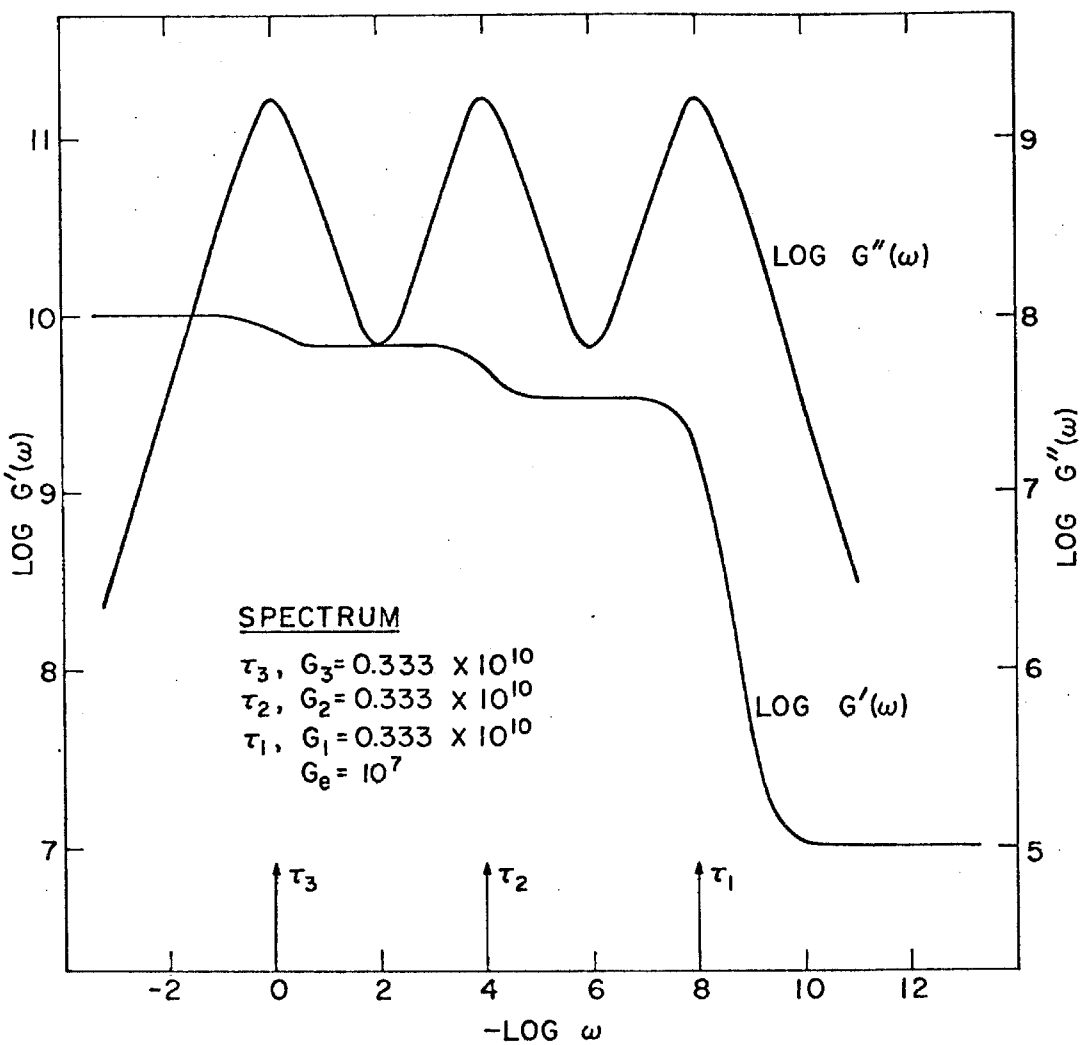
LOG G″(ω)
LOG G′(ω)
SPECTRUM
τ3, G3= 0.333 X 10^10
τ2, G2= 0.333 X 10^10
τ1, G1= 0.333 X 10^10
Ge= 10^7
τ3
τ2
τ1
LOG G′(ω)
LOG G″(ω)
-LOG ω
11
10
9
8
7
9
8
7
6
5
-2
0
2
4
6
8
10
12

Figure 2.

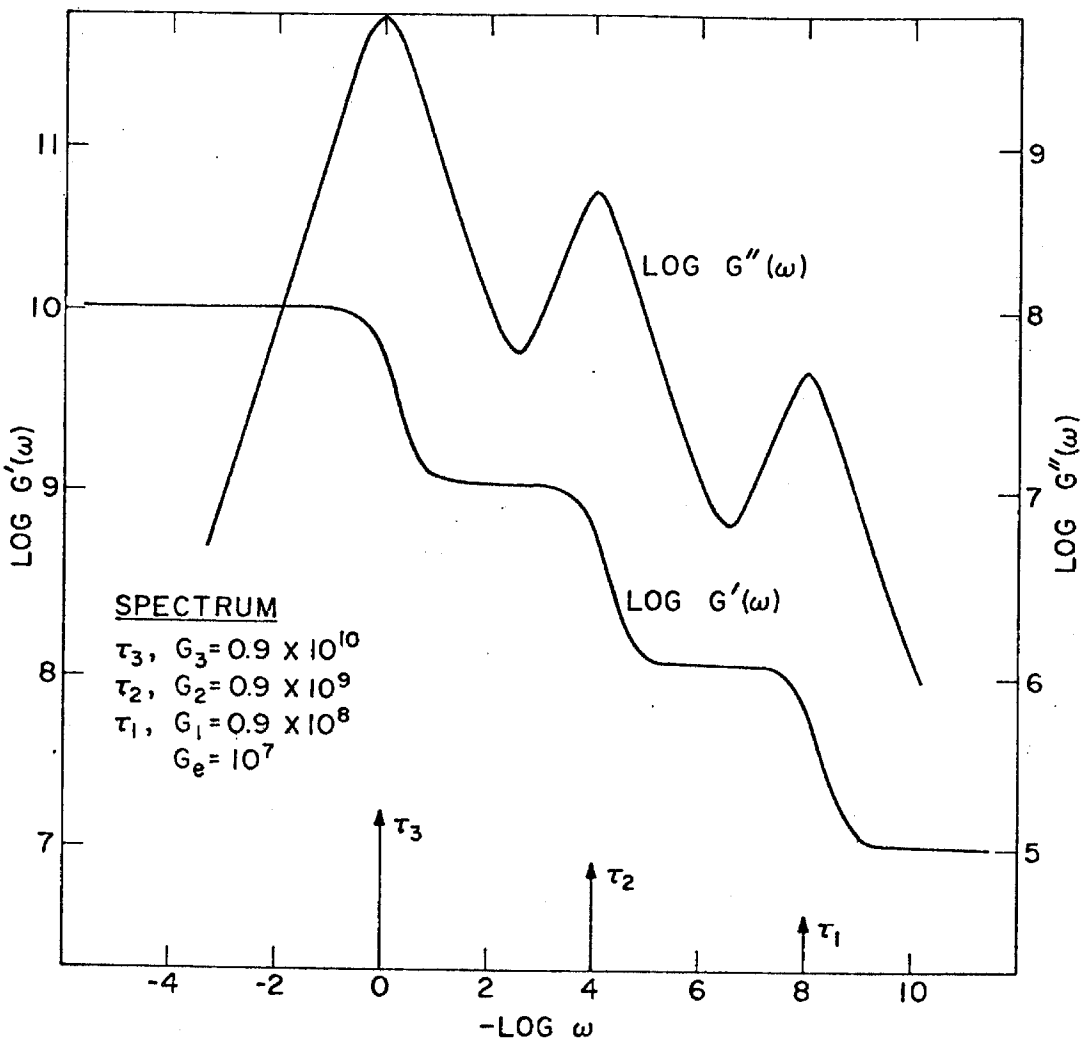
LOG G″(ω)
LOG G′(ω)
SPECTRUM
τ3, G3= 0.9 X 10^10
τ2, G2= 0.9 X 10^9
τ1, G1= 0.9 X 10^8
Ge= 10^7
τ3
τ2
τ1
LOG G′(ω)
LOG G″(ω)
-LOG ω
11
10
9
8
7
9
8
7
6
5
-4
-2
0
2
4
6
8
10

Figure 3.

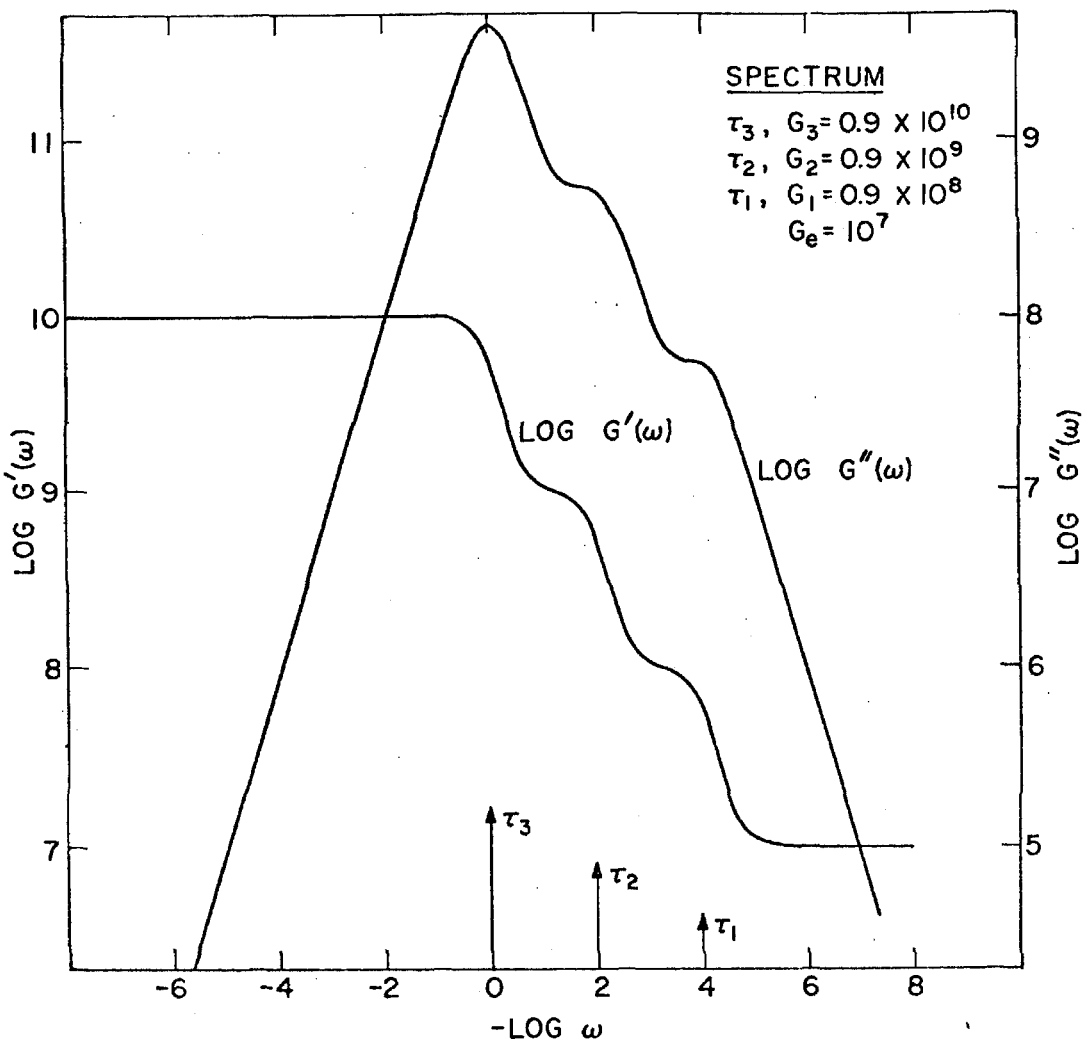
SPECTRUM
τ_3, $G_3 = 0.9 \times 10^{10}$
τ_2, $G_2 = 0.9 \times 10^{9}$
τ_1, $G_1 = 0.9 \times 10^{8}$
$G_e = 10^{7}$
LOG G′(ω)
LOG G″(ω)
τ_3
τ_2
τ_1
LOG G′(ω)
LOG G″(ω)
-LOG ω
11
10
9
8
7
9
8
7
6
5
-6
-4
-2
0
2
4
6
8

Figure 4.

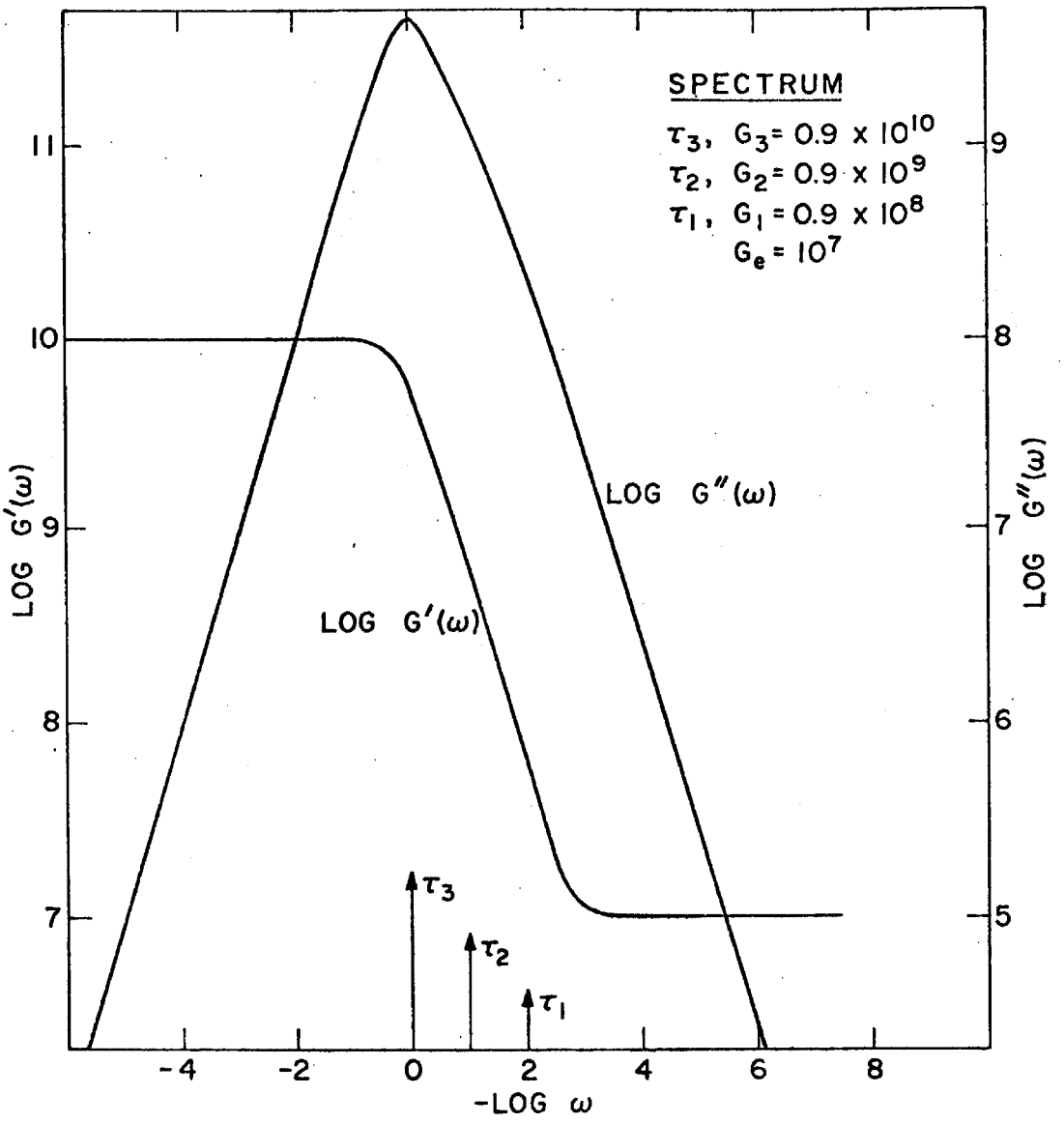
SPECTRUM
τ_3, $G_3 = 0.9 \times 10^{10}$
τ_2, $G_2 = 0.9 \times 10^{9}$
τ_1, $G_1 = 0.9 \times 10^{8}$
$G_e = 10^{7}$
LOG G″(ω)
LOG G′(ω)
τ_3
τ_2
τ_1
LOG G′(ω)
LOG G″(ω)
-LOG ω
11
10
9
8
7
9
8
7
6
5
-4
-2
0
2
4
6
8

Figure 5

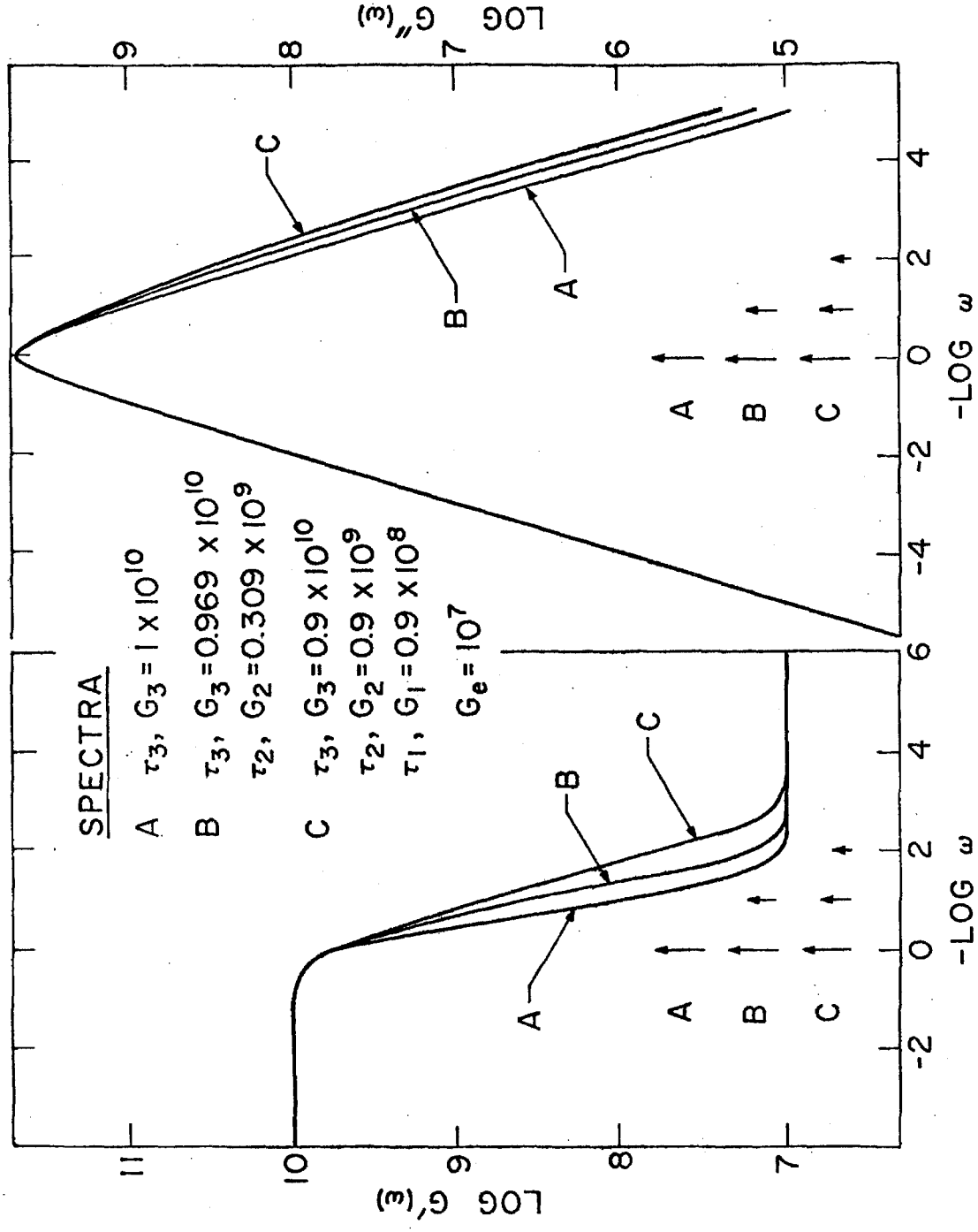
LOG G″(ω)
LOG G′(ω)
-LOG ω
-LOG ω
A
B
C
SPECTRA
A τ3, G3 = 1 X 10^10
B τ3, G3=0.969 X 10^10
τ2, G2=0.309 X 10^9
C τ3, G3=0.9 X 10^10
τ2, G2=0.9 X 10^9
τ1, G1=0.9 X 10^8
Ge=10^7

Figure 6.

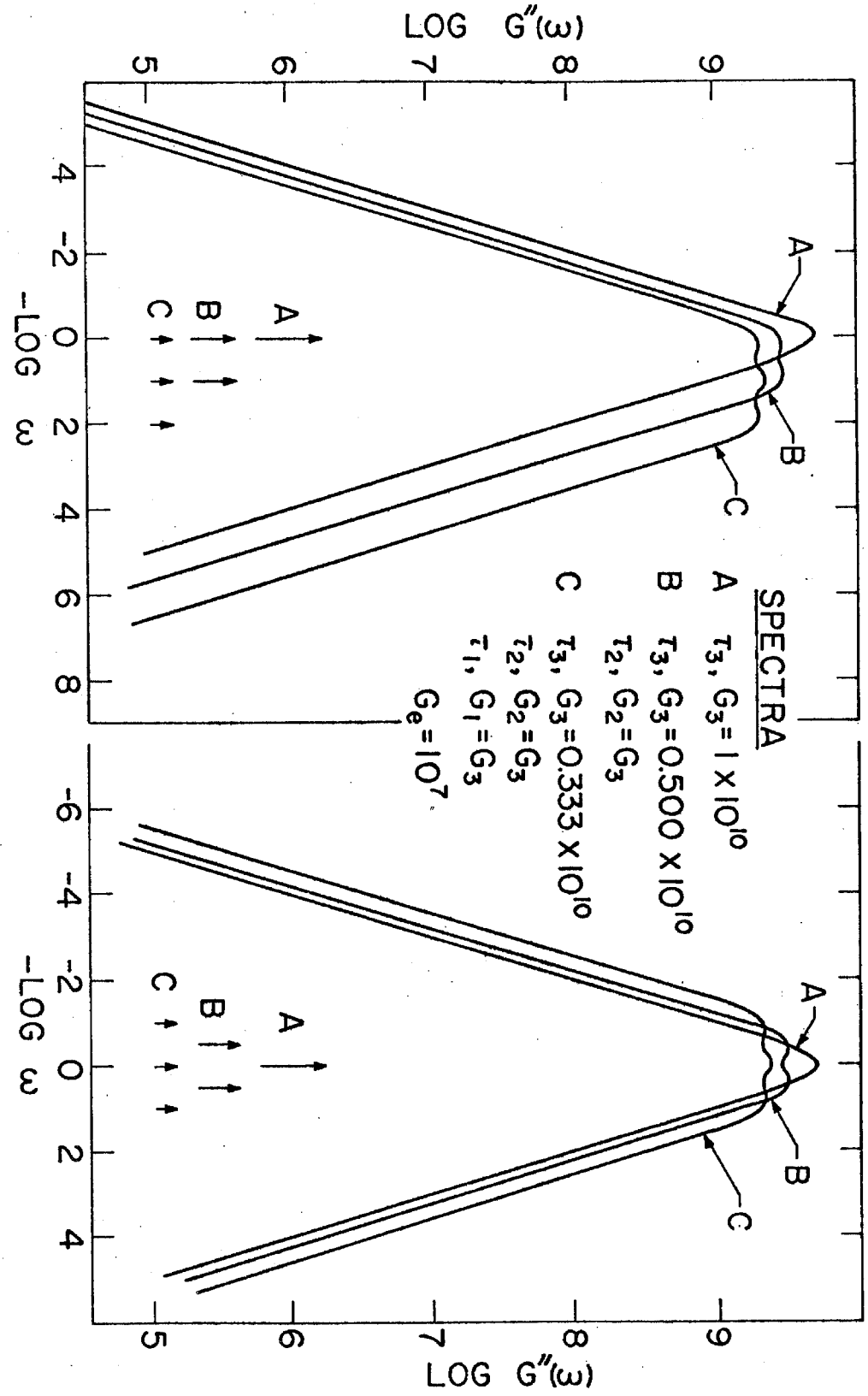
LOG G″(ω)
5
6
7
8
9
-LOG ω
4
2
0
-2
-4
-6
A
B
C
SPECTRA
A τ3, G3= 1 × 10^10
B τ3, G3=0.500 × 10^10
τ2, G2=G3
C τ3, G3=0.333 × 10^10
τ2, G2=G3
τ1, G1=G3
Ge=10^7

Figure 7.

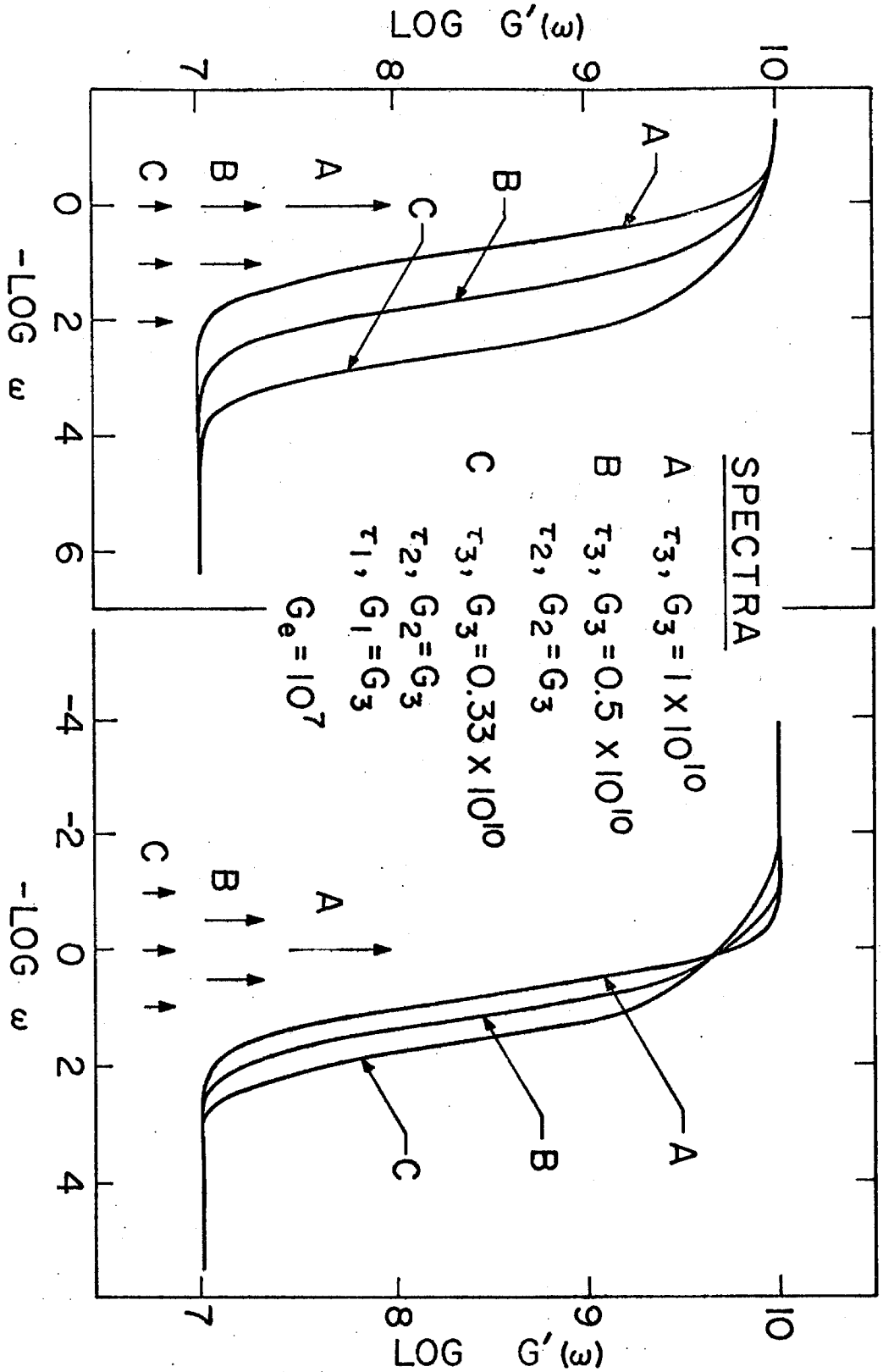
LOG G′(ω)
7
8
9
10
-LOG ω
0
2
4
6
A
B
C
SPECTRA
A τ3, G3 = 1 X 10^10
B τ3, G3 = 0.5 X 10^10
τ2, G2 = G3
C τ3, G3 = 0.33 X 10^10
τ2, G2 = G3
τ1, G1 = G3
Ge = 10^7
-4
-2
0
2
4
-LOG ω
7
8
9
10
LOG G′(ω)

Figure 8.

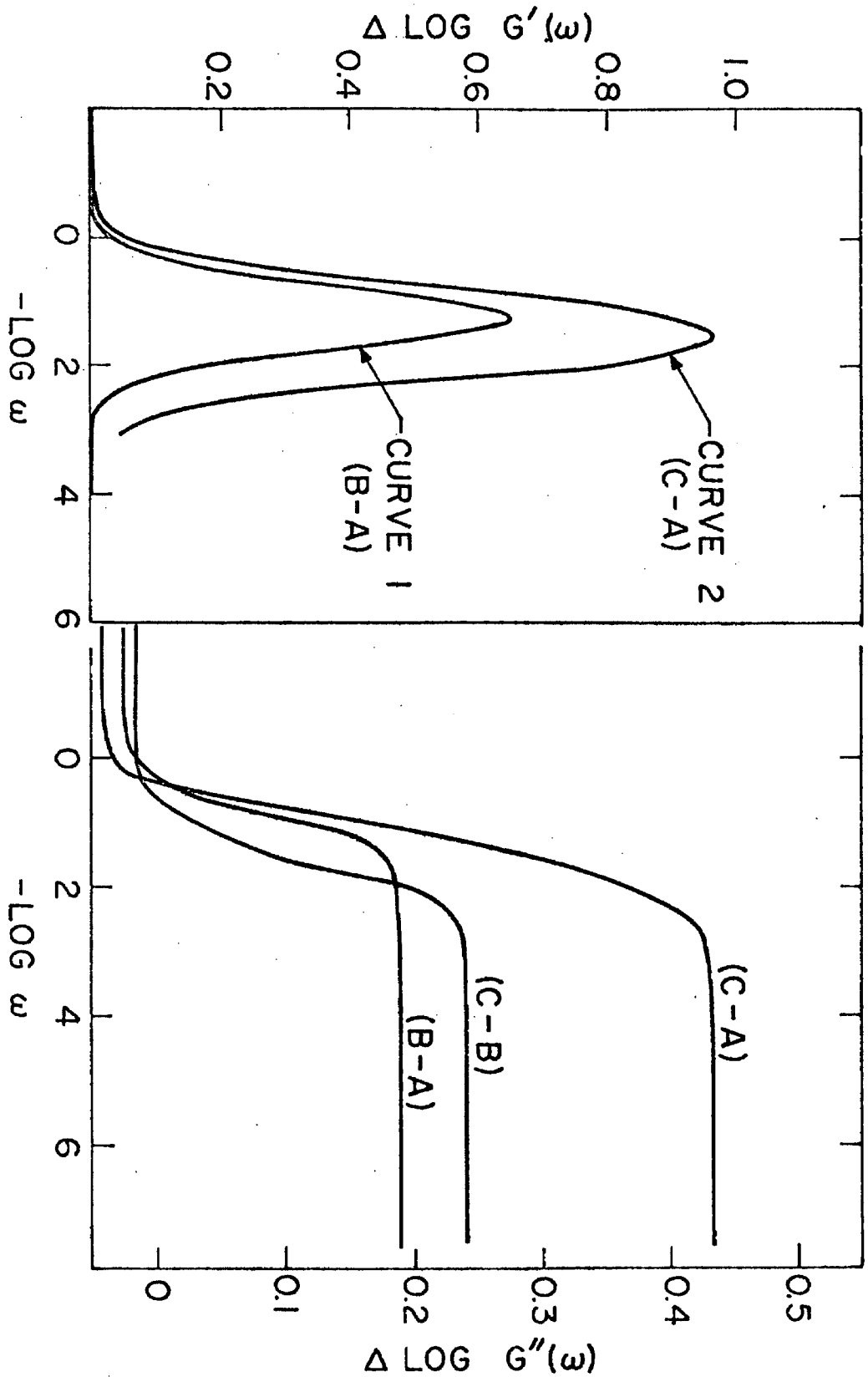
Δ LOG G′(ω)
0.2
0.4
0.6
0.8
1.0
-LOG ω
0
2
4
6
CURVE 1
(B-A)
CURVE 2
(C-A)
-LOG ω
0
2
4
6
(C-A)
(C-B)
(B-A)
0
0.1
0.2
0.3
0.4
0.5
Δ LOG G″(ω)

Figure 9.

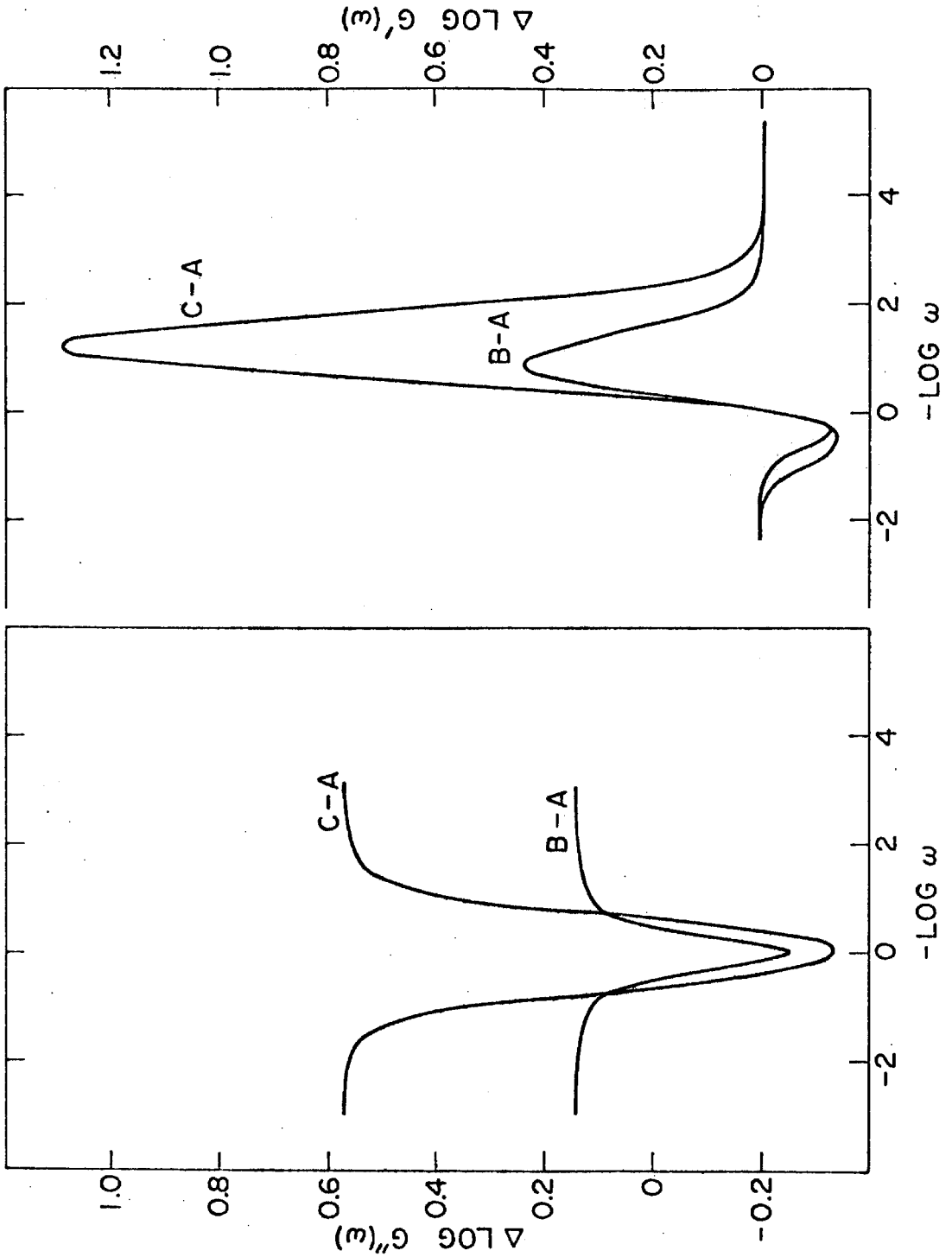
Δ LOG G'(ω)
1.2
1.0
0.8
0.6
0.4
0.2
0
C-A
B-A
4
2
0
-2
-LOG ω
C-A
B-A
4
2
0
-2
-LOG ω
Δ LOG G''(ω)
1.0
0.8
0.6
0.4
0.2
0
-0.2

Figure 10.

References

1. T. Alfrey, Jr., "Mechanical Behavior of High Polymers", Interscience, New York, 1948

2. N. G. McCrum, B. E. Read, G. Williams, "Anelastic and Dielectric Effects in Polymeric Solids", Wiley, London, 1967

3. N. W. Tschoegl, Kolloid Z., 174:113(1961)

PROPOSITION 2

THERMODYNAMICS OF A REVERSE-OSMOTIC PUMP

Abstract

An ingenious reverse-osmotic pump which operates on gravitational energy is analyzed from a thermodynamic point of view. It is demonstrated that the device violates the second law of thermodynamics and therefore must be classed among the many other perpetual motion machines which have appeared over the years. Variations of the original system are also considered and discussed.

Introduction

A recent issue of Scientific American (1) contained an interesting proposal put forth by Professor O. Levenspiel of Oregon State University. Details are given in the next section concerning his suggested method for harnessing gravitational energy to operate a reverse-osmotic pump. Levenspiel indicated that a device of this sort should be capable of creating a perpetual fresh water fountain in the ocean. The feasibility of this proposal was not discussed in Scientific American; instead the proposal was left open to the readers for appraisal.

It is the purpose of this paper to analyze Levenspiel's osmotic pump from a thermodynamic point of view. This author's intuition immediately led him to believe that the proposed situation violated the second law of thermodynamics. Furthermore, the author's experience with Levenspiel's style (2) suggested that the proposal may have been made partially in jest. It is possible that Levenspiel was serving a challenge to his readers, daring them to find a way to disprove his idea.

It is worth noting that this author encountered considerable difficulty before finding the proper method to refute Levenspiel's proposal. It is also of interest that several of the author's colleagues (3) were entirely convinced that the proposal was valid.

Had this author not been exposed to a rather specialized topic concerning the behavior of solutions (4), he too might still believe that one day man could hope to bathe in fresh water brought effortlessly to him from the depths of the ocean via Levenspiel's reverse-osmotic fountain.

Levenspiel's Proposed Fresh Water Fountain

The fresh water fountain was based on the well known principle of reverse osmosis. Figure 1 shows the various situations which can exist when a salt water solution and fresh water are separated by a semipermeable membrane. In Figure 1a the external pressure is identical on both sides of the membrane and fresh water flows spontaneously into the solution chamber. Figure 1b represents the equilibrium situation; the flow of fresh water has been stopped by imposing an excess pressure on the solution. The particular excess pressure which just stops the flow is known as the osmotic pressure. For sea water the osmotic pressure is roughly 22 atmospheres (1). If the excess pressure on the solution is greater than the osmotic pressure, reverse osmosis occurs. As indicated in Figure 1c under these conditions the flow is reveresed, i. e. fresh water flows from the solution into the pure water chamber.

Levenspiel describes two possible water fountains

employing the effects described above. The first is a well known demonstration of osmosis. A tube is closed at one end with a semipermeable membrane. The tube is partly filled with salt water and submerged vertically into a container of fresh water. As in Figure 1a, fresh water diffuses into the tube, and a fountain of increasingly dilute salt water flows out from the top of the tube. The second fountain is the controversial reverse-osmotic pump as pictured in Figure 2. A long pipe is closed with a suitable semipermeable membrane and lowered into the ocean. The key point here is that ocean water is denser (by about 3 percent) than fresh water, and therefore the pressure difference increases across the membrane as the pipe is lowered into the ocean. This means that a depth can be found at which the excess pressure on the sea water side of the membrane is greater than 22 atmospheres even when the pipe is full of fresh water. As a result, Levenspiel suggests that fresh water will diffuse into the pipe via reverse osmosis and perpetually flow out at the top. Levenspiel calculates that a rather formidible depth (about 5 miles) is required, and he admits that no membrane exists which will withstand these conditions. He states, however, that these problems "do not alter the main argument, which relies on gravitational work to separate water from salt, rather than on heat, phase change or other traditional

techniques" (1).

Analysis of the Proposal Using an Ideal Solution of Uniform Concentration

We will begin to analyze the problem by considering an ideal solution of uniform concentration to represent the ocean. The ideal solution has two components: 1-solvent, mole fraction X_1 and 2-solute, mole fraction X_2. The criterion for equilibrium of the solvent across the semipermeable membrane is

$$\mu_1' = \mu_1'' \qquad (1)$$

where μ_1 is the chemical potential (5) of the solvent, and the single and double prime superscripts refer to the solution and pure solvent, respectively. For the chemical potential of the solvent in the solution we have

$$\mu_1' = \mu_1^o(T, P') + RT\ln X_1 \qquad (2)$$

and for the pure solvent

$$\mu_1'' = \mu_1^o(T, P'') \qquad (3)$$

The dependence of the chemical potential on pressure is given as (6)

$$\left(\frac{\partial \mu_1(T, P)}{\partial P} \right)_T = \bar{V}_1(T, 0)(1 - KP) \qquad (4)$$

where $\bar{V}_1$ is the partial molar volume of the solvent at zero (gauge) pressure and K is the compressibility. For the moment we will assume that the solvent is incompressible so that $\bar{V}_1$ is independent of pressure. Then we

obtain

$$\mu' = \mu^*(T) + \overline{V}_1 P' + RT\ln X_1 \qquad (5)$$

$$\mu'' = \mu^*(T) + \overline{V}_1 P'' \qquad (6)$$

Since the temperature is assumed to be equal on both sides of the membrane $\mu_1^*(T)$ has the same value in Equations 5 and 6.

At equilibrium we have

$$\overline{V}_1 P' + RT\ln X_1 = \overline{V}_1 P'' \qquad (7)$$

which can only be true if $P' \neq P''$. In fact if we define $P'-P'' = \pi$ we find that

$$\pi = (-RT\ln X_1) / \overline{V}_1 \qquad (8)$$

The osmotic pressure π is a positive quantity since $X < 1$. As discussed above, π is equal to the required excess pressure on the solution to obtain equilibrium.

Now let us return to Levenspiel's proposed fresh water fountain. The pressure on the solution side of the membrane can be expressed as

$$P' = \rho' g h \qquad (9)$$

where h is the depth measured from sea level, ρ' is the density of seawater, and g is the gravitational constant. Similarly the pressure on the solvent (water) side is

$$P'' = \rho'' g h \qquad (10)$$

where $\rho'' = \rho_1$, the density of pure water. It is pointed out here for later use that, since we are considering an ideal solution, there is no volume change upon mixing. Therefore

$$\rho' = (M_1X_1+M_2X_2)/(\bar{V}_1X_1+\bar{V}_2X_2) \qquad (11)$$

$$\rho'' = (M_1X_1)/(\bar{V}_1X_1) = M_1/\bar{V}_1 = \rho_1 \qquad (12)$$

where the M's are the molecular weights of the solvent and solute, the $\bar{V}$'s are the partial molar volumes, and the X's are the mole fractions.

Equations 9 and 10 may be substituted into Equations 5 and 6 to yield the dependence of the chemical potential on the depth below the surface. This behavior is shown in Figure 3. First we consider curve "a" which represents the variation of the chemical potential, μ_1', of the solvent (water) in the solution. At h=0 the value of μ_1' is $\mu^* + RT\ln X_1$. As h increases, μ' increases due to the increasing pressure, and the rate of change is given by the slope $\rho' g \bar{V}_1$. We can visualize the situation for the pure water in the pipe in two different ways. If we consider curve "b" we are assuming that the pipe is initially empty except for a monomolecular layer of fresh water on the top of the membrane. As the pipe is pushed downward, no water will flow in for values of h less than h* since in this region $\mu_1' < \mu_1''$. At h* the pressure of the solution is exactly equal to the osmotic pressure. At values of h greater than h* fresh water will flow into the pipe since $\mu' > \mu''$. Curve "b"

is drawn with a slope of $\rho''gh$ which means that it represents the change in chemical potential with depth for a column of pure water beginning at $h = h^*$. This means that pure water not only diffuses into an empty pipe when $h > h^*$, but also it is clear that water will continue diffusing in when the pure water column has reached a height of $h-h^*$. Thus, as Levenspiel predicts, the water rises higher in the pipe as the membrane is pushed deeper into the solution. The height of the column of pure water which results in equilibrium is not apparant from this figure. However, by considering curve "c" we can find the limiting depth, h^{**}, for which equilibrium can be obtained. Curve "c" represents the change in chemical potential with depth for a column of pure water beginning at the surface. This means that we are considering the pipe to be full when it is placed into the solution. From Figure 3 we see that when $h < h^{**}$ (Regions A and B) water flows out of the pipe. However between h^* and h^{**} (Region B) the pipe does not empty completely. At $h=h^{**}$ we have equilibrium between the water in the filled pipe and the water in the solution. This condition is given by $h^{**}g(\rho'-\rho'') = \pi$. Moving the pipe down further (Region C) results in μ'' being less than μ', and water flows into the already full pipe. Thus Levenspiel's fountain apparantly works.

Equilibrium Situation for an Ideal Solution in a Gravitational Field

The analysis developed above shows that the reverse-osmotic pump should work for an ideal solution of uniform concentration. However it became apparant to the author that this assumption, i. e. uniformity of concentration, might be the critical concept in this problem. It was only because of his experience with (7) and study of (4) sedimentation equilibrium of polymer solutions that the author was saved from drawing the ignominious conclusion that Levenspiel's proposal was valid. In sedimenatation equilibrium, very large force fields are generated to create concentration gradients in a previously uniform solution. It seemed plausible, therefore, that the gravitational force field sets up an equilibrium concentration gradient in an ideal solution, and in doing so the gravitational potential becomes unavailable for the purposes discussed in the previous sections. The manner in which this connection was made is mentioned here to point out that, in the author's experience, modern texts and courses make little if any mention of the effects of a gravitational field on the equilibrium thermodynamics of solutions. Only the very oldest texts (8,9) available to the author gave any details of this subject.

The following treatment of an ideal solution in a gravitational field was developed by analogy with the

situation for polymeric solutions in a centrifugal force field as discussed by Tanford (4).

Again consider a uniform ideal solution with a mole fraction X_1 of an incompressible solvent. At this point we are considering the equilibrium situation for the solution alone in a gravitational field; no membrane is involved here. As discussed in detail elsewhere (4) it is useful consider small elements of the solution at different levels as separate homogeneous microphases which are part of a much larger constant volume system. Thus the proper condition for equilibrium between the individual elements or phases for an infinitessimal exchange of heat or matter is

$$\sum dE^{(p)} = 0 \qquad (13)$$

where $\sum$ implies a sum over all phases. To analyze the equilibrium situation for the concentration, we are interested in the total energy change associated with the transfer of dn_1 moles of a component from position h_a to position h_b. The energy change is composed of two parts

$$\begin{aligned} dE_{(1)} &= (\mu_{ia} - \mu_{ib})dn_i \\ dE_{(2)} &= (M_i g h_a - M_i g h_b)dn_i \end{aligned} \qquad (14)$$

For an arbitrary quantity of moles transferred we see that the energy change can be zero only if

$$(\mu_{ih} - Mgh) = \text{constant} \qquad (15)$$

or in the terminology of Tanford (4)

$$d(\mu_i)_{total} = 0 \qquad (16)$$

Differentiating Equation15 with respect to h we obtain

$$d\mu_i = Mgdh \qquad (17)$$

But

$$\begin{aligned} d\mu_i &= (\partial\mu_i/\partial X_i)dX_i + (\partial\mu_i/\partial P)dP \\ &= RTd\ln X_i + \bar{V}_i \rho' gdh \end{aligned} \qquad (18)$$

Combining Equations 17 and 18 and substituting for ρ' from Equation 11 we obtain for the solvent in a binary solution

$$RTd\ln X_1 = \left[M_1 - \bar{V}_1 \frac{(M_1X_1 + M_2X_2)}{(\bar{V}_1X_1 + \bar{V}_2X_2)}\right] gdh \qquad (19)$$

This same result was obtained by Guggenheim (8) using a slightly different approach. The importance of Equation 19 is that it predicts that the concentration will change as the depth h changes. Guggenheim (8) has integrated this equation for an ideal binary solution and obtains the following expression for the equilibrium distribution of species in a gravitational field

$$\frac{X_{2b}}{X_{2a}} \left(\frac{X_{1b}}{X_{1a}}\right)^{\frac{\bar{V}_2}{\bar{V}_1}} = \exp\left[g\left[M_2 - M_1\frac{\bar{V}_2}{\bar{V}_1}\right]\left[\frac{h_b - h_a}{RT}\right]\right] \qquad (20)$$

Implications of Gravitational Field Equilibrium with Respect to Levenspiel's Proposed Reverse-Osmotic Fountain

It is immediately apparant that the changing concentration will have an effect on the operation of the proposed fountain discussed above. In particular if we rearrange Equation 19 as follows

$$-(RT/\bar{V}_1)\frac{d\ln X_1}{dh} = \left(\frac{M_1}{\bar{V}_1}\frac{X_1}{X_1}+\frac{M_2}{\bar{V}_2}\frac{X_2}{X_2}-\frac{M_1}{\bar{V}_1}\right)g = \rho' g - \rho'' g \qquad (21)$$

we see that the osmotic pressure, as expressed by Equation 8, is changing with depth according to the right hand side of Equation 21.

Now let us consider that the membrane is at the point h* where the solution pressure is identical to the osmotic pressure. The pipe is still empty and P=0 inside. Moving the pipe downward by an arbitrary distance dh increases the osmotic pressure by an amount given by the right side of Equation 21 multiplied by dh. The pressure on the solution side of the membrane has been increased by an amount $\rho' g\, dh$. Thus the pressure difference across the membrane is greater than the osmotic pressure and fresh water will flow into the pipe. However it will flow in only until a column of fresh water of height dh has been attained since this will exert the required pressure $\rho'' g dh$ to reestablish equilibrium. If the pure water were to rise

in the pipe by any amount greater than the distance the membrane was displaced below h*, the condition $\Delta P < \pi$ would exist, and water would flow out of the pipe until equilibrium was reestablished with the fresh water level at h=h*.

Thus, if we consider the ocean to be in equilibrium in the earth's gravitational field, we should expect in the ideal case that if water enters the pipe at all, it will always rise to the same distance below sea level, h*, no matter how far down the pipe is pushed. This situation, as shown in Figure 4, clearly indicates that Levenspiel's proposal is invalid. The gravitational potential cannot be harnessed as he suggests since it acts to redistribute the species in the solution. To obtain the uniform concentration situation for which the proposed osmotic pump was seen to work, it would be necessary to supply energy to the system, for example by stirring as shown in Figure 5. This is the clearest picture of the way Levenspiel's proposal violated the second law. He was simply trying to get more work out of a system than was available. Therefore his proposed apparatus must be considered to be yet another of the thermodynamic enormities known as perpetual motion machines.

Solvent Compressibility

It has been shown that Levenspiel's proposal is invalid for an ideal solution with incompressible solvent. How would solvent compressibility affect the situation? Guggenheim has shown that osmotic pressure of a solution with a compressible solvent is given by

$$\pi = -(RT/\bar{V}_1^*) \ln X_1 \qquad (22)$$

where

$$\bar{V}_1^* = \bar{V}_1\left(1 - \tfrac{1}{2}K(P_{soln} - P_{solv})\right) \qquad (23)$$

Inspection of Equation 23 shows that $\overline{V_1^*} < \overline{V_1}$ and therefore the osmotic pressure increases with depth for a solution with a compressible solvent. Thus if the pure solvent rose in the pipe to the same height, h*, for all positions of the membrane, the pressure on the solution side would be too great for equilibrium, i. e. the condition $\Delta P < \pi$ would exist and some of the solvent would have to flow out of the pipe for equilibrium. Thus for an ideal solution with a compressible solvent we have the situation shown in Figure 6.

Consideration of Well-Mixed Polymer Solutions at the Theta Temperature

Polymer solutions have much lower osmotic pressures than conventional salt solutions of the same density,

This is the case because osmotic pressure is a colligative property, depending only on the number of solute particles in solution. Therefore it might be reasonable to try to demonstrate Levenspiel's reverse-osmotic fountain using a stirred polymer solution; in this case the critical height for the fountain to operate

$$h^{**} = \pi/\Delta\rho \tag{24}$$

would conceivably be attainable on a laboratory scale since the osmotic pressure is orders of magnitude lower than that of sea water.

Polymer solutions are not well described by the ideal solution formulations discussed above. However it is well known that a certain temperature known as the theta temperature a polymer solution attains a state of ideality. The theta temperature is a characteristic of the particular polymer solution under consideration. At $T=\theta$ we can write

$$\pi = \frac{R\theta}{M_n}\rho_2\phi_2 \tag{25}$$

where $\bar{M}_n$ is the number average molecular weight of the polymer, and ρ and ϕ refer to the density and the volume fraction of the solute (polymer) in the solution. Assuming volumes are additive on mixing we obtain

$$\begin{aligned}\Delta\rho &= \rho_{soln} - \rho_{solv} = \rho_1\phi_1 + \rho_2\phi_2 - \rho_1 \\ &= \phi_2(\rho_2 - \rho_1)\end{aligned} \tag{26}$$

Then the value of h** from Equation 24 becomes

$$h^{**} = \frac{R\theta}{\bar{M}_n}\left(\frac{r}{r-1}\right)$$

where $r = \rho_2/\rho_1$. Thus we see that for a well mixed polymer solution at its theta temperature and with an incompressible solvent, the necessary depth to demonstrate the reverse-osmotic fountain decreases as $\bar{M}_n$ and r increase. Figure 7 gives plots of h^{**}/θ against r-1 on double logarithmeric coordinates. Several different molecular weights were used as the parameter. If we assume that θ is roughly 300°K we find from Figure 7 that a minimum height of about 1.2 meters would be necessary for a polymer of one million molecular weight and a polymer-solvent density ratio of 1.25. These are very advantageous choices of $\bar{M}_n$ and r, and therefore depths much greater than 1.2 meters should be expected for most real polymer solutions. Thus even for well mixed polymer solutions at the theta temperature a demonstration of the reverse-osmotic fountain is not realistic.

(a) osmosis, same pressure on both sides

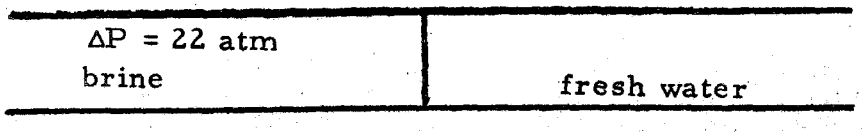

(b)equilibrium, 22 atm excess pressure on brine

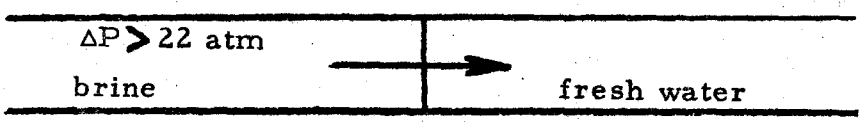

(c)reverse osmosis, more than 22 atm excess pressure on brine

Figure 1. Effect of Excess Pressure on the Flow of Fresh Water. Excess Pressure = $\Delta P = P_{brine} - P_{fresh\ water}$. Arrow indicates direction of fresh water flow. Semipermeable membrane separates the chambers.

Figure 2.

Levenspiel's Proposed Fresh Water Fountain

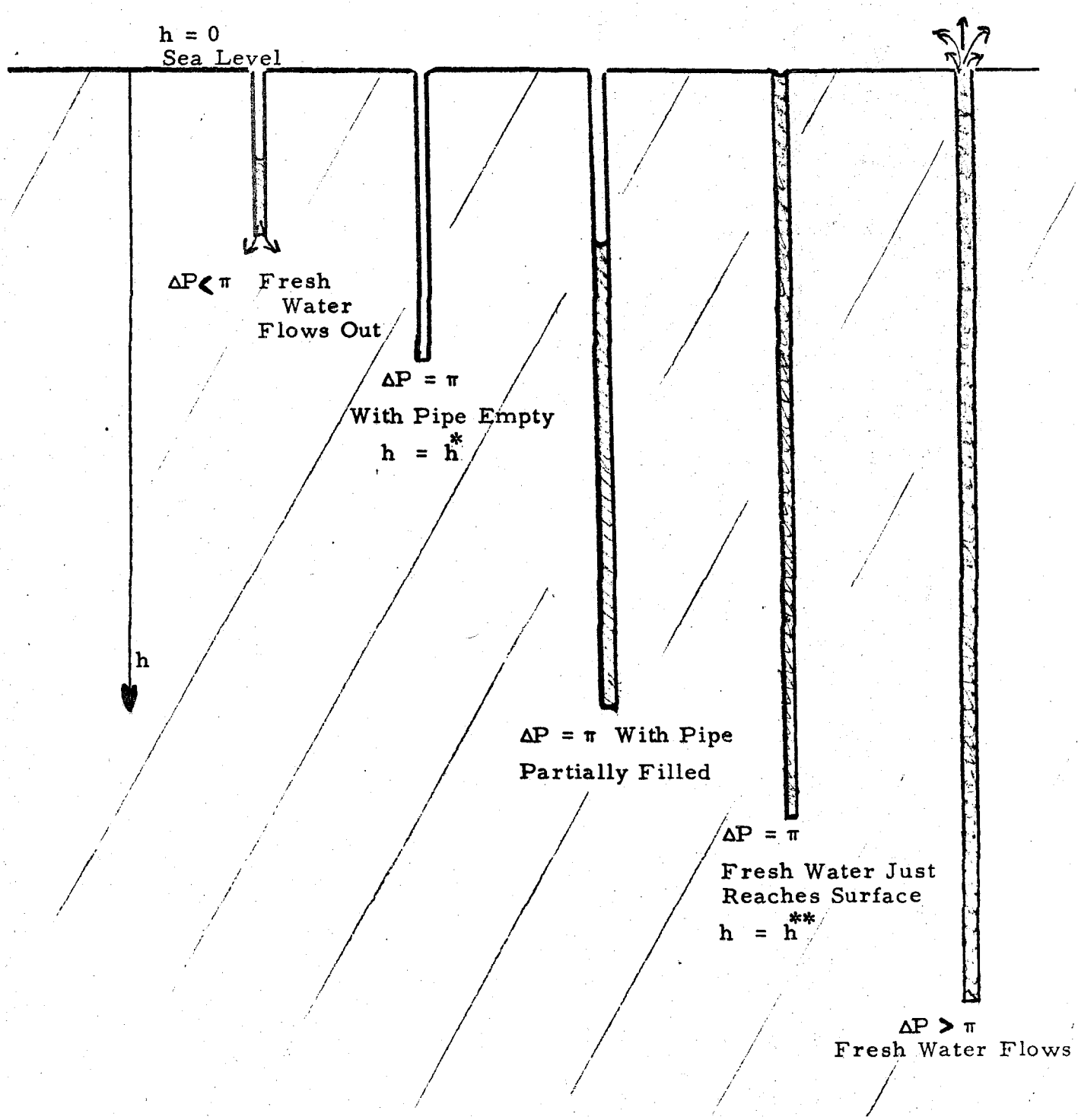

Figure 3.

Variation of the Chemical Potential of Water with Distance Below the Surface for a Hypothetical Ideal Solution of Uniform Concentration

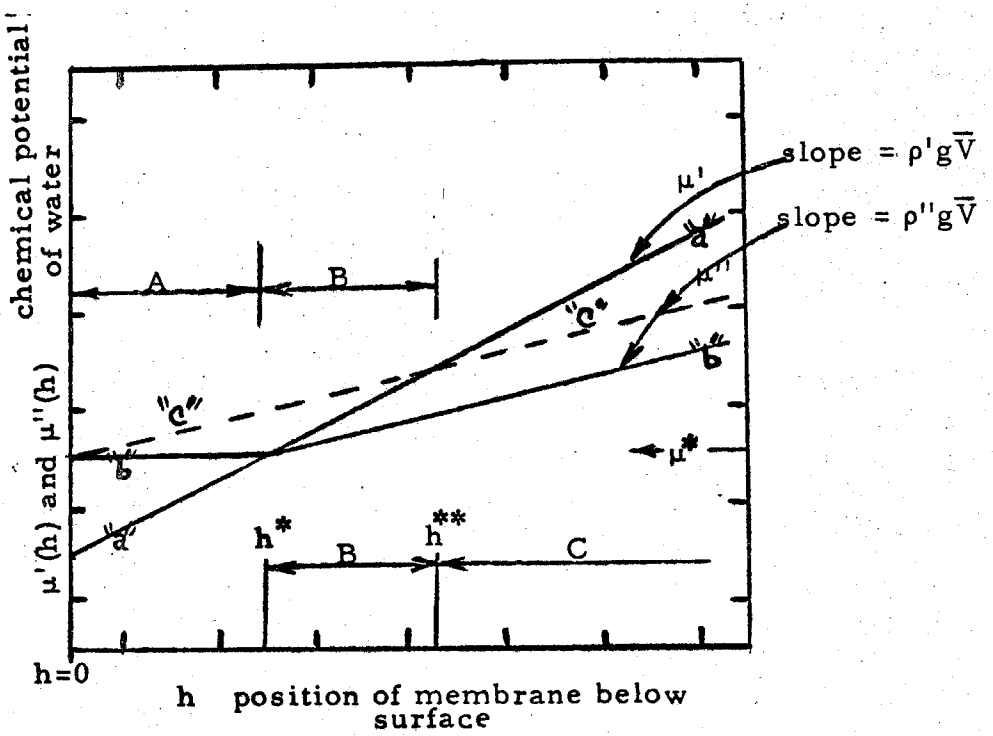

Figure 4.

Situation Predicted by Proper Thermodynamic Analysis
Considering the Solution in Equilibrium in the Gravitational Field

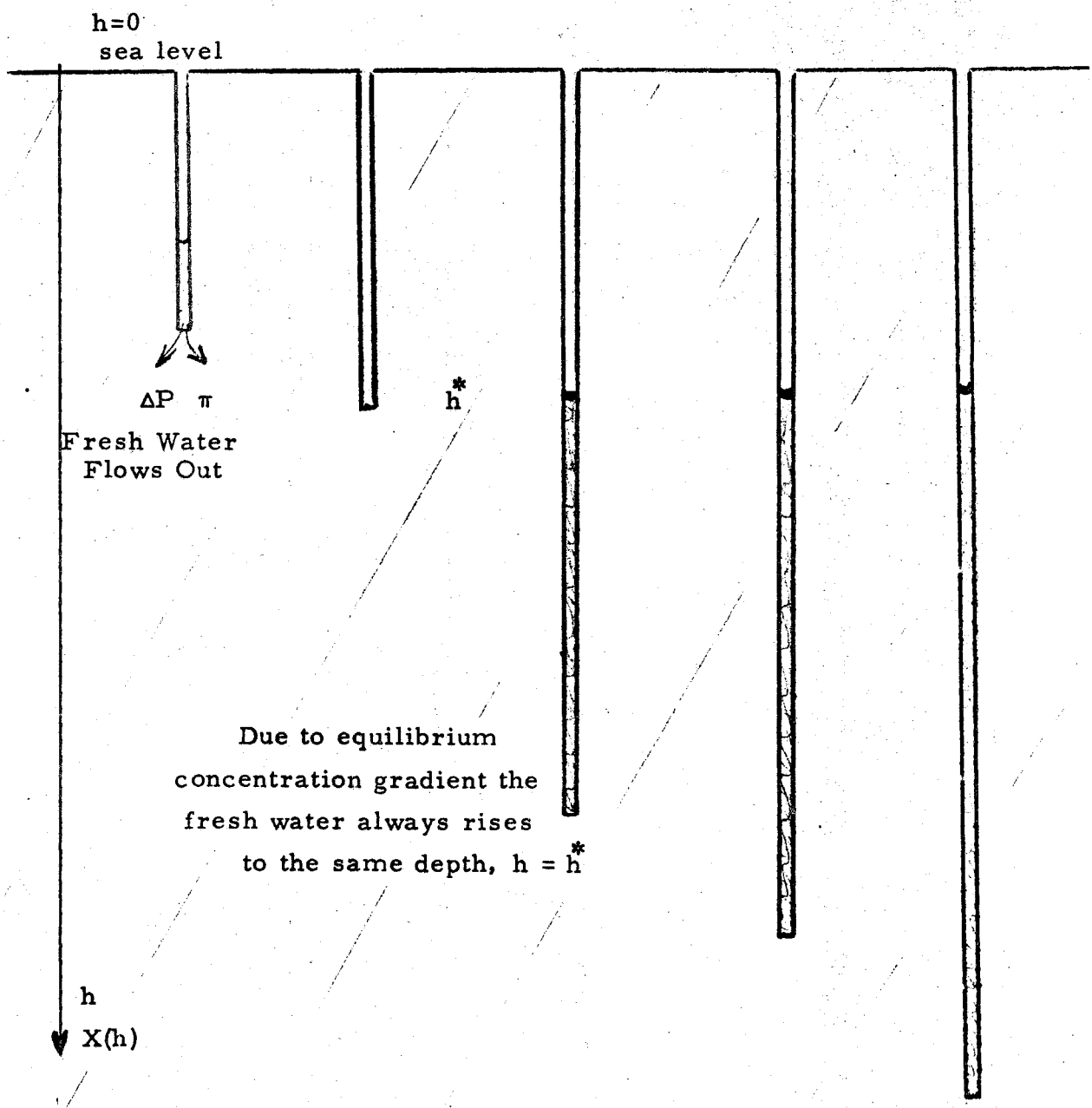

Figure 5.

Solution is Stirred to Return to the Situation of Uniform Concentration in the Gravitational Field

Indicates How the Second Law Was Violated in Fig. 2

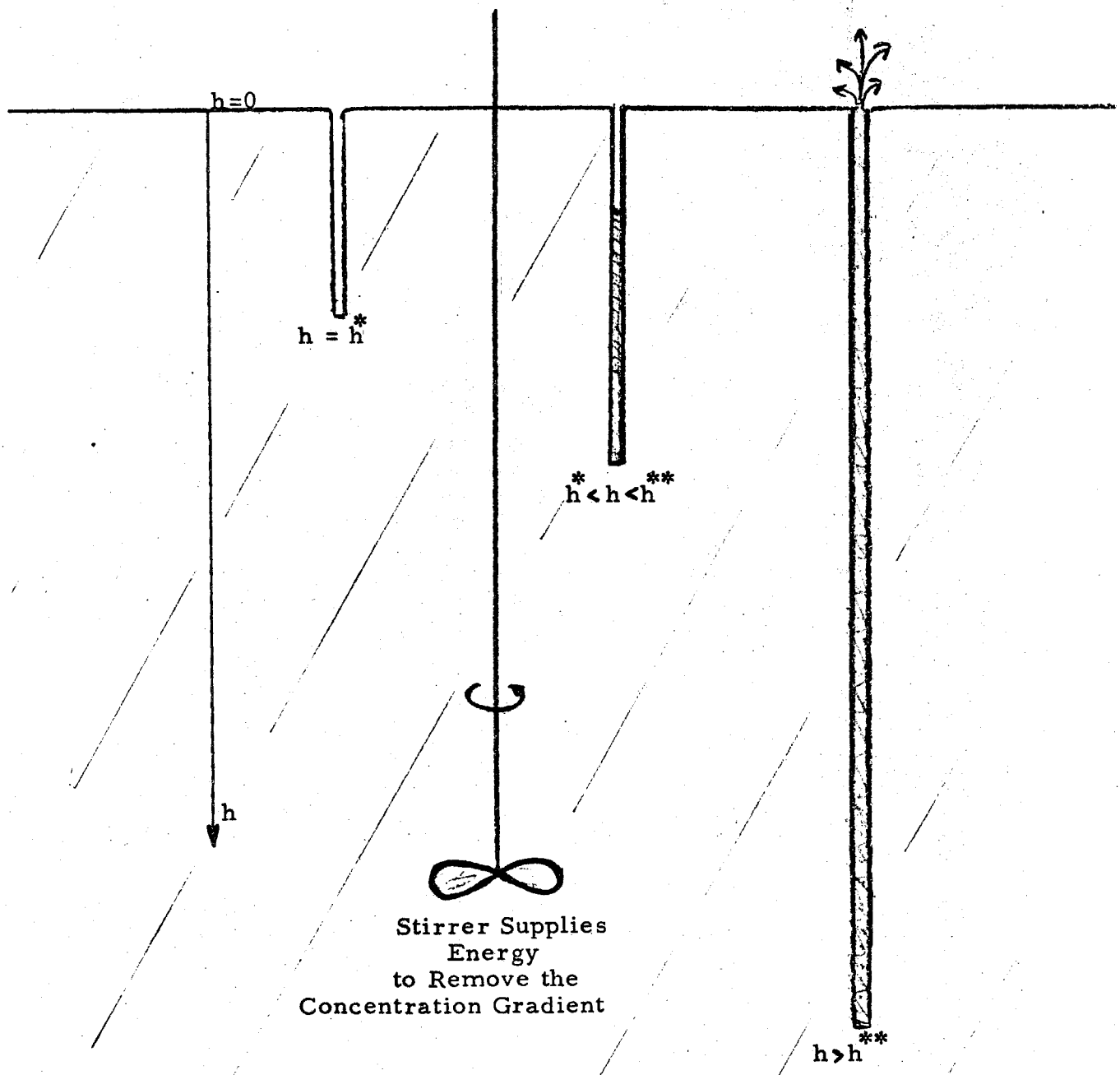

Figure 6.

Situation Which Exixts For an Ideal Solution in Equilibrium in the Gravitational Field when the Solvent is Compressible

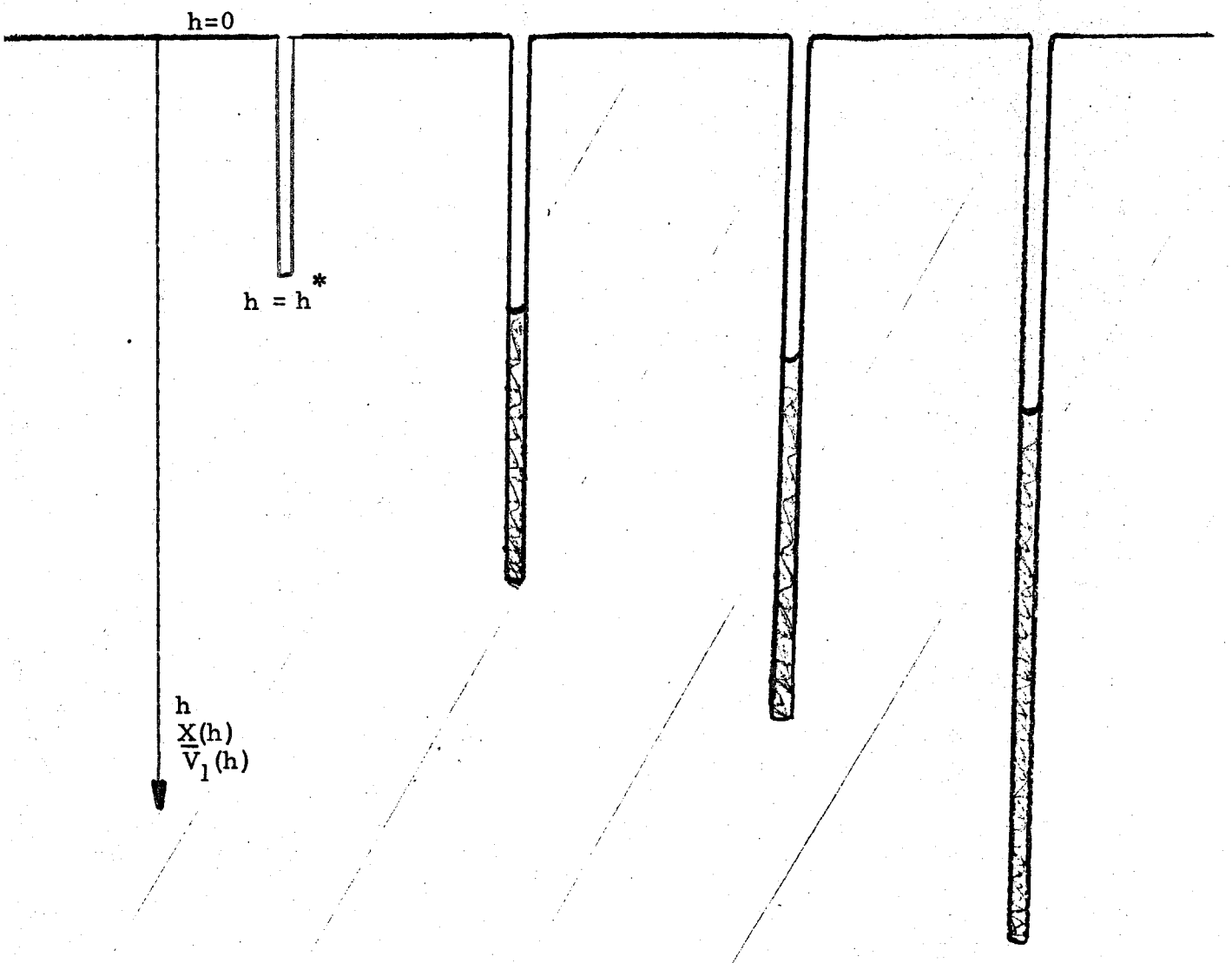

Figure 7.

Estimate of the Depth Required to Show Fountain Effect for Well Stirred Polymer Solutions at the Theta Temperature

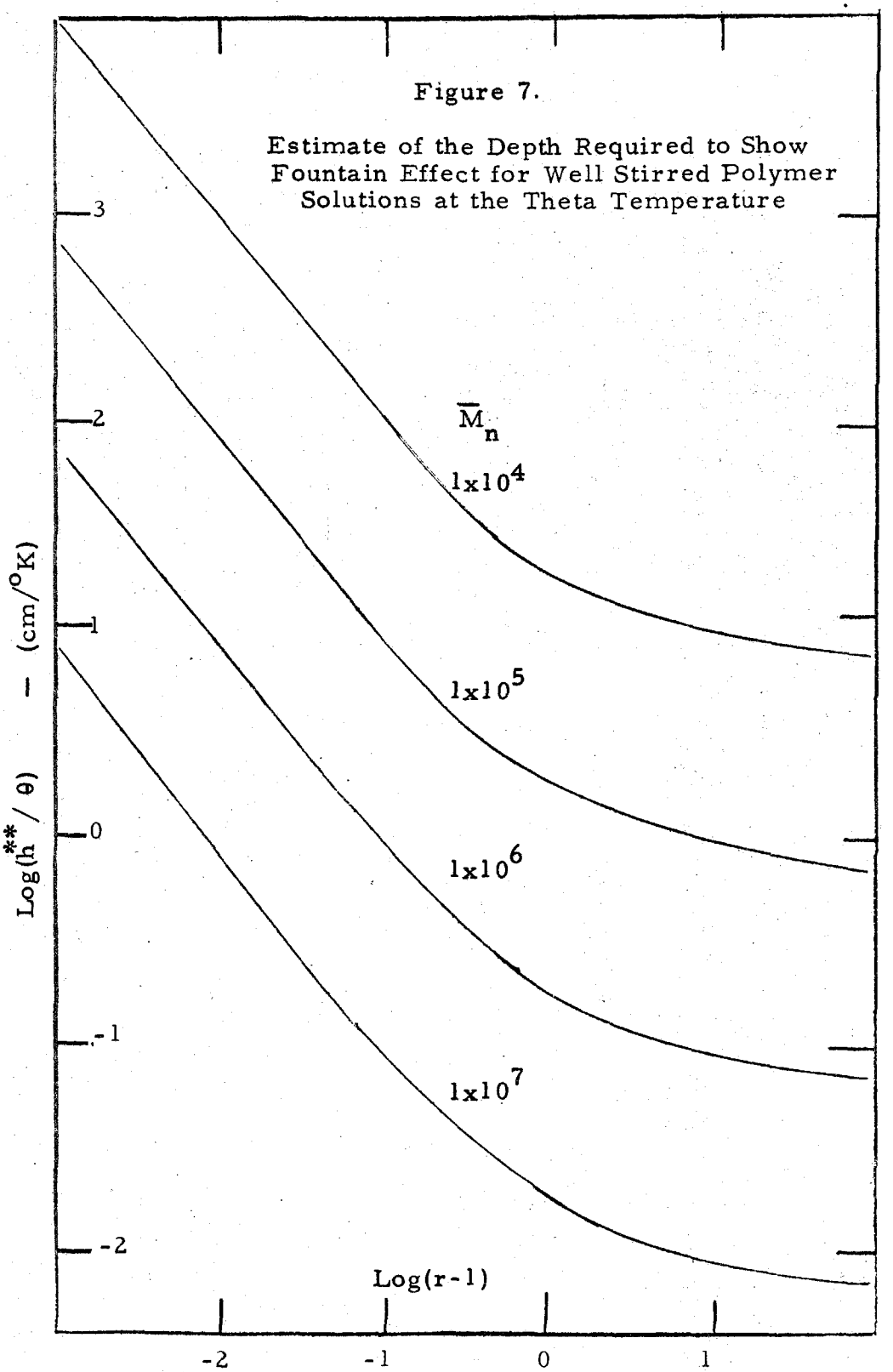

References

1 O. Levenspiel, Scientific American, No 6, p. 100, Dec. 1971

2 O. Levenspiel, "Chemical Reaction Engineering", Wiley, New York, 1962

3 Several Anonymous Caltech Graduate Students, personal communications, 1971 and 1972

4 C. Tanford, "Physical Chemistry of Macromolecules" Wiley, New York, 1961

5 K. Denbeigh, "Principles of Chemical Equilibrium", Cambridge, 1968

6 I. Prigogine and R. Defay, "Chemical Thermodynamics" Longmans, London 1954

7 R. Bowman, personal communications 1969

8 E. A. Guggenheim, "Modern Therodynamics by Methods of Willard Gibbs", Methuen and Co., London 1933

9 J. W. Gibbs, "Collected Works", Yale Univ. Press, New Haven, 1928

Addendum

Several months after Levenspiel first proposed his reverse-osmotic fountain, he again wrote to Scientific American to comment on his earlier contribution. Levenspiel was able to refute his earlier proposal in a single paragraph, a task which required several pages and some time on the part of this author. Levenspiel wrote[1]

> "When a pipe that is closed at the bottom by a semipermeable membrane is lowered into the ocean beyond the critical depth of about 700 feet, fresh water inside the pipe either rises higher as the pipe goes deeper, or it rises only to the critical depth. If the fresh water were to rise higher as the pipe goes deeper, one could construct the machine I have described [*see illustration at right on opposite page*]. In this machine fresh water would run downhill from one pipe to the other through a turbine that would generate electricity. Simultaneously the machine would partly unmix the salty ocean. Brine near the inlet of the deeper membrane would become increasingly salty; brine in the vicinity of the shallower membrane would become less salty. Clearly this action would violate the second law of thermodynamics, which states in effect that natural events proceed without exception in a preferred direction; that substances when left to themselves may mix but will never unmix; that man grows older, never younger, and that a rolling stone eventually stops rolling.

The illustration which accompanied this paragraph is shown on the following page. It is satisfying that the detailed thermodynamic analysis presented earlier gave the same correct result concerning the operation

---

[1] Scientific American, April 1972, page 110.

of the proposed fountain as described so succinctly here by Levenspiel. It is also very clear that there are many ways to draw correct conclusions using thermodynamic arguments, and some of these methods are likely to be easier and much more efficient than others.

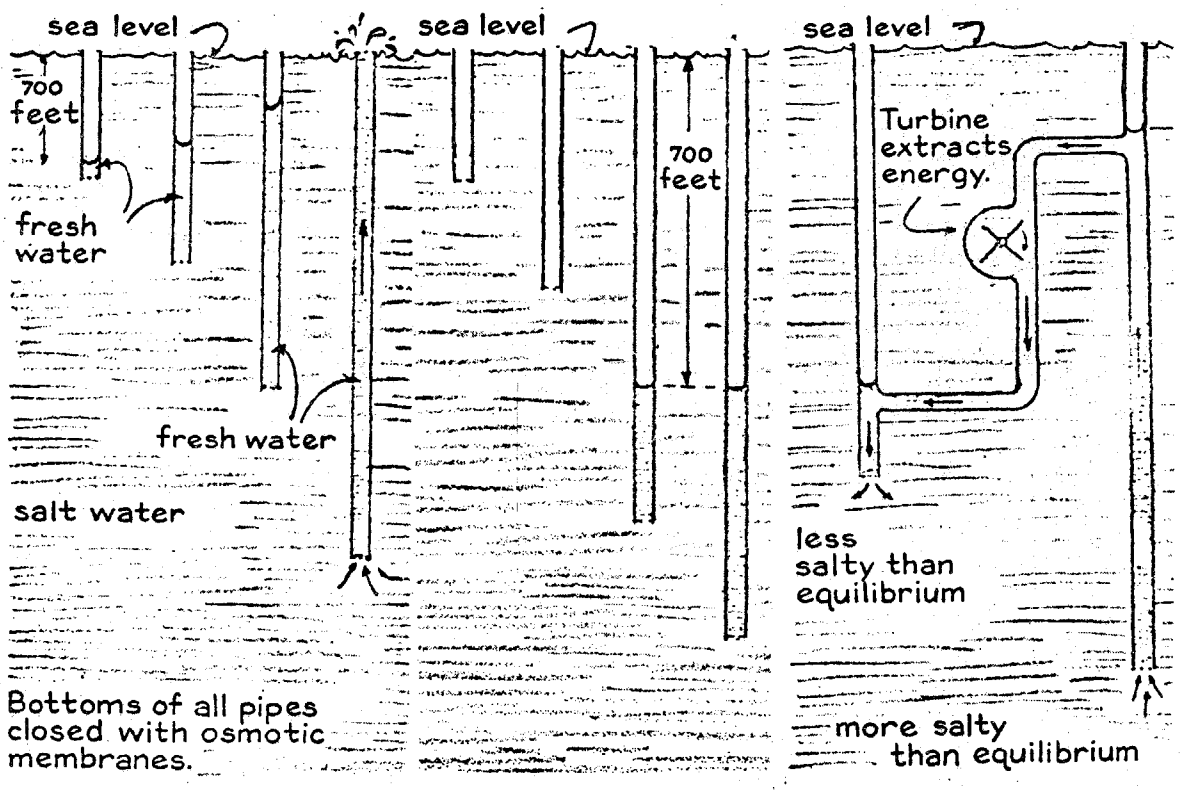

Illustration Included with Levenspiel's Comments
(From Scientific American, April 1972)

PROPOSITION 3

TRANSITORY ASTIGMATISM - AN EXPLANATION FOR SPECTACLE BLURRING IN CONTACT LENS WEARERS

Abstract

The phenomenon of spectacle-blurring experienced by many contact lens wearers is discussed. It is proposed that the condition can be explained by a period of transitory astigmatism which results from a deformation-recovery process in the cornea. Two plausible deformation mehcanisms are discussed which are consistent with the proposed explanation of spectacle-blurring and with all of the observations surrounding this visual phenomenon.

Introduction

It is a common complaint of many contact lens wearers that they experience mildly blurred vision when they remove their contact lenses and return to conventional spectacles. This phenomenon, usually described as "spectacle-blurring" tends to disappear after several hours, and the patient's vision with conventional spectacles then becomes as good as he experienced with his contact lenses in place. Other conditions which are associated with "spectacle-blurring" are the following. The blurred vision is more pronounced and lasts longer for longer wearing periods of the contact lenses. Furthermore, the blurry vision does not arise at all when the patient changes his optical system in the opposite direction; i.e. the patient's vision remains sharp and clear when he changes from conventional spectacles to contact lenses. Finally, some contact lens wearers do not experience "spectacle-blurring" even when their contact lens wearing periods become very long.

The author, being a contact lens wearer himself, has never been able to obtain a satisfactory explanation of the phenomenon described above, either from personal communications with eye specialists or from the literature. Since both optical systems, the contact lenses and the conventional spectacles, are adequate for correcting the

patient's vision in most cases, the phenomenon cannot be explained simply by postulating that there may be differences in the corrective power of the two systems. Instead, the blurred vision experienced during the relatively brief transient period discussed above must reflect some transient effects in the eye itself, particularly in the cornea upon which the contact lenses are placed. It should be noted that the phenomenon discussed here, "spectacle-blurring", is quite different from the phenomenon of gradual blurring of the vision experienced by some patients during prolonged contact lens wearing periods; that problem has been discussed at length in the literature(1). Here an explanation is proposed for the sudden change from sharp, clear vision to mildly blurred vision when a patient exchanges one optical system for a second (and presumably equivalent) system. A proper explanation of this phenomenon should be consistent with all of the other observations listed above, in particular: (a) the transient nature (b) the unidirectionality (i. e. in the direction contact lenses-spectacles but not the reverse) and (c) the nonuniversality (all patients not affected) of the phenomenon.

The Optical Systems

Conventional spectacles and contact lenses differ in the way in which they correct visual deficiencies. Spectacle lenses are positioned at a fixed distance from

the eye. The eye moves in its socket behind the fixed lens so that different regions of the large lens may fall within the line of sight. Contact lenses are placed directly onto the eye and rest upon the fluid layer wetting the surface of the cornea. The small lens moves with the eye, and therefore the line of sight is always through the central region of the lens. In addition, the common spherical contact lens is capable of rotation on the cornea. The rotation is caused by unbalanced forces which may be exerted on the lens as the eyelid passes over it. Because of the freedom of rotation, there is no preferred orientation of the lenses when they are inserted into the eye. Special contacts known as toric corneal lenses (1), have been designed to resist the forces which tend to rotate the lenses. These lenses must be inserted in a given orientation, and they will maintain this orientation during use. The importance of these toric lenses will be discussed later.

The corrective power of contact lenses depends upon the optical properties of both the plastic lenses and the tear fluid upon which they rest. The very important role of the tear fluid is essentially to neutralize most of the refractive power of the cornea (1). Therefore the refraction characteristic of the contact lens-fluid lens optical system is essentially that of the plastic lens only. Thus the contact lens provides the eye with a new

medium of sufficient refractive power to produce the required focal conditions for clear vision. In addition to the fluid layer that completely fills the space between the contact lens and the cornea, it is necessary that the front side of the contact lens be uniformly wetted with a thin layer of tear fluid. Thus the plastic lens is essentially immersed in a fluid medium in front of the cornea.

Astigmatism and Contact Lens Correction

Astigmatism is a common visual disorder which results from differences in the refractive power in different meridians of the eye. There are many physiological causes for astigmatism, but by far the most common is the presence of uniform but unequal curvature of the meridians of the front surface of the cornea. Astigmatism of this variety is known as regular corneal astigmatism. Another type of astigmatism which will be mentioned in later sections is the irregular corneal variety which arises due to non-uniformities of curvature within a given meridian. Irregular astigmatism can result from an abraision injury to the cornea (1,2).

As a result of the unequal curvature of the cornea, the astigmatic eyes cannot focus the light emanating from a point source into a sharp point image. Consequently the vision is blurry. (The word astigmatism comes from Greek roots - a not + stigma point (2).) A schematic diagram (taken, with caption, from Ref 2) showing the

effect of regular corneal astigmatism appears in Figure 1.

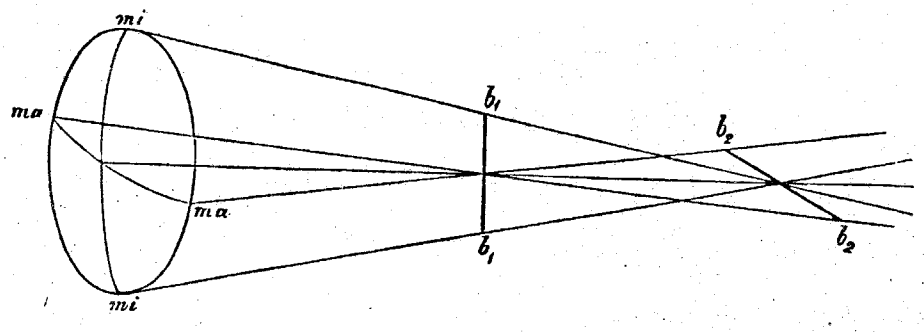

3.9 Effect of corneal astigmatism

The cornea is here assumed to be more strongly curved along *ma ma* than along *mi mi*. The light flux from a point situated on its axis is never re-united into a single focus point, but is concentrated into a vertical focal line b_1 b_1, and further back into another, horizontal, focal line b_2 b_2. (From Fick (1879), 'Dioptrik'. In Hermann's *Handbuch der Physiologie*, Vol. III, Pt I.)

Figure 1

This type of astigmatism is easily corrected by introducing a cylindrical correction into conventional spectacle lenses The cylindrical correction compensates for the different refractive power in the various meridians, and therefore clear vision is restored. In conventional spectacles the cylindrical correction can be combined easily with the spherical component of the lens which corrects for myopia (near-sightedness) or hyperopia (far-sightedness)

This combination of cylindrical and spherical correction is not possible in conventional contact lenses since they rotate on the cornea and most of the time would not be in the proper orientation to correct the patient's astigmatism. However, in most cases of regular corneal astigmatism, a cylindrical correction is not needed since the fluid layer between the contact lens and the cornea

effectively compensates for the differences in refractive power of the cornea. This "repairing" of corneal deficiencies by the fluid layer between the contact lens and the cornea is so good that it has been found to correct a type of irregular astigmatism which is uncorrectable by spectacles, namely the astigmatism associated with roughness of the cornea as discussed above (2). If, however, the patient's astigmatism arises from some cause other than deformities of the cornea surface (1), then the tear fluid layer cannot compensate for the refractive differences, and either conventional spectacles or toric contacts are necessary to correct the patient's vision.

A Proposed Explanation of Spectacle-Blurring-Transitory Astigmatism

Keeping the previous discussion in mind, consider the following: During the period of contact lens wearing, the presence of the plastic lens on the cornea may cause the cornea to deform slowly. The slow deformation will not continue endlessly, but instead the cornea will eventually come to some new equilibrium shape defined by the forces exerted by the lens. During the deformation process, of course, the tear layer is constantly adjusting itself to fill the space between the lens and the cornea.

Now consider how this might affect the vision of a myopic or hyperopic patient who also suffers from regular corneal astigmatism. The patient is wearing his spectacles.

The spherical and cylindrical corrections of his spectacles adequately correct his deficiencies and so his vision is sharp and clear. The patient inserts his contact lenses. The contacts contain the same spherical correction so that the patient's myopia or hyperopia is overcome. In addition the tear fluid immediatily fills the space between the contact lens and the cornea so that the astigmatism is also corrected adequately. Now the cornea begins to deform slowly under the influence of the plastic lens. However since the fluid layer is continuously adjusting itself to fill the space between lens and cornea, the astigmatism is always corrected and the patients vision remains sharp and clear during the contact lens wearing period.

Next consider that the contact lenses have been in the patient's eyes long enough for the cornea to assume a new equilibrium shape; the deformation has stopped. The patient removes his contact lenses. There are three possibilities concerning the behavior of the cornea when the lenses are removed. The cornea might instantanecusly "spring" back to its original shape; it could retain its deformed shape; or it could slowly return to its original shape over a period of time. It will be shown in the following paragraphs of this section that the third possibility, i.e. the slow return of the cornea to its original shape, explains all of the observations surrounding the phenomenon of "spectacle-blurring". In the next section

it will be shown that there are realistic mechanisms which predict that the cornea should behave in the proposed manner.

The patient has removed his contact lenses and replaced them with his conventional spectacles. He finds that his vision is blurry. In view of the above discussion this is not surprising since his conventional spectacles have been ground to correct for corneal astigmatism arising from corneal curvature differences as measured on the patients undeformed cornea. Thus, while the patients vision is immediately corrected by his spectacles for the myopic or hyperopic condition, it will take some time for the cornea to return to its original shape so that the spectacles can correct his normal astigmatic condition. During the period of time when the cornea is returning to its original shape, the cylindrical correction of the spectacles will not correspond to the curvature of the cornea and the patient's vision will be blurry as a result of the improperly corrected astigmatic condition which exists. When the cornea has, after several hours, returned to its orignial shape, the patient's vision is again sharp and clear. Thus a condition of "transitory astigmatism" is the cause of spectacle blurring*.

---

*There is a well known phenomenon known as transitory myopia which can arise from such diverse causes as dietary changes or trauma(1). The phenomenon discussed here is clearly quite different.

The proposed transitory astigmatism explains all of the following conditions which are associated with spectacle-blurring:

1. Unidirectionality-The tear layer continuously compensates for the astigmatism associated with corneal deformation when the contacts are in place. This is not the case when the cornea is returning to its original shape when the spectacles are employed. Thus there is immediate compensation for corneal irregularities whenever contacts are employed, but proper astigmatism correction by the spectacles can be expected only when the cornea is in an undeformed state.

2. Non-universality-If a patient suffers only from myopia on hyperopia but not from astigmatism, spectacle blurring should not arise. During the contact lens wearing period the uniform cornea will either remain undeformed or be deformed uniformly. In either case there is no cylindrical correction in the spectacles which, during the recovery period of the deformed cornea, creates the blurry vision due to improper astigmatic correction.

3. Transient nature-The period of blurry vision is obviously limited to the time it takes for the cornea to return to its original shape. Furthermore, as the cornea gradually approaches the shape for which the spectacle lenses were prescribed, the patient's vision gradually becomes clearer. Also the length of the period of blurry vision

should depend somewhat upon the wearing time of the contact lenses. Surely if the lenses are inserted for only a few minutes, the corneal deformation, and therefore the length of time of blurry vision when the contacts are removed, should be small. However, there should be a maximum period of spectacle blurring, corresponding to the time it takes for the cornea to recover from the proposed equilibrium shape it assumes during long periods of contact lens wearing.

Proposed Mechanisms for Corneal Deformation and Recovery

Before discussing mechansims by which the cornea can slowly change shape and later return to its original shape, it will be useful to have an idea of the composition of the cornea (3,4). Figure 2 shows a stained section of a rabbit cornea. (3)

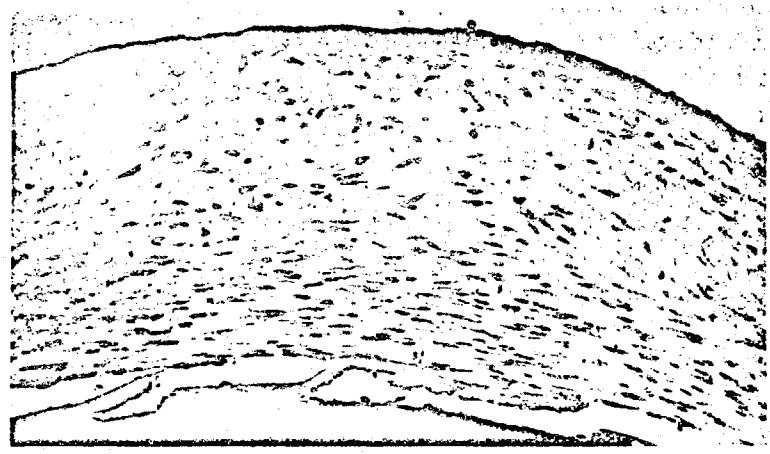

FIG. 1
Section of a rabbit cornea on the 18th day of gestation. Note the well-orientated fibroblasts in the posterior third and indications of the orientation of the collagen fibrils in that region. The cells and their processes in the anterior two-thirds of the cornea are irregularly arranged. The basement membrane underlying the corneal epithelium is visible. Descemet's endothelium is present, but not clearly differentiated from the stromal fibroblasts and no Descemet's membrane has yet appeared to separate them. A fragment of the lens epithelium is adherent to the posterior corneal surface. Mallory's connective tissue stain was used.

Figure 2

The corneal tissue or stroma is a gelantinous substance containing around 20% collagen and around 80% fluid similar to aqueous humor(3). The fluid contains various organic solutes including mucopolysaccharides. The collagen is distributed into bundles of fibrils arranged parallel to the cornea surface. It is difficult to separate the collagen from the mucoid (3), and therefore it is felt that the mucopolysaccharides of the cornea are bound to the collagen bundles by a kind of mucopolysaccharide-protein complex (3,4).

Given this interconnected polymeric nature of the cornea, it is not unreasonable to assume that the cornea deforms and returns to its original shape by the well known creep and creep recovery process commonly observed in synthetic polymers (5). Figure 3 shows this process schematically for a typical cross-linked polymer.

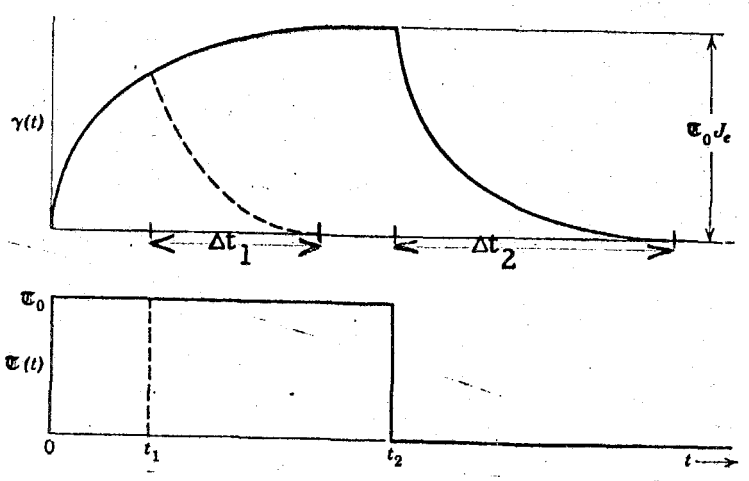

Figure 3

The lower curve shows that the stress is applied instantaneously at time 0 and is held at some constant value until time t_2 at which point the stress is rapidly removed. The upper curve shows the corresponding strain (or deformation) situation. From time 0 the material deforms slowly, approaching an equilibrium deformation. After time t_2, when the stress have been removed, the material slowly returns to its undeformed state. This is in exact correspondence with the proposed situation for the cornea under the influence of contact lenses. At time 0 the lenses are inserted and the cornea experiences a constantly imposed stress as long as the lenses remain in place. At time t_2 the lenses are removed and the stress is reduced to zero. One may wish to speculate on whether the stress act as "gathering" or "spreading" forces on the cornea; this would seem to depend upon the kind of fit provided by the prescribing doctor. In either case the cornea deforms, or creeps, during the contact lens wearing time, i.e. from $t=0$ to $t=t_2$. As discussed above the tear layer compensates adequately for the shape change. It is during the time period after t_2, while the cornea returns to its original shape, that spectacle blurring occurs. The time scale of several hours for recovery is perfectly reasonable based on experience with synthetic polymers. Figure 3 also shows clearly why the spectacle blurring is more pronounced and lasts longer for longer contact lens

wearing periods. The dotted lines in Figure 3 indicate the creep-recovery process observed if the stress is removed before the equilibrium deformation is attained. It is clear that the total deformation is smaller, and also that the recovery time is shorter ($\Delta t_1 < \Delta t_2$). Thus a creep-recovery mechanism is perfectly consistent with the transitory-astigmatism explanation for spectacle-blurring

The true situation may be more complicated than simple creep-recovery if the cornea swells during the contact lens wearing period. It is well known that under certain conditions the cornea will swell, and that most of the swelling takes place in the mucoid material between the collagen fiber bundles (3). At least one theoretical model has been proposed to explain corneal swelling (4). The possibility of corneal swelling during contact lens wearing is likely if the plastic lenses interfere with the oxygen supply necessary for the normal dehydration mechanisms or if they cause changes, perhaps due to a stagnation effect, of the isotonic molarity of the tear fluid. If appreciable swelling takes place, this phenomenon could contribute to the time dependent deformation and recovery of the cornea during and after contact lens use. In this case a swelling-deswelling mechanism must be added to the creep-recovery mechanism discussed above.

Summary and Conclusions

It has been shown that transitory astigmatism is a reasonable explanation for the phenomenon of spectacle blurring The required slow deformation and recovery of the cornea has been described in terms of creep-recovery and swelling-deswelling mechanisms. The occurrence of these particular deformation processes appeared to be quite reasonable considering the structure of the cornea.

Very little is known concerning the time dependent mechanical properties and swelling characteristics of the cornea. Yamada (6) has reported stress-strain data for human and animal cornea but no attention was paid to time effects. It appears to this author that studies of the time dependent mechanisms discussed above would be of great help in finding a solution to the spectacle-blur problem. Solutions to the problem could be of at least two types. The first might be to find a way to increase the rate of recovery, both mechanical recovery and deswelling, so that the period of transitory astigmatism is greatly reduced. The second approach would attempt to eliminate or at least minimize the amount of deformation experienced by the cornea. This would be accomplished by reducing the driving forces for both the creep and swelling mechanisms. The latter approach is clearly the more satisfactory one since it protects the cornea from the trauma of a continuous deformation recovery cycle throughout the patient's lifetime. In any

case, solutions to the problems which give rise to spectacle-blurring would certainly be welcomed by thousands of contact lens wearers.

References

1 I. M. Borish, "Clinical Refraction", Edition 3, Professional Press, Inc., Chicago, 1970

2 M. H. Pirenne, "Optics, Painting and Photography", University Press, Cambridge, 1970

3 The Transparency of the Cornea, a UNESCO and WHO Symposium, Edited by Sir Stewart Duke-Elder and E. S. Perkins, Blackwell Publications, Oxford, 1960

4 S. Hodson, J Theor. Biol., 33 :419-427 (1971)

5 J. D. Ferry, "Viscoelastic Properties of Polymers", Wiley, New York, 1961, page 17

6 H. Yamada, "Strength of Biological Materials", Williams and Wilkins, Baltimore (1970)